FACULTY OF SCIENCES

VUB ENGINEERING

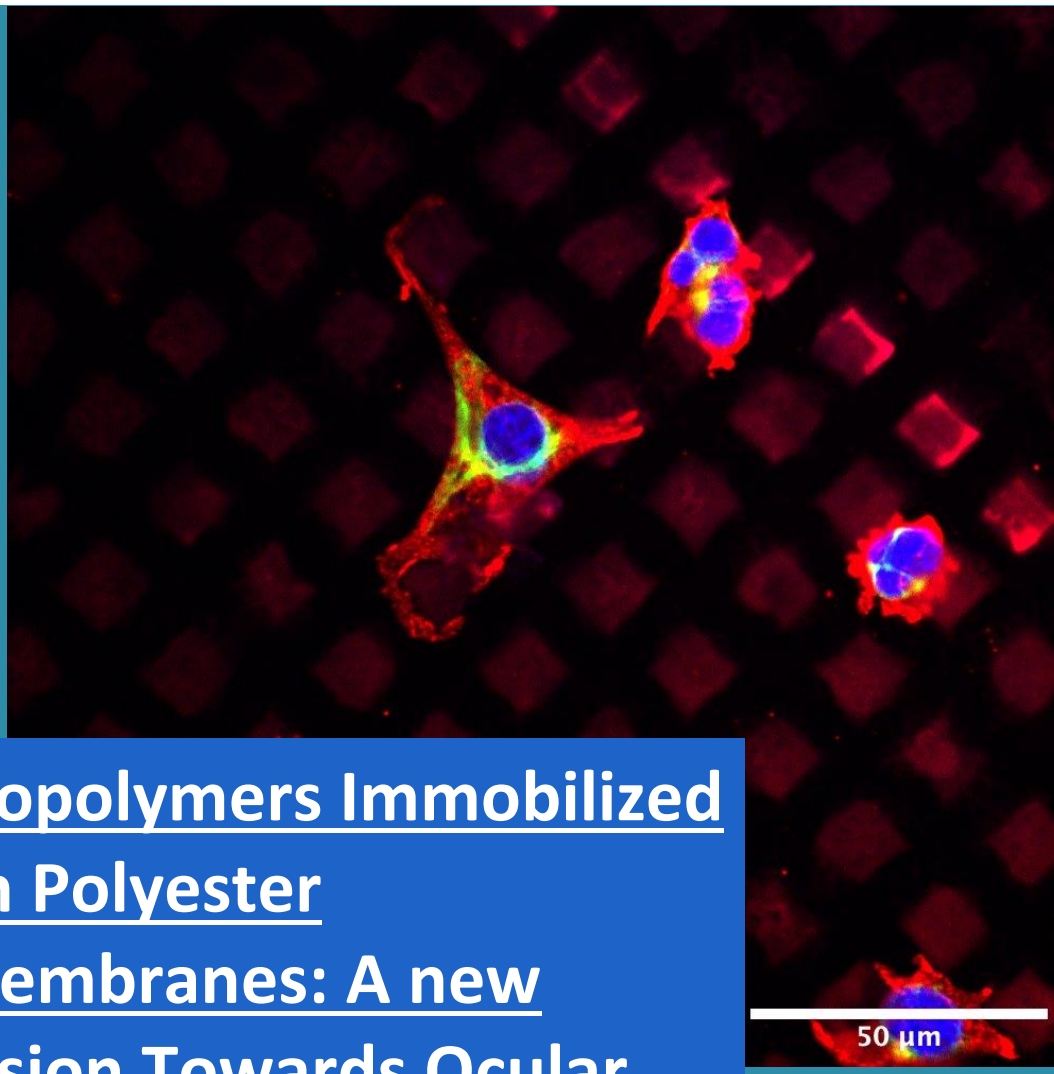

Biopolymers Immobilized on Polyester Membranes: A new Vision Towards Ocular Regeneration

Jasper Van Hoorick
Promotors:
Prof. Dr. S. Van Vlierberghe
Prof. Dr. P. Dubruel
Prof. Dr. Ir. J. Van Erps
Prof. Dr. Ir. H. Thienpont

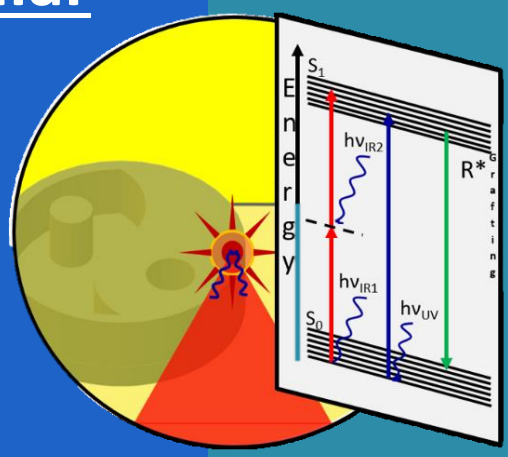

Biopolymers Immobilized on Polyester Membranes: A new Vision Towards Ocular Regeneration

Jasper Van Hoorick

Promotors: Prof. dr. S. Van Vlierberghe, prof. dr. ir. J. Van Erps
Prof. dr. P. Dubruel, Prof. dr. ir. H. Thienpont

Dissertation submitted in fulfillment of the requirements for the academic degree of:

Doctor (Ph.D.) of Science: Chemistry
Doctor (Ph.D.) of Engineering

Department of Organic and Macromolecular Chemistry
Faculty of Sciences
Ghent University

Department of Applied Physics and Photonics
Faculty of Engineering
Vrije Universiteit Brussel

Members of the Examination Committee

Promotors:

Prof. dr. P. Dubruel (Ghent University)

Prof. dr. ir. H. Thienpont (Ghent University)

Prof. dr. S. Van Vlierberghe (Vrije Universiteit Brussel)

prof. dr. ir. J. Van Erps (Vrije Universiteit Brussel)

Jury Members:

Internal (Ugent)

Prof. dr. Filip Du Prez (chairman, Ghent University, België)

Dr. Tom Gheysens (Universiteit Gent, België)

Prof. dr. Richard Hoogenboom (secretary, Ghent University, België)

Internal (VUB)

Prof. dr. ir. Roger Vounckx (co-chair, Vrije Universiteit Brussel België)

Prof. dr. ir. Hubert Rahier (secretary, Vrije Universiteit Brussel, België)

Prof. dr. Steven Ballet (Vrije Universiteit Brussel, België)

External

Prof. dr. Aleksandr Ovsianikov (Technische Universität Wien, Austria)

Prof. dr. Carina Koppen (Universiteit Antwerpen, België)

“None but those who have experienced them can conceive of the enticements of science. In other studies you go as far as others have gone before you, and there is nothing more to know; but in a scientific pursuit there is continual food for discovery and wonder.”
(Frankenstein-Mary Shelley 1818)

Acknowledgement

Finally, the time has come where all the efforts of the past 11 years are condensed in a final manuscript, thereby hopefully resulting in the official end of my university education. It has been a long road (I.e. 11 years) with a lot of tight corners, roadblocks and deviations from the educational highway. Fortunately, there were quite some navigators and travel companions along the way which provided me with the proper sense of direction, thereby making sure I reached the PhD finish line in the end.

It all started in high school with the classes of Mrs. Asselman and Mrs. Moulin, which I would like to acknowledge for guiding me towards the world of science, and more specifically chemistry. As a result, I landed on this world in 2007 by initiating my bachelor in chemistry at Ghent University.

During this adventure, I encountered a lot of chemistry continents, of which I visited repeatedly, until I was introduced to the continent of polymer chemistry. I would like to thank professor Filip Du Prez, for the first introduction to this interesting area, and Professor Peter Dubruel for introducing me to the land of polymer chemistry for biomedical applications.

Additionally, I would specifically like to thank Peter Dubruel, for allowing me to start my master thesis in his research group under the supervision of the then still post-doc Sandra Van Vlierberghe.

Furthermore, I would like to thank Peter Dubruel and Hugo Thienpont, for trusting in me, thereby guided by Sandra's opinion, and providing me with the required funds to start my PhD after a first unsuccessful attempt to consolidate IWT funding. Grateful for this trust, which allowed me to work on the topic of my choice, I was extra motivated to repay this trust via consolidation the IWT grant the next year with success. In this respect, I would also like to thank Hugo, Peter, Sandra and Jürgen for all the help in preparing for this task and all the support afterwards. It was from that moment, that the final destination became clear, obtaining the PhD. However, the road towards it still needed to be paved.

In this respect, I would like to specifically acknowledge Sandra and Jürgen for always being so motivating, constructive and helpful for taking the right strategic decisions. And especially for all the help in writing and correcting the scientific reports and publications. I would also like to specifically thank Sandra for being so motivating, thereby convincing me to always go for the extra mile from the start of my master thesis, until the very end of my PhD. As

a consequence, the road towards the PhD may have become longer, but all the more interesting. In this respect, I always enjoyed her approachable mentality allowing for sufficient independency on the one hand, but also always ready to help thinking about scientific problems, or providing the contacts of the people who could tackle the problems, if her personal knowledge and experience wasn't sufficient. Additionally, I enjoyed the multiple running sessions/meetings which allowed us to discuss both scientific and non-scientific topics in a relaxing atmosphere, and initiating the tradition of running the 20 km of Brussels every year.

In this respect, I would also like to thank my other running buddies Lara, Maxime and Arn for making the lunches so much nicer, while staying in shape. Lara has always been one of the kindest colleagues, always ready to listen to any problems, frustrations I encountered and helping me to take the correct (people related) strategic decisions both work and non-work related. This even resulted in assisting to select the right outfit for my wedding, thereby at least making sure I was properly dressed for the occasion.

Additionally, I would like to thank all my colleagues at PBM for the nice group atmosphere, in the past six years, I have seen a lot of people coming and going. However, I would like to thank some people in particular as they did not only provide me guidance towards the right direction, but also became travel companions and even remained (or will remain) friends after our professional roads separated. Els, Myriam, Elke, Tom, Aysu, Lara, JP, Maxime, Geert-Jan, Liesbeth, Neleken, Veerle, Lana, Babs, Annemie thank you for all the help along the way and all the great discussions/drinks/parties/BBQ's. I am sure we will maintain this atmosphere even when obtaining the PhD is reduced to one of the many stops along the long and winding road of life.

Of course I would like to specifically thank Geert-Jan and Maxime, honorary members of the PolyeSTARs for all the fun, problems and solutions we encountered during the polyester synthesis in lab 1. I am sure that all three of us will always look back on this magical time when we were united in the same lab engulved in an atmosphere of silly puns and clever jokes. Furthermore, Geert-Jan, I couldn't feel more honoured to bear the name of your first-born son.

Tom, your ever so helpful nature has been a real asset to the group both on a professional and personal level. I sincerely hope that in one year we can enjoy our wine together! Also Jasper Delaey, thank you for all the work in

your master thesis, and your critical nature regarding scientific insights. I am sure you will do great in continuing this research.

I would also like to specifically thank Veerle and Tim Courtin for the technical support in all the analysis of the synthesized materials.

Besides the colleagues in PBM, I would also like to thank all the colleagues at B-phot for making the teambuildings, receptions, meetings into some of the nicest events I occurred throughout my PhD.

Furthermore, besides my Belgian colleagues, I also want to thank my colleagues in Vienna Aleks, Marica, Peter, Agi, Markus, Elise, Wolfi, Franziska, Denise. First of all, I would like to thank Aleks, for allowing me to visit his lab very frequently thereby enabling me to learn everything about the coolest and most spectacular 3D printing technique there is. Also Marica, thank you for always being so helpful and kind both professionally as extra-profesionally, a real mother of the group. Peter, the king of 2PP, thank you so much for building the best printer in the world, and for learning me how to operate it properly. I sincerely hope you will conquer the world with UPNano! Wolfi, unfortunately there can only be one king, but if Peter is the king of 2PP, you definitely are the Godzilla of 2PP. Agi and Markus, we met for the first time back in 2015 and I am very happy to have shared so many nice experiences ever since, going from the nice evenings at the TU where we discussed science, beer, wine and feminism to the weekend you guys came to Belgium. I am also happy that we will continue to collaborate in the (near) future! Elise, although we only met more recently, it seems like I have known you for ages, thank you for all the help with the gel-PI synthesis and your ever so contagious (loud) enthusiasm, nice personality and helpful nature. Franziska, although we only met a few times, you are a very helpful and kind person, and I really appreciated you hosting the Godzilla evenings, they always kicked ass! In Brief, thank you all for making Vienna my home away from home, making it into my all-time favourite travel destination. I am sure we will keep seeing each other in the future.

Finally, the last scientific people which deserve my gratitude are Bert, Carina and Nadia from the university of Antwerp. Thank you so much for the help focussing on the ocular application of the developed materials. In this respect, Bert you are a dream to work with, very focussed, very efficient, very constructive and open for discussion. I am happy that we managed to consolidate the FWO grant to continue the work on the membranes towards relevant clinical applications.

Finally, I would like to thank my friends and brothers and especially, Kasper, Barrie, Pieter, Lieven, Xander, Kurt, Dries, Arnout, Maxime, Lara, Steffie, Arman, Jelle, Kevin, Nele for providing me with the correct entertainment to take my mind of the often stressful PhD.

Furthermore, I would like to thank my parents for mentoring me and always believing in me, thereby allowing me to pursue my dreams, even when things didn't always go smoothly

And finally I would like to thank Laura, who was there for me during all the good and bad moments. Especially for always having to deal with my stress and associated bad moods. Always helping me to regain my energy after long and stressful nights. I am happy I managed to convince you to become my wife, so that we can continue our adventure far beyond the end of this PhD.

Jasper Van Hoorick, 02/09/2019

Table of Contents

List of Figures

Chapter 1

List of Tables

Chapter 8

List of Abbreviations

^{1}H-NMR	proton-Nuclear magnetic resonance spectroscopy
2PP	Two-photon polymerization
A	
Ala	Alanine
AEMA	2-aminoethylmethacrylate hydrochloride
Ala	Alanine
AM	Additive Manufacturing
A_{max}	Maximum surface area
A_{CAD}	Surface area according to CAD
APS	Ammonium persulfate
ASC's	Adipose tissue derived stem cells
Asp	Aspartic acid
ATMP	Advanced therapeutic medicinal product
B	
BMSC	Bone marrow stromal cells
C	
CAD	Computer assisted design
CAM	Computer assisted manufcaturing
CEnCs	Corneal endothelial cells
C_n	Flory characteristic ratio
C_v	Heat capacity
Cys	Cysteine
D	
DAPI	4',6-diamidino-2-phenylindole

DAS	tetrapotassium 4,4’- (1,2-ethenediyl) bis (2-(3-sulfo-phenyl) diazenesulfonate)
DBA	diisobutylacrylamide
DLP	digital light projection
DMD	Digital micromirror device
DS(A)EK	Descemet stripping (automated) endothelial keratoplasty
DS	Degree of substitution
DSC	Differential scanning calorimetry
DTP	3,3’-dithiobis(propionic hydrazide)
$Đ_M$	polydispersity
DMEK	Descemet membrane endothelial keratoplasty
DMSO	Dimethyl sulfoxide
DTT	dithiothreitol
E	
ECM	Extra-cellular matrix
EDC	1-ethyl-3-(3-dimethyl aminopropyl)carbodiimide
EDTA	ethylenediaminetetraacetate tetrasodium tetrahydrate salt
EK	Endothelial keratoplasty
F	
FA	Furfuryl amine
FA	Focal adhesions
FDA	U.S. Food & Drug Administration
FECD	Fuchs’ Endothelial Corneal Dystrophy
FI	furfuryl isocyanate
FWHM	Full width at half maximum

G

G	Shear modulus
G’	Storage Modulus
G”	Loss modulus
Gags	glycosaminoglycans
Gel-AA	gelatin-acrylamide
Gel-AC	gelatin-anthracene
Gel-AGE	Gelatin allylglycidyl ether
Gel-boc-AEMA	gelatin with boc protected primary amines and aminoethylmethacrylate coupled to the carboxylic acids
Gel-BTHE	gelatin-3,3’,4,4’-benzophenone tetra carboxylic dihydroxyethylmethacrylate
Gel-cys	Gelatin-cystein
Gel-CYS-2-MPD	gelatin modified with cystein and 2-mercaptopyrimidine-4,6 diol
Gel-FGE	Gelatin furfuryl glycidyl ether
Gel-MA	gelatin-methacryloyl
Gel-MFVF	gelatin-5-(2-(5-methyl furylene vinylene)) furancarboxyaldehyde
Gel-MOD	Gelatin-methacrylamide
Gel-MOD-AEMA	Gelatin-methacrylamide-aminoethylmethacrylate
Gel-NB	Gelatin-norbornene
Gel-NC	Gelatin-nitrocinnamate
Gel-PEG-cys	gelatin-poly(ethylene glycol) cysteine
Gel-S	Thiolated gelatin
Gel-SH	Thiolated gelatin
Gel-T	Gelatin tetrazine

Gel-VE	Gelatin vinyl ester
Gelatin-FA	Gelatin furfuryl amine
Gelatin-FI	Gelatin furfuryl isocyanate
Gelatin-PEG	gelatin-poly(ethylene glycol)
Gelatin-TBA-MNA	gelatin-thiobutylamidine modified with 2-mercaptonicotinic acid (MNA)
Gelatin-tyramine	gelatin modified with tyramine
Gelatin/tyramine/heparin	gelatin modified with tyramine and heparin
gelMA-DA	Gelatin-methacrloyl-dopamine
gelN	Gelatin-norbornene
Gln	Glutamine
Glu	Glutamic acid
Gly	glycine
GMA	Gelatin-methacryloyl-acyl
GM	Göppert-Mayer
GPC	Gel permeation chromatography
GRAS	Generally recognized as safe
H	
HA	Hyaluronic acid
HRP	Horseradish peroxidase
I	
Ile	Isoleucine
i.e.	In exemplum
iPSF	Illumination point spread function
$IPSF^2$	Squared Illumination point spread function
IRgacure 2959	(2-hydroxy-1-(4-(hydroxyethoxy)-phenyl)-2-methyl-1-propanone)

L	.
LAP	Lithium (2,4,6-trimethylbenzoyl)phenylphosphinate
Leu	Leucine
Li-TPO	lithium phenyl-2,4,6-trimethylbenzoylphosphinate
LSM	Laser scanning microscopy
LVE	Linear viscoelastic range
M	
$\overline{Mc}$	Average molecular weight between crosslinks
m_d	Dry mass of hydrogel samples
MFVF	5-(2-(5-methyl furylene vinylene))furancarboxyaldehyde
MHz	Megahertz
MMP-1	Matrix metalloproteinase 1
M_n	Number average molecular weight
MPG	methacrylated poly(ethylene glycol)-modified gelatin
M_r	Average molecular weight of one repeating unit
m_s	Mass of hydrogel at equilibrium swelling
MSC	mesenchymal stem cell
M_w	Weight average molecular weight
MWCO	Molecular weight cut-off
N	
N	Refractive index
NA	Numerical aperture
NHS	n-hydroxysuccinimide
NIR	Near infra-red

NMR	Nuclear magnetic resonance spectroscopy
O	
OPA	ortho-phtalic dialdehyde assay
P	
P2CK	sodium 3,3'-((((1E,1'E)-(2-oxocyclopentane-1,3-diylidene) bis (methanylylidene))bis(4,2-phenylene))bis(methylazanediyl))dipropanoate
P3-A	Tripropylene glycol diacrylate
PA	Dipentaerythritol pentaacrylate
P_{avg}	Average laser power
PBK	Pseudophakic bullous keratopathy
PBL	Poly(γ-butyrolactone)
PBS	Phosphate Buffered Saline
PCL	Poly(ε-caprolactone)
PDLA	Poly(D-lactide)
PDLLA	Poly(D,L-lactide)
PDO	Poly(dioxanone)
PDT	Population doubling times
PEG	Poly(ethylene glycol)
PEG2SH 3400	Poly(ethylene glycol) dithiol with a molecular weight of 3400 g/mol
PEG4SH	4-arm Poly(ethylene glycol)tetrathiol
PEG4SH 10000	4-arm Poly(ethylene glycol) tetrathiol with a molecular weight of 10000 g/mol
PEG4SH 20000	4-arm Poly(ethylene glycol) tetrathiol with a molecular weight of 20000 g/mol
PEGDA	Poly(ethylene glycol) diacrylate
PEGdNB	Poly(ethylene glycol) dinorbornene
PEGDVS	Poly(ethylene glycol) divinylsulphone

PEGTA	4-arm poly(ethylene glycol) tetra acrylate
PGA	Poly(glycolic acid)
pHEMA	Poly(2-hydroxyethyl methacrylate)
PI	Photo-initiator
[PI]	Photo-initiator concentration
PK	Penetrating keratoplasty
PLA	Poly(lactic acid)
PLGA	Poly(lactic-co-glycolic acid)
PLLA	Poly(L-lactide)
PPA	dipentaerythritol pentaacrylate
Pro	Proline
PTA	Pentaerythritol triacrylate
PVA	Poly(vinyl alcohol)
PVA-MA	Poly(vinyl alcohol) methacrylate
PVL	Poly(δ-valerolactone)
Q	
q	Mass swelling ratio
Q	Volumetric swelling ratio
R	
Ru/SPS	Photoinitiator based on a ruthenium complex (tris-bipyridyl-ruthenium (II) hexahydrate) and sodium persulfate (SPS)
RF	Reacted functionalities
RGD	Arginine-glycine-aspartic acid
ROP	Ring opening polymerisation
S	
SLA	Stereolithography

$SnOct_2$	$Sn(2\text{-ethylhexanoate})_2$
SPS	Sodium persulfate
T	
T	Period of the laser pulses
TCP	Tissue culture polystyrene
T_d	Dissociation temperature
TEMED	N,N,N',N' Tetramethylethylene-1,2-diamine
T_g	Glass transition temperature
TEG2SH	Tetraethylene glycol dithiol
T_m	Melting temperature
TNBSA	2,4,6-trinitrobenzene sulfonic acid
TPE	Two-photon excitation
TTA	Trimethylolpropane triacrylate
U	
UDMA	Urethane-dimethacrylate
UV	Ultra violet
V	
Val	valine
$v_{2,s}$	the polymer volume fraction in the swollen state
V_{CAD}	Volume according to CAD design
VF	Volume factor
V_{max}	Maximum volume
W	
WOW 2PP	Widened objective working range 2PP
X	
XPS	X-ray photoelectron spectroscopy
$\dot{\gamma}(t)$	Time dependent shear rate

δ	Phase shift angle
$\delta_u \phi_u$	Two-photon cross section
ξ	Network mesh size
τ_P	Laser pulse duration
$\tau(t)$	Time dependent shear stress
λ	wavelength
κ-carrageenan-MA	kappa-carrageenan-methacrylate
η^*	Complex viscosity
ρ_x	Crosslink density
$\bar{\nu}$	specific volume of gelatin
ω	Frequency of deformation
ω_{xy}	1/e radius in the XY plane of the IPSF² as approximated by a 3D Gaussian distribution
ω_z	1/e radius in the Z direction of the IPSF² as approximated by a 3D Gaussian distribution

Chapter 1: Introduction

Parts of this chapter have been published in:

J. Van Hoorick, L. Tytgat, A. Dobos, H. Ottevaere, J. Van Erps, H. Thienpont, P. Dubruel, S. Van Vlierberghe, *Acta Biomater., **(2019)***

J. Van Hoorick, A. Ovsianikov, P. Dubruel, S. Van Vlierberghe, *Mater. Matters* **(*2018*)**, 13, 75.

1.1. Problem Statement

Corneal diseases are the 4th leading global cause (5.1%) of visual impairment and blindness, which is estimated to affect around 135 million and 45 million people respectively, according to the WHO [1–4]. The cornea is the clear membrane that provides the eye a window to the exterior world (Figure. I.1). Together with the lens, it is responsible for the majority of refractive power of the eye [5,6]. Furthermore, it protects the eye from physical and chemical damage and infections [7]. A significant portion of the patients suffering from corneal diseases suffer from a decompensated cornea due to a dysfunctional corneal endothelium (*vide infra*) [8]. In this respect, Fuchs' endothelial corneal dystrophy (FECD) is one of the most common corneal diseases with a prevalence of 4% of the population over the age of 40 in the U.S. [9]. For FECD, the only viable treatment is corneal transplantation [3,10,11]. FECD is even responsible for 39% of all corneal transplants globally [9,12,13]. However, the transplantation of healthy tissue still poses significant problems[14]. For one, in general, only 1 in 70 people requiring a donor cornea, can be treated [15]. Secondly, although tremendous progress has been made in the field of corneal transplantation, often the long term outcome is unsatisfactory. Reported issues include significant endothelial cell loss (i.e. 39 – 70% after 5 years depending on the performed transplantation procedure[14]), graft detachment, transplant rejection or endothelial decompensation (i.e. secondary failure)[16,17]. Furthermore, success of the procedure is still strongly dependent on issues related to standardization of the procedure[14–17]. Therefore, the need for a sustainable solution for these problems becomes apparent.

1.1.1. Anatomy of the Cornea

The cornea is a transparent, avascular connective tissue which is dome-shaped and composed of five distinct layers. From outside to inside, it consists of the corneal epithelium, the Bowman's layer, the corneal stroma, the Descemet's membrane and the corneal endothelium (Figure I.1 A & B). The epithelium, endothelium and stroma are cellular layers while the Bowman's layer and the Descemet's membrane are acellular membranes [6,7,18,19] (Figure I.1). The cornea has a mean diameter of around 11.71 mm and an average thickness of ± 530 µm at the center up to 650 µm at the periphery [20,21]. It exhibits a curvature radius of ± 7.81 mm at the anterior surface and ± 6.4 mm at the posterior surface [22].The cornea provides the

majority of the refractive power of the eye with a refractive index of 1.376 and a dioptric power of 43 D, whereas the lens only contributes for 20 D [6,21].

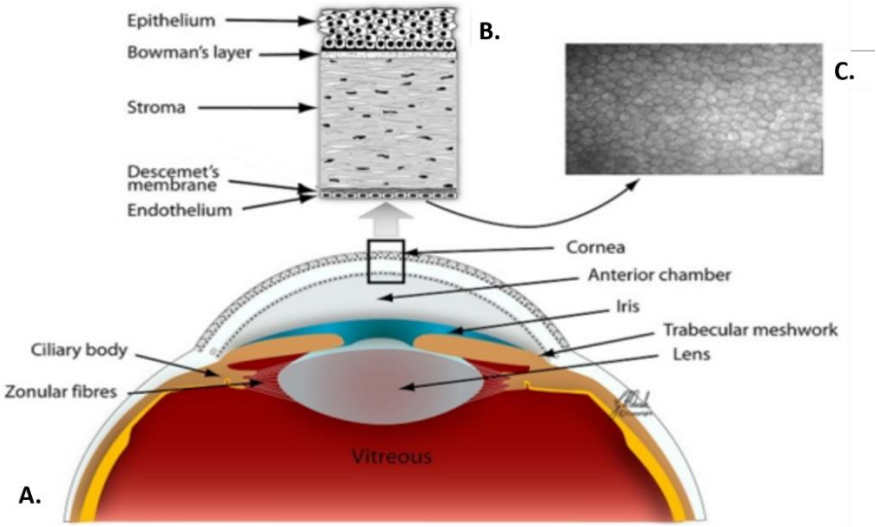

Figure I.1: Schematic representation of the anatomy of the anterior segment of the eye (A); schematic cross-section of the layered cornea structure (B) and visualization of the corneal endothelium (C) (Figure adapted from [18])

The Corneal Epithelium

The corneal epithelium consists of 5 - 7 cell layers and is responsible for around 9% of the overall corneal thickness (i.e. 50 – 90 µm) [5–7,21]. The cells are replaced continuously starting from the corneal limbus with a turnover of 7-10 days [21]. It acts as a biological barrier against pathogens and regulates the transfer of water and solutes to and from the stroma [7]. Furthermore, it is covered by a tear film which smoothens irregularities in the epithelial surface thereby consolidating the required optical properties [19]. Additionally, this tear film also functions as a reservoir for antibacterial components and growth factors, thereby assisting in repair and maintenance of the epithelium [7]. Within this epithelium, three distinct cell types can be identified. The top two layers are composed of non-keratinized, stratified squamous (i.e. thin and flat) epithelial cells which play an important role in tear film stability [21]. Next, there are two to three layers of polyhedral wing cells, which are seated on a basal columnar cell layer [21].

The Bowman's Layer

The epithelium is seated on top of an acellular layer, namely the Bowman's layer, which is a transparent acellular membrane with a thickness of approximately 8 - 14 µm or around 2 % of the total thickness of the cornea [6,21]. It mainly consists of randomly oriented, densely packed, condensed amorphous collagen type I and II fibrils [6,7,20,21]. The Bowman's layer functions as a molecular barrier on the one hand, while it provides rigidity thereby contributing to the shape of the cornea on the other hand [7]. Because it is an acellular layer, it does not possess the capacity to regenerate after injury [21].

The Corneal Stroma

The corneal stroma is responsible for around 88% of the total corneal thickness (i.e. ± 480 µm) [6,21,23]. It consists of collagen fibers which are arranged in up to 200 layers which are referred to as lamellae [21,23]. The collagen network is organised in such way that the collagen fibrils in each lamella are parallel to each other while forming a 90° angle relative to the next lamella thereby minimising forward light scattering [21]. Interweaving of collagen bundles of the adjacent lamellae in the anterior stroma provides a high shear resistance and transfers tensile loads between the lamellae, especially in the anterior stroma when compared to the posterior stroma [7,21]. At the edges of the cornea, the fibrils exhibit a circumferential orientation [21]. Furthermore, besides collagen fibers, it also contains glycosaminoglycans (GAG's), with the posterior stroma being characterised by a higher amount of hydrophilic keratan sulphate GAG's, whereas the anterior part mainly contains less hydrophilic dermatan sulphate GAG's [21]. Finally, the stroma is also sparsely populated with keratocytes which produce the extracellular matrix (ECM) (collagen and proteoglycans) and crystallins (i.e. structural proteins that help in maintaining the transparency of the cornea) [5,7,10,19,20,24].

This highly oriented collagen structure results in a degree of anisotropy in the cornea both from an optical as a mechanical perspective.

From an optical point of view, the presence of this highly oriented collagen structure results in polarizing properties and optical anisotropies also referred to as birefringence and linear dichroism[25]. Moreover, these collagen fibres exhibit two types of birefringence. On the one hand, the intrinsic or crystalline birefringence is a consequence of the presence of many electronic resonators (the π- π*-transitions in the planar peptide bonds) which are oriented in a

preferred direction inside a medium with more than one refractive index. As a result, the whole medium will transmit light with different polarizations in different directions. On the other hand, the form or textural birefringence is a consequence of the sub wave dimension of the collagen fibres which have a specific refractive index and are suspended in a medium with a different refractive index and are very specifically oriented. As a consequence, polarized light microscopy can be used to study the corneal stroma and gain insights in the molecular orientation and aggregational state of the collagen fibres [25]. Therefore, studying this birefringence allows to detect different physiological and pathological conditions of the cornea stroma [25]. For example, during diabetes, nonenzymatic glycosylation of collagen and other ECM proteins can occur which can influence this orientation and aggregation and thereby influence this birefringence [25]. Consequently, diabetes is one of the causes for corneal blindness [25].

From a mechanical point of view, the stroma also exhibits anisotropy which can provide valuable information in terms of diagnosing certain diseases as certain conditions such as keratoconus affect the orientation of the collagen fibrils [23]. In the central region of a healthy cornea, the majority of the fibrils are oriented in the inferior-superior (vertical) or nasal-temporal (horizontal) direction. As these fibrils are responsible for the biomechanical properties of the cornea, their orientation has an influence on the mechanical anisotropy [23]. In general, the inferior-superior direction is characterised by a significantly larger Young's Modulus (i.e. 51.26 ± 8.23 MPa) in comparison to the nasal-temporal direction (i.e. 43.59 ± 7.96 MPa) [23].

The stroma is characterised by a mean refractive index of 1.38 and an elastic modulus in the order of 11 MPa to 100 GPa (i.e. in the longitudinal direction of the fibers) [6]. Both the refractive index and the elastic modulus are dependent on the hydration of the stroma [6,26].

The Descemet's Membrane

The Descemet's membrane is the basement membrane of the corneal endothelium with a thickness of approximately 3 µm at birth up to 10-20 µm at old age (i.e. ± 3% of the total thickness) [21]. It provides an anchoring point for the corneal endothelial layer and consists of an anterior banded layer and a posterior, non-banded layer [6,7]. The banded layer consists of stacked collagen fiber bundles that are present as a 90-120 nm banding, on electron microscopy [19,27] (Figure I.2) . The banded layer has a constant thickness from birth [27] whereas the non-banded layer has an amorphous structure and

thickens with age [19]. In contrast to the Bowman's layer, the Descemet's membrane is continuously synthesized by the corneal endothelium and consequently, it has the ability to regenerate [21]. It is characterised by a Young's modulus of 5 MPa and contains mostly collagen type VIII which is excreted by the corneal endothelium [6,7,28]. Furthermore, it is very resistant to infection, enzymatic degradation and chemical damage [21].

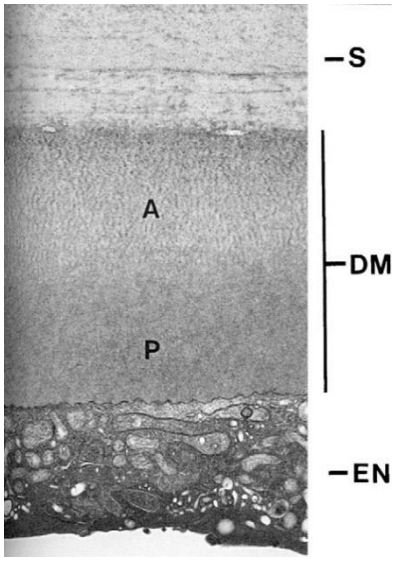

Figure I.2: Cross section of the Descemet's membrane (DM) with part of the stroma (S) and the corneal endothelium (EN). Within the DM the anterior banded region (A) and the posterior, non-banded layer (P) can be distinguished. (Figure reproduced from [19])

The Corneal Endothelium

The corneal endothelium constitutes a monolayer of hexagonally shaped endothelial cells organised in a honeycomb lattice that covers the posterior surface of the cornea. It has a thickness of approximately 5 µm (i.e. ± 1% of the total cornea) [5,18,19,29] (see Figure I.1 C) . The main function of the endothelium is to maintain the stroma in a state of deturgescence which corresponds to a state of relative corneal dehydration thereby maintaining corneal clarity [19,20]. The barrier function of the endothelium is a consequence of the presence of tight junctions between the corneal endothelial cells. Since a healthy cornea is avascular, these tight junctions are interrupted and form incomplete seals thereby acting as a leaky barrier to allow passive diffusion

of nutrients from the anterior chamber to the cornea (i.e. leaking) [7,19,20,28]. However, if this is not counteracted, the cornea inevitably swells thereby turning opaque. Therefore, the endothelial cells actively establish a local ion gradient which results in an osmotic net fluid transport back towards the aqueous humour in the anterior chamber (i.e. pumping) [19]. To this end, the corneal endothelial cells exhibit a high density of Na^+/K^+ ATPase pump sites [19,20]. This precarious balance keeps the human cornea in a physiological state of deturgescence, ensuring optimal tissue transparency and is referred to as the "pump-and-leak" function[30].

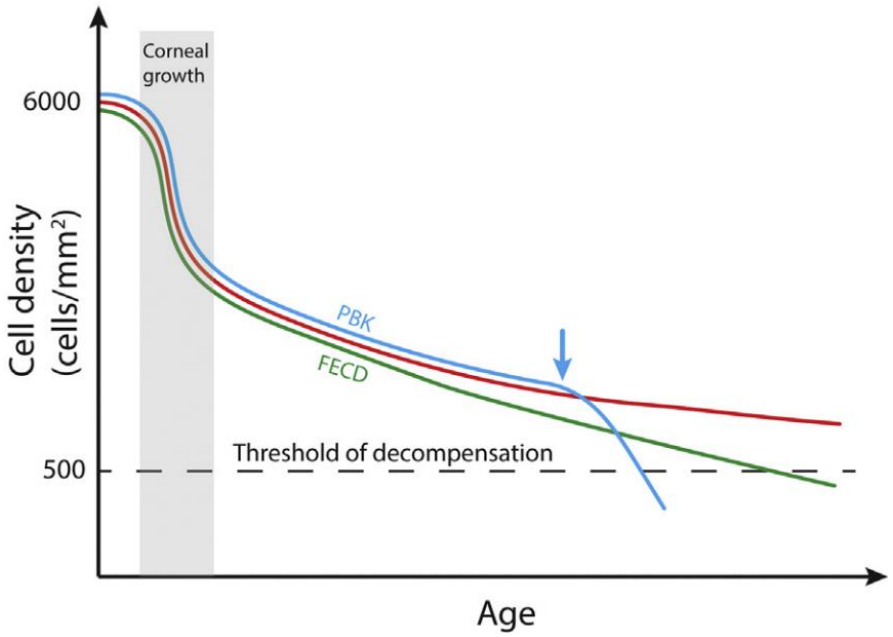

Figure I.3: Cell density of the corneal endothelium as a function of age. In newborns, the cell density is the highest. However, this decreases drastically during expansion of the corneal surface. In a healthy person (red curve), the cell density drops with 0.6 % annually. In case of a trauma or pseudophakic bullous keratopathy (PBK) (i.e. damage during cataract surgery), the cell density can suddenly drop below the decompensation threshold of 500 cells/mm (blue). In patients with FECD, the annual cell loss is higher, resulting in corneal oedema (green curve). (Image reproduced from [31])

Unfortunately, in humans, the endothelium is unable to undergo *in vivo* wound healing (i.e. proliferation to compensate tissue loss). Consequently, the absolute number of cells will only decrease throughout life (Figure I.3). At

birth, a cell density of around 6000 cells/mm^2 is present. However, this number decreases drastically during subsequent expansion of the corneal surface [31]. After being fully grown, the cell density further decreases with age at an average rate of 0.6% per year [31]. Additionally, this phenomenon can be accelerated due to disease or trauma (e.g. pseudophakic bullous keratoplasty (PBK) following cataract surgery) (Figure I.3). During such a trauma, cells surrounding a lesion are only capable to compensate for the damage via migration and enlarging to reinstate the endothelial barrier. However, the decreased cell density results in an overall decreased pumping capacity of the entire cell layer [6,19]. When cell density falls below an arbitrary threshold of 500 cells/mm^2, the aforementioned balance is irreversibly lost and permanent corneal opacification ensues (i.e. corneal decompensation) (Figure I.3) [32].

1.1.2. Fuchs' Endothelial Corneal Dystrophy

The most common condition affecting the corneal endothelium is Fuchs' Endothelial Corneal Dystrophy [14,16,31,33]. FECD is a hereditary disease characterised by a progressive loss of corneal endothelial cells due to apoptotic processes. As a consequence, thickening of the Descemet's membrane and deposition of extracellular matrix results in the formation of bumps or "guttae" (Figure I.4) [9,29,31].

Loss of endothelial cells leads to a breakdown of the barrier function. Although the remaining cells will increase their pump function to compensate, the continued loss of endothelial cells will eventually lead to an uncontrolled influx of fluid from the anterior chamber resulting in corneal oedema [9]. As a consequence, the ordered structure of the collagen fibers is disrupted, thereby resulting in a loss of corneal transparency and concomitant reduced vision [34]. Initially, the Descemet's membrane only thickens at the centre of the cornea, whereas the periphery gets involved as the disease progresses [27].

The disease is categorised in four clinical stages [35]. In the first stage, dome-shaped excrescences called guttae, grow from the Descemet's membrane starting in the centre of the cornea and protrude into the endothelium (Figure I.4). At this stage, the patients are asymptomatic and their vision remains unaffected [9,29,35]. In stage two, the number of corneal endothelial cells reduces which results in a loss of the characteristic hexagonal shape due to spreading of the cells. To compensate for the lost cells the remaining cells become thinner with an enlarged surface. At this stage, the occurrence of

corneal guttae starts to extend towards the periphery of the cornea [9,27]. Mild corneal oedema starts to occur due to loss of pump function of the endothelial cells resulting in a decreased vision [27,29].

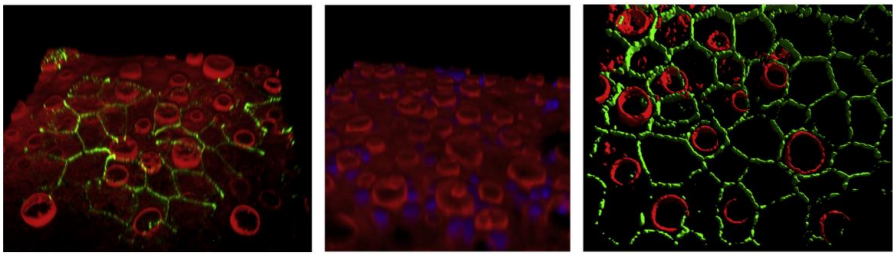

Figure I.4: The presence of guttae at the corneal endothelium as a consequence of FECD. Images obtained from an *ex vivo* corneal endothelium with the ECM being stained in red (laminin), the nuclei in blue (DAPI) and the cellular borders in green (ZO-1). The mushroom cloud appearance of the guttae is clearly visible. (Image reproduced from [31])

In the third stage, epithelial and subepithelial blisters ("bullae") are formed which is concomitant with severe pain upon rupture [35]. The severe pain is a consequence of the fact that the cornea is the most densely innervated tissue in the human body (i.e. 605 nerve terminals/mm²) [21]. Hence, the severity of corneal oedema increases resulting in a further loss of vision [27]. In the fourth stage, opacification and vascularization of the cornea occurs [27]. In this stage the pain recedes and subepithelial scar tissue is formed, thereby severely limiting vision [35].

FECD can be classified into two subtypes being early-onset and late onset. The early-onset type occurs in the 3rd decade of life and is very rare, whereas the late-onset type occurs in the 5th decade of life. Both subtypes have a predominant prevalence in females [14][16][9,31]. Additionally, there appears to be a geological difference in the prevalence of FECD, with low prevalence in Japan and Saudi Arabia but a higher prevalence in western societies (i.e. 4% of the population over the age of 40 in the USA) [9].

1.1.3. Corneal Transplantation

Currently, the only treatment for endothelial cell damage is to remove the dysfunctional cell layer and surgically replace it with a viable donor corneal endothelium [9]. This treatment is necessary when the disease has progressed

beyond the point of potential visual restoration to the patient (i.e. < 500 cells/mm²) [36]. In full thickness corneal transplants, also known as penetrating keratoplasty (PK), all five layers of the cornea are transplanted (Figure I.5 A.) [3,37]. This technique has traditionally been used to treat FECD since 1905 [31,38]. It includes the removal of a full thickness, circular section of the centre of the cornea with a diameter of 7.0 mm to 8.5 mm and the subsequent replacement with a cadaveric donor cornea [34].

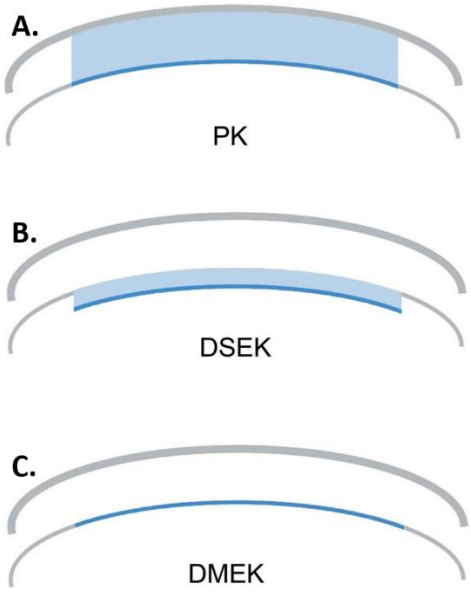

Figure I.5: Figure showing the donor tissue in blue for the differently applied surgical corneal endothelial transplant strategies including Penetrating Keratoplasty (A); Descemet stripping endothelial keratoplasty (B) and Descemet membrane endothelial keratoplasty (C). (Image reproduced from [37])

Besides good visual outcomes, the technique is characterised by a few drawbacks. For example, there can be a geometric mismatch with the donor cornea resulting in astigmatism or refractive errors requiring additional surgeries or correcting hard contact lenses [31,34]. Furthermore, full visual recovery can take up to two years after the procedure [39]. Additionally, there is a risk of suture-related complications and rupture at the graft-host junction, also referred to as traumatic graft dehiscence [40]. Finally, the potential for rejection of the graft also has to be taken into account [31]. Because FECD only affects the endothelium, there has been a shift towards partial thickness endothelial keratoplasty (EK) away from PK, to overcome these drawbacks.

For the latter, only the diseased layers of the cornea are replaced while the healthy layers are retained [3,34]. The two most used types of EK to treat FECD are Descemet stripping (automated) endothelial keratoplasty (DS(A)EK) and Descemet membrane endothelial keratoplasty (DMEK).

In the case of DSAEK, only the Descemet's membrane and the diseased endothelium are removed from the patient. The graft consists of endothelial cells, the Descemet's membrane and some supporting stroma that is inserted using a specialized cannula after which it automatically unfolds in the anterior chamber [31]. During the procedure, the graft is kept in place against the posterior surface of the cornea by means of an air bubble [37,41]. (Figure I.5 B. and Figure V.54)

DMEK is similar to DSAEK except that the donor graft does not contain part of the stroma and only consists of the Descemet's membrane and the endothelium (Figure I.5 C). As a consequence, a thinner graft is obtained which spontaneously rolls up after isolation from the donor. During the procedure, the scroll is inserted in the anterior chamber using a special cannula and rolled open by means of surgical manipulation [30] (Figure V.55). Here, the graft is also placed against the posterior cornea surface in the anterior chamber by means of an introduced air bubble [37,41]. DMEK provides a good and predictable visual recovery that is significantly superior to DSAEK [17,31,37]. However, the DSAEK procedure is typically characterised by better graft attachment to the corneal stroma [14,17].

The advantages of both DSAEK and DMEK over PK are numerous. First of all, the surgeries for DSAEK and DMEK are less invasive in comparison to PK, resulting in shorter operation times, and less complications related to refractive aberrations or astigmatism [21,42]. Furthermore, they generally result in a superior visual outcome and a better biomechanical stability of the cornea [3,31]. Additionally, these procedures are suture-less thereby reducing the risk of suture-related complications. Additionally, visual recovery of the patients is generally significantly faster and more successful [34,41,42]. Since both DSAEK and DMEK only require a small incision, the integrity and associated biomechanical properties of the eye globe is maintained and no ocular surface diseases are encountered that can lead to complications or graft failure in PK [17,37]. Although the eye is an immune-privileged location, there is still a risk of graft rejection. In this respect, both DMEK and DS(A)EK exhibit a lower chance of rejection due to the implantation of a smaller amount of foreign tissue [34].

Although there have been tremendous advances in surgical treatments resulting in good visual outcomes and minimal surgery-related complications, there is a severe global donor shortage that limits the number of corneal (endothelial) transplantations. A recent survey estimates that, in general, only 1 in 70 people requiring a donor cornea, can be treated [15]. Furthermore, over 40 to 50% of this cohort are a result of endothelial dysfunction [8,43]. This unfortunate situation has incited researchers to develop a cell therapy, based on the *ex vivo* expansion of corneal endothelial cells from one donor cornea to provide multiple patients with an answer to their sight-threatening condition. Recently, Kinoshita et al. have treated the very first patients with an injection of an allogenic corneal endothelial cell suspension and reported good visual recovery up to two years later [44]. Nevertheless, currently, the most investigated strategy is to create composite grafts of cells seeded onto a (synthetic) scaffold enabling transplantation similar to the currently applied corneal endothelial grafts [45]. Such cell carriers, however, must exhibit very specific properties, such as transparency (i.e. ≥ 90 % [45]), glucose permeability (i.e. permeability of a natural Descemet's membrane = $1.2 * 10^{-5}$ cm/s [46]), cytocompatibility and above all, they must maintain the correct endothelial cell phenotype [45]. To date, attempts have been made to find an ideal corneal endothelial scaffold, which range from biological and biosynthetic to fully synthetic membranes. Although this idea was already conceived in 1978, to date, the progress is still limited to a preclinical level as no candidate scaffold has met all requirements yet, nor has one effectively entered the clinic [18,47]. Therefore, the need for a synthetic, tissue-engineered membrane becomes relevant. What makes the cornea particularly interesting for tissue engineering is that it does not contain any blood vessels, while being an immune-privileged site and implantation is minimally invasive[21].

In order to produce a synthetic membrane, two different base materials were selected.

Gelatin is selected as an ECM mimic as it is obtained via hydrolysis of collagen, the main constituent of the natural ECM [48]. However, the mechanical properties of gelatin are insufficient as the natural Descemet's membrane is characterized by a Young's modulus of around 5 MPa [6]. Therefore, the gelatin is combined with poly-(lactic acid), a biodegradable polyester. Upon degradation, it forms lactic acid-based degradation products. This is a specific benefit towards corneal endothelial repair as *in vivo,* 85% of the glucose nutrients that enter the cornea are metabolized into lactic acid resulting in high lactic acid concentrations (i.e. up to 13 mM) [49].

1.2. Overview of Applied Materials

1.2.1. Polyesters

Synthetic polymers derived from renewable resources have gained increasing attention over the last decades [50–53]. This is due to the large demand for environmentally degradable polymers (mainly polyesters) for applications such as (food) packaging, biomedical applications (e.g. bio-degradable implants, drug delivery, tissue engineering, sutures, etc.) and due to their decreasing production cost (approximately €2 – 10 per kg) and straightforward processability [54–59]. When degradability is envisaged usually aliphatic polyesters are used due to the presence of ester bonds along the backbone which allow for hydrolytic degradability [60]. Additionally, in general, the synthesis of aliphatic polyesters occurs in a relatively straightforward manner, either via polycondensation or via ring-opening polymerization (ROP) [61]. Depending on the targeted application, polymers with different characteristics are required. Examples thereof include the glass transition temperature (T_g), degradation time, mechanical properties, refractive index, etc..

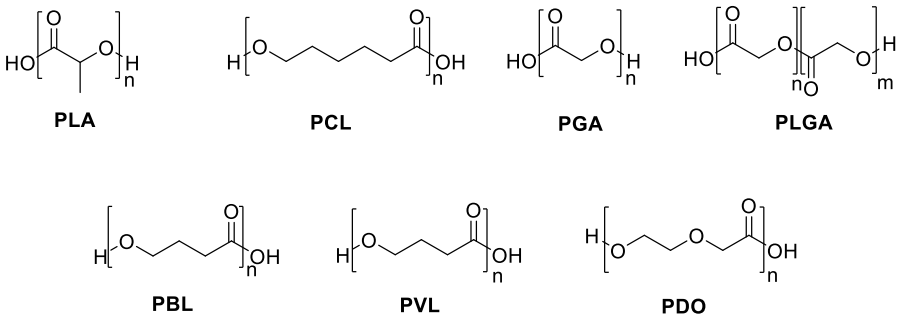

Figure I.6: Overview of commonly applied biodegradable polyesters for biomedical applications including the most commonly applied poly(lactic acid) (PLA); poly(ε-caprolactone) (PCL), poly(glycolic acid) (PGA), poly(lacti-co-glycolic acid) (PLGA) and the less frequently used poly(γ-butyrolactone) (PBL); poly(δ-valerolactone) (PVL); poly(dioxanone)(PDO).

The most common bio-degradable polyesters, include poly(lactide) (PLA) and poly(lactide-co-glycolide) (PLGA), which have a maximal T_g of around 50°C (in case of amorphous polymers) and a maximum degradation time of several weeks up to months, depending on the polymers' chemical composition, the

thickness and morphology of the polymer sample, the molecular weight and the environment in which the polymer is applied [62–66]. In this respect, both bulk degradation and surface erosion occur [67]. This biodegradability makes these lactic acid-based polymers specifically interesting in the field of tissue engineering and regenerative medicine [68,69]. Moreover, polymers with adjustable degradation times can be particularly interesting for example in the case of controlled-release drug carriers for which among others, the degradation rate determines the drug-release profile [56,70,71]. An overview of commonly applied polyesters in biomedical applications is presented in Figure I.6 [71].

Poly(lactic acid)

Poly(lactic acid) (PLA) is a polymer which holds an extensive track record as a scaffolding material for tissue engineering purposes [72,73]. This is due to the fact that it degrades into lactic acid, a component which is also produced inside the human body [74]. Concentrations of lactate in the blood can even go up to 25 m*M* [74]. As a result, it is classified by the Food and Drug Administration (FDA) as a "generally recognized as safe" (GRAS) degradable material [75,76]. It is commonly synthesized in two different ways, either starting from lactide via ring opening polymerization or via a polycondensation reaction of lactic acid (Figure I.7). Furthermore, three different stereochemical forms of PLA can be distinguished, including poly(L-lactide) (PLLA), poly(D-lactide) (PDLA) and poly(D,L-lactide) (PDLLA) [60]. By virtue of its transparency, in the present work the amorphous PDLLA is preferred over the more conventional PLLA and PDLA, that are semi-crystalline to provide structural integrity to the membranes. The presence of these crystalline domains can induce light scattering thereby decreasing transparency [77,78]. Additionally, PDLLA is characterised by a glass transition temperature (T_g) of around 50°C, thereby sufficiently exceeding temperatures observed in the body (i.e. 35 – 40°C) [67]. Furthermore, PDLLA degrades into non-toxic lactic acid-based degradation products (*vide supra*) [74]. This is of specific benefit towards corneal endothelial repair as *In vivo,* 85% of the glucose nutrients which enter the cornea are metabolized to lactic acid, which diffuses back through the corneal endothelium. As a consequence, the tissue is characterized by relatively high lactic acid concentrations (i.e. 13 mM in the cornea and 7 mM in the anterior chamber) [49]. Therefore, it is anticipated that PDLLA is an ideal scaffolding material, as the degradation products will not induce any inflammation and the lactate is even considered to contribute to the anion flux which maintains corneal transparency [49].

Polymerization

The two main polymerization approaches to synthesize PLA are the polycondensation of lactic acid and the ring opening polymerization of lactide (Figure I.7). However, polycondensation reactions generally lead to lower molecular weights and a higher polydispersity in comparison to ROP [79].

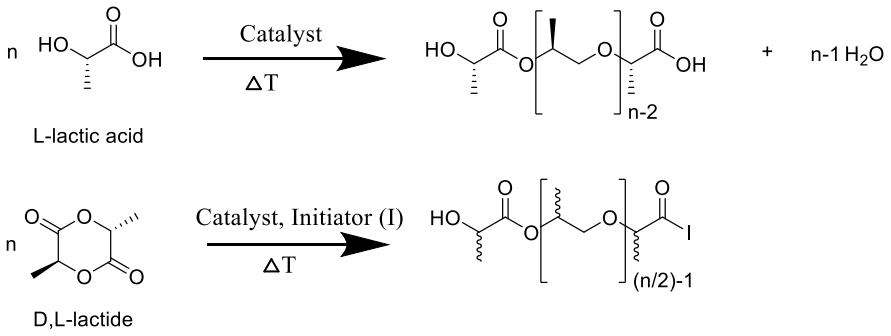

Figure I.7: Polymerization of L-lactic acid to the semi-crystalline PLLA (top) and polymerization of D,L-lactide to the amorphous PDLLA.

For the ROP approach, usually alcohol initiators are used. As a consequence, the molecular weight of the final polymer can be tuned by varying the initiator/monomer ratio [60]. In this respect, a higher initiator/monomer ratio results in lower molecular weights whereas lower initiator/monomer ratios will yield higher molecular weights. Amorphous PDLLA can be obtained via ROP of a racemic D,L-lactide or mixtures of D- and L-lactide or via the polycondensation of a racemic mixture of D- and L-lactic acid [60,80]. The lactic acid monomer used for the polycondensation reaction is generally mass produced by means of microbial fermentation of polysaccharides [60,63,79]. Conversely, the lactide monomer is generally obtained via thermal cracking of low molecular weight PLA that was synthesized via polycondensation [63]. It is important that monomers with a high purity are used for the synthesis of PLA. The presence of hydroxyl impurities can lead to chain transfer and transesterifications, thereby lowering the molecular weight and increasing the polydispersity [63].

Catalysts

A large number of catalysts have already been explored for the ring opening polymerization of lactide. The most commonly used catalysts are metal complexes. Of these, Sn(II)2-ethylhexanoate ($SnOct_2$) is one of the most commonly reported catalysts [81,82]. It is preferred since it is characterised by a low sensitivity to moisture and oxygen, and exhibits lower transesterification side reactions when compared to other organotin catalysts [70,82,83]. Additionally, $SnOct_2$ is an FDA approved food additive due to its relatively low toxicity, rendering it promising to be used in polymers for tissue engineering applications [81]. Another advantage of $SnOct_2$ is its solubility in organic solvents as well as in molten lactide, thereby making it suitable for both solution and bulk polymerizations [63]. Besides tin-based metal complexes, numerous other metal catalysts such as aluminium, yttrium, titanium, lanthanide, magnesium, zinc and iron complexes have also been reported [84]. Furthermore, the possibility for organocatalysis has also been explored using 1,5,7-triazabicyclododecene (TBD), 4-dimethylaminopyridine (DMAP), crown ethers and others as catalysts [63,85].

1.2.2. Gelatin as Extra-Cellular Matrix Mimic

While PDLLA is a degradable and biocompatible material, it is not cell-interactive, making it less suitable for tissue culture. Therefore, it is of predominant importance for the fabrication of membrane scaffolds, that a cell-interactive extra-cellular matrix (ECM) mimic is present in order to ensure cellular attachment to the membranes. In this respect, hydrogels are a promising material class due to their structural similarity to the natural ECM. Hydrogels are polymer networks which are able to absorb large amounts of water without dissolving [86–88]. These polymer networks originate in the linkage of several polymer chains through cross-linking points (cfr. junction knots), preventing the material from dissolving in the presence of large amounts of water. A wide range of hydrogel-based materials is currently under investigation for tissue engineering purposes [86]. First, natural polymers can be considered including chondroitin sulphate, hyaluronic acid, chitosan, cellulose, alginate, collagen, gelatin, etc. [89,90]. Secondly, also hydrogels composed of synthetic polymers have been proposed, including Pluronics [91], PVA [92], pHEMA [93], PEG [94,95], etc. In the present work, gelatin will be selected as hydrogel because of its bio-interactive properties, being a derivative of collagen which is one of the major ECM components [87,90,96–99].

1.2.2.1. Gelatin Hydrogels

Gelatin as an ECM mimic has attracted considerable attention in the field of tissue engineering and biofabrication (i.e. the use of additive manufacturing for regenerative purposes [100]) over the years as it is derived from collagen, which is the main constituent of the natural ECM of mammals [101,102]. It is a denatured protein constituting 18 different amino acids characterized by a repetitive unit of glycine – X – Y in which X and Y can be several different amino acids [103,104]. However, X and Y predominantly consist of proline and hydroxyproline, which provide gelatin a left-handed helix architecture, which enables the formation of triple helices which are stabilised by physical crosslinks via interchain hydrogen bonds [103–105]. As a consequence, the material is characterized by a dissociation temperature (T_d) around 30 – 35 °C [103,106,107]. This implies that it dissolves at elevated temperatures, while forming a hydrated hydrogel below this phase change temperature [103,107–109]. Additionally, the presence of the tripeptide arginine-glycine-aspartic acid (RGD) in the protein backbone results in cell-interactive properties [110,111].

Furthermore, it is enzymatically degradable by metalloproteases such as collagenase, which cleaves sequences such as Gly-Pro-Gln-Gly-Ile-Ala-Gly-Gln between Gly and Ile allowing cells to remodel it [109,112–115]. Due to the harsh acidic or basic denaturation process during the conversion of collagen to gelatin, concerns regarding immunogenicity and pathogen transmittance associated with the use of collagen are circumvented [101,116]. In addition, it is considered safe by the Food and Drug administration (FDA) with a wide track record in the food and pharmaceutical industry [103,104,117]. Furthermore, gelatin is a by-product from the meat industry making it very attractive from an economical point of view [118].

However, due to the solubility at body temperature, the material was originally only applied as a temporary cell carrier to enable more straightforward cell manipulation [118]. To overcome this limitation, strategies were developed to stabilise the material at physiological conditions via the formation of chemical crosslinks. A common approach in this respect, consists of coupling the primary amines present in (hydroxy)lysine and ornithine with the carboxylic acids from aspartic and glutamic acid using carbodiimide chemistry thereby resulting in a zero length crosslinked hydrogel network [116,119]. Alternatively, the nucleophilic functionalities of gelatin can be crosslinked using glutaraldehyde [120]. However, these stabilization techniques offer limited control over the design of the obtained construct, as the material manipulation window is limited in time with little control over the crosslinking process.

A realm shift occurred in 2000 when Van den Bulcke et al. developed and patented the first photo-crosslinkable gelatin derivative (i.e. gelatin-methacrylamide (gel-MA)) [121,122]. Photopolymerization exhibits attractive capabilities in terms of material processing including highly controllable gelation kinetics and predictable degradation capabilities, enabling convenient and straightforward material processing for tissue engineering and biofabrication purposes [107,123,124]. The functionalization occurs by reacting the primary amines in the side chains of (hydroxy)lysine and ornithine with methacrylic anhydride, resulting in the formation of methacrylamide moieties (Figure I.8.A) [107]. Ever since, gel-MA has been applied for a plethora of biofabrication and tissue engineering strategies either as a standalone material or co-crosslinked with other (synthetic) materials (e.g. PEG) to form biohybrid hydrogels. As a result, it became one of the gold standards in the field [106,125–134]. Following this success, it has even started to bridge the gap between academia and industry as it is offered commercially by several companies as a bioink (i.e. a material formulation containing cells prior to processing using additive manufacturing) or a biomaterial ink (i.e. a material

formulation suitable for additive manufacturing and subsequent cell seeding) for research purposes [100,135,136]. Besides gel-MA, several other (photo-)crosslinkable gelatin derivatives have emerged (Figure I.8, I.10, I.11, I.13, I.14, I.15, I.16). These derivatives can be subdivided into different classes based on the applied crosslinking mechanism including chain-growth (Figure I.8) and step-growth polymerization. Within the step-growth classification, several other subclasses can be distinguished based on the applied crosslinking chemistry: thiol-ene (photo-) click chemistry (Figure I.12 red): (thiols: Figure I.10; enes: Figure I.11 red), disulphide linkages (Figure I.10 & I.12 purple), Diels-Alder click (Figure I.8 & I.12: light green), Schiff's-base formation (Figure I.12 grey), π-π cycloaddition (Figure I.14 & I.12: yellow), photooxidation (Figure I.15 & I.12: green) and enzymatic based crosslinking (Figure I.16 & I.12: white).

1.2.2.2. Classification According to Crosslinking Mechanism

Crosslinking via Chain-Growth Polymerization

The most commonly used crosslinkable gelatin derivatives take advantage of a chain growth polymerization crosslinking approach. Here, crosslinking occurs by polymerizing reactive functionalities (typically (meth)acrylates/(meth)acrylamides) immobilized onto gelatin resulting in the formation of short oligomer/polymer kinetic chains in between the gelatin chains [107,114,125,139,146,147] (Figures I.9 A & C). Consequently, a polymer network is generated containing both gelatin polypeptide chains and synthetic oligomer/polymer chains. Crosslinking usually occurs via photo-polymerization, however, also other initiating systems can be applied (i.e. APS/TEMED) [119,131,148]. The benefits of chain-growth polymerization systems include straightforward material handling, consisting of material dissolution and addition of a suitable (photo-)initiator prior to crosslinking without the need for any additional crosslinker. Furthermore, the introduction of methacrylamides to gelatin (gel-MA) involves a straightforward single step reaction resulting in a plethora of applications. (Figure I.8: A) [106,107,126,128,134,149–156]. Besides this success, other derivatives have also been reported to further tune/improve the material properties.

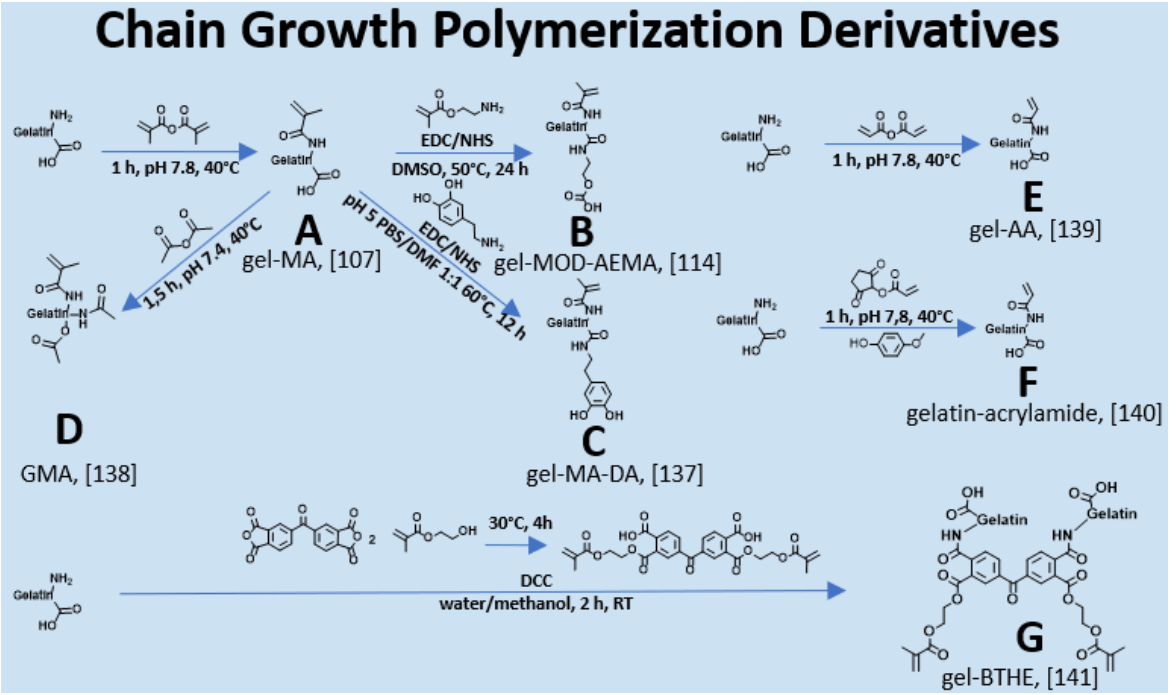

Figure I.8: Non-exhaustive overview of different crosslinkable gelatins including their method of preparation classified according to their crosslinking chemistry: Chain-growth derivatives (blue): gel-MOD/gel-MA(A) [107], gel-MOD-AEMA (B) [114], gel-MA-DA (C) [137], GMA (D) [138], gel-AA (E) [139], gelatin-acrylamide (F) [140], gel-BTHE (G) [141], gel-Boc-AEMA (H) [142], methacrylated poly(ethylene glycol)-modified gelatin(MPG) (I) [143,144], gelatin-PEG-acrylate (K) [145] (Image continued on the next page)

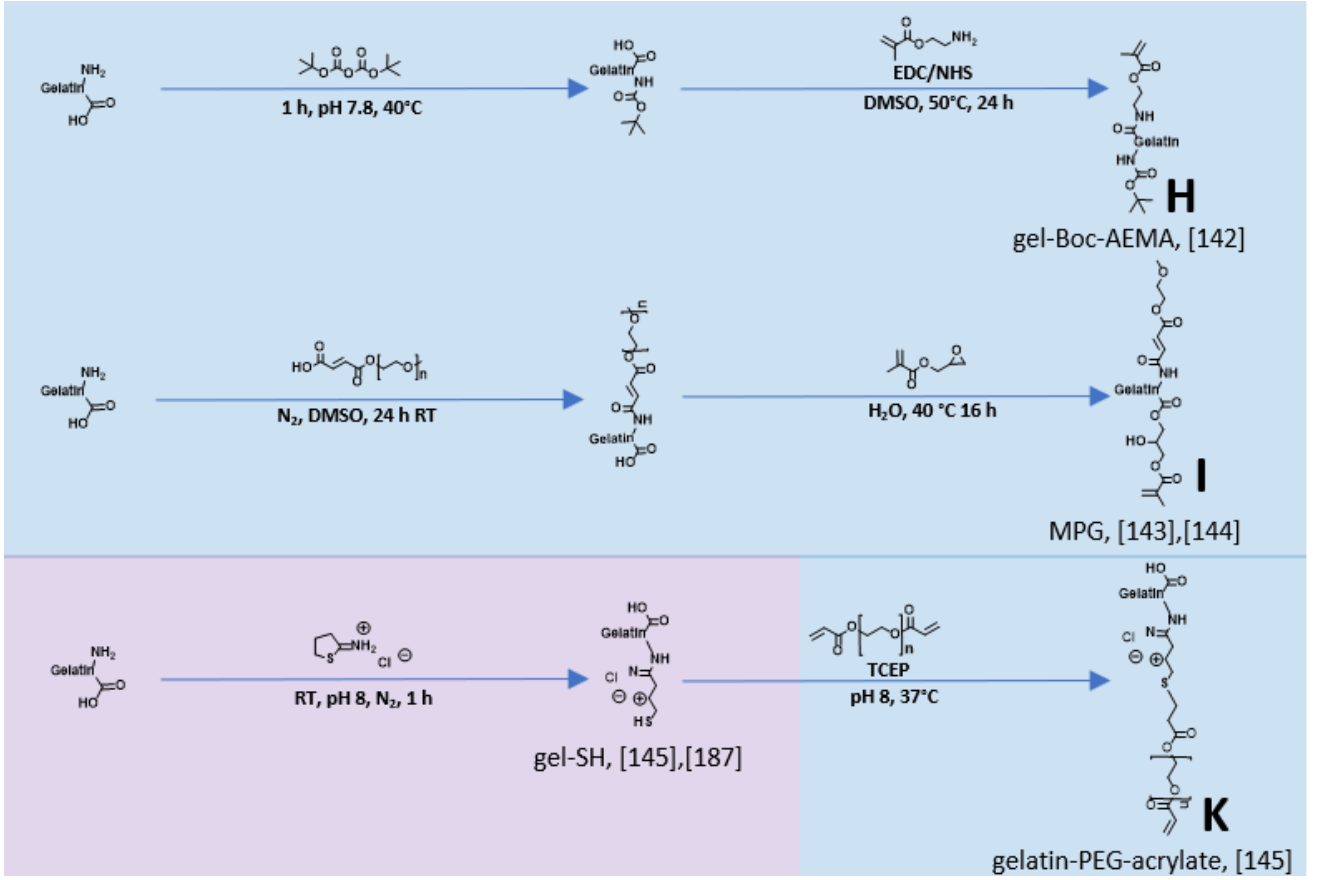
1 h, pH 7.8, 40°C
EDC/NHS
DMSO, 50°C, 24 h
H
gel-Boc-AEMA, [142]
N2, DMSO, 24 h RT
H2O, 40 °C 16 h
I
MPG, [143],[144]
RT, pH 8, N2, 1 h
gel-SH, [145],[187]
TCEP
pH 8, 37°C
K
gelatin-PEG-acrylate, [145]

Examples include the introduction of more reactive functionalities (i.e. acrylates/acrylamides (Figure I.8 E,F) or gelatin-PEG-acrylate (Figure I.8 K) [139,145]) to improve the crosslinking rate. Other attempts aim to increase the mechanical properties of crosslinked gelatin by introducing more crosslinkable sites through modification of the carboxylic acids of glutamic- and aspartic acid, being predominantly present in gelatin in comparison to lysine and hydroxylysine which are usually functionalized. Using this strategy, (additional) methacrylates could be introduced via carbodiimide coupling of 2-aminoethyl methacrylate yielding gel-MOD-AEMA (Figure I.8 B) and gel-Boc-AEMA (Figure I.8 H) [114,142,157]. Finally, Ding et al. explored the incorporation of photocrosslinkable functionalities which already include a photoinitiating moiety (i.e. a benzophenone group linked to the methacrylate functionalities), thereby overcoming the need for the addition of a potentially cytotoxic photoinitiator (PI) (Figure I.8 G) [141,158].

In comparison to the second predominant gelatin crosslinking chemistry (i.e. thiol-ene based systems (vide infra)) in which thiolated crosslinkers are applied to crosslink an “ene” functionalized material, chain-growth gelatin solutions remain stable for longer time periods above the dissociation temperature (cfr. the half-life of dithiotreitol (DTT), a commonly applied crosslinker, shifts from 11 h at 0°C to only 0.2 h at 40°C at pH 8.5 whereas during modification gel-MA can be kept at 40°C for at least 24 hours without any problems). This thermal stability is typically required during most additive manufacturing processes or for cell encapsulation experiments [114,159]. Moreover, chain-growth systems typically yield stiffer hydrogels in comparison to step-growth hydrogels as a result of the kinetic polymer chains which can be a benefit towards stiffer tissue engineering applications including intervertebral discs (i.e. Storage modulus (G’) ranging from 8 – 93 kPa [160]) (Figure I.18 A) [147].

Drawbacks associated with chain growth hydrogels include the formation of a more heterogeneous network due to the presence of these kinetic chains rendering the material prone to shrinkage during crosslinking [141]. Furthermore, the kinetic profile of free radical chain-growth polymerizations is usually more complicated as a consequence of chain-length issues and reaction diffusion limitations resulting in termination which leads to a diminished control over the number of reacted functionalities [161,162].

Moreover, the crosslinking reaction is prone to oxygen inhibition due to rapid radical scavenging by oxygen molecules resulting in the formation of hydroxyperoxides and alcohols, which is undesirable upon targeting cell

encapsulation and also influences reaction reproducibility [163]. These oxygen inhibition effects can be circumvented by using higher PI concentrations in combination with higher spatiotemporal energy (i.e. higher UV power density, longer irradiation times) to crosslink the material [163]. As a result, chain-growth crosslinking typically requires more energy and more PI compared to thiol-ene-based, step-growth hydrogels (*vide infra*) [147]. However, both higher PI concentrations and higher light power densities can induce cellular damage rendering them less favourable for direct cell encapsulation [146,163]. As a consequence, increasing attention is put towards the development of alternative crosslinking chemistries.

Crosslinking via Step-Growth Polymerization

The second major class of photo-crosslinkable gelatin hydrogels involves a step-growth polymerization crosslinking approach. A step-growth mechanism typically occurs between two complementary reactive groups which can ideally only react with one another [162]. A non-exhaustive overview of step-growth crosslinking chemistries applied for gelatin hydrogels is presented in Figure I.12. Of specific interest in this area is the use of “click chemistry”, a concept introduced by Sharpless et al. in 2001. Click chemistry involves chemical reactions which typically occur very fast (i.e. “spring-loaded”), with a high degree of control at high yields under relatively mild conditions (i.e. physiologically stable), without the formation of toxic side products, making them ideal to crosslink hydrogels for biomedical applications [164,165].

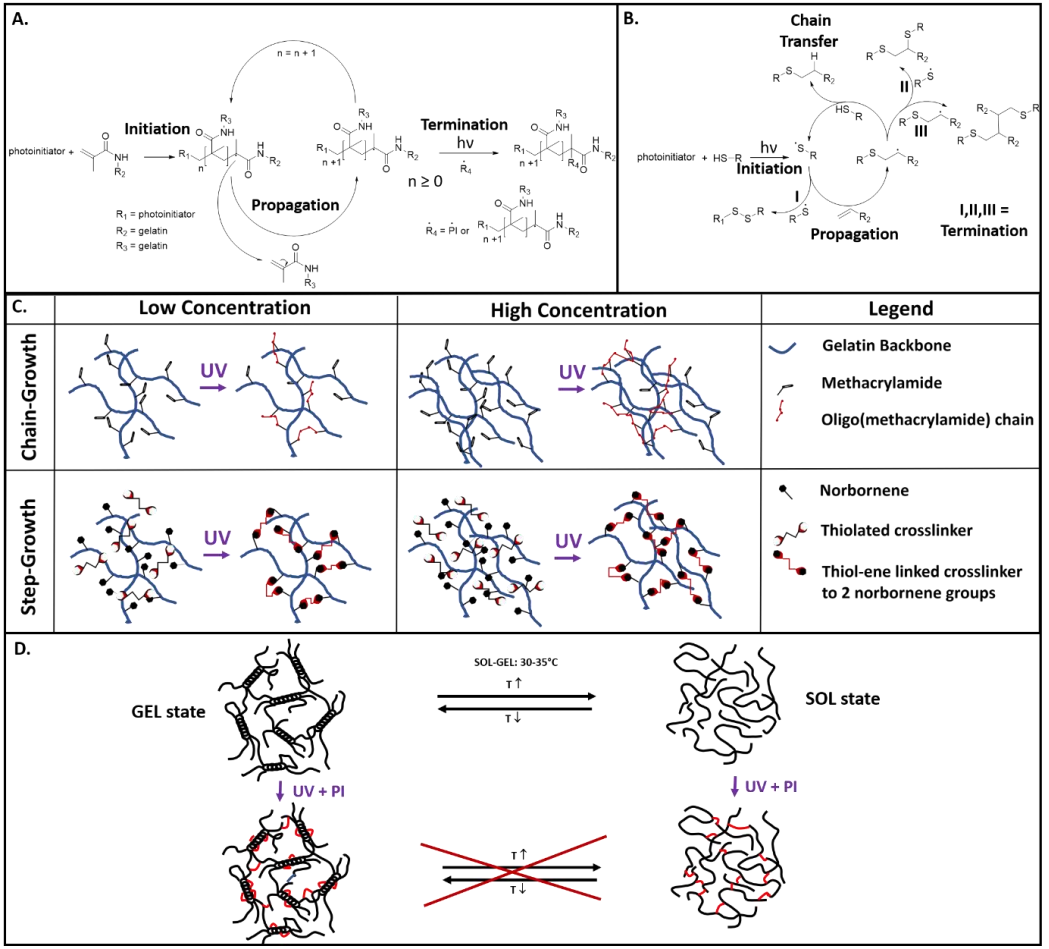
A.
n = n + 1
Initiation
photoinitiator +
Propagation
Termination
hv
n ≥ 0
R1 = photoinitiator
R2 = gelatin
R3 = gelatin
R4 = PI or
B.
Chain
Transfer
photoinitiator + HS–R
hv
Initiation
Propagation
I,II,III =
Termination
C.
Low Concentration
High Concentration
Legend
Chain-Growth
Step-Growth
UV
Gelatin Backbone
Methacrylamide
Oligo(methacrylamide) chain
Norbornene
Thiolated crosslinker
Thiol-ene linked crosslinker
to 2 norbornene groups
D.
GEL state
SOL-GEL: 30-35°C
T↑
T↓
SOL state
UV + PI

Figure I.9: Illustration of the chain-growth (A) vs step-growth (B) crosslinking mechanism using thiol-ene photoclick chemistry. Influence of applied chemistry on network properties (C) demonstrating the presence of kinetic chains in chain-growth crosslinking approaches as compared to a thiol-ene photoclick-based system. (Adapted from [147]) Influence of physical gelation on network density and associated mechanical properties (D.). (Adapted with permission from [114] copyright 2017 ACS (https://pubs.acs.org/doi/abs/10.1021%2Facs.biomac.7b00905))

Thiol-ene Photo Click Crosslinking

The most common “click” crosslinking chemistry applied for gelatin hydrogels is thiol-ene (“photo”-) click chemistry (Figure I.9. B and Figure I.12 (red)). These systems can be applied to form networks by reacting a thiol with an ‘ene’ functionality either following a light-induced, radical-mediated thiol-ene reaction or by the formation of an anionic species resulting in a thiol Michael-type addition (*vide infra*) [162]. The light-induced reaction proceeds via hydrogen abstraction of the thiol resulting in the formation of a thiyl radical which can be generated either in the presence or absence of a photo-initiator (Figure I.9 B: initiation). Next, an anti-Markovnikov addition of this radical to the double bond present in the ‘ene’ species occurs (Figure I.9 B: propagation) [162,166] . After the addition, a radical chain transfer occurs between the formed carbon-centered radical to another thiol group thereby forming another thyil radical (Figure I.9 B: chain transfer) [166]. Finally, termination occurs when two radical species recombine forming either a disulphide bridge (i.e. when two thyil radicals combine (Figure I.9 B: Termination I)), a carbon-sulfur bond (i.e. coupling of a thiyl radical with a carbon-centered radical (Figure I.9 B: Termination II)) or a carbon-carbon bond (i.e. coupling of two carbon centered radicals (Figure I.9 B: Termination III)) [166]. The rate limiting step in this process is the chain transfer step, therefore, thiol-ene reactions proceed slower in systems where this chain transfer is hindered (e.g. in the presence of methyl in methacrylates leading to steric hindrance in contrast to acrylates) [166]. Furthermore, due to the electrophilic nature of the thiyl radical, electron rich enes typically undergo the fastest reaction [166,167]. However, norbornene, methacrylate, styrene and conjugated diene functionalities are exceptions to this rule. Thiol-norbornene reactions are extremely fast due to the ring-strain relief upon thyil addition and the rapid hydrogen abstraction rate [146,168,169]. The methacrylates, styrenes and conjugated dienes, are all characterised by a conjugated system, enabling radical stabilization due to mesomeric delocalization over multiple atoms, which results in slow hydrogen abstraction rates and concomitant lower reactivity [169]. Consequently, the reaction rate of different functionalities relative to each other exhibits the following trend [169]:

Norbornene > vinyl ether > propenyl > alkene ~ vinyl ester > N-vinyl amides > allyl ether > N-vinyl amides > acrylate > acrylonitrile ~ methacrylate > styrene > conjugated dienes.

In general, the reaction can proceed with any type of non-sterically hindered 'ene' functionality. However, if a true step-growth polymerization reaction is pursued, an 'ene' functionality, which cannot undergo competitive chain-growth homo-polymerization (i.e. norbornenes and vinyl ethers) is preferred [162]. As a consequence, superior control over the reaction and concomitant homogeneity within the resulting network is obtained [162]. To develop a thiol-ene photo-crosslinkable gelatin, it has to contain 'ene' functionalities (typically norbornene, vinyl esters, pentenoyls, allyl ethers or acrylates) which can be crosslinked using a multi-functional, thiolated crosslinker (e.g. DTT) [146,147,168,170–173] (Figure I.11, Figure I.9. C and Figure I.12 (red)). Alternatively, gelatin is functionalized with thiols and crosslinked using a multi-functional 'ene' crosslinker (e.g. polyethylene glycol-diacrylate PEGDA, gel-NB or gel-AA) [170–172,174,175] (Figure I.10).

Thiol-ene 'photo-click' hydrogels pose a benefit over chain-growth hydrogels (*vide supra*) as more homogeneous networks are formed with a higher conversion of the functional groups. Furthermore, they exhibit less shrinkage during crosslinking resulting in less post-polymerization stress due to the highly orthogonal nature of the reaction [146,176,177]. Additionally, the crosslinking reaction is not susceptible to oxygen inhibition and exhibits lower radical concentrations (i.e. at least one order of magnitude below chain growth systems) and faster reaction rates as reflected by shorter gel-point times, making them more suitable for cell encapsulation (Figure I.18 B) [146,147,162,166,168,178–180]. Furthermore, the number of reacted functionalities can be fully controlled by varying the thiol-ene ratio prior to crosslinking [147,162,178]. As a consequence, when using ene functionalities which cannot undergo competitive homo polymerization (i.e. vinyl ether, norbornene) pendant ene or thiol functionalities can be retained in the material after crosslinking, thereby allowing post crosslinking grafting or photo-micropatterning with other compounds (i.e. integrin binding sites, growth factors, proteins, etc.) with spatiotemporal control (e.g. when using photomasks, lithography approaches) thereby providing a better biomimetic matrix (see also Chapter 3) [112,181,182]. Drawbacks include the necessity of a multifunctional, thiolated crosslinker present in the reaction mixture which can be susceptible to cross-reactivity with other thiols leading to disulphide formation, especially in oxophilic aqueous systems, thereby resulting in poor stability of the crosslinkable solution [183–186].

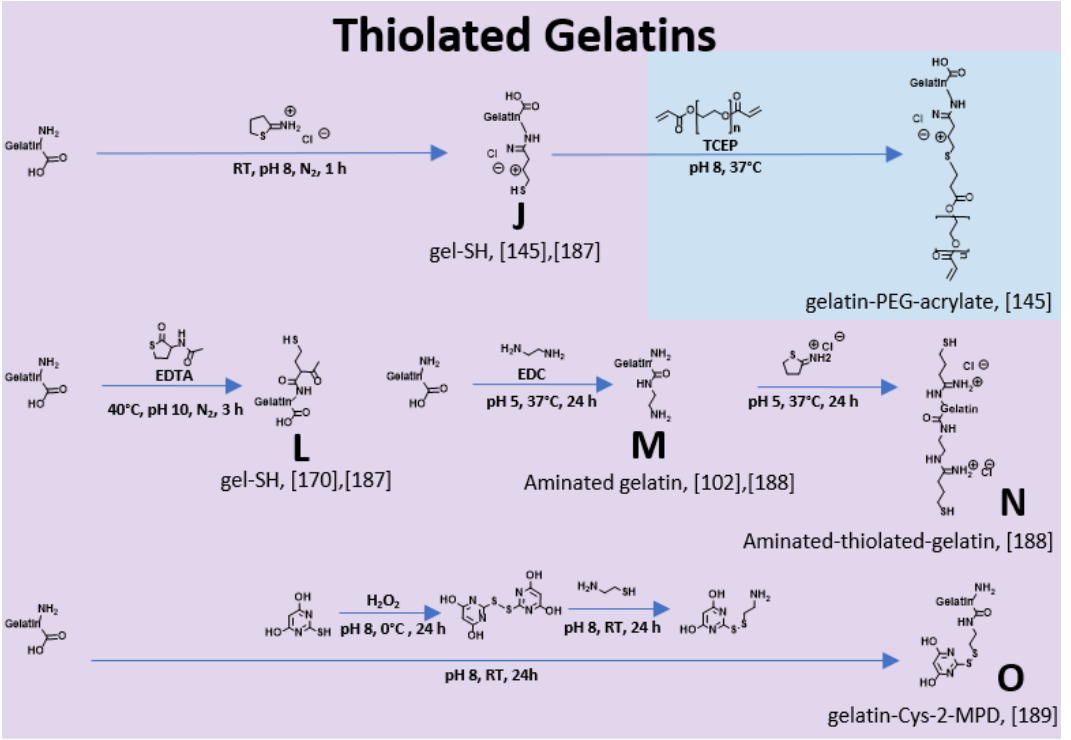

Figure I.10: Non-exhaustive overview of different crosslinkable gelatins including their method of preparation classified according to their crosslinking chemistry: Thiolated gelatins suitable for disulphide chemistry of thiol-ene chemistry (purple): gel-SH (J) [145,187], gel-SH (L) [170,187], aminated gelatin (M) [102,188], aminated-thiolated-gelatin (N) [188], gelatin-Cys-2-MPD (O) [189], gelatin-Cys (P) [189], gel-PEG-Cys (Q) [190], gelatin-TBA-MNA (R) [191], gel-S (S) [192,193], gelatin-thiobutyrolacton (T) [171] (Image continued on the next page)

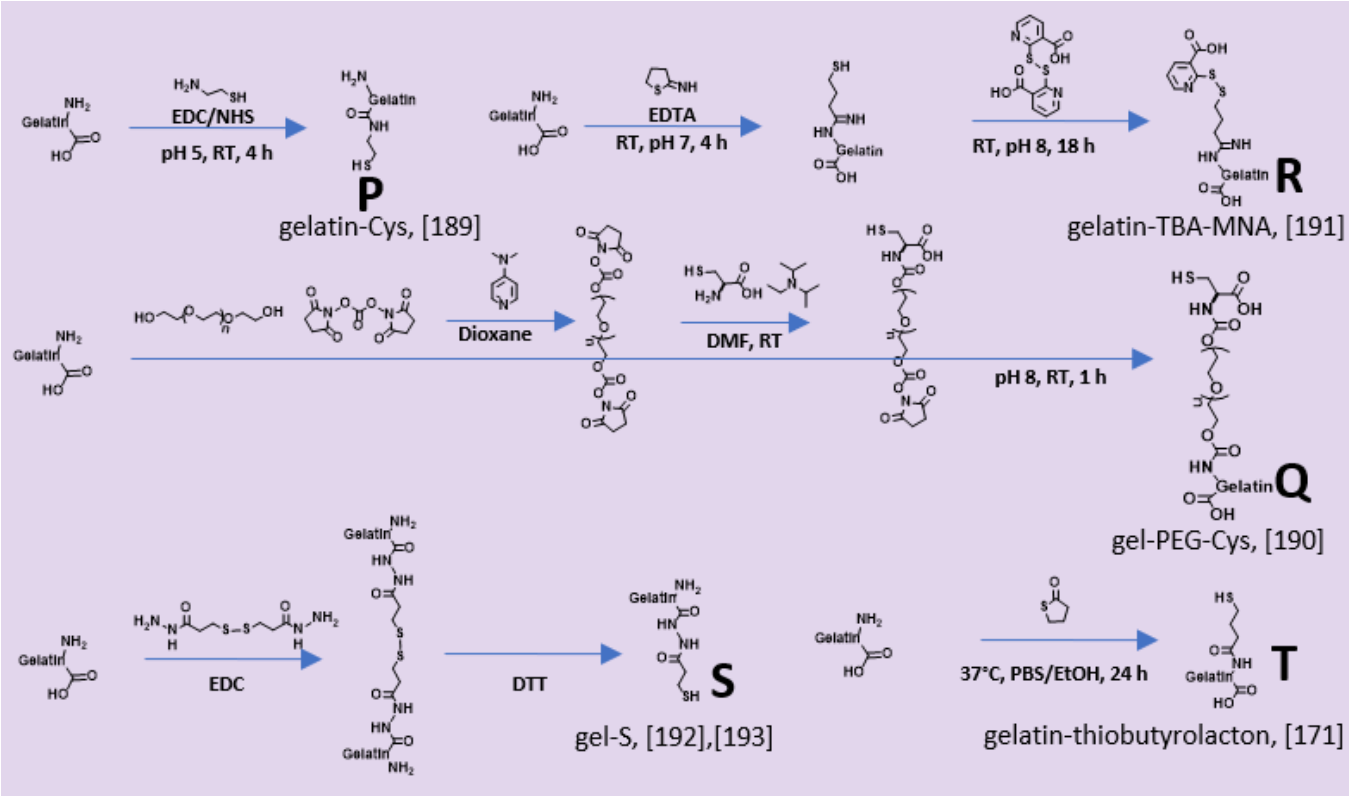
EDC/NHS
pH 5, RT, 4 h
P
gelatin-Cys, [189]
EDTA
RT, pH 7, 4 h
RT, pH 8, 18 h
R
gelatin-TBA-MNA, [191]
Dioxane
DMF, RT
pH 8, RT, 1 h
Q
gel-PEG-Cys, [190]
EDC
DTT
S
gel-S, [192],[193]
37°C, PBS/EtOH, 24 h
T
gelatin-thiobutyrolacton, [171]

Additionally, these thiolated crosslinkers can exhibit reactivity with thiol functionalities present in living cells thereby resulting in cellular damage [194]. Furthermore, the obtained hydrogels are generally characterised by lower storage moduli as compared to their chain-growth counterparts (i.e. storage moduli of 0.6 – 46 kPa are reported for for thiol-ene systems [146] vs 0.07 [145] – 368 kPa [195] for chain growth based systems, Figure I.18 A) [147,168]. Typical gelatin derivatives prone to thiol-ene photoclick crosslinking reactions are depicted in Figure I.11 (enes) and purple (thiolated gelatins) in Figure I.10. Examples of gelatin derivatives with ene functionalities include: gelatin-pentenoate (η) [171], gel-AGE (θ) [146], gel-VE (ι) [196], gel-NB (κ,λ & μ) [115,147,168]. Examples of thiolated gelatin derivatives include: gel-SH (J) [145,187], gel-SH (L) [170,187], aminated-thiolated-gelatin (M) [188], gelatin-Cys (P) [189], gel-PEG-Cys (Q) [190], gelatin-thiobutyrolacton (T) [171];

Thiol-Michael Addition Based Crosslinking

Thiol-Michael addition is the reaction between a thiol and an electron deficient, activated double bond (i.e. alpha, beta unsaturated double bonds: acrylates, acrylamides; maleimides; vinyl sulphones fumarate esters; acrylonitrile; cinnamates and crotonates) via a slightly alkaline or nucleophilic catalysed mechanism [197,198] (Figure I.10 (red)). Thiol-Michael type additions are highly specific nucleophilic additions, which take place without the formation of potentially harmful side products (i.e. radical species) and potentially cytotoxic PI's and (UV) irradiation [193]. Additionally, in contrast to the UV induced thiol-ene reaction, no radical-radical termination side products are formed resulting in quantitative conversion [197]. Furthermore, since the reaction only requires slightly alkaline conditions, the reaction can occur at physiological pH [193]. Although typically slower compared to thiol-ene photoclick reactions, it still exhibits relatively fast crosslinking kinetics with reported gel-points in the range of a few minutes [175] (Figure I.18 B). As a consequence, thiol-Michael addition is an ideal candidate for cell encapsulation purposes [175,193].

Drawbacks include the relatively fast reaction profile, without any spatiotemporal control, making it less straightforward for biofabrication applications. Examples of gelatin derivatives which have been applied in thiol-Michael type additions include: gel-SH (Figure I.10 J) [145,175] and gel-S (Figure I.10 S) [192,193].

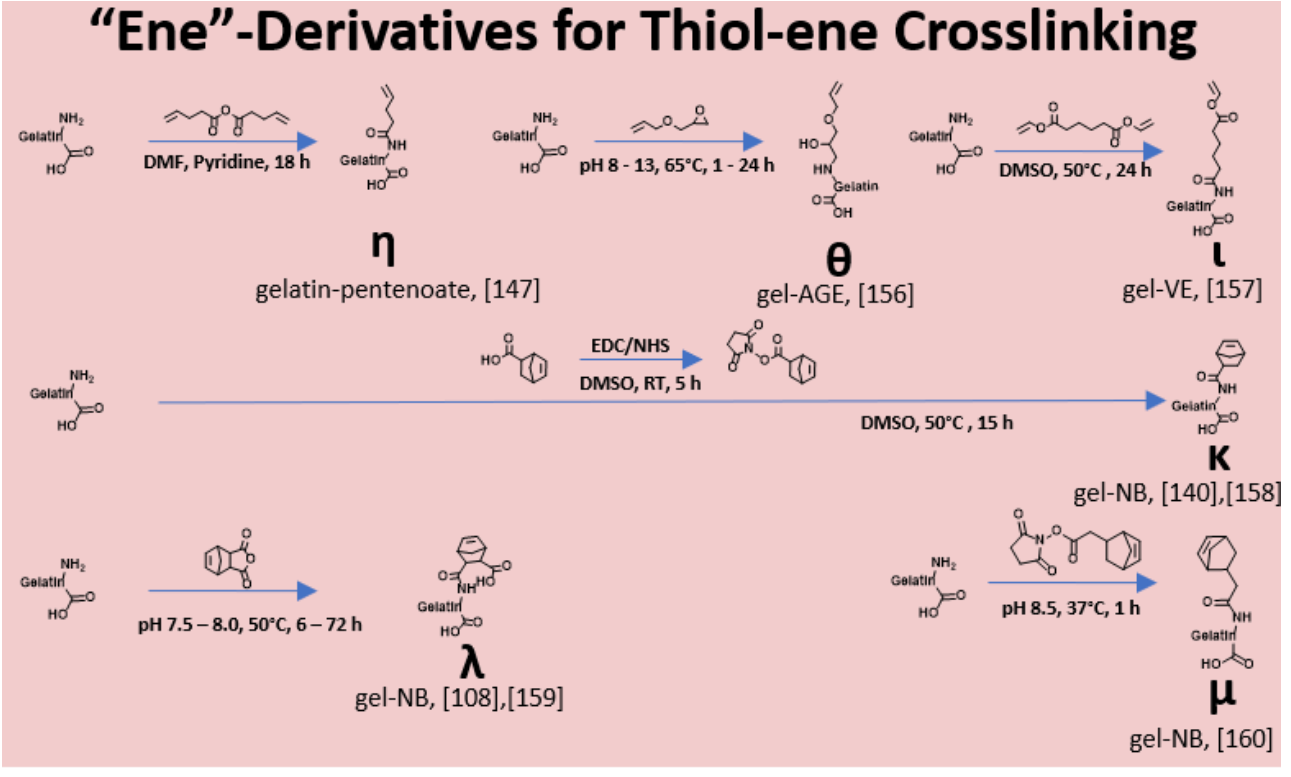

Figure I.11: Non-exhaustive overview of different crosslinkable gelatins including their method of preparation classified according to their crosslinking chemistry: *„ene" derivatives suitable for Thiol-ene chemistry (red) : gelatin-pentenoate (η)* [171]**, *gel-AGE (θ)*** [146]**, *gel-VE (ι)*** [196]**, *gel-NB (κ)*** [147,170]**, *gel-NB (λ)*** [115,168]**, *gel-NB (μ)*** [199]

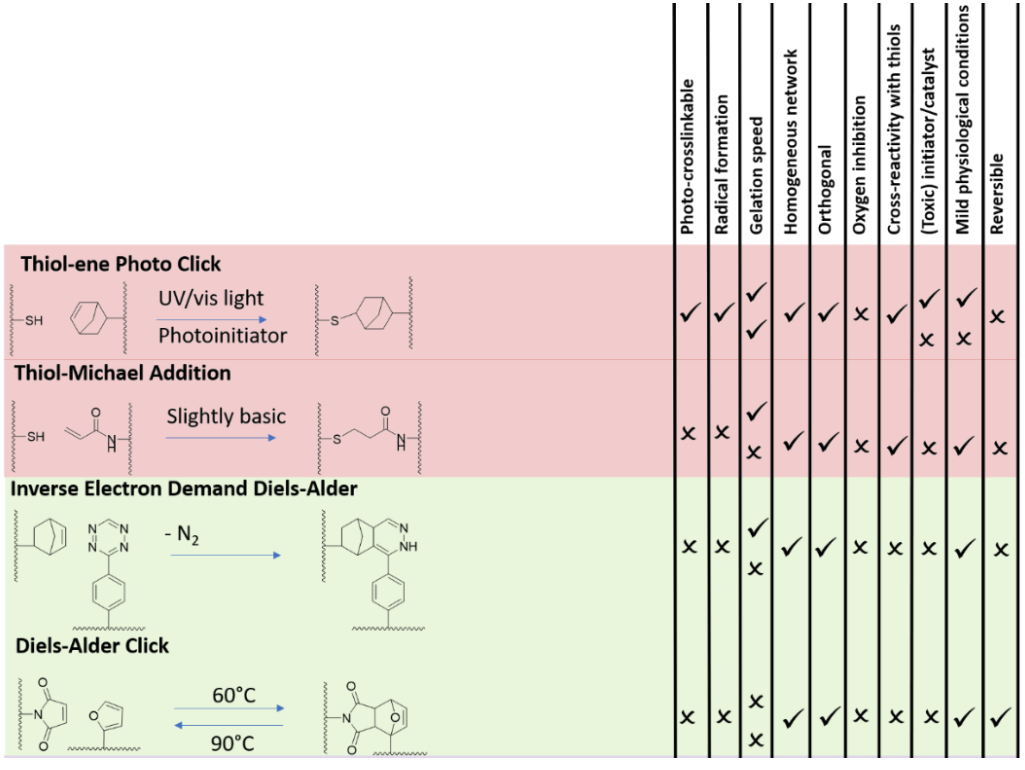

Figure I.12: Overview of different step-growth crosslinking chemistries applied to gelatin including: thiol-ene (photo-)click (red), Diels-Alder click (light green), disulphide formation (purple), Schiff's base formation (grey), π-π cycloaddition (yellow), photo-oxidation (dark green) and enzymatic crosslinking (white).

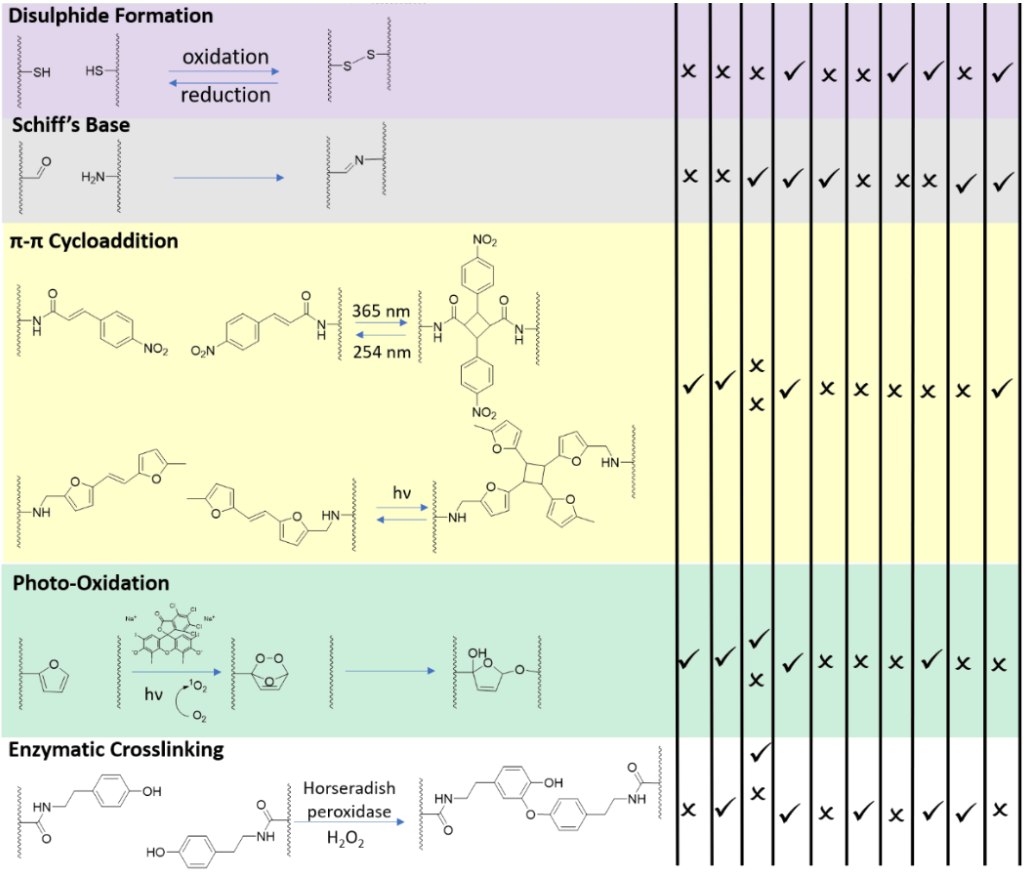
Disulphide Formation
oxidation
reduction
Schiff's Base
π-π Cycloaddition
365 nm
254 nm
hv
Photo-Oxidation
hv
Enzymatic Crosslinking
Horseradish
peroxidase
H_2O_2

Diels-Alder Based Click Systems

Inverse Electron Demand Diels-Alder Based Systems

Although thiol-ene photo-click systems pose some benefits over the conventional chain-growth crosslinking systems, both mechanisms still involve harmful radical species, while for thiol-ene systems (both thiol-ene photo click as thiol-michael addition), a cross reactivity can occur with thiols present in other proteins or the cells during cell (photo-)encapsulation [194]. Therefore, researchers are also exploring alternative "click" crosslinking mechanisms [165,198,200]. Koshy et al. evaluated a norbornene-tetrazine click system which allows crosslinking in the absence of any other trigger (i.e. UV irradiation, PI, catalyst, etc.) (Figure I.13 ε, ζ; Figure I.12 (light green)) [194]. The crosslinking occurs via an inverse electron demand Diels-Alder click reaction with the formation of nitrogen (Figure I.12 (light green)) [181]. Furthermore, the reaction is quantitative with high atom efficiency producing only nitrogen gas as side product [181,184]. Due to these aspects, tetrazine chemistry is increasingly applied in the field of polymer chemistry. By preparing a gelatin-norbornene component (gel-NB, Figure I.13 (ε)) and a gelatin-tetrazine (gel-T, Figure I.13 (ζ)) a stable, non-toxic hydrogel can be obtained after mixing (ClickGel) [181,194]. Furthermore, the gelation time can be tuned by varying the introduced dienophile. In this respect, norbornene provides a good compromise between reaction rate and sample manipulation time after mixing [181]. What's more, upon encapsulation with 3T3 fibroblasts, higher cell-viabilities were observed when compared to the gel-MA reference due to the absence of harmful UV irradiation [194].

Reversible Diels-Alder Based Click Systems

Alternatively, Garcia-Astrain et al. explored the use of a Diels-Alder based "click" type reaction consisting of a (4 + 2) thermo-reversible π-π cycloaddition between a dienophile and a diene to crosslink gelatin [200,201] (Figure I.12 (light green)). Similar to the earlier discussed norbornene-tetrazine scheme, the reaction occurs in the absence of light, catalysts or initiators. They introduced furan functionalities as diene to gelatin (gel-FGE Figure I.13 δ) by reaction of the primary amines with furfuryl glycidyl ether [200]. Crosslinking of the material occurred using a modified Jeffamine-based bismaleimide as dienophile [200,201].

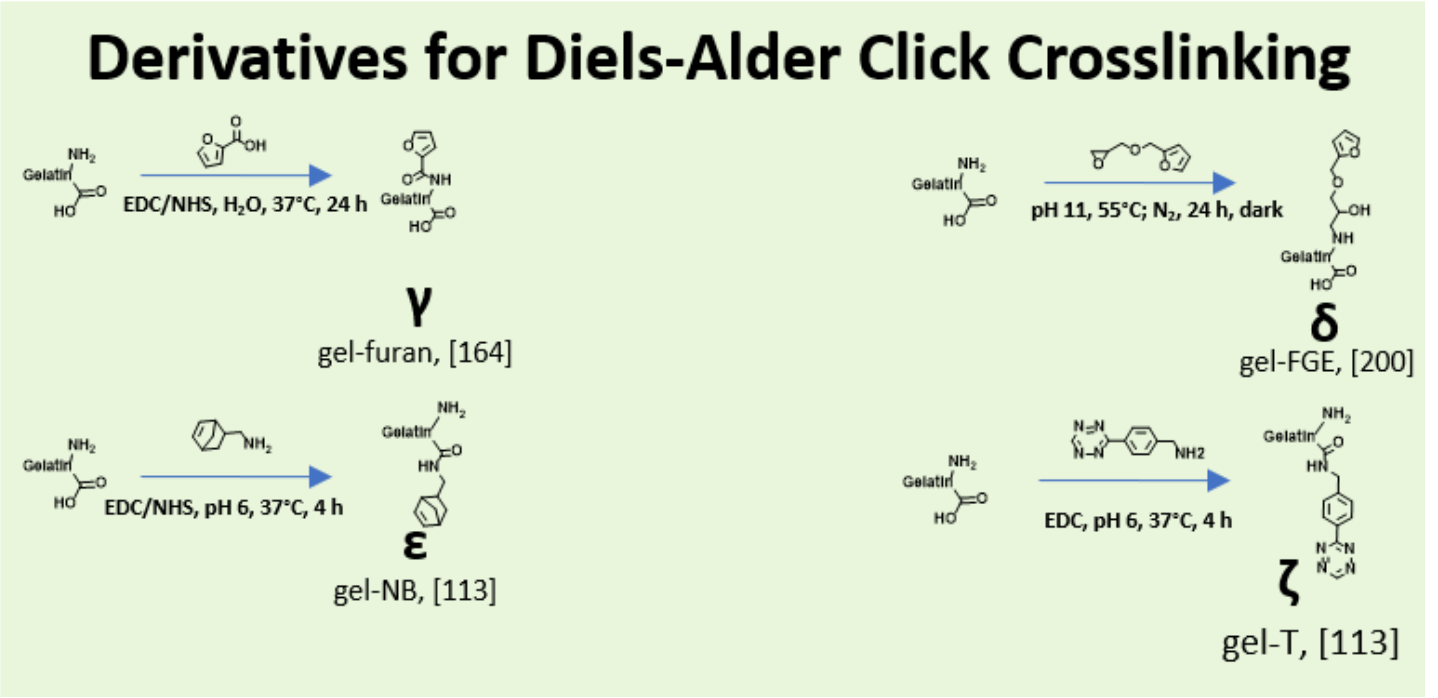

Figure I.13: Non-exhaustive overview of different crosslinkable gelatins including their method of preparation classified according to their crosslinking chemistry: Derivatives suitable for Diels-Alder click (light green): gel-furan (γ) [164], gel-FGE (δ) [200], gel-NB (ε) [113], gel-T (ζ) [113]

Thermal crosslinking occurred at 65°C during 5 hours using a 60 wt% gel-FGE aqueous solution with different crosslinker amounts. De-crosslinking occurred by heating the hydrogel to 90°C to induce the retro Diels-Alder reaction. Although the presence of water typically favours the Diels-Alder reaction over the retro Diels-Alder reaction which complicates network cleavage, the authors managed to monitor the reaction using UV-VIS spectroscopy, thereby proving reformation of the diene and dienophile [200]. Another similar Diels-Alder based crosslinking approach applied for gelatin crosslinking, involves the reaction between a furan moiety introduced onto gelatin (gel-furan, Figure I.13 γ), which is crosslinked using a bismaleimide [164] (Figure I.12 (light green)).

Gelatin derivatives benefitting from thermoreversible Diels-Alder click chemistry include: gel-furan (Figure I.13 (γ) [164], and gel-FGE (Figure I.13 (δ)) [200].

Reversible Disulphide Linkage-Based Crosslinking

Another reversible system, inspired by nature, involves the application of reversible thiol/disulphide formation. Disulphide bridges between thiols can be formed using an oxidative trigger (e.g. hydrogen peroxide), while cleaving of these bonds can be realised in the presence of reducing agents (e.g. DTT or glutathione) [185,186,202–204] (Figure I.12 (purple)). An additional benefit associated with thiolated systems is the fact that thiolation of polymers leads up to a 140-fold improvement of mucoadhesion via the formation of disulphide linkages between the polymer and glycoproteins within the mucosal layer [186,188,189,191,203,205]. Due to the combination of this property and the controllable reversible nature of this chemistry, thiolated gelatins and thiolated hydrogels in general prove to be ideal candidates for controlled drug release studies [204,205]. However, although gelatin is a protein consisting of around 18 different amino acids, it does not contain cysteine in its backbone. Therefore, disulphide chemistry can only occur after chemical introduction of thiols [145,171,187–193]. To this end, Van Vlierberghe et al. introduced thiols either via reaction of the primary amines with n-acetylhomocysteine thiolactone (Figure I.10 L) or Traut's reagent (Figure I.10 J) to yield gel-SH [187]. They reported a linear correlation between storage modulus G' of the resulting gel and degree of amine substitution [171]. Using this strategy, a maximum of 300 µmol thiols/g of gelatin was achieved [187].

In an attempt to further increase the number of incorporated thiols, Duggan et al. first modified part of the carboxylic acid side chains present in the

glutamic and aspartic acid amino acids by coupling ethylene diamine using carbodiimide click chemistry [188,206]. Next, both the native and the introduced amines were reacted with Traut's reagent resulting in up to 660 µmol of thiols/g of gelatin. Although crosslinking of the material proved successful, no attempts were made to de-crosslink the material afterwards by reducing the disulphide linkages [188].

An important drawback associated with thiols and thiolated polymers is their short shelf life due to the potential of auto-oxidation resulting in premature crosslinking [185]. To overcome this limitation, it can be useful to incorporate protected thiols onto gelatin [185,189,191]. To this end, Rohrer et al. applied thiols functionalised with a 2-mercaptopyrimidine-4,6 diol as a protective leaving group for mucoadhesive drug delivery applications (gelatin-Cys-2-MPD; Figure I.10 O) [189] or protected thiolated gelatin with mercaptonicotinic acid (gelatin-TBA-MNA; Figure I.10 R) [191].

Other thiolation strategies include the reaction of the primary amines with gamma-thiobutyrolactone [171] (Figure I.10 T), reaction of the carboxylic acids with cysteamine to yield gelatin-Cys (Figure I.10 P) [189], reaction of the carboxylic acids with 3,3'-dithiobis(propionic hydrazide) (DTP) using carbodiimide chemistry followed by cleaving of the disulphides with DTT yielding gel-S (Figure I.10 S) [192,193], the reaction of the primary amines with one side of a N-hydroxysuccinimide (NHS)-bifunctional PEG followed by linking the primary amine of cysteine to the other NHS functionality to yield gel-PEG-Cys (Figure I.10 Q) [190].

Although the concept of a reversible hydrogel is very interesting due to the aforementioned reasons, the use of disulphide linkages as crosslinks requires the use of oxidizing chemicals including hydrogen peroxide which can induce cellular damage. Furthermore, the introduced thiols can undergo side reactions with thiolated functionalities present in the cell [194]. As a consequence, the system is less suitable for cell-encapsulation purposes [190,207].

Schiff's-base reaction

Another step-growth based strategy is reacting the primary amine groups from gelatin with aldehyde groups from a crosslinker in the absence of light (Figure I.10 grey). This chemistry is referred to as a Schiff's-base crosslinking reaction [102,208,209]. A potential crosslinker in this respect is dextran or alginate which can be oxidized with periodate to generate aldehyde functionalities

[102,208,210]. As a consequence, a suitable ECM mimic is formed since the natural ECM also consists of proteins and polysaccharides. Furthermore, the Schiff's base is prone to hydrolysis resulting in reversible degradation of the crosslinks afterwards [211]. In order to render gelatin water soluble at room temperature (*vide infra*) while introducing additional amines to increase the crosslink density, Pan et al. reacted the carboxylic acids in gelatin with ethylene diamine using carbodiimide coupling chemistry [102]. In an attempt to increase the mechanical properties of a dextran-gelatin based system formed via Schiff's base reaction, Liu et al. first introduced methacrylate functionalities to dextran prior to the periodate oxidation. As a consequence, a denser network with higher storage moduli could be obtained which was successfully applied to encapsulate vascular endothelial cells [210].

Photo-Reversible Systems: π-π Cycloaddition

A proposed photo-reversible crosslinking system takes advantage of functionalities that can undergo a photo-reversible dimerization reaction by irradiation at different wavelengths [212] (Figure I.12 (yellow)). Examples of such functionalities are Furanic chromophores (gel-MFVF [213] Figure I.14 Z) and nitrocinnamate (gel-NC [212] Figure I.14 β) which can undergo a photo-reversible (π2+π2) photocycloaddition reaction with the formation of a cyclobutane ring as a consequence (Figure I.12 (yellow)).

Alternatively, anthracene (gel-AC Figure I.14 α) can also undergo a photo-reversible (π4 + π4) cycloaddition [212,214].

Garcia-Astrain et al. introduced furan containing chromophores (i.e. 5-(2-(5-methyl furylene vinylene)) furancarboxyaldehyde (MFVF)) onto gelatin (gel-MFVF Figure I.14 Z), resulting in moderate crosslinking at 365nm (Figure I.12 (yellow)). However, photo-reversibility was not explored in the reported work [213].

Furthermore, Gattas-Asfura et al. introduced nitrocinnamate functionalities onto gelatin (gel-NC) which was successfully crosslinked in the absence of a photo-initiatior by irradiation at 365 nm, while subsequent irradiation at 254 nm allowed the (partial) photocleavage of the material (Figure I.14). In another attempt to develop a photo-reversible gelatin, Gattas Asfura et al. synthesized gelatin with anthracene side groups. Although the modification proved successful, quantification was not possible due to solubility issues of the synthesized gelatin [212].

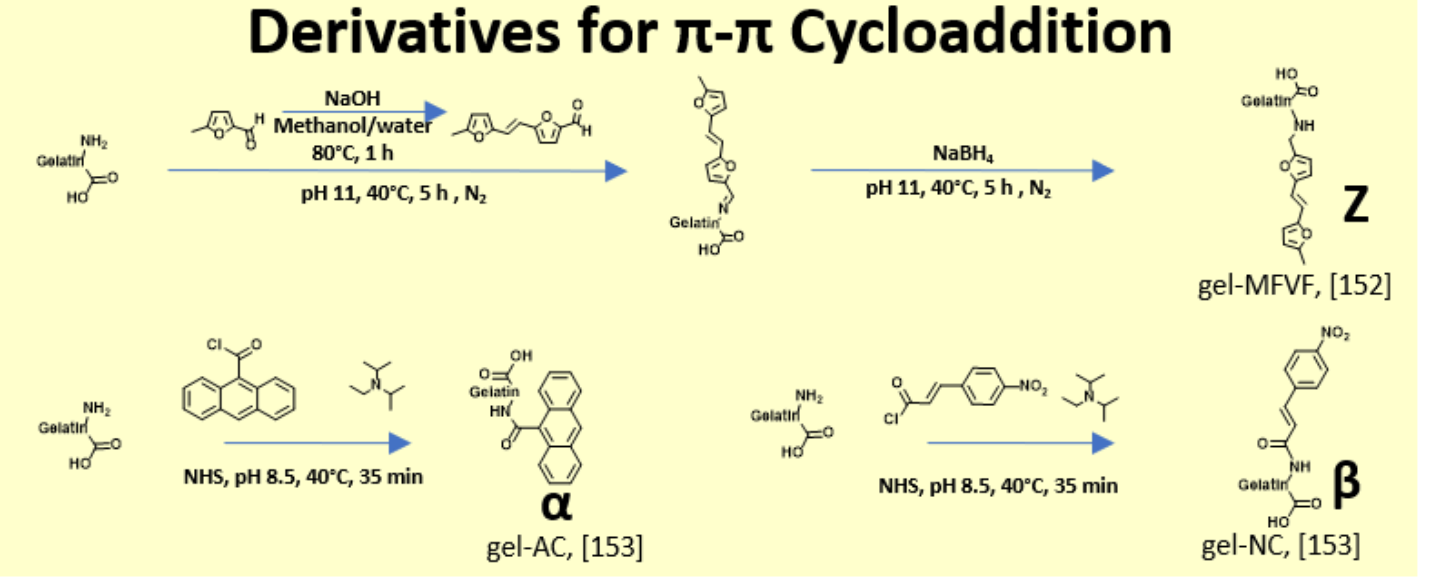

Figure I.14: Non-exhaustive overview of different crosslinkable gelatins including their method of preparation classified according to their crosslinking chemistry: π- π cycloaddition (yellow): gel-MFVF (Z) [213], gel-AC (α) [212], gel-NC (β) [212];

The use of a photo-reversible system can have benefits in drug release applications, since the release of an active compound can be triggered locally using irradiation [212,214,215]. Alternatively, when using selective photocleavage with a high degree of spatiotemporal control, localised cleaving of a matrix material can aid towards guiding cell migration [216,217] .

In general, these systems can undergo dimerization in a relatively straightforward way when immobilized on a polymer resulting in a crosslinked network. However, there are some problems associated with the reversible reaction as typically the materials do not fully cleave upon irradiation [212]. Furthermore, using UV light and especially, UV-C light as a trigger also poses some drawbacks, since it has poor penetration depth into tissue and can additionally pose carcinogenic effects [218]. Therefore, these systems require further development before becoming viable for real biofabrication applications.

Photo-Oxidation Based Systems

In an alternative approach to previously mentioned systems, Son et al. applied visible light irradiation to activate an introduced functionality rendering it prone to crosslinking (Figure I.12 (dark green)). To this end, they took advantage of photo-oxidation of furfuryl groups introduced onto gelatin (gel-FI; Figure I.15 X) [219]. To yield gelatin with furfuryl side groups, two modification strategies have been reported to date. The first consisted of reaction of the primary amines in gelatin with furfuryl isocyanate (FI) to yield gelatin-FI with a DS of 98% (Figure I.15 X) [219]. In order to further optimise the reactivity, another approach applies carbodiimide crosslinking to link the primary amines of furfuryl amine (FA) to the carboxylic acids of gelatin thereby yielding gelatin-FA [220] (Figure I.15 W). Finally, in a third approach, the primary amines of gelatin were linked to furfuryl glycidyl ether yielding gel-FGE (Figure I.15 Y) [221,222].

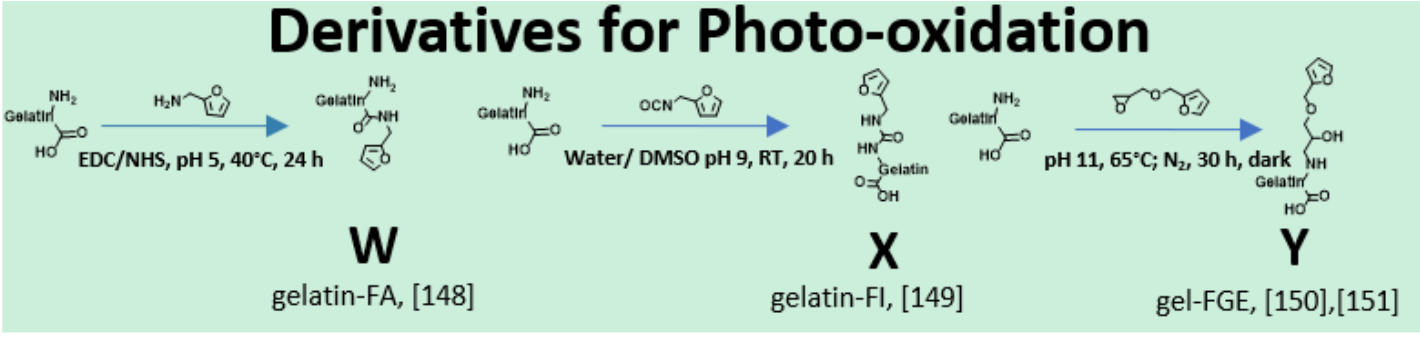

Figure I.15: Non-exhaustive overview of different crosslinkable gelatins including their method of preparation classified according to their crosslinking chemistry: Derivatives suitable for photo-oxidation (green): gelatin-FA (W) [220], gelatin-FI (X) [219] gel-FGE (Y) [221,222]

In order to crosslink the gelatin, first, the furfuryl groups are oxidized using the photo-induced formation of singlet oxygen by rose bengal upon irradiation with visible light. As a result, a (π2 + π4)-cycloaddition of singlet oxygen to the diene of the furan moiety leads to the formation of an endoperoxide [223]. Next, the formed endoperoxides on the furfuryl rings can undergo polycondensation to form a conjugated polymer [219]. Consequently, a crosslinked network can be formed using visible light (Figure I.12 (dark green). Therefore, the need for potential damage due to UV irradiation is circumvented [219]. Additionally, the reaction is not prone to oxygen inhibition and even requires the presence of oxygen in order to proceed [224]. Furthermore, both the rose bengal (a common food dye) and the gelatin-FI as such did not exhibit any cytotoxicity [219].

However, the formation of singlet oxygen is known to negatively influence cellular survival, and is often applied in photodynamic therapy to efficiently eliminate cancerous cells [129,180]. As a consequence, the chemistry is less suitable for cell encapsulation. However, Mazaki et al. applied a gelatin furfuryl system (gel-FA; Figure I.15 W) in combination with rose bengal as photosensitizer. In their study they indicated that the presence of the gel-FA (Figure I.15 W) exhibited a cytoprotective effect on encapsulated bone marrow-derived stromal cells in the presence of 0.05% rose bengal in comparison to a blank solution containing only rose bengal. They reported a viability of 87% 24 hours after encapsulation whereas the reference solution only exhibited around 10% survival. This effect is probably a consequence of the very fast reaction of the furfuryl groups in gelatin with the generated singlet oxygen, thereby acting as a singlet oxygen scavenger [220].

Furthermore, Son et al. applied gel-FI (Figure I.15 X) in combination with rose Bengal as a photosensitizer in dental pulp regenerating experiments followed by in situ irradiation, thereby outperforming the calcium hydroxide control [219].

Enzymatic crosslinking

Enzymatic crosslinking approaches can be of interest due to mild reaction conditions in combination with a high specificity of the enzymes to selectively crosslink the required functionalities, rendering it very suitable for cell encapsulation purposes [101].

Additionally, it is typically faster (i.e. seconds to minutes) in comparison to most other non-light (non-click chemistry based) induced systems (i.e. glutaraldehyde, carbodiimide) which typically require multiple hours [101,225].

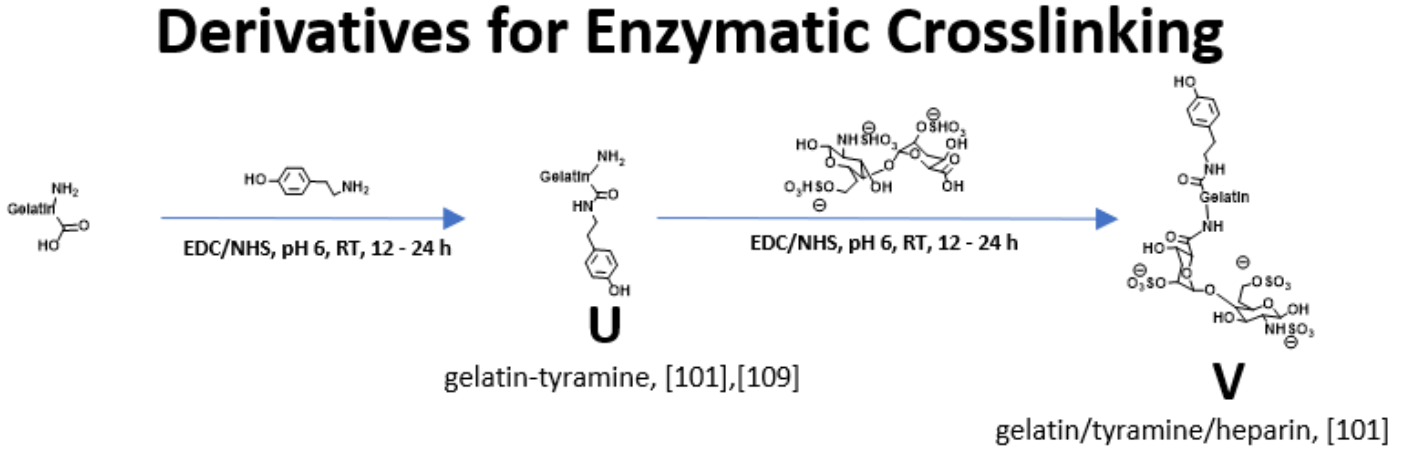

Figure I.16: Non-exhaustive overview of different crosslinkable gelatins including their method of preparation classified according to their crosslinking chemistry: Derivatives for enzymatic crosslinking (white): gelatin-tyramine (U) [101,109], gelatin/tyramine/heparin (V) [101]

A typical enzymatic crosslinking approach is the use of peroxidase catalysts for the oxidation of electron donors using H_2O_2, enabling linking of polyphenols at the aromatic ring (Figure I.12 (white)). To benefit from this approach, Li et al. introduced tyramine side chains onto gelatin in order to provide enzymatic crosslinking points after material injection (gelatin-tyramine; Figure I.16 U) [101,109,225]. Crosslinking can be achieved by the addition of horseradish peroxidase (HRP) and hydrogen peroxide (Figure I.12 (white)) [101,109]. The rate of crosslinking can be increased by increasing the HRP concentration and decreasing the hydrogen peroxide concentration, resulting in crosslinking within seconds [109]. This is a consequence of the fact that besides acting as a catalyst, H_2O_2 also deactivates HRP in high concentrations [109]. The crosslinking approach also proved to be non-cytotoxic despite the use of low quantities of H_2O_2 and allowed for encapsulation of L929 cells or Bone Marrow Stromal Cells (BMSCs) with over 95% viability [109,225]. A drawback of this approach is that this reaction is also prone to oxygen inhibition [226]. Recently, studies also indicated the potential towards photo-crosslinking of phenolic hydroxyl moieties, thereby clearing the road towards light-based additive manufacturing technologies [227].

Alternatively, transglutaminase can be used to crosslink gelatin without the prior need of a chemical modification [116]. Transglutaminase can catalyse the reaction between the gamma-carbonyl group of glutamine and the epsilon-amino group of a lysine amino acid resulting in the formation of an amide bond [116].

1.2.2.3. Overview of Applied Photoinitiators

When using light-based crosslinking chemistries, typically a photo-initiator is required to initiate the crosslinking reaction. Since gelatin is a hydrogel material, suitable photo-initiators need to be water-soluble, thereby limiting the options. A non-exhaustive overview of photo-initiators applied for gelatin crosslinking is presented below, which can be classified according to their activation behaviour.

Norrish Type I photo-initiators

Norrish type I photo-initiators are characterized by photocleavage into different smaller molecule radical species [228]. This type of PI is usually active in the UV-region and rarely exhibits activity in the visible spectrum. The most commonly applied photo-initiator for crosslinking and biofabrication purposes

of gelatin derivatives is Irgacure 2959 (2-hydroxy-1-(4-(hydroxyethoxy)-phenyl)-2-methyl-1-propanone) which is most efficient at 254 nm (Figure I.17). This water-soluble photo-initiator has been considered as one of the gold standards since it has been commercially available for a long time (i.e. over 2 decades) [121,163]. Furthermore, at low concentrations (below 2.24 mM, corresponding to 0.05 wt%), it is considered highly biocompatible which makes it suitable for biological applications [128,146]. Cytotoxic effects have been reported at concentrations exceeding 0.1 wt% corresponding to 4.46 mM [146]. Since short wavelength (UV) irradiation has a low penetration depth and can induce cellular damage, research has also shifted towards visible light initiators [115,146,163,229]. Unfortunately, Irgacure 2959 has proven to be very inefficient in the UV-A to visible light spectrum (i.e. molar absorptivity at 365 nm: 4 M^{-1} cm^{-1} [133]). Therefore, researchers are increasingly substituting Irgacure 2959 by alternative photo-initiating systems. In this respect, lithium phenyl-2,4,6-trimethylbenzoylphosphinate (LAP or Li-TPO) (Figure I.17) has witnessed an increased use due to its higher efficiency in the visual spectrum (i.e. molar absorptivity at 365 nm: 218 M^{-1} cm^{-1} [115]; at 400 nm: 30 M^{-1} cm^{-1} [115] ; at 405 nm: 50 M^{-1} cm^{-1} [133]) and its superior water solubility while exhibiting a comparable biocompatibility to Irgacure 2959 [115,128]. Alternatively, also the use of VA-086 has been reported. VA-086 is an azo initiator resulting in the formation of nitrogen gas upon irradiation leading to the formation of gas bubbles in the hydrogel network (Figure I.17) [127]. The photo-initiator is substantially less efficient in comparison to Irgacure 2959 as typically, a tenfold increase in concentration is required to yield comparable hydrogel properties [127]. However, Billiet et al. indicated an increase in cell viability using hepatocarcinoma cells during cell encapsulation experiments even at these high concentrations.

A final important class of PI's are 2PP-active PI's as 2PP has gained increasing attention in the field of biofabrication. The first two-photon activated type I photo-initiator was DAS (tetrapotassium 4,4'-(1,2-ethenediyl)bis(2-(3-sulfo-phenyl)diazenesulfonate)) which is a diazosulfonate-based initiator suitable for 2PP applications (*vide infra*) (Figure I.17) [230]. However, DAS is not suitable to function as a conventional photo-initiator for linear absorption applications. Despite its lower activity in comparison to other 2PP-PI's at 800 nm as reflected by a lower two photon absorption cross-section (i.e. 40 GM at 800 nm), it is the only Type I photo-initiator suitable for cell encapsulation experiments during 2PP processing. Similar to VA-086, it is an azo initiator, implying that it produces nitrogen gas upon activation [230].

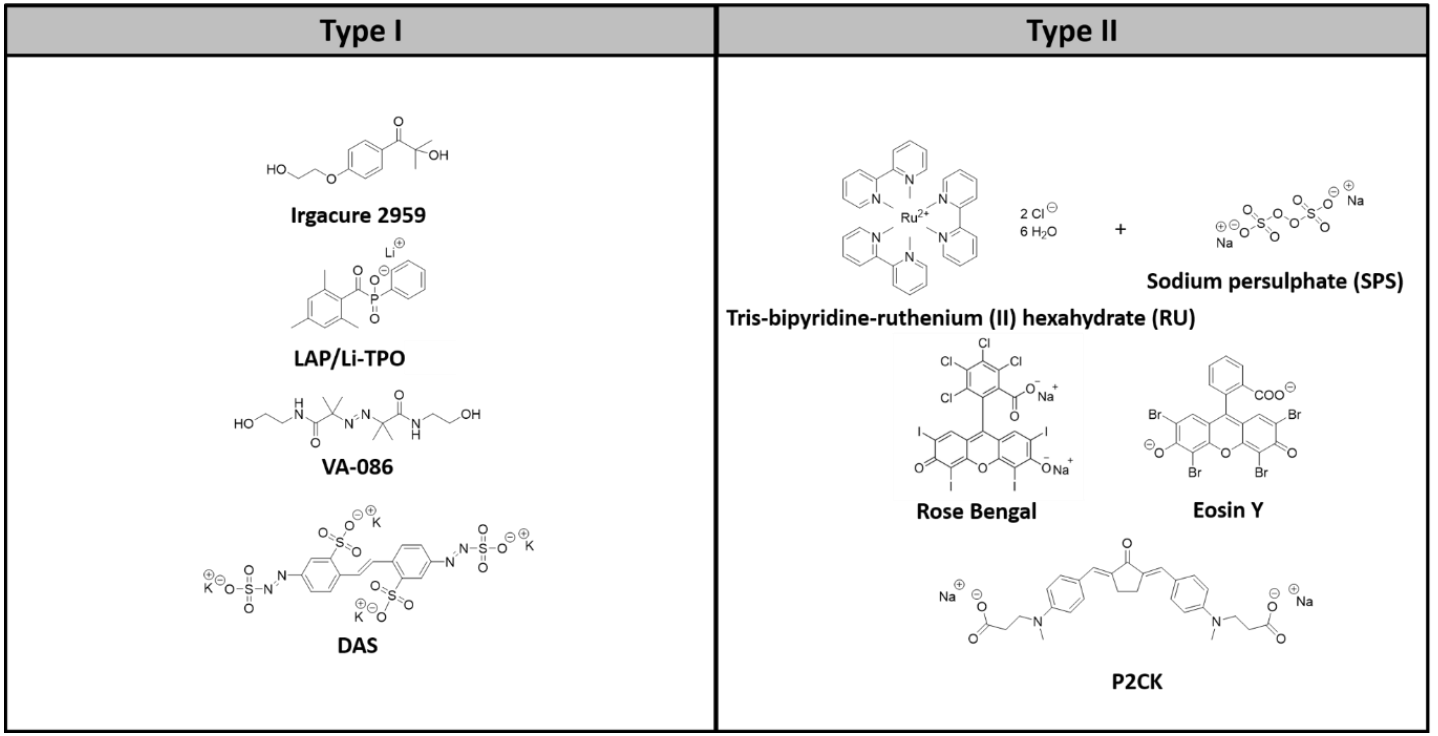

Figure I.17: Overview of different photoinitiators applied for crosslinking of gelatin derivatives classified according to their initiation mechanism.

Norrish Type II Photo-initiators

Type II initiators are initiators which can generate radicals without cleaving into smaller molecules [228]. Typical commercial examples of such molecules include eosin Y, rose bengal and ruthenium/SPS [115] (Figure I.17). In contrast to type I PI's, most type II PI's require a (strong base) co-initiator (i.e. triethanolamine) to achieve a suitable reactivity for biofabrication approaches [124]. However, a lack of initiator reactivity can sometimes be overcome by using more reactive crosslinking chemistries. To this end, thiol-norbornene systems have for example shown to overcome the drawbacks associated with less efficient initiators [147]. Greene et al. have shown that eosin Y can be applied to crosslink gelatin-norbornene with thiolated 4-arm PEG in the absence of a co-initiator using visible light (i.e 550 nm) [115]. Furthermore, they demonstrated its increased initiator efficiency, as 40 times more LAP was required to reach similar mechanical properties in comparison to eosin Y upon visible light irradiation (i.e. absorptivity of eosin Y: 100000 M^{-1} cm^{-1} at 525 nm [115]). Additionally, eosin Y at a concentration of 0.1 mM exhibited an increased reactivity in comparison to LAP at 4 mM as evidenced by a shorter gel-point (24 s vs 42 s) [115]. Furthermore, eosin Y exhibits comparable cytotoxicity to LAP [115].

Another example of a type II visible light initiation system which is gaining increasing attention in the field of biofabrication is a ruthenium complex (tris-bipyridyl-ruthenium (II) hexahydrate) and sodium persulfate (SPS) as co-initiator and is referred to as Ru/SPS [133,146,163,229]. Upon irradiation, Ru^{2+} is photoexcited to Ru^{3+} followed by donating electrons to SPS, that in turn dissociates into sulphate anions and radicals [163,231]. Ru/SPS can be considered a very efficient PI as it is characterized by a high molar absorptivity: 14600 M^{-1} cm^{-1} at 450 nm [133].

Finally, the most commonly applied PI to enable 2PP of hydrogel materials is also a type II initiator, namely P2CK (sodium 3,3'-(((1E,1E') -(2-oxocyclopentane-1,3-diylidene) bis (methanylydiebe)) bis(4,1-phenylene)) bis(methylazanediyl)) dipropanoate) [114,129,147,232–234] which has proven to be very efficient (i.e. two photon absorption cross-section: 176 GM at 800 nm) [232]. However, despite being a very efficient 2PP PI, P2CK is not really suitable for cell encapsulation, as it can penetrate the cell membrane. Thereafter upon irradiation, it will generate singlet oxygen, resulting in cytotoxicity making it an attractive candidate for two-photon based photodynamic therapy [129,180,235].

1.2.2.4. Important Considerations During Gelatin Modification Strategies

Since gelatin is a biopolymer consisting of around 18 different amino acids with various functionalities in different ratios, the material is characterised by a specific behaviour towards solvents, reaction conditions, temperature, pH, etc.

Therefore, it is important to take a closer look at some of the aspects that need to be considered when modifying or processing gelatin(-based) materials.

Gelatin Functionalities Suitable for Chemical Modification and Analysis Thereof

Gelatin contains a large number of functionalities in the side chains of the different amino acids which are prone to reaction. It contains amine functionalities in the side chains of lysine, hydroxylysine and ornithine (in gelatin type B), carboxylic acids in the side chains of glutamic and aspartic acid and hydroxyl functionalities in the side chains of serine, threonine and hydroxylysine [236]. Although most modification strategies discussed above use the primary amines as a handle to introduce functionalities, also the hydroxyl functionalities exhibit nucleophilic behaviour and can therefore compete in these reactions [150]. Depending on the reaction conditions, reports show that either both functionalities participate in the reaction or only one. Recently, Claassen et al. reported that during the modification of gelatin into gelatin methacryloyl (gel-MA) (Figure I.8 A), the hydroxyl functionalities participate in the reaction when a tenfold excess of methacrylic anhydride is added, while this is not the case when only two equivalents are added [150].

Additionally, Van Hoorick et al. investigated the degree of substitution (DS) of gel-MA and gel-NB using ^{1}H-NMR spectroscopy based on the signals of the introduced functionalities (i.e. methacrylamide or norbornene signals) using the amino acid composition of the applied gelatin (see chapter 3). They compared the obtained results with a spectrometric indirect amine determination technique based on ortho-phthalic dialdehyde. Both techniques yielded comparable results in terms of amine DS, thereby indicating only modification of the primary amines upon adding 1 equivalent methacrylic anhydride and upon applying a reaction time of 1 hour or by adding 0.75 or 2 equivalents of 5-norbornene-2-carboxylic acid succinimidyl ester and reacting

for 20 hours thereby confirming that only modification of the primary amines occurs when using low molar excesses of reagents enabling the introduction of functionalities as reported by Claassen *et al.* [147].

Furthermore, Garcia-astrain et al. reported on a comparable DS for the modification of gelatin with furfuryl glycidyl ether after 24 hours of reaction as indicated via ^{1}H-NMR spectroscopy, based on the signals of the furan ring and through a spectroscopic amine determination assay. This proves that also during this reaction, the hydroxyl functionalities remained unaffected [200].

In contrast, Shuster et al. reported on the modification of both the primary amines (100%) and the carboxylic acids (35%) during modification with glycidyl methacrylate at a molar excess of 17.75 equivalents at 40°C during an overnight reaction [237].

Bertlein et al. investigated the predominant site of modification during the functionalization of gelatin with allyl glycidyl ether. To this end, they calculated the number of reacted amines indirectly using a TNBSA (2,4,6-trinitrobenzene sulfonic acid) assay and compared this result with the DS as obtained via ^{1}H-NMR spectroscopy. Furthermore, they looked into the reactivity of other functional groups by reacting model compounds including poly(allylamine), poly(vinyl alcohol) (PVA) and poly(acrylic acid) under the same reaction conditions. From this experiment, they observed that only 13% of the hydroxyl groups in PVA and only 10.8% of the carboxylic acids in poly(acrylic acid) were reacted whereas full conversion was obtained for the amines in poly(allylamine) indicating the primary amines as the primary sites of reaction. However, an overestimation of the amount of introduced functionalities via ^{1}H-NMR spectroscopy relative to the TNBSA assay was obtained when performing the modification under strong basic conditions, which is anticipated to be a consequence of the formation of additional primary amines due to basic hydrolysis of the amide functions along the backbone as further substantiated by GPC measurements [146]. Therefore, it can be concluded that indeed the hydroxyl functionalities can participate in the reactions targeting primary amine functionalization. However, this will only lead to a significant contribution when using large molar excesses of the applied reagent and for prolonged reaction times (i.e. more drastic reaction conditions).

Influence of Modification on Triple Helix Formation

As already briefly discussed, gelatin is primarily composed of lysine, proline and hydroxyproline, of which proline and hydroxyproline are responsible for

the helical architecture and the formation of hydrogen bonds resulting in triple helix formation [104,238]. Upon cooling below the dissociation/denaturation or gel temperature, the random coils in the gelatin solution start to aggregate to form microcrystalline junction zones resulting in physical crosslinks and therefore gel formation [103]. Reports have shown that introducing (bulky) groups (i.e. acyl groups) to the side chains of gelatin can hamper the triple helix formation and the associated renaturation properties associated to the physical gelation of gelatin (Figure I.8 B, D, C, M) [114,194,200,213,239]. Since the transition from helix to coil is accompanied by endothermal heat, the effect of a modification on the triple helix formation and associated physical gelation properties can be quantified using differential scanning calorimetry (DSC). These measurements can either be performed in solution or in the gel state during which the associated energies related to the physical gelation around 30°C can be assessed [114,142,240]. Alternatively, also strategies were reported in which the sample is first dehydrated by heating above 100°C followed by rapid cooling to prevent renaturation and by performing a second heating run during which differences in the glass transition (Tg), which is associated to the triple helix formation of gelatin, can be compared [188,200,213].

More recently, another approach to assess the triple helix formation has been elaborated which involves the use of modulated DSC. In modulated DSC experiments, complex and overlapping thermal effects can be distinguished by superimposing a sinusoidal wave on the linear heating ramp. The resulting signal can be subdivided into a non-reversing and a reversing component via a deconvolution procedure [103,241]. As a consequence, time-dependent processes such as triple helix dissociation are present in the non-reversing signal whereas specific heat changes are visible in the reversing signal. Therefore, a straightforward distinction between the dissociation temperature (T_d) and the T_g becomes possible [103]. By performing this method, Steyaert et al. indicated that the T_g decreases from about 104 °C down to 10 °C with moisture levels increasing from 0 to 23 wt%. Furthermore, this T_g completely disappears in hydrogels, in contrast to the T_d that is associated to the triple helices which remain present both in the dry as in the hydrogel state and decrease with increasing water content since water acts as a plasticizer between the gelatin chains [103]. However, at high water content, which is typically encountered in hydrogels, a T_d plateau is obtained around 30°C [103].

At high modification degrees, typically observed when besides the primary amines, also other functionalities are modified, the physical gelation is no longer apparent, rendering mammal origin gelatin accessible to light-based additive manufacturing techniques including stereolithography [102,114,242,243].

In this respect, several research groups have attempted to render gelatin soluble at room temperature via the reaction of the carboxylic acids with ethane diamine (Figure I.8 J) [102], 2-aminoethylmethacrylate (Figure I.8 B) [114], dopamine (Figure I.8 C) [137] or through acetylation of the hydroxyl groups (Figure I.8 D) [242,244]. Another approach is the partial hydrolysis of gelatin, as it is known that the T_d decreases with decreasing molecular weight [104,144,237].

Bertlein et al. reported on the absence of physical gelation of gel-AGE based on porcine skin gelatin A at room temperature due to the modification of the primary amines with allyl glycidyl ether in alkaline conditions (Figure I.8 θ) resulting in partial hydrolysis of the gelatin, thereby rendering it suitable for SLA applications [146]. However, when less basic conditions were applied during the synthesis of gel-AGE, the material did maintain its physical gelation behaviour at room temperature [146].

Alternatively, when aiming at light-based additive manufacturing, the physical gelation behaviour of gelatin can be overcome by using gelatin originating from cold water fish which is already soluble at room temperature due to the lower concentrations of proline and hydroxyproline present within the backbone [245–247].

Finally, drastically increasing the surface to volume ratio of gelatin by electrospinning also results in cold water solubility. However, it should be noted that although the material becomes cold water soluble, it forms a hydrogel again within minutes [103].

1.2.2.5. Degradation Behaviour of Gelatin

Degradation of the Gelatin Backbone

Gelatin is a material which is composed of robust amide bonds and will therefore not degrade under physiological conditions when crosslinked [164]. However, the material can be degraded by specific enzymes present in the natural ECM including collagenase, also referred to as matrix metalloproteinase 1 (MMP-1), which cleaves sequences such as Gly-Pro-Gln-Gly-Ile-Ala-Gly-Gln between Gly and Ile, resulting in complete material degradation [114,115]. This effect was further substantiated by Koshy et al. who observed cell stretching of encapsulated 3T3 fibroblasts in an inverse electron demand Diels-Alder crosslinked system at low gelatin concentrations due to matrix remodelling (i.e. the breakdown of the hydrogel and substitution by own ECM) occurring by the cells. In a control experiment during which the

cells were treated with marimastat, which is an MMP inhibitor, the cells did not exhibit this stretching behaviour, thereby proving the enzymatic degradability of the material [194].

Another enzyme which allows gelatin degradation is chymotrypsin, which cleaves C-terminal peptide bonds preceding large hydrophobic amino acids (i.e. tryptophan, proline and tyrosine) present in gelatin [112].

The crosslink density of the material has a crucial effect on the degradation process [114,164]. Materials with a low crosslink density exhibit a linear correlation between mass loss and time indicating a surface erosion mechanism [114,115]. Besides longer degradation times, highly crosslinked gels typically first exhibit an increase in mass (in the hydrated state) due to cleavage of some crosslinks, while maintaining structural integrity resulting in an increased water uptake capacity. Only after longer degradation times, the materials start exhibiting a linear decrease in mass as a consequence of degradation [112,114,115,124,164]. Therefore, highly crosslinked gelatin materials exhibit a combination of bulk degradation and surface erosion behaviour [112].

The degradation mechanism can be of crucial importance when using gelatin hydrogels for drug or growth factor delivery as it will influence the release profile [112].

Furthermore, numerous studies indicate that gelatin hydrogels degrade in the presence of cells as evidenced by differences in swelling ratio or storage moduli during culture [112]. For example, Greene et al. observed a decrease in storage modulus over 14 days of culture in the presence of hepatocytic carcinoma cells, while the gels (gel-NB/PEG4SH 1-7wt%) remained intact over a course of 14 days [112].

In order to prove the difference in network type between gelatin hydrogels crosslinked via a chain growth polymerization mechanism (gel-MA) and a step growth polymerization mechanism (gel-AGE + DTT), Bertlein et al. performed a partial collagenase degradation assay, by carrying out an acidic hydrolysis treatment followed by GPC analysis of the hydrolysis products. They observed the presence of non-degradable higher molecular weight fractions in the gel-MA hydrogels in comparison to the gel-AGE gels, as a consequence of the presence of the kinetic poly(methacrylamide chains) that are typically present in chain-growth hydrogels as discussed above [146].

Degradation of Introduced Crosslinks

The degradation behaviour of crosslinked gels can be tuned by selecting appropriate crosslinkers. For example when using ester-containing crosslinkers (i.e. PEGDA), hydrogels will degrade relatively fast even in the absence of enzymes. Conversely, when using a crosslinker with a more robust functionality (i.e. PEGDVS), degradation will only occur in the presence of enzymes [193]. As a consequence, the gelatin hydrogel composition can be tailored to tune the degradation properties, in particular when using multicomponent step-growth based systems. Some crosslinking chemistries focus specifically on the introduction of reversible crosslinks that can be cleaved when subjected to an external trigger including light resulting in spatiotemporal control over the degradation (Section 1.2.2.2.: photo-reversible systems) or chemical triggers (Section 1.2.2.2. Reversible Diels-Alder based Click systems and Reversible Disulphide linkage-based Crosslinking).

1.2.2.6. Controlling the Mechanical Properties of Crosslinked Gelatin Hydrogels

The mechanical properties of photo-crosslinkable gelatin hydrogels can be tuned in various ways either during gelatin modification or during material processing.

Influencing the Mechanical Properties by Chemical Modifications of Gelatin

By varying the number of introduced crosslinkable functionalities, the mechanical properties of the crosslinked hydrogel can be controlled [106,114,124,244]. For most derivatives, the number of reacted primary amines (i.e. DS) can be controlled by varying the molar ratio of the functionalizing reagent (e.g. methacrylic anhydride [106], carbic anhydride [168], 5-norbornene-2-carboxylic acid [147], etc.) with respect to the primary amines present in gelatin. When all primary amines are converted into crosslinkable functionalities, the mechanical properties can be increased even further by subsequent modification of the carboxylic acids present in the side chains of aspartic acid and glutamic acid with additional crosslinkable functionalities (e.g. 2-aminoethyl methacrylate) [114]. As a consequence, up to 5 times stiffer hydrogels can be obtained [114]. However, it should be noted that increasing

the degree of modification will not always lead to an increase in hydrogel stiffness. Indeed, the introduction of additional functionalities can hamper triple helix formation (*vide supra*). Covalently crosslinked gels prove to be stronger when crosslinking occurs after physical gelation, since the triple helices formed can be 'locked' resulting in a smaller mesh size and associated superior mechanical properties [114,244,248] (Figure I.9 D). Alternatively, the mechanical properties of gelatin-methacrylamide can be altered through covalent linking to another biopolymer (e.g. alginate) prior to crosslinking [111]. Although weaker hydrogels have been reported compared to gelatin-methacrylamide, the modification enabled to fine-tune the mechanical properties through incorporation of divalent cations to physically crosslink the alginate chains [111]. An additional benefit of this approach is the formation of a network containing both protein and polysaccharide chains, thereby resulting in a more accurate ECM mimic with respect to chemical composition [111]. Further approaches focussing on the formation of a superior ECM mimic comprising both proteins and glycosaminoglycans (GAGs) include the use of thiolated hyaluronic acid to crosslink gel-NB [124], the introduction of heparin onto gel-NB prior to crosslinking via coupling of the primary amines of gel-NB to the carboxylic acids in heparin using carbodiimide chemistry [112]. The introduction of heparin poses the additional benefit that it has specific domains to bind growth factors including VEGF and hepatocyte growth factor [101,112]. Furthermore, heparin even provides a stabilizing effect on growth factors as it protects them from denaturation and proteolytic degradation [101]. The incorporation of heparin loaded with hepatocyte growth factor in gel-NB gels resulted in the establishment of increased hepatocyte-specific functions for hepatocellular carcinoma cells (Huh7) [112].

Influencing the Mechanical Properties During Hydrogel Processing

After the introduction of crosslinkable functionalities onto gelatin, there are several methods to influence the mechanical properties of the hydrogel construct during processing. The most straightforward approach to vary the mechanical properties of a hydrogel is to vary the applied gelatin concentration for which higher concentrations typically lead to stiffer gels (Figure I.18 A) [106,114,124,139,147,175,249–251]. However, evidence suggests that high gelatin concentrations (> 15 w/v%) can compromise the biocompatibility and cellular response in cell-encapsulation applications due to the presence of a too densely crosslinked network [139,249,252].

It should be noted that if the mechanical properties are altered by altering the crosslinkable gelatin content, also the concentration of RGD functionalities alters and therefore, the biological response cannot only be attributed to the stiffness of the gel [112].

One way to overcome this limitation is through co-crosslinking gelatin with another photo-crosslinkable material which can either be natural (e.g. a polysaccharide) or synthetic (e.g. poly(ethylene glycol) (PEG) [112,124,168,233,253]. This co-crosslinking approach can be applied for chain-growth as well as step-growth polymerization systems. However, due to the high degree of supramolecular interactions occurring between the gelatin chains, that result in triple helix formation, the use of a secondary co-crosslinking material can result in phase separation as the secondary material can be excluded during physical gelation [110,254]. For example, Van Nieuwenhove et al. observed the formation of starch granules when co-crosslinking gel-MA with starch-pentenoate [110].

Examples of co-crosslinked materials using a chain-growth approach include κ-carrageenan-MA [255], starch-pentenoate (using DTT, via a step growth concurrent approach) [110], PEGDA [233,256], PEGTA [257], PVA-MA [133], HA-MA [148], pentaerythritol triacrylate (PTA) [144], trimethylolpropane triacrylate (TTA) [144], diisobutylacrylamide (DBA) [144], urethane-dimethacrylate (UDMA) [144], tripropylene glycol diacrylate (P3-A) [144], dipentaerythritol pentaacrylate (PPA) [144].

For step-growth polymerization of materials, a crosslinker is required which has a great influence on the mechanical properties of the resulting hydrogel. In this respect, especially the number of crosslinkable groups per molecule is of crucial importance [124]. For example, the use of a 4-arm PEG-SH in comparison to a bifunctional DTT results in increased mechanical properties [168]. Additionally, Shih et al. compared the use of 4-arm PEG-NB (20 kDa) with PEG-dinorbornene (10 kDa) to crosslink thiolated PVA hydrogels which resulted in an almost doubling of the hydrogel stiffness [124].

Examples of different applied crosslinkers in thiol-ene systems in which gelatin contains the -ene functionality (e.g. norbornene, allylether, pentenoyl, etc.) include DTT [147,168], PEG4SH 10kDa [112,115,168], thiolated polyvinylalcohol (TPVA) [124], thiolated hyaluronic acid (THA) [124,193] and thiolated gelatin [170,171].

Examples of applied crosslinkers in thiol-ene systems in which gelatin contains the thiol functionality include PEGDA [190,193], hyperbranched

acrylated PEG [175], pentenoyl gelatin [171] , PEG-divinylsulfone (PEGDVS) [193], gel-NB [170].

In some cases, additional co-crosslinked materials can be introduced besides the crosslinker to influence the mechanical properties of the hydrogel. For example, Greene et al. applied PEG4NB together with a gel-NB/PEG4SH system resulting in a 10-fold increase in storage modulus (i.e. 0.8 kPa up to 8 kPa) when incorporating up to 1.68 wt% PEG4NB into 2 wt% gel-NB/PEG4SH gels without varying the biologically active component (i.e. gelatin) [112]. Shih et al. added PEG4SH to a gel-NB/gel-SH system to increase the mechanical properties without increasing the total gelatin concentration in the mixture [124]. Examples of co-crosslinked materials which do not function as crosslinker in thiol-ene systems include PEG4NB 20 kDa [112] , PEG-dinorbornene 10 kDA (PEGdNB) [124] and thiolated-HA [193].

Furthermore, Greene et al. observed that the presence of low gelatin concentrations (i.e. 1 - 3 wt% gel-NB) in crosslinked gel-NB/PEG4SH gels resulted in lower cell survival of encapsulated Huh7 hepatic carcinoma cells in comparison to higher concentrations (i.e. 5 - 7 wt%) [112].

Thiol-ene systems have another benefit over chain-growth hydrogels in the sense that by varying the thiol-ene ratio, the gelatin content can be tuned without changing the network density nor the associated mechanical properties [112,124,147,162,168]. To this end, Greene et al. managed to vary the gel-NB content from 1 to 7 wt% while keeping the thiolated crosslinker concentration constant, resulting in similar mechanical properties throughout the complete concentration range [112]. When using the same gelatin content, but varying the stiffness of the gel by varying the thiol-ene ratio in gel-NB gels, it was shown that hepatocyte cells exhibit a higher metabolic activity in gels with lower stiffness for an identical gelatin content [112].

Another handle to tune the mechanical properties of the crosslinked network is a variation in the applied irradiation dose for crosslinking [107,112,114,127,139,250,251]. Generally, lower doses result in weaker hydrogels as lower crosslink densities are obtained [112,127,139]. However, influencing the mechanical properties by varying the irradiation dose also affects the number of unreacted, potentially cytotoxic functionalities. Additionally, when chain-growth hydrogels are applied, varying the irradiation dose often is concomitant with a reduced reproducibility due to the complex kinetic profile of the reaction in combination with oxygen inhibition occurring during

crosslinking [162]. Furthermore, when using highly reactive thiol-ene systems (e.g. norbornene), the influence of the dose will be less apparent, since already at very low irradiation doses (during 2PP: 20 mW at 100 mm/s for gel-NB with a fully crosslinked network from 40 mW onwards vs ≥ 80 mW for gel-MA with a clear correlation between irradiation energy and swelling degree), the material will be fully crosslinked [114,147].

A final strategy is combining gelatin hydrogels with other materials (e.g. polyesters) for their mechanical properties without covalent linking [149,271]. This can either be done by combining it with a stiff scaffolding material (e.g. polyesters) obtained either via macro- or microprinting [128,131,149,271]. For example, Visser et al. managed to drastically improve the mechanical properties of gelatin via the incorporation of PCL fibres produced via melt electrowriting resulting in a stronger scaffold in comparison to the pure PCL scaffold or a pure gelatin pellet [149], whereas Markovic et al. applied a PLA scaffold obtained via fused deposition modelling and introduced a gel-MA bioink as an ECM mimic containing pre-osteoblasts inside in order to benefit from the stiff PLA for mechanical properties [128].

All these aspects render gelatin hydrogels suitable to cover a broad range of mechanical properties. A non-exhaustive overview of the range of mechanical properties of earlier reported gelatin derivatives compared to the mechanical properties of different tissues can be found in Figure I.18 [114] . As a consequence, gelatin-based materials prove to be versatile tools for mimicking the mechanical properties of a plethora of tissues.

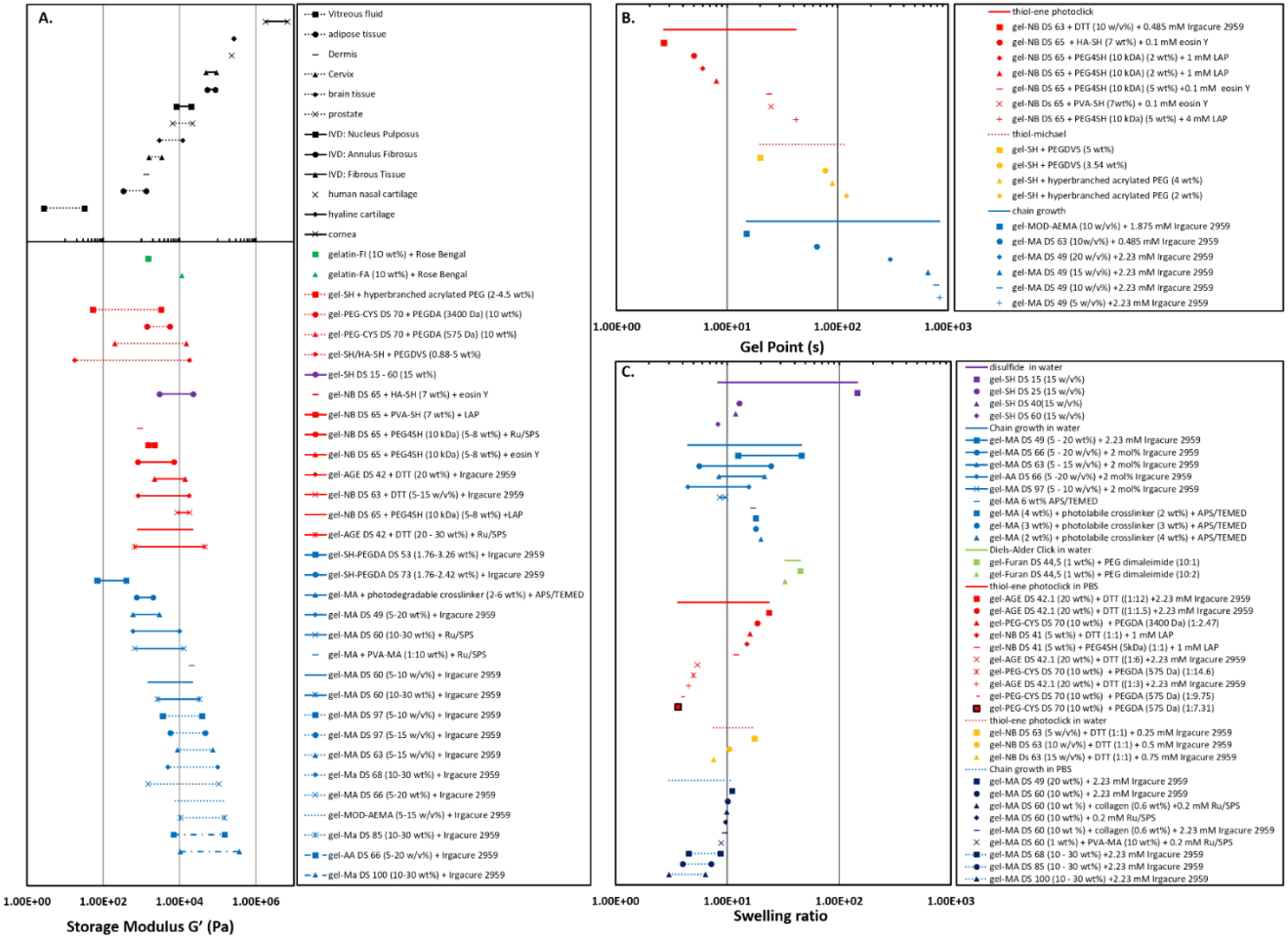
A.
Vitreous fluid
adipose tissue
Dermis
Cervix
brain tissue
prostate
IVD: Nucleus Pulposus
IVD: Annulus Fibrosus
IVD: Fibrous Tissue
human nasal cartilage
hyaline cartilage
cornea
gelatin-FI (10 wt%) + Rose Bengal
gelatin-FA (10 wt%) + Rose Bengal
gel-SH + hyperbranched acrylated PEG (2-4.5 wt%)
gel-PEG-CYS DS 70 + PEGDA (3400 Da) (10 wt%)
gel-PEG-CYS DS 70 + PEGDA (575 Da) (10 wt%)
gel-SH/HA-SH + PEGDVS (0.88-5 wt%)
gel-SH DS 15 - 60 (15 wt%)
gel-NB DS 65 + HA-SH (7 wt%) + eosin Y
gel-NB DS 65 + PVA-SH (7 wt%) + LAP
gel-NB DS 65 + PEG4SH (10 kDa) (5-8 wt%) + Ru/SPS
gel-NB DS 65 + PEG4SH (10 kDa) (5-8 wt%) + eosin Y
gel-AGE DS 42 + DTT (20 wt%) + Irgacure 2959
gel-NB DS 63 + DTT (5-15 w/v%) + Irgacure 2959
gel-NB DS 65 + PEG4SH (10 kDa) (5-8 wt%) +LAP
gel-AGE DS 42 + DTT (20 - 30 wt%) + Ru/SPS
gel-SH-PEGDA DS 53 (1.76-3.26 wt%) + Irgacure 2959
gel-SH-PEGDA DS 73 (1.76-2.42 wt%) + Irgacure 2959
gel-MA + photodegradable crosslinker (2-6 wt%) + APS/TEMED
gel-MA DS 49 (5-20 wt%) + Irgacure 2959
gel-MA DS 60 (10-30 wt%) + Ru/SPS
gel-MA + PVA-MA (1:10 wt%) + Ru/SPS
gel-MA DS 60 (5-10 w/v%) + Irgacure 2959
gel-MA DS 60 (10-30 wt%) + Irgacure 2959
gel-MA DS 97 (5-10 w/v%) + Irgacure 2959
gel-MA DS 97 (5-15 w/v%) + Irgacure 2959
gel-MA DS 63 (5-15 w/v%) + Irgacure 2959
gel-Ma DS 68 (10-30 wt%) + Irgacure 2959
gel-MA DS 66 (5-20 wt%) + Irgacure 2959
gel-MOD-AEMA (5-15 w/v%) + Irgacure 2959
gel-Ma DS 85 (10-30 wt%) + Irgacure 2959
gel-AA DS 66 (5-20 w/v%) + Irgacure 2959
gel-Ma DS 100 (10-30 wt%) + Irgacure 2959
1.00E+00
1.00E+02
1.00E+04
1.00E+06
Storage Modulus G' (Pa)
B.
thiol-ene photoclick
gel-NB DS 63 + DTT (10 w/v%) + 0.485 mM Irgacure 2959
gel-NB DS 65 + HA-SH (7 wt%) + 0.1 mM eosin Y
gel-NB DS 65 + PEG4SH (10 kDA) (2 wt%) + 1 mM LAP
gel-NB DS 65 + PEG4SH (10 kDA) (2 wt%) + 1 mM LAP
gel-NB DS 65 + PEG4SH (10 kDA) (5 wt%) +0.1 mM eosin Y
gel-NB Ds 65 + PVA-SH (7wt%) + 0.1 mM eosin Y
gel-NB DS 65 + PEG4SH (10 kDa) (5 wt%) + 4 mM LAP
thiol-michael
gel-SH + PEGDVS (5 wt%)
gel-SH + PEGDVS (3.54 wt%)
gel-SH + hyperbranched acrylated PEG (4 wt%)
gel-SH + hyperbranched acrylated PEG (2 wt%)
chain growth
gel-MOD-AEMA (10 w/v%) + 1.875 mM Irgacure 2959
gel-MA DS 63 (10w/v%) + 0.485 mM Irgacure 2959
gel-MA DS 49 (20 w/v%) +2.23 mM Irgacure 2959
gel-MA DS 49 (15 w/v%) +2.23 mM Irgacure 2959
gel-MA DS 49 (10 w/v%) +2.23 mM Irgacure 2959
gel-MA DS 49 (5 w/v%) +2.23 mM Irgacure 2959
1.00E+00
1.00E+01
1.00E+02
1.00E+03
Gel Point (s)
C.
disulfide in water
gel-SH DS 15 (15 w/v%)
gel-SH DS 25 (15 w/v%)
gel-SH DS 40(15 w/v%)
gel-SH DS 60 (15 w/v%)
Chain growth in water
gel-MA DS 49 (5 - 20 wt%) + 2.23 mM Irgacure 2959
gel-MA DS 66 (5 - 20 w/v%) + 2 mol% Irgacure 2959
gel-MA DS 63 (5 - 15 w/v%) + 2 mol% Irgacure 2959
gel-AA DS 66 (5 -20 w/v%) +2 mol% Irgacure 2959
gel-MA DS 97 (5 - 10 w/v%) + 2 mol% Irgacure 2959
gel-MA 6 wt% APS/TEMED
gel-MA (4 wt%) + photolabile crosslinker (2 wt%) + APS/TEMED
gel-MA (3 wt%) + photolabile crosslinker (3 wt%) + APS/TEMED
gel-MA (2 wt%) + photolabile crosslinker (4 wt%) + APS/TEMED
Diels-Alder Click in water
gel-Furan DS 44,5 (1 wt%) + PEG dimaleimide (10:1)
gel-Furan DS 44,5 (1 wt%) + PEG dimaleimide (10:2)
thiol-ene photoclick in PBS
gel-AGE DS 42.1 (20 wt%) + DTT ((1:12) +2.23 mM Irgacure 2959
gel-AGE DS 42.1 (20 wt%) + DTT ((1:1.5) +2.23 mM Irgacure 2959
gel-PEG-CYS DS 70 (10 wt%) + PEGDA (3400 Da) (1:2.47)
gel-NB DS 41 (5 wt%) + DTT (1:1) + 1 mM LAP
gel-NB DS 41 (5 wt%) + PEG4SH (5kDa) (1:1) + 1 mM LAP
gel-AGE DS 42.1 (20 wt%) + DTT ((1:6) +2.23 mM Irgacure 2959
gel-PEG-CYS DS 70 (10 wt%) + PEGDA (575 Da) (1:14.6)
gel-AGE DS 42.1 (20 wt%) + DTT ((1:3) +2.23 mM Irgacure 2959
gel-PEG-CYS DS 70 (10 wt%) + PEGDA (575 Da) (1:9.75)
gel-PEG-CYS DS 70 (10 wt%) + PEGDA (575 Da) (1:7.31)
thiol-ene photoclick in water
gel-NB DS 63 (5 w/v%) + DTT (1:1) + 0.25 mM Irgacure 2959
gel-NB DS 63 (10 w/v%) + DTT (1:1) + 0.5 mM Irgacure 2959
gel-NB Ds 63 (15 w/v%) + DTT (1:1) + 0.75 mM Irgacure 2959
Chain growth in PBS
gel-MA DS 49 (20 wt%) + 2.23 mM Irgacure 2959
gel-MA DS 60 (10 wt%) + 2.23 mM Irgacure 2959
gel-MA DS 60 (10 wt %) + collagen (0.6 wt%) +0.2 mM Ru/SPS
gel-MA DS 60 (10 wt%) + 0.2 mM Ru/SPS
gel-MA DS 60 (10 wt %) + collagen (0.6 wt%) + 2.23 mM Irgacure 2959
gel-MA DS 60 (1 wt%) + PVA-MA (10 wt%) + 0.2 mM Ru/SPS
gel-MA DS 68 (10 - 30 wt%) +2.23 mM Irgacure 2959
gel-MA DS 85 (10 - 30 wt%) +2.23 mM Irgacure 2959
gel-MA DS 100 (10 - 30 wt%) +2.23 mM Irgacure 2959
1.00E+00
1.00E+01
1.00E+02
1.00E+03
Swelling ratio

Figure I.18: Scheme representing the physico-chemical properties of reported gelatin hydrogels (A) .Storage moduli of reported gelatin derivatives grouped according to crosslinking mechanism including photooxidation (green): gelatin-FI and gelatin-FA [220]; Thiol-Michael addition (red, dashed): gel-SH + hyperbranched PEG [175], gel-PEG-Cys [190]; gel-SH/HA-SH + PEGDVS [193]; Disulphide formation (purple): gel-SH [187]; Thiol-ene photoclick (Red, solid): gel-NB DS 65 + HA-SH [124], gel-NB DS 65 + PVA-SH [124], gel-NB DS 65 + PEG4SH (10 kDa) [115], gel-AGE DS 42 [146], gel-NB DS 63 [147]; Chain growth (Blue): gel-SH-PEGDA [145], gel-MA + photodegradable crosslinker [216], gel-MA DS 49 [258]; gel-MA DS 60 + Ru/SPS [146], gel-MA + PVA-MA [133], gel-MA DS 60 (5-10 w/v%) [106], gel-MA DS 60 (10-30 wt%) [146], gel-MA DS 97 [106,114], gel-MA DS 63 [147], gel-MA DS 68 [195], gel-MA DS 66 [139], gel-MOD-AEMA [114], Gel-MA DS 85 [195], gel-AA DS 66 [139], gel-MA DS 65 + CS-MA [259], gel-MA DS 100 [195] - in comparison to the mechanical properties of different human tissues including: vitreous fluid [260], adipose tissue [261,262], dermis [263], cervix [264], brain tissue [265], prostate [266], intervertebral disc (IVD): nucleus pulposus [267], annulus fibrosus [267], fibrous tissue [267], human nasal cartilage [195,268], cornea [269].

(B) Overview of reported gel points for different gelatin derivatives organized according to crosslinking mechanism including: thiol-ene photoclick (red): gel-NB DS 63 [147], gel-NB DS 65 + HA-SH [124], gel-NB DS 65 + PEG4SH (10 kDa) [115], gel-NB + PVA-SH [124]; thiol-Michael (red dashed, orange): gel-SH + PEGDVS [193], gel-SH + hyperbranched acrylated PEG [175]; Chain-growth (blue): gel-MOD-AEMA [114], gel-MOD DS 63 [147], gel-MA DS 49 [258].

(C) Mass swelling ratios of different reported gelatin derivatives organized according to crosslinking mechanism and applied solvent: disulphide in water (purple): gel-SH [187], chain growth in water (blue): gel-MA DS 49 [258], gel-MA DS 66 [139], gel-MA DS 63 [147], gel-AA DS 66 [139], gel-MA DS 97 [106], gel-MA 6 wt% + photolabile crosslinker [216]; Diels-Alder click in water (green): gel-FA, gel-FI [220]; thiol-ene photoclick in PBS (red): gel-AGE [220], gel-PEG-cys [190], gel-NB DS 41 [168]; thiol-ene photoclick in water (red dashed, orange): gel-NB DS 63 [147]; chain growth in PBS (dark/dashed blue): gel-MA DS 49 [258], gel-MA DS 60 [163], gel-MA DS 60 (1wt%) + PVA-MA (10 wt%) [133], gel-MA DS 68,85 & 100 [195]

(If the elastic modulus E' was presented in the original document, an estimation of the shear storage modulus was obtained using E' = 2G'(1+μ)) in which μ is 0.5 for ideal rubbery networks) [270].

1.3. Two Photon-Polymerization

Two-photon polymerization (2PP) or multiphoton lithography is a laser-based additive manufacturing (AM) technique which applies highly focused pulsed laser light to solidify a photo-sensitive material. It is based on the non-linear absorption of laser light to induce crosslinking in a photosensitive resin. By tightly focusing a femtosecond laser (often in the near infrared spectrum) beam into the material, the simultaneous interaction of a photo-initiator molecule with two photons, each possessing half the required energy to bridge the band gap required for photo-initiator excitation can be met to initiate localised free-radical polymerization [114,272,273] (Figure I.19). Compared to conventional light-based additive manufacturing techniques using linear (i.e. single-photon) absorption, for which polymerization can occur throughout the entire beam path and is only limited by its penetration depth into the material, 2PP allows polymerization only in a small volumetric element (voxel) enabling the fabrication of structures with resolutions below the diffraction limit (Figure I.19). The maximum achievable resolution is determined by the size of the voxel which depends on the applied optics and laser source [114,274,275]. As a consequence of this unique principle, this is the only additive manufacturing technology which allows processing of gelatin in the physically crosslinked state. Moreover, processing in the physically crosslinked state not only leads to more efficient crosslinking, but also provides support to the structures during crosslinking, resulting in the possibility to generate more complicated architectures [114,129,147].

In 2011, our research groups were the first to report on 2PP processing of modified gelatin (gel-MA, Figure I.8 A) for the generation of scaffolds for tissue engineering purposes using primary adipose tissue-derived stem cells (Figure I.20 C) [130]. Ever since, multiple studies reported on 2PP processing of modified gelatin being mainly gel-MA [96,196,234,276]. In 2014, Ovsianikov et al. reported the first study on 2PP in the presence of living cells [129]. Although the cells did not survive direct exposure to the laser during structuring, it was possible to use 2PP to entrap cells within 3D microstructures [129]. Furthermore, the research indicated that the cytotoxicity was not a result of the applied laser intensity, but could be attributed to the formation of cytotoxic species (i.e. singlet oxygen) within the cells as a side-product of P2CK photo-initiator activation [129,180] . This hypothesis was later substantiated by the development of a macromolecular photo-initiator based on hyaluronic acid, which did enable 2PP processing combined with the encapsulation of living cells in the exposed areas as well [235]. The study indicated that the previously

observed cytotoxicity originated from the penetration of the low molecular weight photo-initiator through the cell membrane, thereby resulting in photo-oxidative damage within the cell during irradiation. By immobilizing the photo-initiator onto a macromolecule, it could no longer penetrate the cell membrane, thereby allowing 2PP in the presence of living cells [235]. Additionally, a different approach using a type I cleavable diazosulfonate PI (DAS) (Figure I.17) has been developed for direct encapsulation of living cells in gel-MA hydrogels. As a result, cell survival was five times higher when compared to P2CK, while maintaining high writing speeds (1000 mm/s) thereby further demonstrating its potential as a biocompatible photo-initiator for 2PP [230] (Figure I.20 E).

Despite these successful approaches, gelatin-methacryloyl is characterized by some limitations in the context of 2PP processing. In general, the poor reaction kinetics and associated mechanical properties require relatively high light doses (e.g. 70 mW at 1000 mm/s scan speed) to crosslink the material. Furthermore, the subsequent swelling of the 2PP-produced structures can compromise the high-resolution capacity of this technology [230].

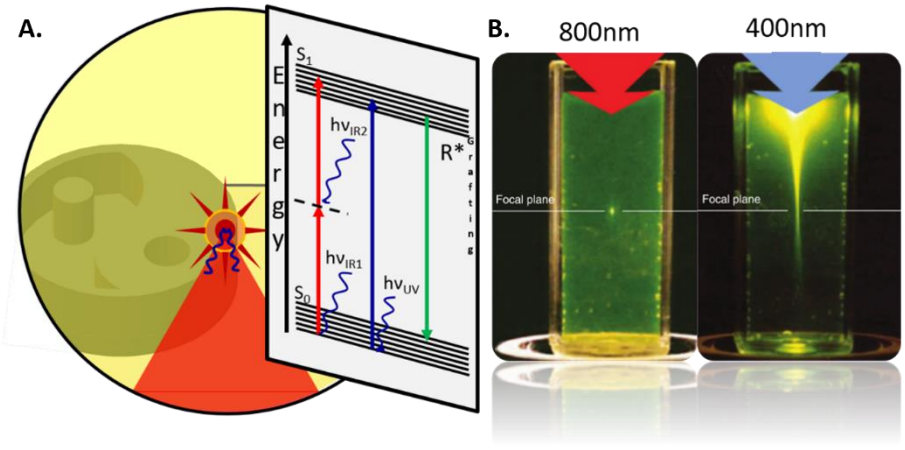

Figure I.19: Schematic representation of the two-photon polymerization principle using a Jablonski diagram demonstrating the theoretical background for which single photon excitation (blue) is compared to two-photon excitation (red) (A). Practical implications of the absorption throughout the beam path for single photon absorption (blue) versus only excitation in the very small voxel for two-photon polymerization (red) (B) (image adapted from [277] and [275])

Several approaches have already been developed to overcome the poor mechanical properties and low reactivity associated with gel-MA for 2PP structuring. The mechanical properties could be improved by using a secondary material to function as/contribute to mechanical support [191,233,278].A second strategy consisted of co-crosslinking low concentrations of PEGDA (1%) for the formation of a co-network. In this respect, processing benefits from the higher mechanical properties of PEG, along with superior acrylate-based reaction kinetics [233]. Alternatively, benefitting from an indirect approach, first a stronger material (e.g. a mixture of hydrophobic acrylates) can be structured to function as support, followed by subsequent gel-MA structuring [278] .

Another approach to improve the properties of gel-MA is to modify the material chemically. To this end, a gelatin derivative was developed where all primary amines were modified into methacrylamides (0.385 mmol/g gelatin), while additional methacrylates were introduced onto the carboxylic acids, resulting in 1 mmol crosslinkable groups per gram gelatin (Figure I.8 B) (*vide infra &* Chapter 2) [114,157]. As a consequence, a denser gelatin network can be formed exhibiting higher stiffness along with less to no occurrence of post-production swelling. Additionally, the reaction kinetics were improved compared to conventional gelatin-methacrylamide resulting in a broader 2PP spatiotemporal processing range (Figure I.20 A) [114,157]. Furthermore, 2D biocompatibility experiments indicated a comparable biocompatibility towards both fibroblasts (L929) and osteoblasts (MC3T3) for gel-MOD-AEMA and the well-established gel-MA [114] .

Although the introduction of these additional functionalities resulted in a drastic improvement in terms of 2PP processing, the crosslinking reactions remain subject to the drawbacks associated with chain-growth polymerizable hydrogels as discussed earlier. Therefore, to further improve the material processing range, 2PP experiments have also been explored using thiol-ene photoclick hydrogels [196]. Qin et al. reported the synthesis of gelatin hydrolysate vinyl esters that were copolymerized with reduced derivatives of bovine serum albumin as a thiolated crosslinker. In a different system, gelatin type B was modified with norbornene functionalities (Figure I.8 κ) (see chapter 3 & 4)[196]. Gel-NB was processed via 2PP using DTT as thiolated crosslinker resulting in a drastically improved spatiotemporal 2PP processing range compared to all previously reported gelatin derivatives. On the one hand, only half of the energy was required to result in reproducible crosslinking (i.e. 20 mW at 100 mm/s for gel-NB + DTT DS 63 vs 40 mW at 100 mm/s for gel-MOD-AEMA) despite a four times decreased concentration of crosslinkable

functionalities (i.e. 0.24 mmol/g for gel-NB vs 1 mmol/g for gel-MOD-AEMA)(see chapter 2 & 3). Additionally, from 40 mW onwards, further increasing the laser power did not influence the hydrogel swelling behaviour, indicating that the material was already fully crosslinked, in contrast to gel-MOD-AEMA for which a further increase of the laser power resulted in concomitantly decreasing swelling ratios [114,147]. Furthermore, also a broader concentration range could be applied for 2PP processing, because reproducible structuring was reported for the first time below a 10 w/v% gelatin concentration (i.e. 5 w/v%) (see chapter 3) [147].

It should be noted that when comparing to gel-MA with a comparable DS, gel-NB is characterized by significantly lower swelling ratios due to the higher degree of conversion during structuring [147]. As a consequence, a superior CAD-CAM mimicry is observed when using gel-NB + DTT in comparison to gel-MA, while the lower required spatiotemporal energy for full conversion leads to stiffer gels at lower laser powers. As a consequence, the material could also be applied for the fabrication of complex structures able to support their own weight despite the presence of only small support structures or micro-scaffolds, that were fully populated by fibroblasts after 7 days of cell culture (Figure I.20 A) [147] .

Another application of 2PP-assisted photomanipulation of gelatin-based hydrogels has been reported by Pennacchio et al. They incorporated an azobenzene crosslinker into acrylamide-modified gelatin hydrogels (Figure I.8 F, Figure I.20 D). Upon 2PP illumination, the azobenzene molecules undergo isomerization from the more planar (trans) to a bent (cis) configuration. This transformation triggers changes in the material properties such as the mesh size, stiffness and/or its swelling behaviour resulting in a dynamic hydrogel platform for 3D cell culture (Figure I.20 D) [140].

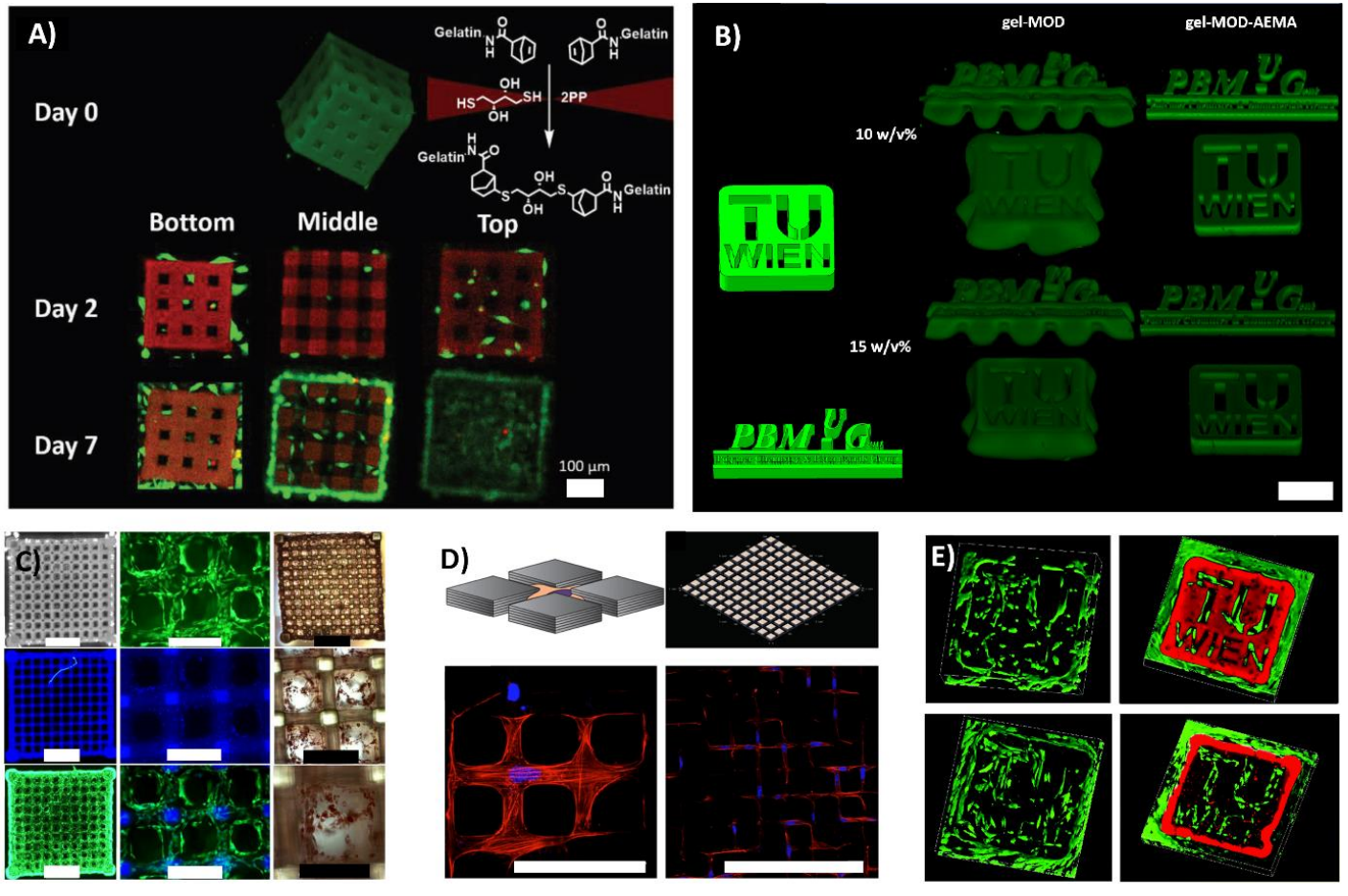
A)
Day 0
Day 2
Day 7
Bottom
Middle
Top
Gelatin
2PP
100 µm
B)
gel-MOD
gel-MOD-AEMA
10 w/v%
15 w/v%
C)
D)
E)

Figure I.20: Different examples of 2PP on gelatin derivatives (A) Scheme demonstrating the thiol-ene photoclick crosslinking of gelatin into a microscaffold, subsequent cell culture in the presence of L929 fibroblasts after 2 and 7 days cell culture (reproduced from [147] with permission). The scale bar represents 100 µm. (B) Difference in shape fidelity between gel-MOD and gel-MOD-AEMA due to post-production swelling as compared to the CAD model. (scale bars represent 100 µm) (Image adapted from [114] with permission; copyright 2017 ACS (https://pubs.acs.org/doi/abs/10.1021%2Facs.biomac.7b00905)). (C) First reported gelatin scaffold obtained via 2PP seeded with primary adipose-derived stem cells. The scale bars represent from top to bottom 1000 µm, 300 µm and 200 µm respectively) (Reprinted with permission from [130] under the CC BY 3.0) (D) Micropattern of a photoresponsive gelatin derivative, enabling light-based control over swelling properties (reprinted with permission from [140]). The scale bar represents 100 µm (E) 2PP structures recorded in gel-MA hydrogels, using DAS (left) and P2CK (right) as PI, thereby proving viability of the cells (green cells) inside the structured material when using DAS. The red signal shown for the P2CK samples is caused by the autofluorescence of the 2PI. The dimensions of the structures are 500 x 500 x 125 µm³ (reprinted with permission from [230]).

1.4. Aim of the PhD

The current PhD aims to develop a synthetic Descemet's membrane to manufacture *ex vivo* corneal endothelial grafts. Using this approach, it is anticipated that the damaged endothelium in visually impaired patients can be replaced with a synthetic cell containing scaffold to restore their vision. The project aims to tackle current hurdles towards an advanced therapeutic medicinal product (ATMP). These hurdles include:

1. Standardisation issues related to the elasticity of the rolls in DMEK.

2. The presence of visual aberrations encountered for currently applied techniques due to the thickness of the transplant and differences in refractive index.

3. The problems associated with lack of donor availability (1/70 patients).

4. The fact that currently, most donor Descemet's membranes originate from older patients, which already have a (partially) compromised endothelium.

The importance to the field becomes apparent since currently no approaches to restore the corneal endothelium have reached the clinic. Furthermore, due to the ageing population, there will be an increasing need for donor corneas as the number of cataract surgeries is rising, the latter being strongly correlated with increased intraoperative endothelial damage. As a result, the present research can have a great impact on the field.

A critical analysis of the state-of-the-art yields insights into the ideal scaffold properties for corneal endothelial regeneration. Based on a literature study, the ideal scaffold is biodegradable, exhibits a transparency of over 90% throughout the entire visual spectrum (390 - 700 nm), a thickness below 50 µm and a glucose permeability coefficient of at least $1.2*10^{-5}$ cm/s [45,279,280]. Furthermore, the material needs to be surgically tangible, and therefore has to be at least as strong as natural Descemet's membranes. To this end, a Young's modulus of at least 2.57 – 5 MPa is desirable [6,45,279].

In order to succeed in this approach the research performed in the current PhD project can be divided in two large sections. On the one hand, a large part of the research was performed focussing on material development in order to further improve and tailor the properties of photo-crosslinkable gelatin derivatives functioning as ECM mimics. To this end, specific attention was provided to improve the 2PP processing potential, as it is known that

micropatterns can influence cellular behaviour [281–283]. To this end, efforts were made to improve the reactivity and concomitant attainable writing speeds and maximal attainable resolution by decreasing the swelling behaviour. On the other hand, research was performed on the development and fabrication of membranes to serve as scaffolds for corneal endothelial regeneration.

In **Chapter 2** the capabilities of chain growth gelatin-based hydrogels are explored in terms of obtainable mechanical properties, 2PP processing capabilities and decreasing swelling properties. It is anticipated that the mechanical properties and processing conditions can be improved via the formation of a more densely crosslinked network. To this end, the widely applied gelatin-methacryloyl (gel-MOD or gel-MA) is further modified by the introduction of crosslinkable methacrylate functionalities via the coupling of 2-aminoethyl methacrylate (AEMA) to the carboxylic acids present in gel-MOD using conventional carbodiimide coupling chemistry [284]. Next, the influence of the modification is assessed in terms of physico-chemical properties, *in vitro* biological performance and 2PP processing properties.

In **Chapter 3** the processing capabilities of photo-crosslinkable gelatin derivatives are further expanded via the use of a step-growth thiol-ene based photo-click approach. To this end, the primary amines in gelatin type B are modified with norbornene functionalities via coupling to the carboxylic acids of 5-norbornene-2-carboxylic acid using conventional carbodiimide coupling chemistry. The success of this strategy is assessed using DTT as thiolated crosslinker and benchmarked to the gel-MA gold standard in terms of physico-chemical properties, *in vitro* biological performance and 2PP processing capabilities. To this end, also the influence of varying the thiol-ene ratio as an extra tool to tune the final network properties is assessed. Finally, the potential of thiol-ene based photo-grafting is assessed.

Besides variation in the thiol-ene ratio, also the identity of the applied crosslinker provides a way to tune the final network properties (vide infra) of thiol-ene based hydrogels. To this end, in **Chapter 4,** the effect of different thiolated crosslinkers on the physico-chemical properties of the obtained hydrogels is assessed. More specifically, gel-NB is crosslinked in the presence of different thiolated crosslinkers being DTT, tetratethylene glycol dithiol (TEG2SH), poly(ethylene glycol) dithiol with a molecular weight of 3400 g/mol (PEG2SH 3400), Poly(ethylene glycol) tetrathiol with a molecular weight of 10 000 g/mol (PEG4SH 10000) and 20 000 g/mol (PEG4SH 20000). Additionally, gelatin type B is functionalised with thiol functionalities via the

reaction of the primary amines with n-acetyl homocysteine thiolactone to result in a multifunctional thiolated crosslinker which is anticipated to result in a more homogeneous network. The performance of these different systems is benchmarked to gel-MA with a comparable DS in terms of physico-chemical properties, *in vitro* biological performance and 2PP processing range.

In the second part of this PhD, the different developed gelatin hydrogel materials are combined with a biodegradable amorphous lactic acid-based polyester (i.e. PDLLA) to generate suitable biodegradable/biointeractive membranes to act as scaffolding membranes for corneal endothelial regeneration. In **Chapter 5,** the fabrication of these membranes using a multistep spin-coating approach is performed. The use of this multi-step spin-coating approach not only results in a straightforward fabrication method but also allows easy isolation of the membrane for implantation. To this end, four different gelatin hydrogel formulations were applied as coatings on the PDLLA membranes to assess the optimal combination towards corneal endothelial regeneration applications. After production, the membranes are characterised in depth towards functionality as a corneal endothelial transplant scaffold in terms of thickness, transparency throughout the visual spectrum and glucose permeability. Additionally, the *in vitro* biological performance of the different substrates is assessed using corneal endothelial cells in terms of adhesion and expression of the correct phenotype. Furthermore, some qualitative experiments were performed to assess the potential towards surgical manipulation while maintaining sample integrity. Finally, preliminary experiments on the influence of the presence of gelatin patterns obtained via 2PP on the membranes on the cellular behaviour are performed.

In **Chapter 6** the main conclusions and the future perspectives of the current research are discussed.

In **Chapter 7**, the materials and methods section is discussed which provides the details of the performed experimental work. Furthermore, in this section, information is provided covering the applied analysis and processing techniques.

Finally, in **Chapter 8,** a Dutch summary of the PhD research is provided.

Chapter 2:
Stretching the Boundaries of Chain-Growth Based Gelatin Hydrogels to Improve the Two-Photon Polymerization Potential

The *in vitro* cell work mentioned in this chapter has been performed by dr. Marica Markovic. The NMR samples were measured by Dhr. Tim Courtin. The HR-MAS NMR samples were measured by dr. Geert-Jan Graulus and dr. Maxime Vagenende

Parts of this chapter have been published in:

> **J. Van Hoorick**, P. Gruber, M. Markovic, M. Tromayer, J. Van Erps, H. Thienpont, R. Liska,A.Ovsianikov, P. Dubruel and S. Van Vlierberghe, *Biomacromolecules, **(2017)*** **18** 3260–72

2.1. Introduction

In the present chapter, the use of chain-growth gelatin hydrogels as suitable ECM mimics for tissue engineering and biofabrication applications is explored. The aim is the development of novel photo-crosslinkable chain-growth gelatin derivatives resolving swelling-related deformations and compromised spatial resolution as the two most persisting issues in laser-based processing of hydrogel building blocks. The amount of photo-crosslinkable functionalities in gel-MOD is determined by the limiting amount of primary amines. Therefore, we anticipated that an increase in photo-reactive functionalities using the gelatin carboxylic acids would positively affect the crosslink density of the resulting hydrogels and consequently, the processing capabilities.

To this end, a good starting point is one of the most commonly applied hydrogel materials for biofabrication and tissue engineering, namely methacrylamide-modified gelatin (gel-MOD) or gelatin-methacryloyl (gel-MA) (see Chapter 1). It can be obtained by the functionalization of the primary amines of the (hydroxy)lysine and ornithine side groups present in gelatin with methacrylic anhydride [86,89,90,139,242,285–290] (Figure II.21 A). As a result, a photo-crosslinkable derivative is obtained that is suitable for laser-based rapid prototyping techniques including two photon polymerization (2PP) [96,97,129,233,276]. Important material limitations however remain in terms of mechanical and swelling properties after crosslinking. Consequently, several strategies were proposed to tackle these issues: varying the degree of substitution, grafting of other biomolecules [111], the formation of interpenetrating networks [291] or combining the gelatin with a second (synthetic) material (e.g. polyesters) to increase the overall stiffness of the final construct [149,292,293]. (see Chapter 1)

2PP of naturally derived polymers has gained increasing interest for the development of porous constructs with (sub-)micron scaled features for tissue engineering purposes [96,97,129,294]. Unfortunately, laser-based processing of natural polymers mimicking the ECM is often concomitant with limitations including swelling-related deformations and compromised spatial resolution. As an example, Ovsianikov et al. previously performed 2PP on gelatin-based hydrogels (gel-MOD/gel-MA) at relatively high concentrations (20 wt%) with and without cells to explore the tissue engineering potential of the developed scaffolds [96,97,129]. However, the reported structures did not fully match the implemented computer assisted design (CAD) because of post-processing

aberrations as a consequence of swelling and inferior mechanical properties [96]. Since these scaffolds were fabricated from precursor concentrations close to the gelatin solubility limit, no substantial improvement in CAD model reproducibility can be realized by further increasing the gelatin concentration. With the aim to overcome the above-mentioned limitations to improve the 2PP potential of gelatin hydrogels, the present chapter elaborates on a novel photo-crosslinkable gelatin. The 2PP potential refers to several aspects of 2PP including the minimally required spatiotemporal energy to obtain reproducible structures. This spatiotemporal energy is defined both by the applied laser power as well as the scan speed of the voxel. Additionally, the 2PP potential also refers to the mimicry between the applied CAD and the final structure obtained. This feature is determined both by post- production swelling of the hydrogel during the development process as well as the mechanical properties of the material. Indeed, a higher stiffness results in superior load bearing capabilities, rendering the support of smaller features possible. Additionally, reproducible structuring at lower concentrations can also be considered as part of the "2PP potential." As a consequence, it is anticipated that a novel photo-crosslinkable gelatin possessing a higher number of cross-linkable functionalities compared to the gold standard gel-MOD can increase this 2PP potential. We anticipate that this higher number of crosslinkable functionalities in the hydrogel precursor will result in a higher network density after crosslinking, thereby outperforming currently reported gelatin derivatives [125,134,187,295] (e.g. gel-MOD/gel-MA, gel-VE, etc.) with respect to 2PP potential.

2.2. Modification of Gelatin type B via the Introduction of Methacrylamides and Methacrylates: Reaction Condition Study

In order to improve the properties of gel-MOD, the effect of the introduction of additional crosslinkable functionalities was assessed. Furthermore, the gel-MOD starting material was also used as a benchmark. First, this gel-MOD was obtained according to a previously reported protocol starting from gelatin type B obtained via an alkaline pretreatment of bovine hides with a known amino acid composition [121] (Table II.1). In order to introduce additional functionalities to gel-MOD, an approach was selected where a partial modification of the carboxylic acid functionalities present in the glutamate and aspartate side chains of gelatin was envisaged using carbodiimide coupling chemistry. In this respect, it is important that all primary amines present in the

(hydroxy)lysine and ornithine amino acids are consumed during the modification into gel-MOD. It is known from literature, that full modification can be performed via the addition of 2.5 equivalents methacrylic anhydride, relative to the number of primary amines present in gelatin type B [296] (Figure II.21 A). Based on the amino acid composition (Table II.1), this corresponds to 0.97 mmol (i.e. 0.385 mmol/g * 2.5 equivalents) of methacrylic anhydride which should be added per gram of gelatin [296]. The modification of the primary amines was confirmed using ^{1}H-NMR spectroscopy [289]. As gelatin consists of more than 20 different amino acids (Table II.1), a complex ^{1}H-NMR spectrum is typically obtained, yet, a complete elucidation of the spectrum was beyond the scope of the present work. The current study only aims at the quantification of the DS by examining the characteristic peaks present in the spectrum as a consequence of the reaction. The selected reference peak is present at 1.01 ppm, which corresponds to the resonance of the methyl groups present in the valine (Val), the leucine (Leu) and the isoleucine (Ile) side chains (Figure II.12). These hydrophobic alkyl side chains can be considered chemically inert and therefore, the methyl groups can serve as a suitable reference. Based on the amino acid composition (Table II.1), it is known that the total amount of protons from the Val, Leu and Ile corresponds to 0.3836 mol/100 g gelatin (i.e. 6 protons in Val, 6 protons in Leu and 6 protons in Ile). By comparing the integration of the signal corresponding to the characteristic protons present on the introduced methacrylamides (Figure II.21 A) with the integration of the reference signal thereby taking into account the total amount of primary amines available for reaction (i.e. 0.0385 mol/100 g) the DS can be calculated as indicated in the left equation in Figure II.21 [289]. As a result, gel-MOD with a DS of 97 % (i.e. 0.37 mmol methacrylamides/g) was obtained.

For the subsequent carboxylic acid modification of the glutamate and aspartate side chains, a good leaving group was introduced to the carboxylic acids via conventional carbodiimide coupling chemistry using ethyl(dimethylaminopropyl) carbodiimide (EDC) while N-hydroxysuccinimide (NHS) was also added to stabilize the activated carboxylic acid groups. Next, a nucleophilic substitution to the carbonyl was realized using the primary amine present in 2-aminoethyl methacrylate (AEMA).

As a result, both methacrylate as methacrylamide functionalities were introduced onto gelatin (Figure II.21 B (red)). The DS of the obtained derivatives was determined via ^{1}H-NMR spectroscopy in a similar fashion as for gel-MOD. To this end, the integration of the characteristic methacrylate signals at 6.20 and 5.80 ppm were normalized against the reference signal

for Val, Leu and Ile at 1.01 ppm (Figure II.21 C). The integration of this reference signal corresponds to a total of 0.3836 mol protons/100 g gelatin [289]. The methacrylate signal corresponds to two protons and based on the amino acid composition, a total of 0.1098 mol carboxylic acids from Asp and Glu are present in 100 g gelatin type B. Therefore, the DS of the carboxylic acids can be calculated in a similar fashion as for the amines in gel-MOD by using the right formula depicted in the top panel of Figure II.21.

Table II.1: Amino acid composition of the gelatin type B applied throughout the present PhD [297].

Amino Acid composition	**Gelatin B** **Bovine hides** **(g/100g)**
Aspartate	5.01 ± 0.14
Glutamate	9.2 ± 0.20
Serine	2.76 ± 0.05
Histidine	0.61 ± 0.01
Glycine	22.12 ± 0.59
Threonine	2.18 ± 0.05
Arginine	6.74 ± 0.14
Alanine	8.76 ± 0.18
Tyrosine	0.21 ± 0.01
Valine	2.63 ± 0.08
Methionine	0.86 ± 0.02
Hydroxylysine	1.26 ± 0.03
Phenylalanine	1.76 ± 0.04
Isoleucine	1.68 ± 0.04
Ornithine	0.97 ± 0.04
Leucine	3.24 ± 0.07
Lysine	3.49 ± 0.08
Proline	14.35 ± 0.40

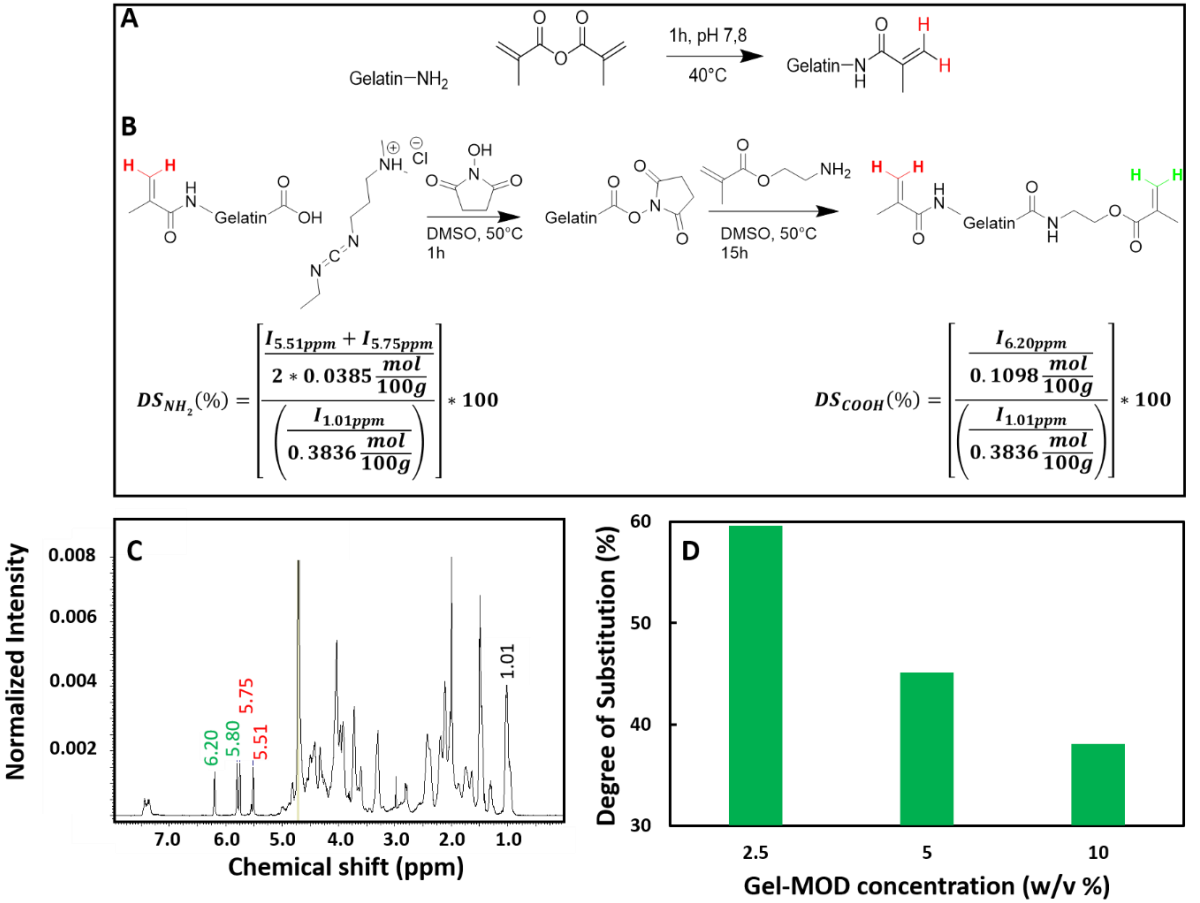
A
Gelatin–NH2
1h, pH 7,8
40°C
Gelatin–N
H
H
B
Gelatin
OH
DMSO, 50°C
1h
Gelatin
NH2
DMSO, 50°C
15h
Gelatin
$DS_{NH_2}(\%) = \left[\frac{\frac{I_{5.51ppm} + I_{5.75ppm}}{2 * 0.0385 \frac{mol}{100g}}}{\left(\frac{I_{1.01ppm}}{0.3836 \frac{mol}{100g}}\right)}\right] * 100$
$DS_{COOH}(\%) = \left[\frac{\frac{I_{6.20ppm}}{0.1098 \frac{mol}{100g}}}{\left(\frac{I_{1.01ppm}}{0.3836 \frac{mol}{100g}}\right)}\right] * 100$
C
Normalized Intensity
0.008
0.006
0.004
0.002
6.20
5.80
5.75
5.51
1.01
7.0
6.0
5.0
4.0
3.0
2.0
1.0
Chemical shift (ppm)
D
Degree of Substitution (%)
60
50
40
30
2.5
5
10
Gel-MOD concentration (w/v %)

Figure II.21: Reaction scheme of the development of gel-MOD (A) and gel-MOD-AEMA (B) with the corresponding equations to calculate the degree of substitution (DS). (C) ^{1}H-NMR spectrum of gel-MOD-AEMA with the characteristic methacrylamide signals at 5.75 ppm and 5.51 ppm depicted in red, the methacrylate signals at 6.20 ppm and 5.80 ppm depicted in green and the reference signal corresponding to the -CH_3 groups present in valine, leucine and isoleucine at 1.01 ppm depicted in black. (D) Influence of gel-MOD concentration on the carboxylic acid DS of gel-MOD-AEMA.

Variation of the selected reaction conditions resulted in gel-MOD-AEMA derivatives with a different carboxylic acid DS. Experiments indicated that rather than increasing the amount of added reagents (data not shown), the gelatin concentration of the reaction mixture provides control over the DS. Indeed, a decreasing amount of methacrylate functions of 56% ± 11 % (0.60 mmol methacrylates/g gelatin) to 35% (0.38 mmol methacrylates/g gelatin) was obtained when increasing the gel-MOD concentration from 2.5 to 10 w/v % in the reaction mixture (Figure II.21 D). It is anticipated that this trend is a consequence of the superior gelatin chain mobility in DMSO at lower concentrations (cfr. the concentration-dependent viscosity) [142]. As a result, the accessibility of the carboxylic acids is increased, rendering them more prone to reaction [142].

When comparing the amount of cross-linkable double bonds of gel-MOD to gel-MOD-AEMA, it can be concluded that the proposed gelatin functionalization scheme enables a tripling of the total amount of crosslinkable functionalities (0.99 mmol/g gel-MOD-AEMA vs 0.37 mmol/g gel-MOD).

Table II.2: Effect of functionalization on the gelatin molecular weight as determined by gel permeation chromatography.

	Gelatin type B	Gel-MOD	Gel-MOD-AEMA
Mn (Da)	47900	35400	32800
Mw (Da)	97900	90600	77500
$Đ_M$	2.04	2.56	2.36

The original aim of the newly developed gel-MOD-AEMA was to obtain higher crosslinking densities to reduce post-production swelling and to improve the mechanical properties of the resulting hydrogels in comparison to gel-MOD. Therefore, all further experiments throughout the chapter are performed using gel-MOD-AEMA with the highest carboxylic acid DS (i.e. 56 %).
As the proposed functionalization scheme involves the reaction of gelatin with the primary amine functionalities of AEMA, gel permeation chromatography (GPC) was performed to reveal possible effects on the molecular weight (Table II.2). The results indicate that the influence of carboxylic acid modification on the molecular weight can be considered moderate (i.e. ± 7 % decrease in M_n) in comparison to the hydrolysis occurring during the

established primary amine modification procedure to obtain gel-MOD (i.e. ± 26 % decrease in M_n).

2.3. Influence of the Chemical Modification of Gelatin on the Physical and Covalent Crosslinking Properties of the Gelatin Hydrogels

2.3.1. Determination of the Physical Gelation Behaviour of Functionalized Gelatins via Differential Scanning Calorimetry

Gelatin is a protein which is characterized by a dissociation temperature (T_d) upon dissolution in water. This means that the material forms collagen-like triple helices below the T_d resulting in the formation of a physical network. The T_d is influenced by several key factors including the amino acid composition, the polymer molecular weight, the hydrophilicity/hydrophobicity and the DS (i.e. the number of incorporated functionalities) [121]. Visual observations of the herein developed materials indicated that, in contrast to unmodified gelatin and gel-MOD, solutions of gel-MOD-AEMA at concentrations of ≤ 15 w/v % remain soluble at room temperature rather than forming a physical gel. The latter observation was further substantiated by differential scanning calorimetry (DSC) experiments, following a protocol previously described in literature [142,240].

Similar dissociation temperatures (around 30°C) were observed for both gelatin derivatives and pristine gelatin type B (Figure II.22). The latter implies that triple helix formation occurs for all evaluated gelatin derivatives [240,298]. However, large differences in denaturation enthalpy could be distinguished (Figure II.22 B). The denaturation enthalpy is proportional to the number of hydrogen bonds associated with triple helix formation [120]. Indeed, the introduction of methacrylamides into the side chains of gelatin thereby forming gel-MOD resulted in a 7% decrease in intramolecular interactions including hydrogen bonds. The introduction of both methacrylamides and methacrylates in gel-MOD-AEMA resulted in a drastic decrease (70 %) in denaturation enthalpy (Figure II.22 B).

This drastic decrease may be attributed to several factors. First, it is known that variation of the average molecular weight of gelatin alters the physical gelation properties. However, because GPC measurements indicated only moderate hydrolysis, the contribution of the molecular weight to the

denaturation enthalpy can be regarded as limited. A more important effect can be attributed to the functionalization of the side chains thereby hampering efficient triple helix formation.

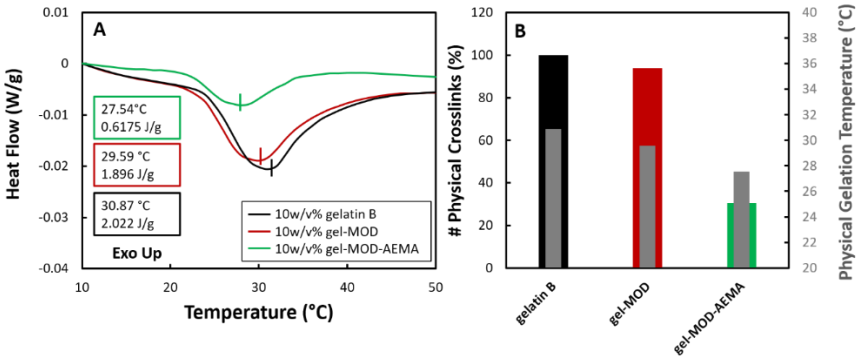

Figure II.22: DSC thermograms of 10 w/v % (functionalized) gelatin solutions (A). Physical gelation temperature and associated physical interactions of 10 w/v % gel-MOD and 10 w/v % gel-MOD-AEMA relative to the denaturation enthalpy of pristine gelatin type B (B).

The observed effect is more pronounced for gel-MOD-AEMA when compared to gel-MOD since more carboxylic acids are present in gelatin in comparison to primary amines. Consequently, the introduced functionalities will interfere more with triple helix formation resulting in the formation of less extended junction zones (cfr. shorter helices). The latter is in accordance with literature reports illustrating that the DS of gelatin can influence its physical gelation properties [121,138,187,295]. For the herein developed gel-MOD-AEMA, the amount of physical crosslinks as revealed by DSC, is apparently insufficient to induce gel-like behavior, as observed by the inverted tube method (data not shown). As a consequence, the derivative exhibits liquid-like behavior when solubilized in an aqueous environment at room temperature. This behavior is in accordance with the results obtained by Hoch et al. who observed a similar trend upon modifying the hydroxyl functionalities present in the hydroxyproline, serine, threonine, tyrosine and hydroxylysine amino acids [138][150]. Consequently, the material becomes more versatile for processing via additive manufacturing techniques which require room temperature solubility including digital light processing, widened objective working range (WOW) 2PP (i.e. meso scale 2PP benefitting from moving of the objective through the applied resin) as well as stereolithography [299].

2.3.2. Determination of the Mechanical Properties of Chain-growth Hydrogels Based on Functionalized Gelatins via (Photo-) Rheology

The observed differences in physical gelation properties of gel-MOD-AEMA were further studied through rheology experiments with the aim to reveal possible effects on the hydrogel mechanical properties. In a first assay, the crosslinking occurred via a photo-induced, chain-growth free radical polymerization mechanism and was monitored using photo-rheology. In this respect, the storage modulus G' was monitored as this provides an indication of the elastic behavior of a sample, which is related to the number of crosslinks present in a material [111]. During the experiment, a comparison based on the evolution of G' was made between crosslinking in the presence (Figure II.23 A) or absence (Figure II.23 B) of physical interactions. To this end, 10 w/v% precursor solutions were either cooled down to 5°C to induce physical gelation prior to UV exposure (Figure II.23 A) or heated to 37°C prior to UV-induced crosslinking to preclude the influence of physical interactions on the efficiency of chemical crosslinking (Figure II.23 B).

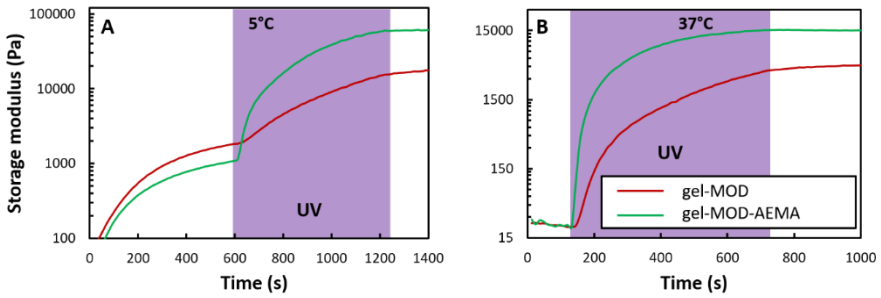

Figure II.23. Evolution in storage modulus of 10 w/v % gel-MOD and 10 w/v % gel-MOD-AEMA during UV-A-induced crosslinking at 500 mW/cm² with (A) and without (B) 10 min physical gelation at 5°C as determined by rheology. All experiments were performed in the presence of 2 mol% Irgacure 2959.

A clear difference in mechanical properties induced by physical gelation can be observed between 10 w/v% solutions of gel-MOD and gel-MOD-AEMA. Gel-MOD clearly outperforms gel-MOD-AEMA in terms of physical gelation (i.e. 2000 Pa for gel-MOD vs 1000 Pa for gel-MOD-AEMA) within the observed time frame which is in good agreement with the earlier discussed DSC results. However, the presence of these physical interactions does

significantly and positively affect the final stiffness after covalent crosslinking for both derivatives. Indeed, when inducing triple helices by lowering the temperature below the T_d prior to UV irradiation, the gelatin chains will organize. On the one hand this brings the crosslinkable functionalities in closer proximity to each other leading to more efficient crosslinking [248,300]. This hypothesis is substantiated by literature as similar observations were reported by Houben *et al.* for a synthetic crosslinkable hydrogel building block, for which self-organization due to crystallization induced phase-separation increased the observed crosslinking reactivity and associated mechanical properties [301]. On the other hand, the formed triple helices are partially locked by the covalent crosslinks thereby further increasing the final mechanical properties [248,300] (Figure I.9 D). As a consequence, UV-A irradiation of a physical network results in a more efficient crosslinking reaction, which is reflected by a substantially higher storage modulus obtained after crosslinking for both gel-MOD (i.e. 18 ± 1.3 vs. 4.7 ± 0.3 kPa) and gel-MOD-AEMA (i.e. 60.6 ± 0.6 vs. 14.9 ± 0.2 kPa) (comparison of Figure II.23 A & B).

Furthermore, the introduction of additional crosslinkable functionalities also positively affects the kinetics of the photo-induced crosslinking as indicated by the steeper slope of the G' curve during crosslinking for gel-MOD-AEMA in Figure II.23 A & B**.** Additionally, the increased crosslink density results in a higher stiffness of the crosslinked hydrogels as evidenced by a 3.0 to 3.6 fold increase in final storage modulus for gel-MOD-AEMA vs gel-MOD both in the presence (i.e. from 18 ± 1.3 kPa to 60.6 ± 0.6 kPa) and absence of physical interactions prior to crosslinking (i.e. from 4.7 ± 0.3 kPa to 14.9 ± 0.2 kPa) (comparison of Figure II.23 A & B).

Additionally, variation of the applied light intensity provides control over the final mechanical properties (Figure II.24 A). Lower light intensities result in a less densely crosslinked network and concomitant lower storage modulus [139]. This phenomenon can be considered very relevant when applying 2PP for material processing since the technique is characterized by a high spatiotemporal control in terms of the locally applied irradiation dose. As a consequence, the material could be applied to obtain structures with locally tuned stiffness, thereby mimicking natural tissue to a greater extent.

Since these *in situ* crosslinking experiments only provide insight in the mechanical properties of the hydrogels in the relaxed state prior to equilibrium swelling, crosslinked hydrogel films after equilibrium swelling were also monitored. Therefore, hydrogel films were prepared from different concentrations of both gelatin derivatives. Next, these films were equilibrium swollen in double distilled water at physiological temperature (37°C) and the

storage modulus was determined under the same conditions over a frequency range of 0.01-10 Hz.

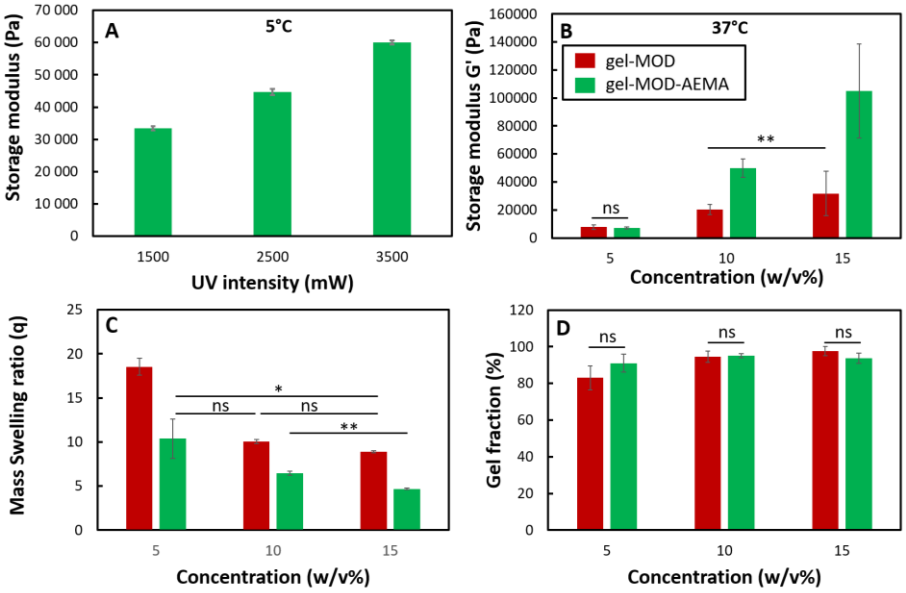

Figure II.24. Influence of applied UV-A irradiance on the final mechanical properties of 10 w/v % gel-MOD-AEMA with prior cooling at 5°C for 10 minutes and subsequent crosslinking for 10 min (A). Effect of gelatin functionalization and – concentration on the storage modulus of 1 mm thick equilibrium-swollen hydrogel films prepared via film casting at a UV-A irradiance of 2 * 4 mW/cm^2 after 30 min crosslinking (B). Mass swelling ratio (C) and gel fraction (D) of these thin films. All experiments were performed in the presence of 2 mol% Irgacure 2959. (in all images red refers to the use of gel-MOD and green refers to gel-MOD-AEMA) (all differences significant with P < 0.001 except when denoted otherwise with ** P < 0.01, * P < 0.05 and ns indicating no statistical significance)

The average storage moduli and associated standard deviations are presented in Figure II.24 B. First, the experiment indicated a frequency independent G' and G", indicating the presence of a crosslinked rubbery network [302] (data not shown). Secondly, besides variations in applied UV irradiation dose and the gelatin DS, varying the precursor concentration is another parameter that influences the mechanical properties of the resulting hydrogel[127,139]. The results indicate that gel-MOD-AEMA outperforms gel-MOD in equilibrium swollen conditions over the entire concentration range in terms of stiffness except at 5 w/v% for which no significant differences were

observed (Figure II.24 B). As a consequence, a higher amount of crosslinkable functionalities in the hydrogel precursor allows gel-MOD-AEMA to reach the same mechanical properties as gel-MOD albeit at lower concentrations. This is very relevant as previous findings from our group indicated that high gelatin concentrations negatively affect the biocompatibility [139]. It should be noted, that similar gel fractions (close to 100%, no significant differences) were obtained for all studied hydrogel films.

As a consequence, stable hydrogel films were formed for both derivatives and observed differences in stiffness cannot be attributed to incomplete crosslinking (Figure II.24 D).
In conclusion, when looking into potential tissue engineering applications, literature reports state that the obtained mechanical properties match the mechanical properties of a series of tissues (Figure II.25). These tissues range from soft tissue including brain tissue (G' = 3 to 12 kPa) [265] to relatively hard tissues including the intervertebral discs (G' = 8 to 93 kPa) [303]. Furthermore, a comparison between the obtained mechanical properties and those earlier reported for biomaterials, indicates that gel-MOD-AEMA scores more towards the higher end of the mechanical spectrum. In this respect, it outperforms all reported gelatin derivatives to date which have been crosslinked in the absence of a second material (e.g. Chondroitin sulphate, hyaluronic acid)[90][263] (Figure II.25). Additionally, the obtained mechanical properties are comparable to those described earlier for crosslinked collagen despite the less pronounced physical interactions inherent to gelatin [304,305].
The combination of the observed faster crosslinking kinetics with the superior mechanical properties of gel-MOD-AEMA are anticipated to be beneficial for lithography-based additive manufacturing purposes, as this can lead to shorter structuring times.

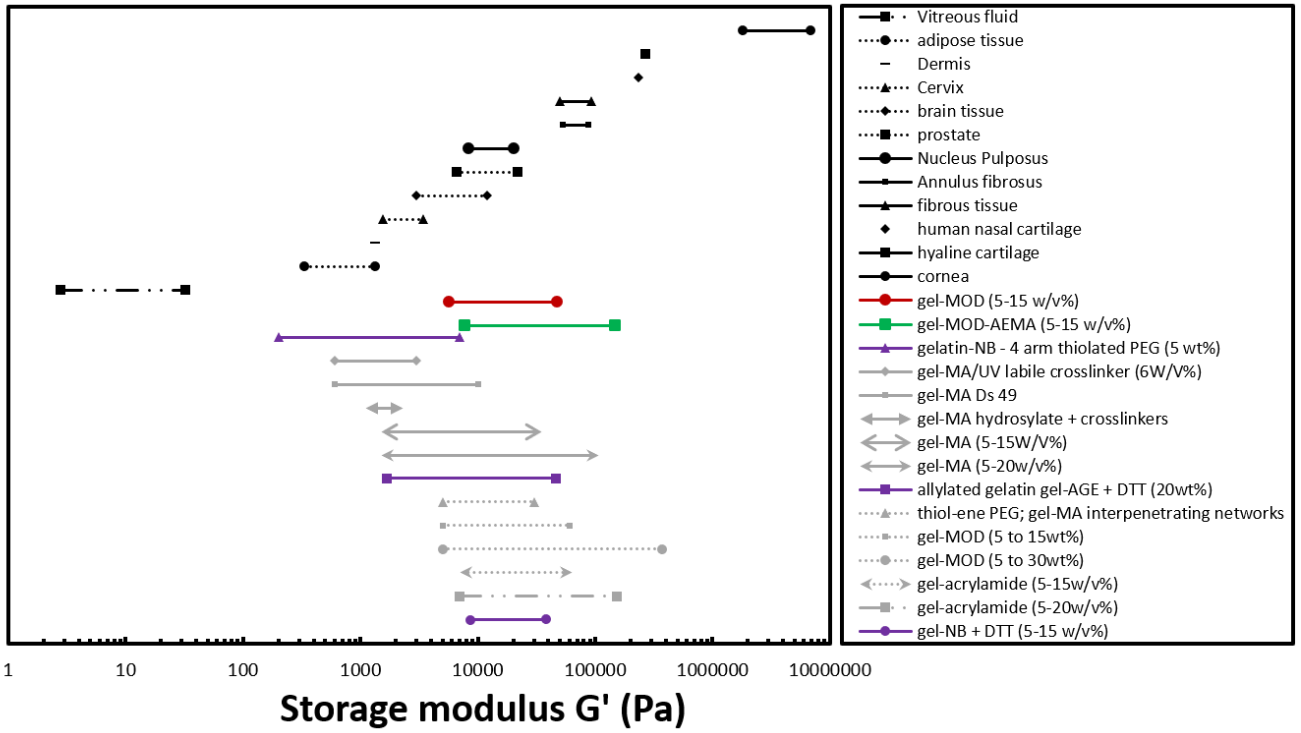

Figure II.25: Scheme presenting the mechanical properties of the gel-MOD and gel-MOD-AEMA hydrogels developed in the present chapter compared different crosslinked gelatin hydrogels reported in literature and the mechanical properties of various tissue types. Native tissues are depicted in black, chain-growth hydrogel systems are depicted in grey, step-growth hydrogel systems are depicted in purple.)(Adapted from [306] & [284])

2.3.3. Effect of Gelatin Functionalization and Concentration on the Hydrogel Gel Fraction, Water Uptake Capacity And Network Density

Hydrogel materials are generally excellent candidates for tissue culture since they mimic the aqueous environment present in the extracellular matrix, while providing mechanical support to the cells. Therefore, the equilibrium swelling degree of a hydrogel material is an important characteristic for ECM mimics. To this end, swelling at equilibrium was determined gravimetrically for both derivatives at varying precursor concentrations (Figure II.24 C).
The assay indicated that while still being able to absorb large quantities of water (≥ 350 %), the gel-MOD-AEMA derivative exhibits a significant reduction in equilibrium swelling compared to gel-MOD, this can again be attributed to a more densely crosslinked network. To further substantiate these observations, a more thorough comparison of the obtained network density can be calculated via the rubber elasticity theory using the average molecular weight, the equilibrium swelling ratio and the mechanical properties[139,307,308].

Rubber Elasticity Theory

This theory allows to obtain an estimation of several important parameters including the polymer volume fraction in the swollen state ($v_{2,s}$), the volumetric swelling ratio (Q), the average molecular weight between crosslinks ($\overline{Mc}$), the network mesh size (ξ) and the crosslink density (ρ_x). Q and $v_{2,s}$ are both indications for the amount of liquid that can be imbibed inside a hydrogel which can be calculated starting from the mass swelling ratio q [139,309].

$$v_{2,s} = \frac{V_p}{V_g} = \frac{1}{Q} = \frac{\left(\frac{1}{\rho_{gelatin}}\right)}{\left(\frac{q}{\rho_{H_2O}}\right) + \left(\frac{1}{\rho_{gelatin}}\right)} \quad (1)$$

Herein, V_p and V_g represent respectively the polymer volume and the hydrogel volume at equilibrium swelling, while ρ_{H_2O} and $\rho_{gelatin}$ represent the density of water and gelatin respectively. The density of water is 1 g/cm³ while the density of gelatin was estimated to be around 1.36 g/cm³ based on previous reports from literature [139,258,310,311]. Since all network chains within the characterized hydrogels follow the Gaussian statistics model (Figure II.26),

the obtained volumetric swelling ratio could be applied to determine $\overline{Mc}$ using the following equation [308,312].

$$G = \left(\frac{cRT}{\overline{Mc}}\right) * \left(1 - \frac{2\,\overline{Mc}}{M_n}\right) * \left(\frac{1}{Q^{1/3}}\right) \quad (2)$$

in which G is the shear modulus (atm), c is the concentration of gelatin in the solution, R is the universal gas constant (L*atm*K^{-1}*mol^{-1}), T is the temperature (K) and $\overline{Mc}$ is the average molecular weight between crosslinks (Da). Literature states that the shear modulus of hydrogels can be derived from the mean peak value of the storage modulus G‘, since the contribution of the loss modulus G“ to the shear modulus can be considered negligible for all analyzed hydrogel samples [139,302,313].

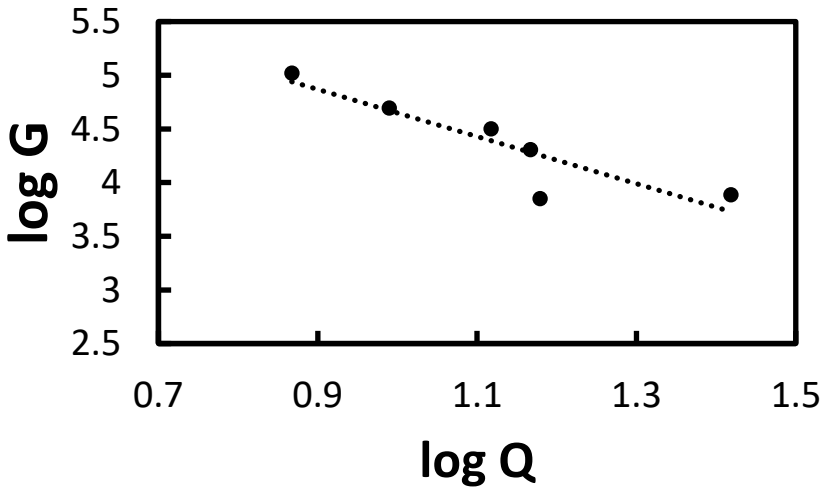

Figure II.26. Plot of log G vs log Q for all analyzed hydrogel films used in the rubber elasticity theory calculations.

To obtain the average weight between crosslinks ($\overline{Mc}$), equation (4) can be rewritten as:

$$\overline{Mc} = \frac{1}{\left(\frac{G}{cRTQ^{-1/3}}\right) + \left(\frac{2}{M_n}\right)} \quad (3)$$

Once the average molecular weight between crosslinks ($\overline{Mc}$) is known, an estimation of the average mesh size at equilibrium swelling (ξ) can be obtained using the following equation [248].

$$\xi = \left(\frac{2C_n\,\overline{Mc}}{M_r}\right)^{(1/2)} * l * Q^{(1/3)} \qquad (4)$$

with C_n being the Flory characteristic ratio which corresponds to 8.26 for gelatin based on reports from literature [248], M_r is the average molecular weight of one repeating unit or one amino acid (assumed to be around 94.7 g/mol) [236,248] and l is the length of a bond along the polymer backbone. Furthermore, it should be noted that equation (4) is derived from the Flory-Rehner theory which is only strictly valid for simple systems like vinyl polymers. Therefore, the factor 2 has to be replaced by a factor 3 since the repetitive unit contains 2 bonds in contrast to 1 bond in vinyl polymers [248]. For the same reason, the bond length along the polymer backbone was approximated as the average bond length of one bond along the polymer backbone, taken as the arithmetic mean of one carbonyl C-C bond (1.53 Å) one C-N bond next to the carbonyl (1.32 Å) and a C-N bond (1.47 Å) [248,314]. The crosslink density ρ_x is a measure for the number of crosslinks present per unit of volume and can be calculated from $\overline{Mc}$ and $\bar{\nu}$, in which $\bar{\nu}$ corresponds to the specific volume of gelatin, that was determined to be 0.735 cm³/g according to a previous study using the same batch of gelatin [139].

$$\rho_x = \frac{1}{\bar{\nu}\,\overline{Mc}} \qquad (5)$$

A summary of the experimentally obtained results based on GPC, rheology and gravimetric swelling assays is presented in Table 3, along with the calculated results obtained using the rubber elasticity theory.

The results clearly indicate a correlation between the initial gelatin concentration, the amount of crosslinkable functionalities and the density of the obtained network. This is reflected by a decreased average molecular weight between crosslinks (M_c) and increased crosslink density (ρ_x) both upon increasing the precursor concentration and increasing the amount of crosslinkable functionalities.

Table II.3. Influence of concentration and gelatin derivative on gel fraction, mass swelling ratio, Q, G', Mc, ξ and ρ_x. In this table, the columns denoted with * are measured values and columns denoted with ‘ are calculated from these measurements.

sample	# crosslinkable functionalities (mmol/$g_{gelatin}$)	initial concentration (% w/v)	Gel fraction*	mass swelling ratio*	G' at 37°C (kPa)*	Q	Mc ‘(g/mol)	ξ (Å)	ρ_x (*10^{-4}) (mol/cm^3)
gel-MOD	0.37	5	83.0 ± 6.5	18.5 ± 1.0	5.7 ± 0.3	26.21	5326	160	2.55
		10	94.5 ± 3.0	10.1 ± 0.2	22.1 ± 0.3	14.68	3752	110	3.63
		15	97.7 ± 2.5	8.9 ± 0.1	47.5 ± 0.8	13.11	2892	93	4.7
gel-MOD-AEMA	0.99	5	91.0 ± 4.9	10.4 ± 2.2	7.7 ± 0.4	15.11	4783	126	2.84
		10	95.1 ± 1.2	6.4 ± 0.2	56.2 ± 1.2	9.76	1899	69	7.16
		15	93.7 ± 2.9	4.7 ± 0.1	147.1 ± 2.9	7.37	1248	51	10.9

As a result, the observations from swelling assays as well as rheological measurements can be attributed to network density. Furthermore, it should be noted that rheology and swelling experiments were performed above the T_d of the gelatin derivatives (27°C – 30°C as determined by DSC) (Figure II.22). Consequently, the obtained crosslink densities can only be attributed to the presence of covalent crosslinks without the influence of interfering physical interactions. However, as previously discussed, physical interactions prior to covalent crosslinking did result in an increased final gel strength and therefore, a more densely crosslinked network.

2.4. Effect of Gelatin Functionalization and Concentration on Enzymatic Degradation

To assess to what extent the biodegradable properties of gelatin were preserved upon derivatization and subsequent crosslinking, *in vitro* degradation experiments have been performed in the presence of collagenase (100 CDU/ml). The results indicated that gel-MOD-AEMA remains fully enzymatically degradable as previously reported for other crosslinked gelatin derivatives [312]. However, the presence of additional crosslinks (i.e. 25.5 & 36.3 mmol/cm³ for respectively 5 & 10 w/v % gel-MOD and 28.4 & 71.6 mmol/cm³ for respectively 5 & 10 w/v% gel-MOD-AEMA) in combination with a decreased water uptake capacity results in a reduced inter-crosslink chain mobility. This effect combined with the fact that more bonds need to be cleaved for denser crosslinked networks, results in a longer degradation time. Indeed, the degradation time for gel-MOD-AEMA is substantially larger (up to a factor of 7.5 for both 5 and 10 w/v% hydrogels) (Figure II.27)**.** It should be noted that for gel-MOD-AEMA only the extrapolated final degradation times are presented. However, the materials were fully degradable since after somewhat less than 30 hours, no material was left after washing and freeze-drying for all studied samples.

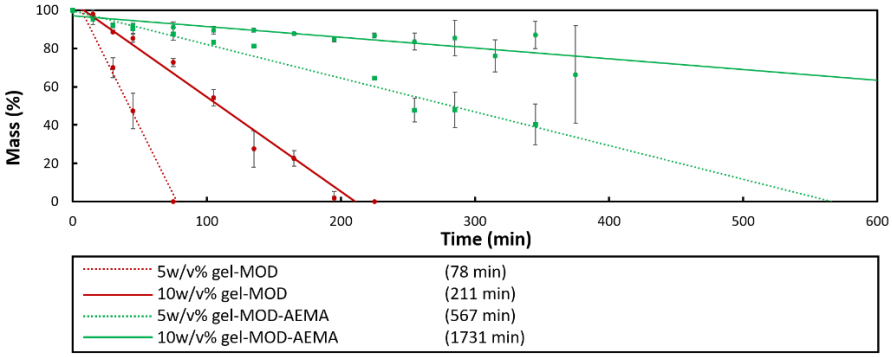

Figure II.27. *In vitro* degradation behavior of gel-MOD (red) and gel-MOD-AEMA (green) in the presence of 100 CDU/ml collagenase starting from different polymer concentrations (5 versus 10 w/v %). The extrapolated final degradation times are given in between brackets.

2.5. Influence of Gelatin Functionalization on *In Vitro* Biocompatibility

Despite the beneficial material properties, the developed derivative has to retain its favorable cell-interactivity to remain suitable for tissue engineering purposes. Therefore, *in vitro* biological tests were performed on hydrogel coated glass slides using both MC3T3-E1 pre-osteoblasts and L929 fibroblasts. To this end, the metabolic activity of the cells was monitored over the course of 7 days at regular time points using a Presto-blue based assay. The results of the assays are depicted in Figure II.28**.** To ensure a more quantitative comparison, all samples were normalized against the TCP control after 7 days of culture (= 100%). Since a clear increase in metabolic activity is observed as a function of time, the cells can be considered healthy and proliferating on all substrates throughout the course of the experiment. It should however be noted that for the MC3T3 cells, the increase in metabolic activity between day 3 and day 7 is less pronounced. This is a phenomenon also observed in literature for this cell type as typically the metabolic activity reaches a plateau corresponding to the confluence state [315]. In the performed assay, confluence was indeed reached between day 3 and day 7 resulting in a plateau in metabolic activity. Furthermore, no significant difference in metabolic activity could be observed between gel-MOD-AEMA and gel-MOD, which is currently one of the gold standards in the field of biofabrication and tissue engineering [125,316] (see also Chapter 1). Additionally, for the MC3T3 cells, all substrates exhibited a metabolic activity of > 70% after 7 days of culture, while the metabolic activity for the L929 cells exceeded 90% for all

substrates. As a consequence, both materials can be considered biocompatible and suitable for tissue culture of both cell types.

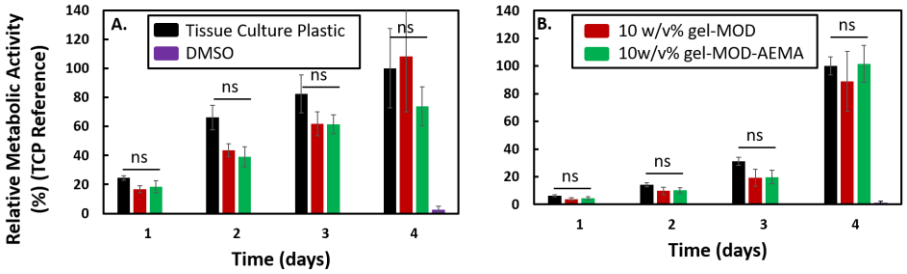

Figure II.28. Presto blue assay performed on hydrogel coated glass slides, expressing the metabolic activity of MC3T3-E1 pre-osteoblasts (A) and L929 fibroblasts (B), relative to a tissue culture plastic (TCP) reference and DMSO as a negative control.

2.6. Influence of Gelatin Functionalization and Concentration on Two-Photon Polymerization Potential

To prove the suitability of the material for laser-based additive manufacturing purposes, 2PP experiments were performed comparing gel-MOD to gel-MOD-AEMA solutions. By scanning a tightly focused femtosecond pulsed (70 fs at 80 MHz) near infrared (800 nm) laser beam through the solutions in the presence of a suitable photoinitiator, local polymerization can occur in the focal spot (voxel) as a result of the simultaneous absorption of two photons by the photoinitiator (Figure II.22 A). As a result, the photoinitiator will generate radicals, thereby locally inducing a chain-growth free radical polymerization reaction between the methacrylamides and methacrylates resulting in crosslinking (Figure II.29 A). Consequently, a complex 3D hydrogel construct can be fabricated by scanning the focal spot through the precursor solution according to a CAD model followed by dissolution and washing away of uncrosslinked material. In the majority of reports, 2PP fabrication using gelatin-based solutions has only been reported for concentrations starting from 20 wt% functionalized gelatin or when using an additional crosslinker [96,97,129,233,276] (see also Chapter 1).

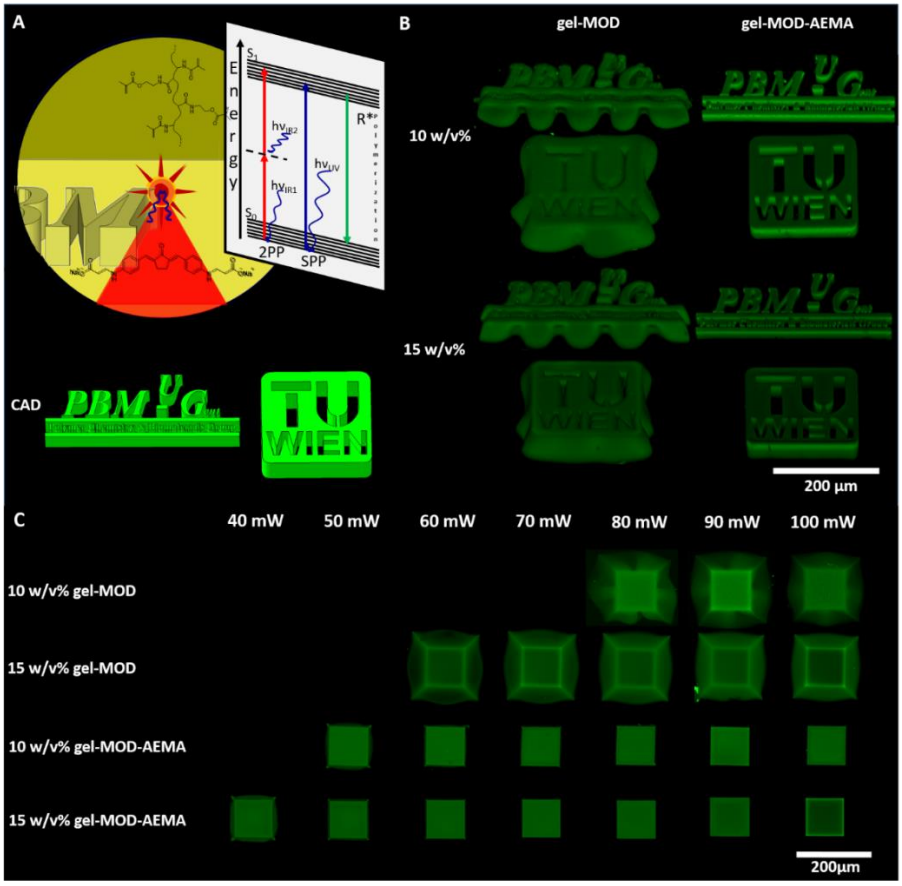

Figure II.29. Schematic representation of the two-photon polymerization (2PP) principle on gel-MOD-AEMA in the presence of P2CK as photoinitiator including a Jablonski diagram demonstrating the theoretical background for which single photon excitation (blue) is compared to two photon excitation (red) (A). Applied CAD model and structured logos expressing clear differences in swelling and swelling-related deformations between gel-MOD and gel-MOD-AEMA at different concentrations (B). (TU Wien logo printed with permission from the TU Wien, PBM logo printed with permission from the Polymer Chemistry and Biomaterials research group at Ghent university) Semi-quantitative analysis of structuring range and related swelling (observed as a ‚halo' around the square) for both derivatives via 3D renderings of the generated cubes (r = 100 µm) imaged through the glass slide after 24 hours of incubation at 37°C (C). (all experiments were performed in the presence of 2 mol% P2CK at a laser scanning speed of 100 mm/s).

Due to the higher reactivity and superior mechanical properties, the reported gel-MOD-AEMA precursors are anticipated to be a superior alternative for gel-MOD from a processing perspective. In order to prove this hypothesis, the swelling properties and the CAD mimicry of conventionally applied gel-MOD and the novel gel-MOD-AEMA derivative have been compared using different polymer concentrations (5-15 w/v%) and various average laser powers (10-100 mW) in solutions containing 2 mol% P2CK, a biocompatible and efficient 2PP photoinitiator [129,232,294] (Figure II.29 B & C and Figure I.17).

The degree of volumetric swelling obtained after 2PP was assessed. The swelling not only provides insight in the crosslink density of a material but is also very relevant when targeting additive manufacturing and, more specifically 2PP. As a consequence of post-production swelling, adaptations are often required to the CAD model to compensate for these deformations to result in reproducible computer aided manufacturing (CAM) [317]. Furthermore, swelling is also correlated with the applied irradiation dose (Figure II.29 C). Unfortunately, swelling is often not uniform and even design-dependent. As a result, it becomes challenging to anticipate and correct for post-production swelling-related morphological changes when generating the CAD design. Inhomogeneous swelling can induce local stress areas and result in distortions of the construct architecture as depicted for gel-MOD in Figure II.29 B [233]**.** Therefore, the correlation between swelling, irradiation dose and precursor concentration was qualitatively assessed by imaging cubes polymerized on methacrylated glass via 2PP. The bottom (100 * 100 µm) of the hydrogel structures is covalently attached to the methacrylated glass thereby preventing swelling and mimicking the dimensions of the CAD model. The top part of the structure however, is free to swell during development of the sample. Consequently, a ‚halo'-like contour is present behind the bottom surface when imaged through the glass slide (Figure II.29 C). These qualitative observations were quantified by comparing the length of one side of the cube of the bottom slice attached to the glass with the length of the equilibrium swollen top section of the cube (Figure II.30 A). Clearly, the concentration and the applied average laser power affect the swelling of gel-MOD structures, especially at lower polymer concentrations. However, for gel-MOD-AEMA the effect, although still present, is less pronounced since swelling is nearly absent for average laser powers of 80 mW onwards both for 10 and 15 w/v% solutions. As a consequence, a close CAD/CAM shape fidelity of gel-MOD-AEMA hydrogels is demonstrated (Figure II.29 C and Figure II.30 A). This significantly reduced swelling behavior is a consequence of a decrease in average molecular weight between the crosslinking points.

As a result, the mobility of the polymer chains within the network is lowered and the water uptake capacity decreases, as discussed earlier [139,258]. A second observation was the fact that no reproducible structures could be obtained starting from 5 w/v% solutions of gel-MOD or gel-MOD-AEMA. To obtain more insight in this matter, an estimation of the amount of crosslinkable functionalities present in one voxel was calculated for both derivatives at the applied precursor concentrations. An estimation of the two-photon excitation (TPE) volume of one voxel was calculated by approximating the illumination point spread function² (IPSF²) (Figure II.30 B) as a three-dimensional Gaussian analytical integration [275].

$$V_{TPE} = \pi^{3/2} \omega_{xy}^2 \omega_z \quad (6)$$

To calculate this Gaussian volume, the 1/e width in the lateral (ω_{xy}) and axial (ω_z) dimension was calculated using the following formulas as described in literature [275].

$$\omega_{xy} = \frac{0.325\,\lambda}{\sqrt{2}\,NA^{0.91}}\ NA\ (if\ NA > 0.7) \quad (7)$$

$$\omega_z = \frac{0.532\,\lambda}{\sqrt{2}} \left(\frac{1}{n - \sqrt{n^2 - NA^2}} \right) \quad (8)$$

The numerical aperture (NA) of the applied objective is 0.85 as provided by Zeiss. The NA of a system is defined by half the maximum angle of the focussing cone exiting the objective and the refractive index of the objective according to the following formula [318].

$$NA = n \sin \theta \quad (9)$$

With n being the refractive index (i.e. 1.33 as it is a water-immersion objective) and θ being half the maximum angle of the focussing cone exiting the objective. The refractive index of the crosslinkable gelatin solutions was measured using a refractometer and is presented in Figure II.30 C.

To calculate the amount of double bonds present in the voxel, the concentration of the applied gelatin solution was combined with the calculated amount of double bonds present in the material to obtain the number of double bonds/volume (Figure II.30 C).
It should be noted that, although more crosslinkable functionalities are present in 5 w/v % solutions of gel-MOD-AEMA as compared to 10 w/v % gel-MOD, no reproducible structures could be obtained starting from 5 w/v % gel-MOD-AEMA although the polymerization could be monitored during

structuring. However, the poor mechanical properties of the material starting from a 5 w/v % concentration render it insufficiently strong to support its own weight during structuring and lead to a partial loss of the structure during the development. As a consequence, only parts of the structure remained after development (data not shown).

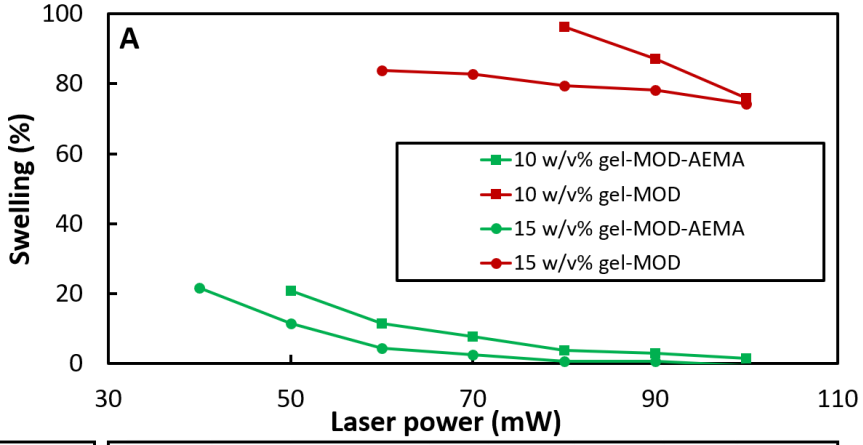

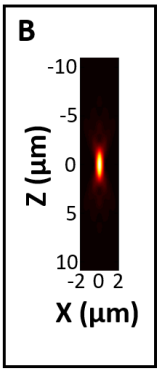

C

Material	# Double Bonds/ g	Concentration (w/v%)	n	ω_{xy} (nm)	ω_z (nm)	V_{TPE} (µm³)	# Double Bonds/ Voxel (mmol)
gel-MOD	0.37	5	1.349	213.15	998.643	0.252	4.67E-15
	0.37	10	1.347	213.15	996.136	0.252	9.32E-15
	0.37	15	1.355	213.15	1004.060	0.254	1.41E-14
gel-MOD-AEMA	0.99	5	1.348	213.15	997.133	0.252	1.25E-14
	0.99	10	1.350	213.15	998.921	0.253	2.50E-14
	0.99	15	1.354	213.15	1002.735	0.253	3.76E-14

Figure II.30. Semi-quantitative swelling analysis performed on printed cubes (r = 100 µm) by comparison of the surface area of the bottom slice attached to the glass and the top slice of the printed cube after equilibrium swelling (A). The structuring range of both derivatives as well as the influence of the applied average laser power on the swelling is demonstrated. Exemplary schematic representation of the point spread function as a consequence of tight focusing exhibiting an ellipsoid morphology (B)[319]. Table estimating number of double bonds within the same volume voxel of different materials (C). (all experiments performed in the presence of 2 mol% P2CK at a laser scanning speed of 100 mm/s)

Furthermore, the combination of more crosslinkable functionalities per voxel (Figure II.30 B) combined with more favorable crosslinking kinetics for gel-MOD-AEMA results in the formation of denser networks, even at low concentrations (as mentioned before). Therefore, lower irradiation doses enable the generation of similar mechanical properties for gel-MOD-AEMA when compared to gel-MOD even at higher concentrations and average laser powers (e.g. 10 w/v % gel-MOD-AEMA exhibits a similar stiffness compared to 15 w/v % gel-MOD, Figure II.24 B). Consequently, it is anticipated that higher writing speeds can be applied to gel-MOD-AEMA to obtain similar mechanical properties in combination with a lower swelling degree relative to gel-MOD.

To visualize the true CAD/CAM fidelity for the novel gel-MOD-AEMA precursors, more complex structures were also constructed starting from 10 and 15 w/v % concentrations (Figure II.29 B). Furthermore, it is demonstrated that even fine features (down to 1 µm with high aspect ratio 1:40 as evidenced by the small features apparent in the PBM logo) were closely reproduced using the novel gelatin derivative (Figure II.29 B). Consequently, sub-cellular dimensions (≤ 10-20 µm) [320] could be realized with high aspect ratios using gel-MOD-AEMA as starting material. It is therefore anticipated that the combination of gel-MOD-AEMA and 2PP will become a powerful tool in the study of cellular responses towards ultra-small biocompatible hydrogel structures, thereby influencing cellular behavior, and to guide cells into a desired morphology or pathway [321].

Additionally, it should be noted that usually in a physical gel, the structures are typically written in a bottom up approach, meaning that the laserbeam is focused from the bottom through a glass slide on top of which the crosslinkable resin is situated. However, in that respect, there are severe size limitations in the z-direction related to the focal length of the objective. For example, in the currently applied 32X objective, the focal length (f) is 1.1 mm (as provided by Zeiss), meaning that the maximum attainable construct height equals 1.1 mm – 0.17 mm (thickness of the glass) or 930 µm. Furthermore, when a bottom-up approach is performed, there will be additional issues with spherical aberrations due to refractive index mismatch between the glass and the material on the one hand, and between the crosslinked and uncrosslinked material. As a consequence, elongation of the voxel will occur when writing the upper parts of the structure [322]. A strategy to circumvent this issue is the use of dip-in laser lithography or widened objective working range-2PP where the objective is immersed inside a liquid resin [299,323]. In this respect, especially WOW-2PP is of interest, because there, a glass slide is placed on top of the objective, with glass matching immersion oil in between [299]. As a

result, polymerization occurs immediately in the focal spot, without resulting in voxel elongation due to a refractive index mismatch between the glass and the material. As a consequence, high resolution meso-scale 2PP becomes accessible, as larger designs can be split up in smaller sections, which can be structured next to each other. However, in order to perform this technique, a liquid resin is required. Therefore, in contrast to gel-MOD, gel-MOD-AEMA does not form a physical gel at room temperature (*vide supra*), it allows for meso-scale production via 2PP thereby drastically increasing the maximum attainable construct size from the µm to the mm scale.

2.7. Conclusions

The combination of primary amine functionalization with subsequent carboxylic acid modification to introduce crosslinkable moieties proves to be an elegant tool to increase the 2PP potential of gelatin-based hydrogel precursors following a chain-growth polymerization crosslinking approach. In addition to superior material stiffness, gel-MOD-AEMA also exhibits faster crosslinking kinetics compared to conventionally applied photo-crosslinkable chain-growth gelatin derivatives. Furthermore, nearly no post-processing swelling occurred upon applying gel-MOD-AEMA while the material biocompatibility with respect to *in vitro* tissue culture potential was sufficiently maintained. The above-mentioned factors render the material ideal for 2PP processing at high-resolution (feature sizes of around 1 µm) and increase the additive manufacturing potential of gelatin precursors in general for which faster crosslinking kinetics, lower swelling ratios and superior mechanical integrity can increase the maximum attainable writing speeds in combination with a higher shape fidelity for the applied CAD without compromising biocompatibility. Furthermore, the absence of visually observable physical gelation at room temperature increases the potential of gel-MOD-AEMA for layer-by-layer and WOW/dip-in laser lithography techniques which drastically increases the maximum attainable construct sizes. This aspect clears the road towards the production of patient-specific macro-structures, up to several millimeters in size, containing ultraprecise micro-features to optimize the desired cellular behavior. Furthermore, the applied polymer functionalization can be translated towards other (bio)polymers containing free carboxylic acids including collagen, elastin and glycosaminoglycans. In this respect, the ECM-mimicking toolbox can be further expanded towards a new platform consisting of highly specific processable materials enabling close reproductions of living tissue.

Chapter 3:
Expanding the Capabilities of Photo-Crosslinkable Gelatin Hydrogels Using a Step-Growth Crosslinking Approach

The *in vitro* cell work in the present chapter was performed by dr.. Marica Markovic.The NMR spectra of the gelatin derivatives were measured by dhr. Tim Courtin

Parts of this chapter have been published in:

> **J. Van Hoorick**, P. Gruber, M. Markovic, M. Rollot, G-J. Graulus, M. Vagenende, M. Tromayer, J. Van Erps, H. Thienpont, J. C. Martins, S. Baudis, A. Ovsianikov, P. Dubruel, S. Van Vlierberghe, *Macromolecular Rapid Communications **(2018)**,* **39**(14) 1800181

3.1. Introduction

In the previous chapter, attempts were made to improve the capabilities of chain-growth gelatin-based hydrogels. Although the introduction of additional crosslinkable functionalities resulted in a higher network density and associated superior mechanical properties and decreased swelling resulting in improved 2PP processing capabilities, there was still room for improvement in terms of reaction kinetics. Furthermore, previous studies indicated that the presence of a too densely crosslinked network has a negative influence on cell viability and migration, especially when aiming to use the material as a bioink (i.e. in case of cell encapsulation)[100,139,152,252] (Figure III.31).

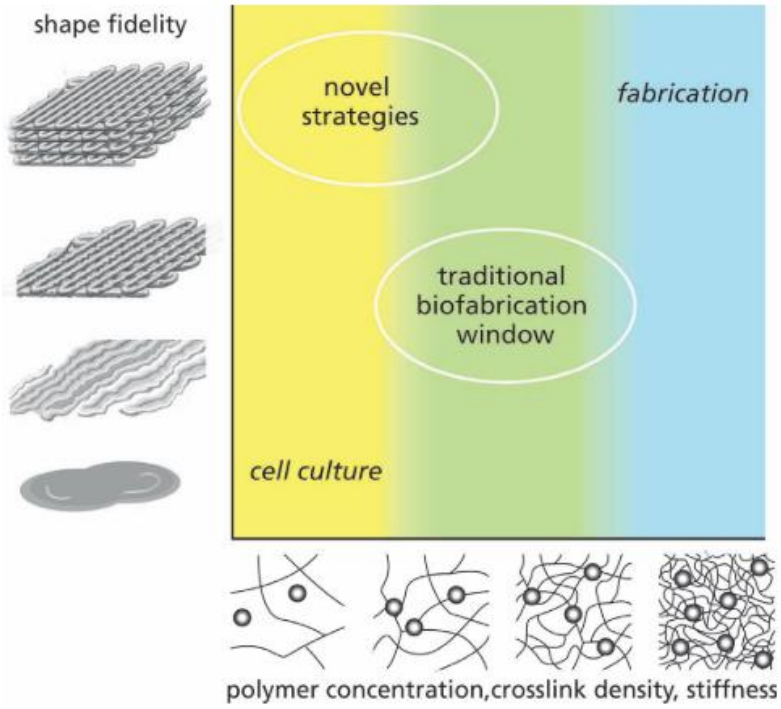

Figure III.31: visualization of the paradox between shape fidelity and biocompatibility of hydrogels. (Image reproduced from [252])

Therefore, in the present chapter, a different, more reactive crosslinking approach is applied benefitting from thiol-ene photo-click chemistry. As a result, hydrogel networks can be obtained that can be crosslinked using a step-growth crosslinking approach via the reaction of complementary

functionalities. As a consequence, the obtained network does not contain non-degradable hydrophobic kinetic poly(methacryloyl) chains resulting in network inhomogeneity [146] (Figure I.9 C).

Thiol-ene photo-click hydrogels are typically characterized by a higher reactivity and the formation of more homogeneous networks due to their orthogonal nature [146]. Consequently, they exhibit superior compatibility towards cell encapsulation since the crosslinking reaction can efficiently take place in the presence of oxygen while also being characterized by lower radical concentrations [115,146,162,168,324]. To perform thiol-ene chemistry, several functionalities have already been reported in literature including vinyl ethers, acrylates, methacrylates and norbornene moieties (Figure I.8) [146,176,325]. Of specific relevance is the use of norbornene, as it cannot undergo competitive homo-polymerization in contrast to e.g. acrylates [115,162,176]. Additionally, the ring strain present in norbornene renders it more reactive towards thiols in comparison to vinyl ethers [167]. As a result, only efficient step-growth polymerization crosslinking will occur in the presence of a complementary thiolated crosslinker [176]. Therefore, the present chapter focusses on the modification of gelatin using 5-norbornene-2-carboxylic acid to yield Gel-NB for subsequent 2PP processing.

3.2. Modification of Gelatin Type B with Norbornene Functionalities: Reaction Condition Study

The introduction of norbornene functionalities was pursued using conventional carbodiimide/N-hydroxysuccinimde coupling (EDC/NHS) chemistry between the carboxylic acid functionality of 5-norbornene-2-carboxylic acid and the primary amines of gelatin (Figure III.33 A). A one-pot approach was targeted consisting of two reaction steps. First, the carboxylic acid of 5-norbornene-2-carboxylic acid was converted into an active succinimidyl ester via reaction with EDC/NHS to enable subsequent reaction with the primary amines of gelatin. However, during this synthesis, the presence of unreacted EDC molecules should be eliminated as they can on the one hand result in the formation of zero-length crosslinks between the primary amines present in the (hydroxy)lysine and ornithine amino acids and the carboxylic acids of the glutamic and aspartic acid amino acids present gelatin [48,284]. On the other hand, it is of predominant importance that all the EDC is reacted prior to the addition of the gelatin, as the combination of a carbodiimide and an acid catalyst (i.e. 5-norbornene-2-carboxylic acid) in DMSO could result in oxidation of the alcohols present in the hydroxyproline, serine, threonine, tyrosine and hydroxylysine amino acids in gelatin into their

respective aldehyde or ketone following a Pfitzner-Moffatt-oxidation [326] (Figure III.32). These aldehydes can also result in crosslinking of gelatin via reaction with the primary amines of gelatin resulting in Schiff's base formation [48].

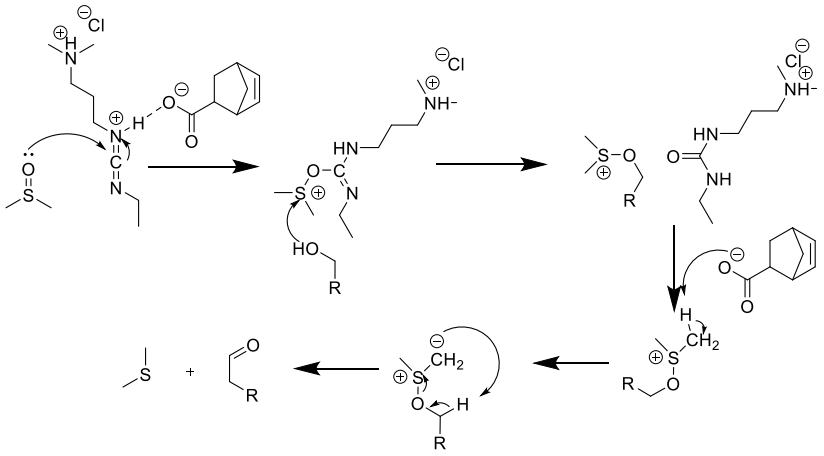

Figure III.32: Undesired Pfitzner-Moffatt Oxidation which can occur with DMSO in the presence of EDC and 5-norbornene-2-carboxylic acid.

The reaction efficiency was quantified using ^{1}H-NMR spectroscopy. To this end, a comparable methodology was performed as with gel-MOD using the proton signals of the "ene" functionality in norbornene (see Chapter 2) (Figure III.33 B) [289]. However, since the applied norbornene derivative is a mixture of both the endo- and exo-isomer of 5-norbornene-2-carboxylic acid, four signals are observed instead of two, of which two peaks correspond to the endo-form (6.33 ppm (m, 0.06-0.75 H depending on the DS) and 6.00 ppm (m, 0.06-0.75 H depending on the DS)) and the two other signals (6.28 ppm (m, 0.05-0.45H depending on the DS) and 6.26 ppm (m, 0.05-0.45H depending on the DS)) to the exo-derivative [327]. Consequently, the four peaks need to be taken into account for the integration. Furthermore, because the peaks of the exo-derivative cannot be separated fully, these signals are grouped and the DS can be obtained by taking the average of these signals and comparing it to the reference signal at 1.01 ppm (s, 9.96 H) resulting in the following equation:

$$DS(\%) = \left[\frac{\frac{I_{6.33\ ppm} + I_{6.28\ \&\ 6.26\ ppm} + I_{6.00\ ppm}}{2 * 0.0385\ mol/100g}}{\frac{I_{1.01\ ppm}}{0.3836\ mol/100g}} \right] * 100$$

$$= \left[\frac{I_{6.33\ ppm} + I_{6.28\ \&\ 6.26\ ppm} + I_{6.00\ ppm}}{2 * I_{1.01\ ppm}} \right] * 9.96 * 100 \qquad (10)$$

This method was further verified using an ortho-phtaldialdehyde assay for primary amine detection using n-butylamine standards [187] (Data not shown). A parametrical optimization study investigating the influence of the reaction time and of the 5-norbornene-2-carboxysuccinimidyl-ester/gelatin primary amine ratio on the final degree of substitution (DS) was performed (Figure III.33 C). On the one hand, a minimal reaction time of 15 h yielded the highest DS (after a 25 h reaction yielding the succinimidyl ester). On the other hand, varying the 5-norbornene-2-carboxysuccimidyl-ester/gelatin primary amine ratio present in the reaction mixture can be applied to control the DS. This can be achieved by varying the EDC and associated 5-norbornene-2-carboxylic acid content as this is the limiting reagent in the modification. The highest DS was obtained using 2 equivalents of EDC, 3 equivalents of NHS and 2.5 equivalents of 5-norbornene-2-carboxylic acid and a reaction time of 15 h yielding 0.35 mmol norbornene functionalities/g of gelatin (DS ~ 90%). The addition of 0.75 equivalents of EDC, 1.5 equivalents of NHS and 1.2 equivalents of 5-norbornene-2 carboxylic acid combined with a reaction time of 15 h yields a DS of 63% or 0.23 mmol/g gelatin.

Although the use of 5-norbornene-2-carboxylic acid has previously been reported for the modification of gelatin [324], it is the first time that the modification has been performed yielding Gel-NB with a high degree of substitution (DS) (i.e. > 45% or > 0.22 mmol/g) [115,324]. Additionally, this high DS can be obtained via a one-pot synthesis approach. It should be noted that Munoz et al. also reported on a one-pot synthesis yielding gel-NB via the reaction of carbic anhydride with the primary amines in gelatin [168]. However, after optimization of the reaction conditions, the DS did not exceed 45%. Additionally, this high DS was obtained after 70h of reaction, whereas the proposed synthesis route in the present chapter results in a maximal DS of ± 90% after 40 h of reaction [168].

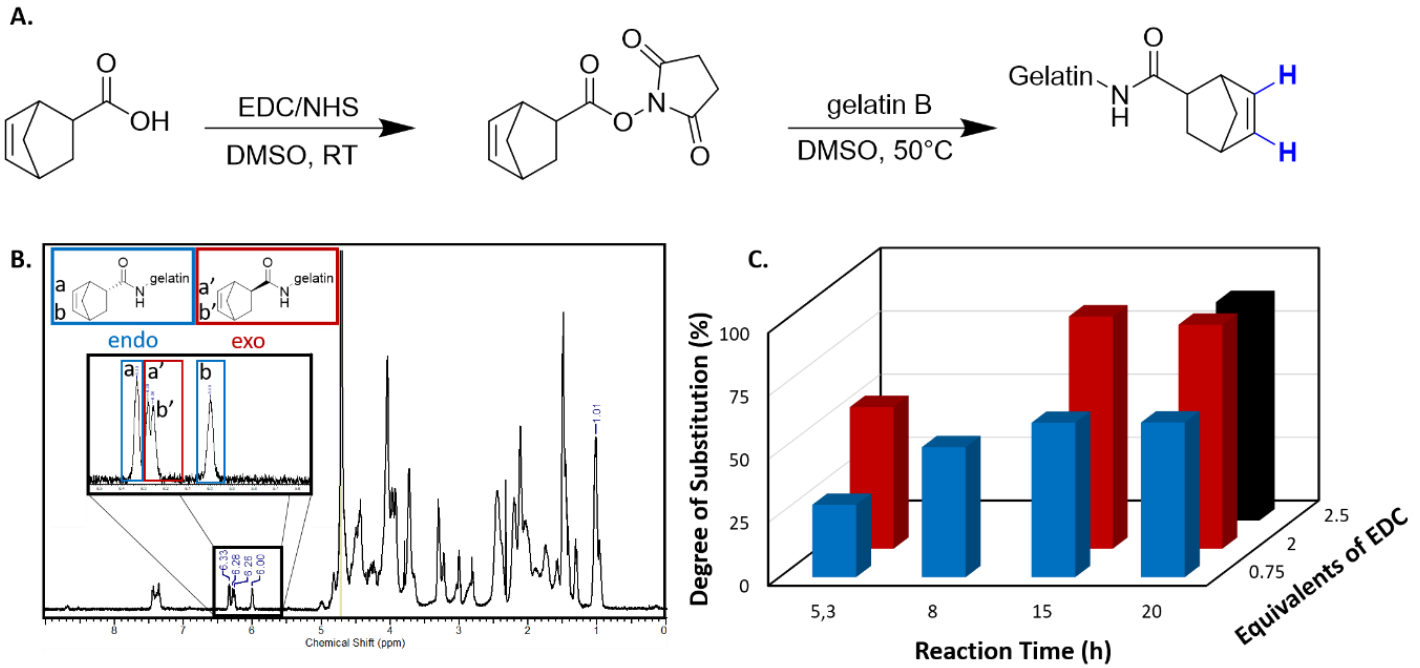

Figure III.33: Reaction scheme showing the modification of gelatin B to Gel-NB; (B) 1H-NMR spectrum indicating the coupling of both the endo- and the exo-5-norbornene-2-carboxylic acid to gelatin; (C) Parametric optimization of the reaction parameters to yield Gel-NB (only the assessed conditions are displayed

Additionally, although the use of thiol-ene crosslinkable gelatin hydrogels has already been described for the use in biofabrication and additive manufacturing [146], this is the first time that a thiol-norbornene crosslinking scheme is reported using 2PP to process gelatin derivatives. In order to obtain quantitative insights in the performance of the reported Gel-NB, it is benchmarked to the widely used Gel-MOD in terms of physico-chemical characteristics, 2PP processing as well as biocompatibility.

3.3. Quantitative Physico-Chemical Characterization of the Developed Hydrogels

Gel-NB was benchmarked to Gel-MOD with a similar DS (~65%) in all further experiments to allow a quantitative comparison. All Gel-NB characterization experiments were performed in the presence of 0.5 equivalents of DTT corresponding to an equimolar thiol/norbornene ratio unless stated otherwise. In a first assessment, the influence of the modification of the gelatin into gel-NB on the molecular weight of gelatin was assessed using GPC and benchmarked to gel-MOD (Table III.4). The results indicate that the modification with norbornene functionalities results in more hydrolysis in comparison to gel-MOD as reflected by a larger decrease in M_n (i.e. 16% and 25% respectively). However, in this respect, it should be noted that the differences in weighted average molecular weight (M_w) are almost not present. Furthermore, the introduced norbornene functionalities exhibit a higher hydrophobicity in comparison to the introduced methacrylamides in gel-MOD (i.e. $LogP_{5\text{-norbornene-2-carboxylic acid}} = 1.31$ vs $logP_{methacrylamide} = -0.23$) [328].

Table III.4: Effect of the introduction of norbornene functionalities on the molecular weight of the gelatin as determined by gel permeation chromatography.

	Gelatin type B	Gel-MOD	Gel-NB
Mn (Da)	50500	42500	37700
Mw (Da)	83400	80100	82100
$Đ_M$	1.65	1.88	2.17

As a consequence, the modification will result in a decrease in hydrodynamic volume, resulting in longer retention times on the column, as the eluent was

a buffer solution [329]. As a result, an underestimation of the molecular weight can occur [187,330,331]. Therefore, it can be anticipated that a similar degree of hydrolysis occurs between both modifications.
The higher reactivity for crosslinking of the thiol-ene photo-click-based Gel-NB was proven by *in situ* photo-rheology experiments (Figure III.34 A) and clearly reveals the benefit of thiol/ene photo-click crosslinking over conventional free radical polymerization of Gel-MOD. Furthermore, the crossover between the storage and loss modulus (gel point) already occurs within 2.7 s ± 0.1 after applying UV irradiation for gel-NB + DTT in contrast to 64.7 s ± 6.1 for Gel-MOD. At the latter time point, the storage modulus (G') of Gel-NB has already increased by two orders of magnitude (Figure III.34 A). However, after 10 minutes crosslinking, the slower crosslinking Gel-MOD reached similar mechanical properties (i.e. 4.576 kPa ± 0.225) compared to Gel-NB (i.e. 4.728 kPa ± 0.045).

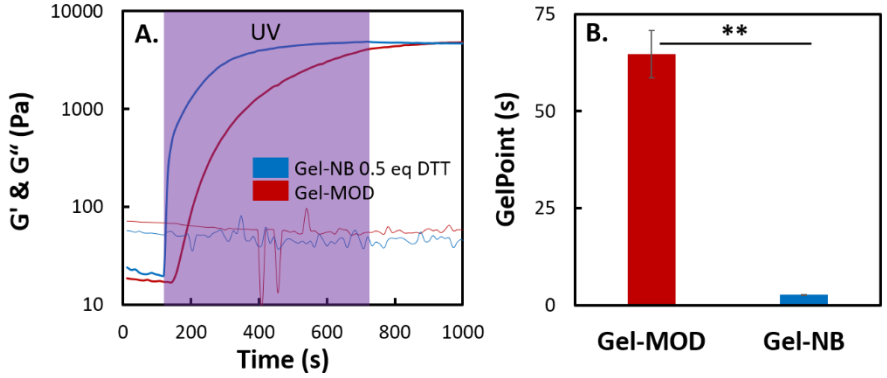

Figure III.34: *In situ* photo-rheology on 10 w/v% solutions of Gel-MOD and Gel-NB + 0.5 eq DTT in the presence of 2 mol% Irgacure 2959 at 37 °C (A); Gel points of Gel-NB and Gel-MOD based on *in situ* photo-rheology experiments (B) (n = 3). All experiments were performed using 2 mol% Irgacure 2959 and 0.5 equivalents DTT with respect to Gel-NB unless stated otherwise. (all differences significant with P < 0.001 except when denoted otherwise with ** P < 0.01, * P < 0.05 and ns indicating no statistical significance)

For tissue engineering applications, hydrogels are typically in an equilibrium swollen state. Therefore, the storage moduli were also quantified for crosslinked hydrogels after equilibrium swelling at 37 °C (Figure III.34 A). The test indicated a close correlation between the crosslinking parameters (gelatin concentration, crosslinker thiol/ene ratio) and the final mechanical properties [284]. In general, Gel-MOD exhibits higher storage moduli than Gel-NB throughout the studied concentration range (i.e. 5 – 15 w/v%) despite higher

swelling ratios (i.e. 21.6 ± 0.7 (Gel-MOD) vs 17.5 ± 2.4 (Gel-NB) at 5 w/v% and 8.4 ± 0.3 (Gel-MOD) vs 7.5 ± 0.2 (Gel-NB) at 15 w/v%) (Figure 27 E). This phenomenon becomes even more apparent at higher concentrations (i.e. 75.563 kPa ± 4341 (Gel-MOD) vs 38.330 kPa ± 1.421 (Gel-NB) at 15 w/v%) and is absent at low concentrations (i.e. 8.939 kPa ± 0.331 (Gel-MOD) vs 8.666 kPa ± 0.220 (Gel-NB) at 5 w/v%) for which no statistical differences are observed. This phenomenon can be attributed to the nature of the crosslinking reaction (Figure III.35 A). Indeed, in an orthogonal step-growth polymerization crosslinking reaction (Gel-NB), each norbornene functionality is only linked to one other functionality through the bifunctional crosslinker (DTT). Consequently, each junction knot in the network only links two functionalities, which results in a homogeneous network [176]. However, in a free radical chain growth polymerization, each junction knot can link multiple functionalities into a short oligo-methacrylamide chain resulting in more local strain (Figure I.9 C). As a result, a stiffer, more heterogeneous network is formed. Furthermore, the probability to obtain longer oligo-methacrylamide chains is higher at elevated gelatin concentrations (i.e. > 5 w/v%).

The insignificant difference in stiffness of Gel-MOD versus Gel-NB at low concentrations (i.e. 8939 Pa ± 331 (Gel-MOD) vs 8666.67 Pa ± 220 (Gel-NB) at 5 w/v%) further substantiates this hypothesis as the probability to link more than two methacrylamide functionalities will be limited due to the high dilution. In this case, the Gel-NB derivative exhibits a comparable stiffness while exhibiting a more pronounced decrease in equilibrium swelling, this can be attributed to the more efficient thiol-ene crosslinking reaction as evidenced by HR-MAS ^{1}H-NMR spectroscopy results and the more pronounced hydrophobicity for the norbornene functionalities. (Figure III.35 A, B, C).

This hypothesis is further substantiated by literature, which describes roughly five times higher storage moduli when using a tetrafunctional crosslinker (4-arm thiolated poly(ethyleneglycol) PEG4SH) compared to applying bifunctional DTT [168]. Consequently, it is anticipated that comparable mechanical properties can be obtained by using multivalent thiolated crosslinkers (Chapter 4). Another relevant parameter to tune the mechanical properties of the final gel is the thiol:ene ratio. Intuitively, the highest storage moduli would be obtained for an equimolar thiol:ene ratio, as also confirmed by literature [168]. Further increasing this ratio again results in a decreased storage modulus because some crosslinkers will only react at a single side, thereby resulting in less dense networks (Figure III.35 A).

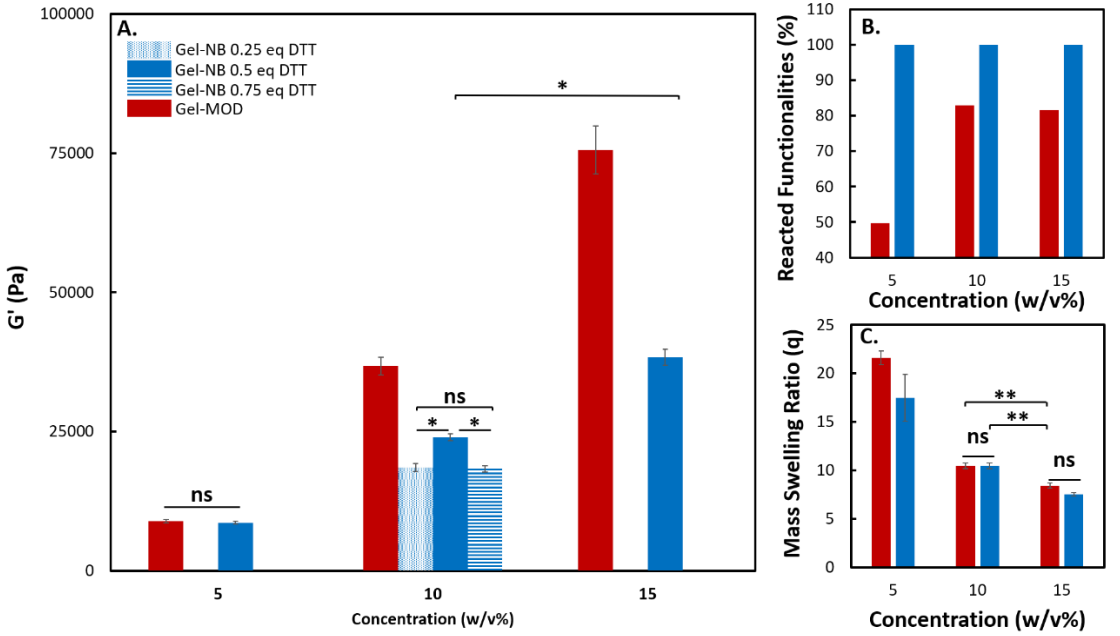

Figure III.35: Effect of gelatin concentration and gelatin/crosslinker ratios (for Gel-NB) on the storage moduli of equilibrium-swollen Gel-MOD and Gel-NB films after 30 mins UV-A irradiation (A). (n ≥ 2); Conversion of Gel-MOD and Gel-NB based on HR-MAS ^{1}H-NMR spectroscopy (B); Comparison between mass swelling ratio of Gel-MOD and Gel-NB at different gelatin concentrations (C). (n ≥ 6); All experiments were performed using 2 mol% Irgacure 2959 and 0.5 equivalents DTT with respect to Gel-NB unless stated otherwise. (all differences significant with P < 0.001 except when denoted otherwise with ** P < 0.01, * P < 0.05 and ns indicating no statistical significance)

By exploiting this phenomenon, tight control over the number of reacted functionalities becomes possible. Consequently, remaining norbornene functionalities can be applied for post-production grafting of functional compounds (e.g. pharmaceuticals, growth factors, ECM components, etc.) by thiol-ene coupling (*vide infra*) [182].Finally, when evaluating the water uptake behavior, it is clear that the water uptake capacity decreases with increasing gelatin concentration, as anticipated for denser networks which is in agreement with literature reports [284] (Figure III.35 C) (Chapter 1 & 2). Generally, Gel-NB exhibits similar swelling ratios at higher concentrations (i.e. > 5 w/v%) in comparison to Gel-MOD despite the lower storage moduli. It is anticipated that this is a consequence of the fact that Gel-NB hydrogels are characterized by full conversion of the crosslinkable functionalities in contrast to the methacrylamides incorporated in Gel-MOD, as evidenced by HR-MAS ^{1}H-NMR spectroscopy (Figure III.35 B). The comparable swelling behavior in combination with the faster crosslinking kinetics is an additional benefit of Gel-NB over Gel-MOD when aiming at high resolution additive manufacturing (e.g. 2PP) as lower intensities and faster writing times can be applied resulting in a similar CAD/CAM mimicry [126,284].

3.4. Two-photon Polymerization Processing

The 2PP structuring performance of Gel-NB in comparison to Gel-MOD was evaluated by writing cubes (r = 100 µm) in both materials dissolved in PBS using P2CK, a highly efficient water-soluble 2-photon photoinitiator at different gelatin concentrations and laser powers [332] (Figure III.36 A & Figure I.17). The swelling behavior of the developed gelatin derivatives was obtained by comparing the surface area of the top slice to the applied CAD design [284] (Figure III.36 C). At the applied processing conditions (i.e. laser power: 10-100 mW, scanning speed: 100 mm/s), Gel-MOD could not be processed at all, thereby demonstrating the tremendous improvement with respect to reactivity of the gel-NB derivative as already indicated by *in situ* photo-rheology experiments.

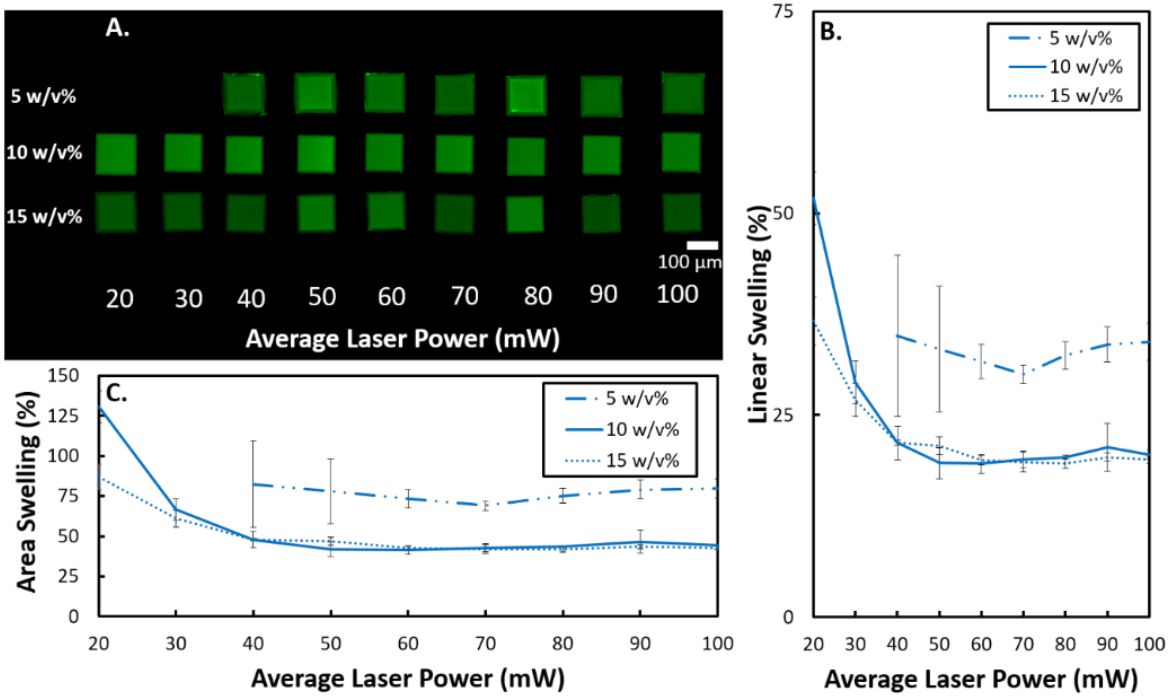

Figure III.36: (A) Laser scanning microscopy Z-stack images of cubes (r = 100 µm) using different Gel-NB concentrations and laser powers and a writing speed of 100mm/s. (B) Semi-quantitative analysis of post-production linear swelling of the structured cubes. (C) Semi-quantitative analysis of post-production area swelling via comparison of the surface area of the top of the cube to the CAD design. All experiments were performed in the presence of 2 mol% P2CK and 0.5 equivalents of DTT; error bars represent the standard deviation (n ≥ 3)

Furthermore, Gel-NB can be processed at lower polymer concentrations (5 w/v%) in contrast with any previously reported gelatin derivative [284]. Additionally, even at this concentration, structuring was already feasible at a lower spatiotemporal energy (40 mW @ 100 mm/s) in contrast with any earlier reported gelatin derivative irrespective of the applied polymer concentration (i.e. ≥ 10 w/v% using ≥ 40 mW @ 100 mm/s) [126,284]. At higher concentrations (i.e. ≥ 10 w/v%), even lower laser powers (20 mW @ 100 mm/s) resulted in reproducible structures (Figure III.36 A,B & C).
In addition, the linear swelling of the material is rather limited (20 – 40 % in contrast to ≥ 70 % for previously reported Gel-MOD with higher DS [284]) thereby resulting in minor deviations from the applied CAD design (Figure III.36 B). Although one previously reported gelatin derivative (Gel-MOD-AEMA, see Chapter 2[277]) was fully precluded from swelling, Gel-NB exhibits a broader processing range and can be developed through a one-pot modification approach, as described earlier. Additionally, a “plateau” in swelling ratio can be observed starting from laser powers of 40 mW and above (at 100 mm/s) for all applied precursor concentrations indicating that from this laser power onwards, crosslinking is complete.

3.5. In vitro Biocompatibility and 3D Cell Culture Assays

Biocompatibility experiments using L929 fibroblasts were conducted on glass slides coated with crosslinked Gel-NB or Gel-MOD. This assay indicated that the introduction of norbornene functionalities does not result in any cytotoxicity as no significant differences were observed between the gel-MOD and the gel-NB throughout the culture period (Figure III.37 A). Over the first three days, the positive control (i.e. tissue culture polystyrene) exhibited a significantly higher metabolic activity in comparison to both gelatin derivatives. However, after 7 days of culture, no significant differences were observed, indicating a comparable cytocompatibility for both derivatives. Since Gel-MOD is considered a benchmark for biofabrication, Gel-NB can be considered at least equally suitable from a biological perspective while exhibiting substantial benefits in terms of reactivity and processing [125,284]. Furthermore, in the course of time, all substrates including the positive control, exhibited a similar linear increase in metabolic activity with a comparable slope (i.e. slopes: 16.15 for TCP; 16.41 for gel-NB and 14.85 for gel-MOD) indicating that the cells were proliferating at a similar rate on all substrates (Figure III.37 B).

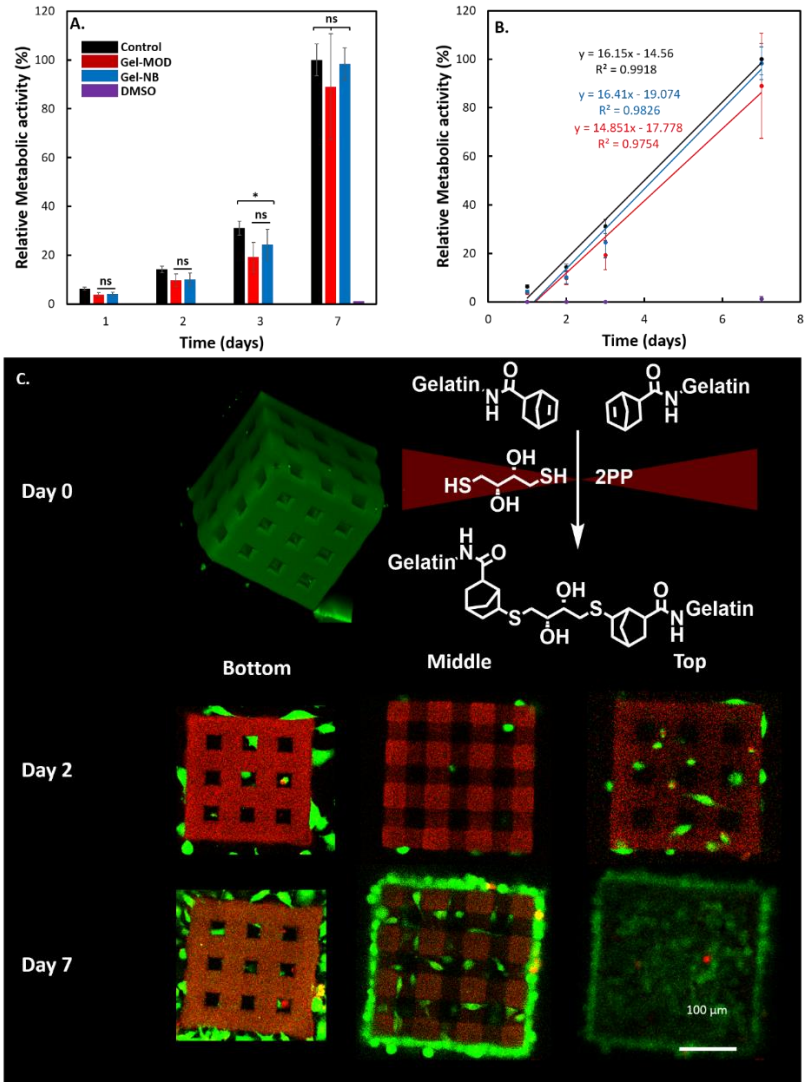

Figure III.37: (A & B) Presto Blue metabolic activity assay performed on L929 fibroblasts cultured on 10 w/v% hydrogel-coated glass slides relative to tissue culture polystyrene and DMSO as respectively positive and negative control. (C) Crosslinking scheme and micro-scaffold (r = 200 µm) containing 30 µm pores generated using 2PP starting from a 10 w/v% solution of Gel-NB in the presence of 0.5 equivalents DTT and 2 mol% P2CK. Live (green)/dead (red) staining images of scaffold cross-sections at different time points during L929 culture. (all differences significant with P < 0.001 except when denoted otherwise with ** P < 0.01, * P < 0.05 and ns indicating no statistical significance)

Additionally, after 7 days of culture, no significant differences were observed between the gelatin derivatives and the positive control (TCP) (Figure III.37 A).
As a proof-of-concept towards biofabrication, a cubic micro-scaffold (i.e. r = 200 µm with pores of 30 µm and struts of 30 µm) was generated using 2PP. After equilibrium swelling this corresponded to an average pore diameter of 33.6 µm ± 1.5 and an average strut size of around 39.6 µm ± 4.7 . Next, this structure was seeded with L929 fibroblasts which are characterized by sizes of around 10 – 20 µm (Figure III.37 C). After equilibrium swelling, the Live/dead staining indicated that nearly no cell death occurred after seeding and during the remaining cell culture period (i.e. 7 days). Furthermore, although few cells were present on the structure initially, the cells infiltrated throughout the fabricated structure. As a result, the material holds great potential towards more complex biofabrication designs in comparison to the previously reported gelatin derivatives due to the increased shape fidelity.

3.6. Photo-Grafting Proof-of-Concept Experiments

Another benefit of using a thiol-ene photo-click system encompasses the ability to precisely control the number of reacted functionalities (Figure III.35 A). As a result, when thiol:ene ratios below 1 are applied during crosslinking, unreacted norbornene functionalities remain present within the hydrogel that remain prone to reaction. Gramlich et al. already reported the use of thiol-ene systems for the grafting of thiolated compounds to thiol/norbornene-hyaluronic acid hydrogels with high spatiotemporal control [182]. It is anticipated that a similar strategy can be applied for the developed Gel-NB hydrogels. As a proof of concept experiment, the ability to introduce 7-mercapto-4-methylcoumarin, a fluorescent dye, on crosslinked Gel-NB hydrogels was assessed [333]. It is known that 7-mercapto-4-methylcoumarin as such does not result in fluorescence in water. However, after alkylation of the thiol functionality, it becomes highly fluorescent due to the inability to form a thione-tautomer resonance structure, resulting in a loss of aromaticity [333] (Figure III.38). Indeed, during the thiol-ene photoclick reaction, the thiol reacts with the double bond of norbornene thereby preventing the formation of the non-fluorescent resonance structures (Figure III.38 & III.39 A). As a consequence, it is an ideal candidate to assess the success of thiol-ene photo-grafting, as uncoupled residual molecules will not induce fluorescence [333].

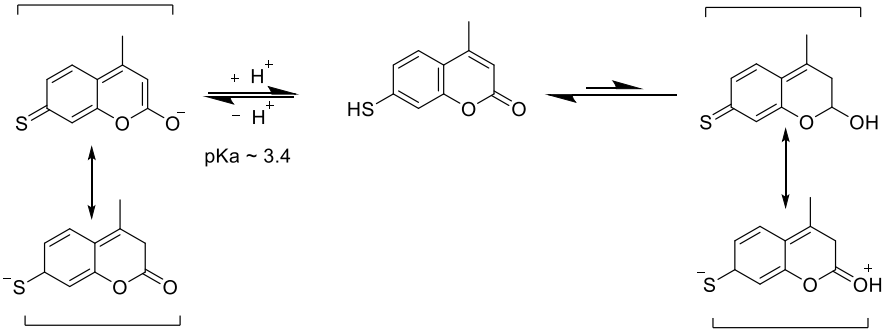

Figure III.38: Influence of pH on resonance structures of 7-mercapto-4-methylcoumarin that are prevented after alkylation of the thiol due to thiol-ene click reaction.

In order to assess the viability of this thiol-ene grafting strategy, crosslinked hydrogels were prepared at a thiol/ene ratio of 0.5. As a consequence, 50% of the norbornene functionalities (i.e. ± 0.12 mmol of norbornene functionalities/g Gel-NB) remain unreacted in the hydrogel. Next, an assay was performed to assess the grafting potential (Figure III.39 B). In this assay, first the crosslinked hydrogel samples were allowed to reach equilibrium swelling at 37°C in a solution containing 10 mmolar of 7-mercapto-4-methylcoumarin in DMSO. DMSO was selected as a solvent because of the poor water solubility of 7-mercapto-4-methylcoumarin [333]. After equilibrium swelling, the samples were subjected to 30 minutes of UV-A irradiation to induce the photo-click reaction. Finally, the samples were washed three times with DMSO to remove uncrosslinked 7-mercapto-4-methylcoumarin and three times with water to allow equilibrium swelling. In order to assess the success of the grafting also three control samples were prepared at different conditions. In this respect, Gel-NB/DTT samples were prepared in parallel either in the absence of 7-methyl-4-coumarin (Figure III.39 E) or in the presence of the dye without UV irradiation (Figure III.39 C). Finally, also a Gel-MOD control sample was applied to demonstrate the benefits of the thiol-ene gels (Figure III.39 D). The first observation of the photo-grafted Gel-NB sample (Figure III.39 F) is the deep yellow colour as a consequence of successful grafting of the yellow dye. This colour is completely absent in the sample that was not incubated in the dye-containing solution (Figure III.39 E) but is faintly visible in the Gel-MOD and Gel-NB dark control samples. For the gel-NB dark sample, this is probably a consequence of traces left after washing. For the Gel-MOD sample, it is anticipated that thiol-ene grafting has also occurred to some extend since not all methacrylamide functionalities were consumed during photo-crosslinking (Figure III.35 B). As a result, these

methacrylamides can also undergo thiol-ene photo-click reactions. However, the yellow colour is less pronounced because methacrylamides are less prone to thiol-ene click chemistry due to stabilization of the radical on the one hand [167]. On the other hand, there are less methacrylamides available for reaction in comparison to the norbornene in Gel-NB gels because only 20% of the methacrylamides (i.e. 0.05 mmol/g) remain unreacted after crosslinking (Figure III.35 B).

A second proof of successful grafting is the decreased volume of the samples after equilibrium swelling due to the introduction of the hydrophobic dye in comparison to the blank sample. The smallest dimensions are clearly obtained for the grafted yellow sample with a diameter of only ± 5.5 mm (Figure III.39 F) in comparison to the control sample with a diameter of ± 8 mm (Figure III.39 E) and the gel-MOD sample with a diameter of ± 6 mm (Figure III.39 D).

Although these proof-of-concept single photon polymerization experiments are promising, the real added value of photo-chemistry lies in the fact that it enables large degrees of spatiotemporal control for the reaction. To this end, especially 2PP offers extreme benefits due to the highly localised non-linear absorption of multiple photons resulting in high spatiotemporal control over all 3 dimensions that can even expand beyond the diffraction limit [274]. Additionally, due to the small dimensions, also thermal effects are limited using this technique resulting in relatively mild reaction conditions [274]. In this respect, Ovsianikov et al. already reported on the potential of multiphoton grafting of aromatic azides as a consequence of photolysis [334]. However, it is anticipated that the use of thiol-ene photo-click chemistry allows to further expand this potential.

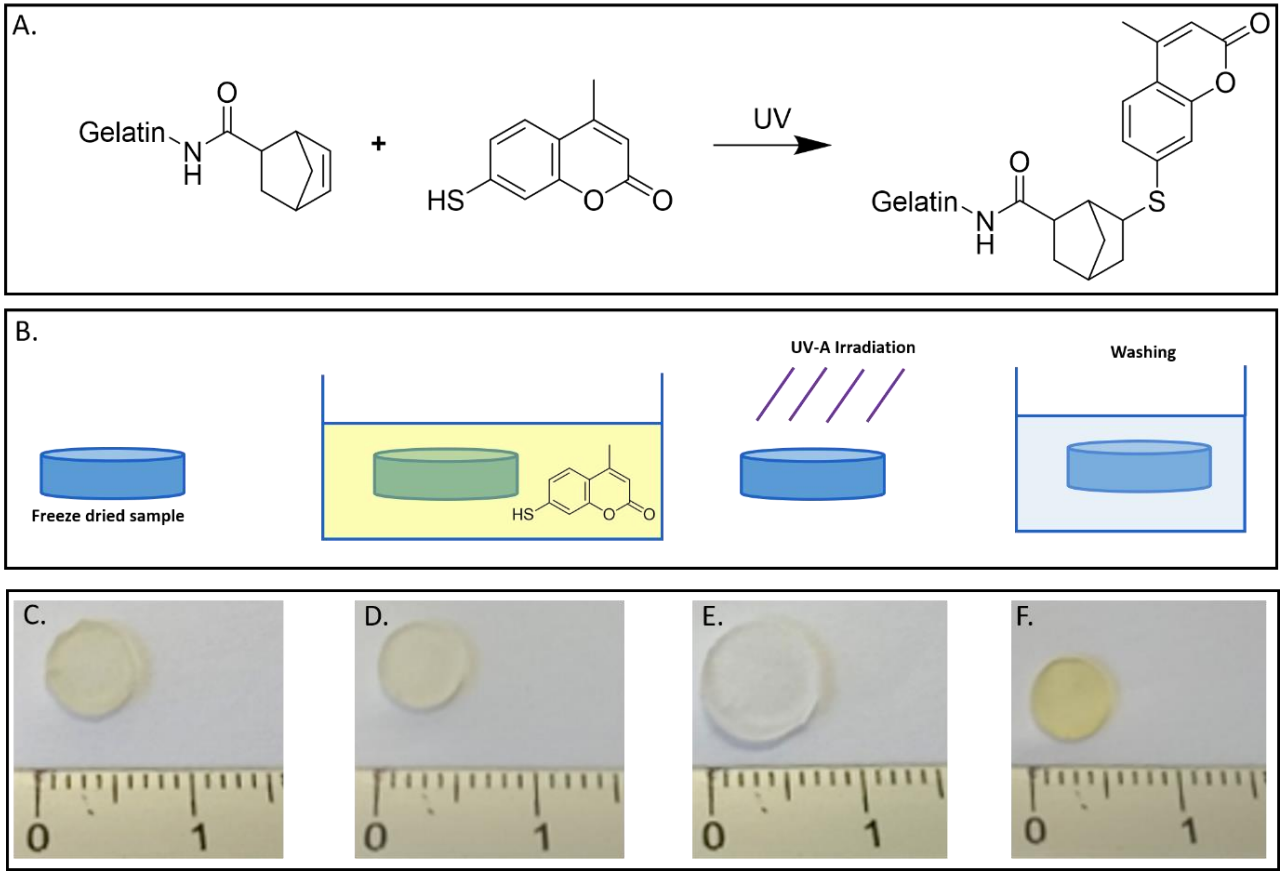
A.
Gelatin
N
H
O
+
HS
O
O
UV
Gelatin
N
H
O
S
O
O
B.
Freeze dried sample
HS
O
O
UV-A Irradiation
Washing
C.
D.
E.
F.
0
1

Figure III.39: Single-photon grafting experiments. (A) Thiol-ene photo-grafting reaction between the norbornene functionalities present on Gel-NB and 7-mercapto-4-methylcoumarin present in the solution upon applying UV irradiation. (B) Experimental set-up: in a first step, different freeze-dried samples crosslinked at a thiol/ene ratio of 0.5 were incubated and allowed to reach equilibrium swelling in DMSO in the presence of 10 mmolar of 7-mercapto-4-methylcoumarin (the dye). After equilibrium swelling, samples were taken from the solution and crosslinked upon UV-A irradiation followed by incubation in DMSO (3 times) to remove ungrafted dye and in water (3 times) to remove the DMSO. (C-E) Images of equilibrium swollen samples after washing: (C) a Gel-NB/DTT sample without UV irradiation prior to washing; (D) a Gel-MOD control sample; (E) a Gel-NB/DTT sample subjected to the same treatment without incubation in the presence of the dye; (F) Gel-NB/DTT sample processed as mentioned in B.

Firstly, thiol-ene reactions can proceed in the absence of a PI, thereby not requiring the aromatic azide system. Secondly, thiols are functionalities that are present in a plethora of biological components and growth factors (i.e. peptides, proteins, ECM components, etc.).Consequently, this approach has the potential to graft active components onto the hydrogel matrix in a very controlled fashion to provide cellular cues or initiate localised differentiation of stem cells.

To assess the feasibility of multi-photon initiated thiol-ene photo-grafting, a similar assay was executed comparable to the single photon grafting experiments. However, instead of UV-irradiation, the hydrogel samples were subjected to photopatterning using a femtosecond pulsed NIR (i.e. 800 nm, 70 fs, 80 MHz) laser in the presence of the dye at different scanning speeds (i.e. 25 – 150 mm/s) and average laser powers (i.e. 50 – 200 mW) (Figure III.40). For control, the same test was performed on a Gel-NB/DTT hydrogel in the absence of the coumarin dye. During writing, the structures were visible when applying higher laser powers (i.e. ≥ 100 mW at all writing speeds) (see figure III.33 B). During 2PP processing, the structuring is usually visible through the microscope objective as a result of the formation of a crosslinked network, resulting in a difference in refractive index between the crosslinked structure and uncrosslinked matrix [317,335]. However, during the photo-grafting experiments, this is counterintuitive, as no additional crosslinking that would result in a denser network and associated increase in refractive index can occur in the highly orthogonal thiol-ene systems. It should be noted that at the highest laser powers, this effect can be attributed to thermal hydrolysis of the hydrogel matrix resulting in air bubble formation during structuring (Figure III.41 C & D). However, at intermediate laser powers (Figure III.41 A & B), no air bubble formation was observed indicating that this effect is due to photo-hydrolysis of the hydrogel matrix (see Chapter 4).

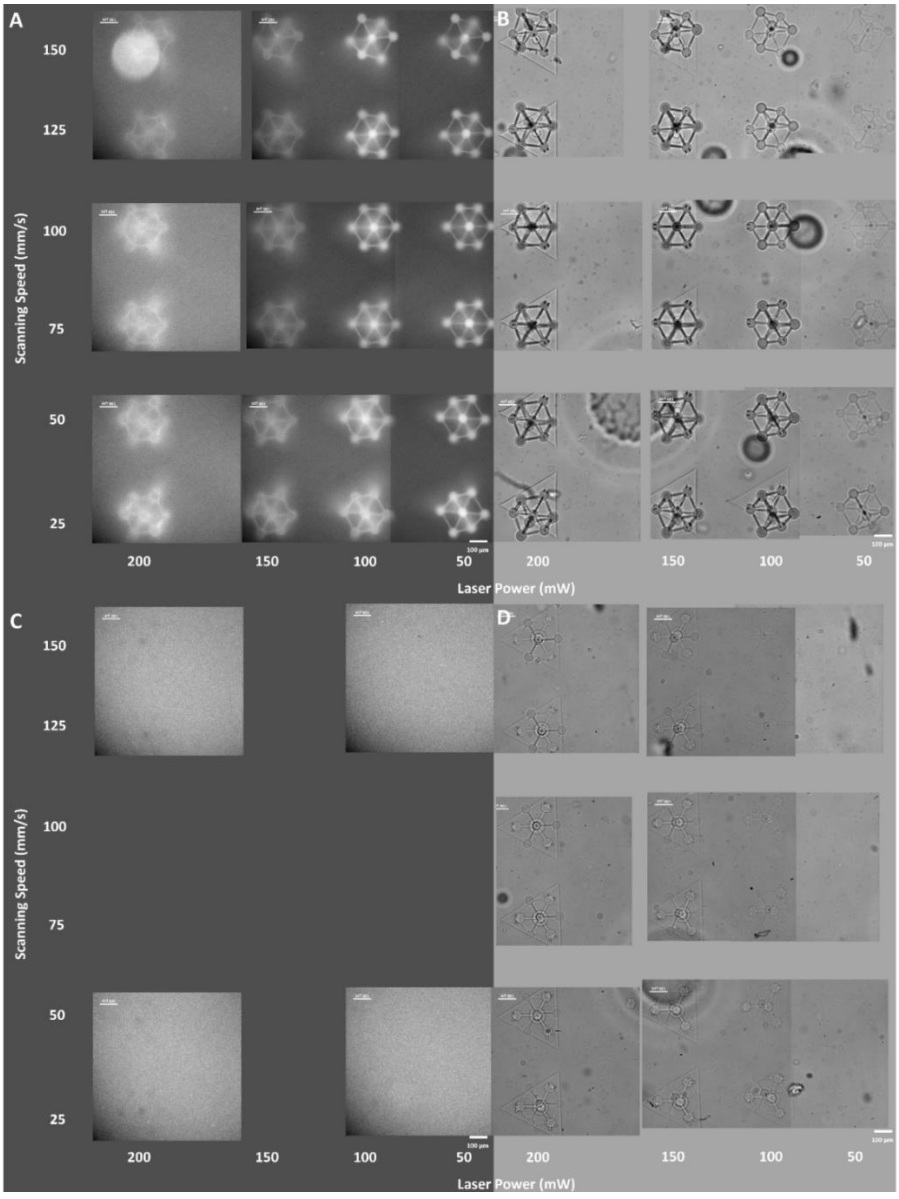

Figure III.40: Fluorescence microscopy images of 340nm excitation (A & C) and Brightfield microscopy images (B & D) of 7-mercapto-4-methylcoumarin grafted using 2PP at different scanning speeds and laser powers inside a crosslinked Gel-NB/DTT gel at a thiol/ene ratio of 0.5 (A & B) and a control in the absence of 7-mercapto-4 methyl coumarin (C & D).

When looking at the brightfield microscopy images (Figure III.40 B and D), it is clear that the structures are already visible at lower laser powers for the samples in the presence of the dye. This is intuitive as the introduction of the hydrophobic dye will result in localised shrinkage of the hydrogel and an associated increase in refractive index. The successful grafting of the dye was further confirmed via fluorescence microscopy.

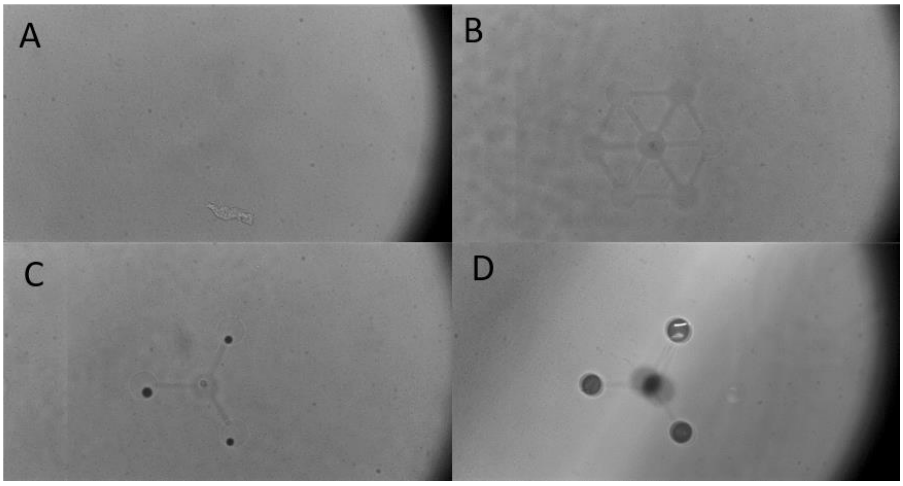

Figure III.41: Different effects observed during multiphoton photo-grafting: (A) Very faint structure visible due to grafting/photocleaving of the hydrogel. (B) Faint structure visible due to grafting/photocleaving (occurring at 100 mW from 25 – 75 mm/s and at 150 mW from 125 – 150 mm/s onwards). (C) Occasional small bubble formation due to thermally induced hydrolysis/ablation of the hydrogel matrix (occurring at 150 mW from 25 – 100 mm/s). (D) Bubble formation due to severe thermally induced hydrolysis/ablation of the hydrogel matrix (occurring at 200 mW at all scanning speeds).

To this end, the sample was irradiated with UV light at 340 nm which is close to the absorption maximum of 7-mercapto-4-methylcoumarin, resulting in emission in the visible spectrum (Figure III.40 A) [333]. For the latter, the grafting is clearly visible, whereas in the control sample, no fluorescence could be detected at any spatiotemporal energy (Figure III.40 C). Additionally, the high precision spatiotemporal control due to the non-linear absorption is clearly visible, as the fluorescence is only observed within the structured complex Atomium geometries and completely absent throughout the remaining hydrogel matrix. It should also be noted that fluorescence is already clearly visible at the lowest spatiotemporal exposure doses (i.e. 50 mW & 150 mm/s) for which the structures are almost absent in the brightfield

microscopy images (Figure III.40 A & B). Furthermore, at high energy (i.e. 200 mW) the fluorescence is poor due to concurrent thermal ablation as evidenced via air bubble formation (Figure III.41).

Consequently, multi-photon induced thiol-ene photo-click chemistry proves to be very promising towards the generation of complex artificial tissues, because different mechanical- and biological cues can be incorporated within the same hydrogel to form a superior mimic of the complex natural ECM.

3.7. Conclusions

In the present work, a one-pot modification protocol is reported to yield Gel-NB with a broad range of degrees of substitution (up to 90%), enabling a subsequent highly efficient thiol-ene photo-click crosslinking. Quantitative physico-chemical characterization experiments enabled benchmarking of the newly developed material compared to Gel-MOD and indicated a drastic increase in crosslinking speed. The nature of the reaction also allows control over the number of reacted functionalities, thereby holding potential to use remaining functionalities on the obtained hydrogels for post-processing grafting of bioactive molecules to further tailor the constructs towards specific needs. In this respect, especially the use of multi-photon assisted grafting holds great promise due to the increased spatiotemporal control in comparison to conventional single photon lithography approaches. In addition, Gel-NB also exhibits a comparable biocompatibility in comparison to Gel-MOD, which is considered one of the gold standards in the field of biofabrication and regenerative medicine. Finally, an unprecedented efficiency towards 2PP processing of gelatin derivatives was demonstrated. Both lower concentrations and lower spatiotemporal energies compared to the state-of-the-art materials could be applied to obtain reproducible structures. Combining all these advantages renders the reported Gel-NB very suitable for tissue engineering applications and more specifically, for light-based biofabrication techniques, exhibiting a high degree of tailoring potential.

Chapter 4:
Influence of Thiolated Crosslinker on Network Properties and Laser-Based Processing of Thiol-Norbornene Gelatin-Based Hydrogels.

The *in vitro* cell biology experiments were performed together with dr. Marica Markovic. Part of the 2PP and LSM experiments in the present chapter were performed by Agnes Dobos. The gel-SH was synthesized together with Liesbeth Tytgat. The NMR spectra of the gelatin derivatives were measured by Tim Courtin

Parts of this chapter have been submitted as:

> **J. Van Hoorick**, A. Dobos, L. Tytgat, M. Markovic, P. Gruber, J. Van Erps, H. Thienpont, A.Ovsianikov, P. Dubruel and S. Van Vlierberghe, *Biofabrication* **(submitted 2019)**

4.1. Introduction

In the previous chapter, the benefits of thiol-ene photo-click chemistry was demonstrated over the more conventional chain growth-based systems in terms of laser-based additive manufacturing as well as laser-based grafting of/onto gelatin. Although substantial research has been performed on thiol-ene photo-click gelatin hydrogels, little attention has been given to the influence of the applied thiolated crosslinker on the network properties along with the material processability. To date, either DTT or PEG-based thiolated crosslinkers were applied [168] (see Chapter 1 & 3).

Therefore, in the present chapter, gel-NB was developed with a high degree of substitution (i.e. 90 %) to investigate the influence of six different thiolated crosslinkers on the hydrogel properties in terms of physico-chemical characteristics, biological performance upon encapsulating adipose tissue-derived stem cells (ASCs) and on the laser-based (using 2PP) processing potential. Throughout this chapter, all assays were benchmarked against gel-MOD with a comparable degree of substitution (i.e. 95 %) [48,125] (see also Chapter 1).

4.2. Development of a Macromolecular Crosslinker Through Gelatin Thiolation

One of the proposed crosslinkers was gelatin based namely, thiolated gelatin (gel-SH) with a DS of 72% (i.e. 0.277 mmol/g gelatin) due to its structural similarities with the gel-NB. In this respect, it is anticipated that no issues related to phase separation of both components will be encountered in contrast to what was previously reported when using different polymer backbones [48,296].

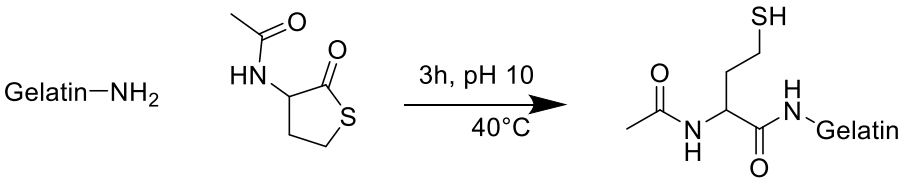

Figure IV.42: Development of gel-SH via reaction of the primary amines in gelatin with N-acetyl-homocysteine thiolactone.

Additionally, it should result in an even more homogeneous network in comparison to the previously applied thiol-ene gelatins, as only gelatin based

components are used. Gel-SH was obtained via the reaction of the primary amines present in gelatin with N-acetyl-homocysteine thiolactone using a previously reported protocol (Figure IV.42) [187].

4.3. Influence of Thiolated Crosslinker on Physico-Chemical Properties of Gelatin Hydrogels

The assessed thiolated crosslinkers are depicted in Figure IV.43 (A) and include thiolated gelatin (gel-SH with a DS of 72%), dithiothreitol (DTT), tetra(ethyleneglycol) dithiol (TEG2SH), polyethylene glycol dithiol with a molecular weight of 3400 g/mol (PEG2SH 3400), 4-arm polyethylene glycol tetrathiol with a molecular weight of 10000 g/mol (PEG4SH 10000) and 4-arm polyethylene glycol tetrathiol with a molecular weight of 20000 g/mol (PEG4SH 20000). DTT was also selected because it is an often reported crosslinker exploited in the framework of thiol/ene systems[168,176,336–338].

Besides DTT, also different thiolated PEG derivatives were selected, differing in molecular weight (i.e. 220 – 20 000 g/mol) and/or number of thiols per crosslinker (i.e. 2 or 4) as PEG-based thiolated crosslinkers have also already been extensively reported in literature. However, there has been very little research on the comparison of different (PEG-based) crosslinkers[112,115,168]. The use of different PEG-based crosslinkers allows to screen towards specific effects of molecular weight and number of thiols on the physico-chemical properties of the crosslinked hydrogel without changing the chemical functionalities. Finally, a thiolated gelatin was also selected as it is anticipated that this will lead to a more homogeneous network without the incorporation of any synthetic, non-degradable macromolecular species (i.e. PEG) while also having the benefit of exhibiting a relatively high number of thiols being present per crosslinker (i.e. ± 14 thiols per gelatin chain). Therefore, it could potentially result in a stiffer hydrogel network. Despite these potential beneficial aspects, there are very few reports in literature using thiolated gelatin as crosslinker for ‘ene’-functionalized gelatins[171,172,339].

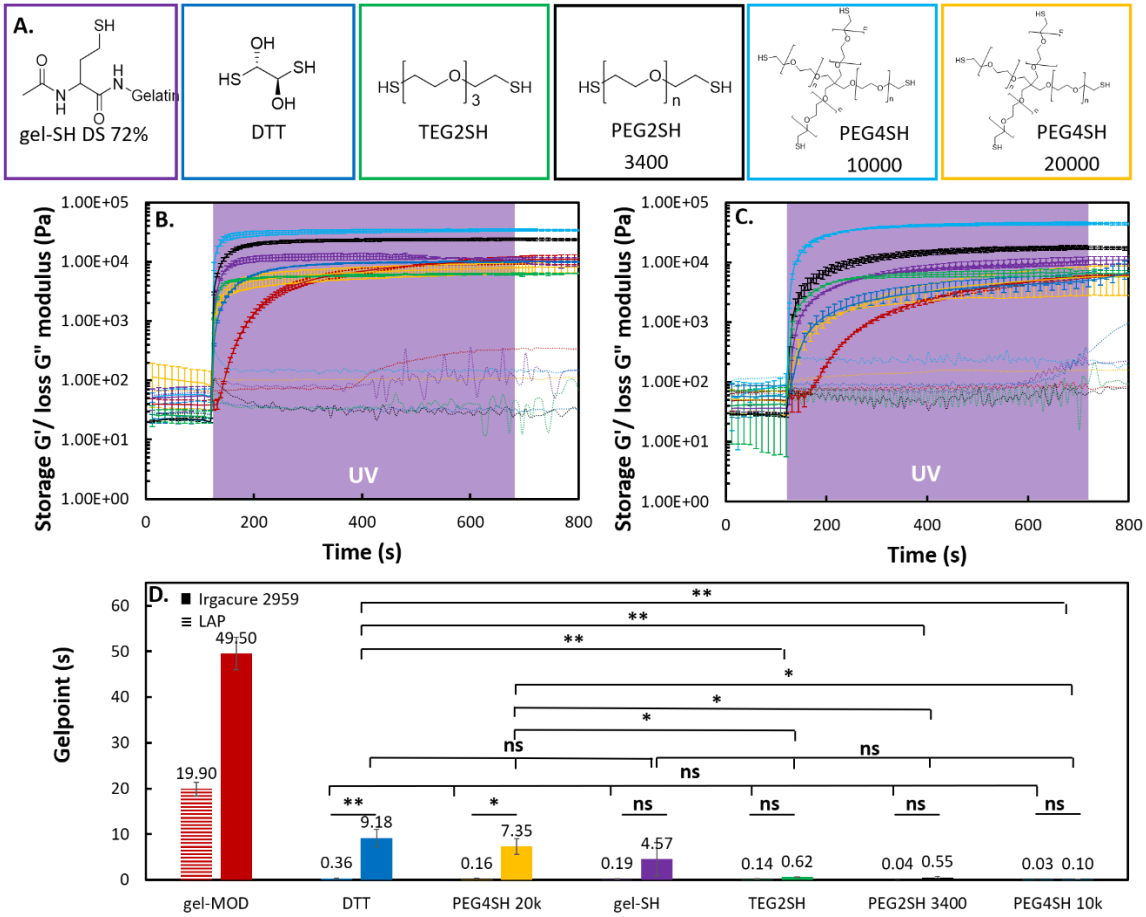
A.
gel-SH DS 72%
DTT
TEG2SH
PEG2SH
3400
PEG4SH
10000
PEG4SH
20000
B.
C.
Storage G' / loss G" modulus (Pa)
1.00E+05
1.00E+04
1.00E+03
1.00E+02
1.00E+01
1.00E+00
UV
0
200
400
600
800
Time (s)
D.
Irgacure 2959
LAP
Gelpoint (s)
60
50
40
30
20
10
0
49.50
19.90
9.18
0.36
7.35
0.16
4.57
0.19
0.14
0.62
0.04
0.55
0.03
0.10
**
*
ns
gel-MOD
DTT
PEG4SH 20k
gel-SH
TEG2SH
PEG2SH 3400
PEG4SH 10k

Figure IV.43: Overview of the different applied thiolated-crosslinkers (A); *In-situ* photo-rheology of the different thiol-ene formulations with a 1:1 thiol-ene ratio using gel-MOD DS 95 % as reference in the presence of LAP (B) or Irgacure 2959 (C) as PI. The UV irradiation time is indicated with a purple square. Calculated gel points (based on crossover between G' and G " in panel B and C) of the gel-MOD reference and the different thiolated crosslinkers applied to crosslink gel-NB with the values obtained using LAP or Irgacure 2959 as PI (D). All statistical differences are significant with P < 0.001 unless stated differently with ** P < 0.001, * P < 0.05 and ns indicating no statistical significance.

4.3.1. Influence of the Applied Photoinitiator and Crosslinker on the Crosslinking Kinetics

A first characteristic to compare different photo-crosslinkable systems includes the crosslinking kinetics. To this end, photo-rheology was performed using either 2 mol% (relative to the number of “ene” functionalities) LAP (Figure IV.43 B) or Irgacure 2959 (Figure IV.43 C) as PI (see also Figure I.17). LAP was assessed as an alternative to Irgacure 2959 due to its better water solubility and higher reactivity, especially in the UV-A to visual spectrum, while exhibiting a comparable biocompatibility to Irgacure 2959 [115,128,133] (see Chapter 1). When monitoring the storage modulus (G’) over time, the difference in reactivity between the thiol-ene step-growth systems and the conventional chain growth gel-MOD system becomes apparent. The chain-growth systems are characterized by a lag phase upon UV irradiation. This lag phase is a consequence of oxygen inhibition occurring during the reaction. Indeed, before the polymerization is initiated, the oxygen has to be consumed first by the radicals, which is not the case for the step-growth thiol-ene systems resulting in the observed faster crosslinking reaction [179]. Furthermore, the crosslinking typically occurs faster in the presence of LAP (Figure IV.43 B) in comparison to the more conventional Irgacure 2959 (Figure IV.43 C). This is reflected more quantitatively by assessing the gel points or crossover points between the storage (G’) and loss (G”) moduli indicating a transition from predominantly viscous to elastic behaviour for the different formulations [340] (Figure IV.43 D). The difference in reactivity between both PI’s is especially apparent for the gel-MOD derivative as this is characterized by lower reaction kinetics in comparison to the thiol-ene systems[336]. This is a consequence of the higher efficiency of LAP in the UV-A region as it is characterized by a molar absorptivity at 365 nm of 218 M^{-1} cm^{-1} [115] vs 4 M^{-1} cm^{-1} [133] for Irgacure 2959. This means that in the presence of LAP, more radicals will be formed upon UV irradiation. Because high radical concentrations can compensate for the oxygen inhibition due to the rapid oxygen consumption, resulting in shorter lag times and concomitantly, faster gel points [48,163]. However, the difference in reactivity between both photoinitiators is not significant for gel-SH, TEG2SH, PEG2SH and PEG4SH 10000 because of the spring loaded behaviour of the thiol-norbornene, and the absence of oxygen inhibition. When comparing the kinetics of the different formulations, there is no significant difference in gel point between the different thiol-ene systems when using LAP (Figure IV.43 D). However, when Irgacure 2959 is used, some differences in reactivity can be observed as DTT

and PEG4SH 20000 exhibit a significantly lower reactivity in comparison to the other crosslinkers, albeit non-significant relative to one another (Figure IV.43 D). Additionally, no significant difference in storage modulus (G') with respect to gel-MOD is observed after 10 minutes crosslinking for most thiol-ene formulations (i.e. 6 – 10 kPa when using LAP and 5 – 11 kPa when using Irgacure 2959 as PI) with the exception of PEG2SH 3400 (i.e. 17500 ± 1100 Pa for Irgacure 2959 and 23950 ± 1200 Pa for LAP) and PEG4SH 10000 (i.e. 44600 ± 2000 Pa for Irgacure 2959 and 34550 ± 1400 Pa for LAP) that outperform the conventional gel-MOD derivative, while PEG4SH 10000 is even outperforming all evaluated crosslinkers in terms of mechanical properties. Furthermore, the thiol-ene systems already exhibit their final mechanical properties after ± 60 s crosslinking, whereas gel-MOD requires 10 min to reach similar storage moduli.

4.3.2. Influence of the Applied Crosslinker on the Mechanical Properties of the Hydrogel at Equilibrium Swelling.

During *in situ* photo-rheology, the mechanical properties of a hydrogel in relaxed state are obtained. This relaxed state is less relevant because in the final application they are in the hydrated state. Therefore, a second assay was performed during which the water uptake capacity and the rheological properties of equilibrium-swollen, crosslinked hydrogel films at physiological conditions were assessed (Figure IV.44 & 45). In a first experiment, the films were crosslinked using either Irgacure 2959 or LAP immediately after film casting. Under these circumstances, higher storage moduli were obtained when using LAP as PI. On the one hand, this effect is related to the higher efficiency of the PI around 365 nm. On the other hand, the acylphosphinate functionality in LAP will cleave upon activation which results in the loss of the light-absorbing chromophore [340]. As a consequence, a larger penetration depth of UV-light during crosslinking is ensured, which is not the case for Irgacure 2959 [340]. The fact that the samples are 1 mm thick can result in a more densely crosslinked network on the inside and concomitantly higher storage moduli when using LAP as PI. This is further substantiated by the swelling ratio as in general, lower swelling ratios are obtained for the hydrogels that were crosslinked in the presence of LAP (Figure IV.44 B).

It is generally known that chain growth hydrogels (i.e. gel-MOD) exhibit a higher stiffness due to the presence of kinetic chains resulting in the linking of different functionalities in the same junction knot (see Chapter 1). For thiol-ene systems this is not the case. However, the number of functionalities linked

in one junction knot depends on the number of thiols present on the crosslinker molecule and the relative distance between the thiols on the crosslinker due to the reaction of complementary functionalities [48]. The present research indicates that the applied thiolated crosslinker has a substantial influence on the final mechanical properties as previously reported by Munoz *et al* [168]. In the present work, the highest storage modulus was observed when PEG4SH 10000 was applied as crosslinker which is a consequence of several aspects (Figure IV.44 A). First, the crosslinker contains 4 thiol functionalities, resulting in the coupling of 4 norbornene functionalities in one junction knot, whereas the other applied crosslinkers, with the exception of gel-SH and PEG4SH 20000, only exhibit 2 functionalities, thereby resulting in a less densely crosslinked network, as also reflected by the higher swelling ratio.

However, both PEG2SH 3400 and PEG4SH 10000 exhibit superior mechanical properties compared to the hydrogels crosslinked using gel-SH that contains ± 14 thiol groups/crosslinker. This is a consequence of the fact that all systems were crosslinked in a 1:1 thiol/ene ratio while keeping the total gelatin concentration at 10 w/v%. Indeed, changing the gelatin content would also result in a variation of the amount of RGD functionalities that can influence the biological response, irrespective of the applied crosslinker [112]. This means that for gel-NB/gel-SH, the total polymer concentration was 10 w/v% whereas for gel-NB/PEG2SH 3400, the total concentration was ± 16 w/v% and for gel-NB/PEG4SH 10000, this was ± 20 w/v% resulting in the observed better mechanical properties. In addition, also a lower swelling ratio was obtained for these samples, due to a higher initial polymer mass resulting in a higher dry mass after crosslinking. This increase in total polymer mass is negligible for the low molecular weight crosslinkers, resulting in poor mechanical properties for the TEG2SH and DTT formulations(i.e. 3.3 – 6.8 kPa) along with a high swelling ratio (i.e. 24 – 32) (Figure IV.44 A & B).

Furthermore, it should be noted that based upon this reasoning, superior mechanical properties are anticipated upon applying PEG4SH 20000, which in practice results in the weakest gels. This might be due to the larger distance between the thiols on the one hand and phase separation phenomena occurring between gelatin and PEG resulting in a heterogeneous mixture on the other hand. This hypothesis was also confirmed during 2PP experiments (*vide infra)*.

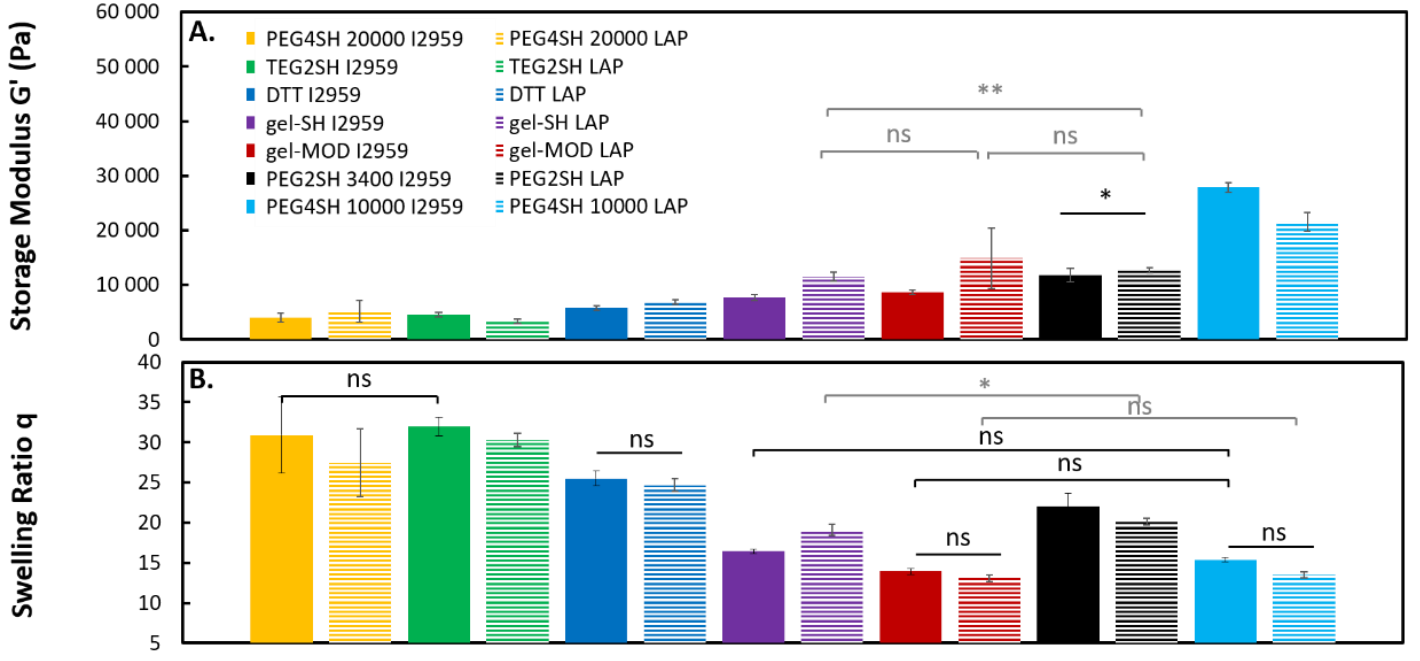

Figure IV.44: Influence of PI on storage modulus (A) and associated swelling ratio (B). The full bars represent hydrogels crosslinked in the presence of 2 mol% Irgacure 2959 and the dashed bars were crosslinked in the presence of 2 mol% LAP. All statistical differences are significant with p < 0.001 unless stated differently with ** p < 0.001, * p < 0.05 and ns indicating no statistical significance.

Despite the fact that the use of a multifunctional, branched, thiolated crosslinker results in similar or higher storage moduli compared to gel-MOD, the gel-MOD hydrogels are characterized by the lowest swelling ratio (Figure IV.44 A & B). This is in line with previous reports from literature [146,339]. In this respect, the gel-MOD hydrogels are characterized by the presence of hydrophobic oligo-methacrylamide kinetic chains, resulting in a lower water uptake capacity [168]. Furthermore, in case of chain growth hydrogels, several methacrylate functionalities on the same gelatin chain can react with each other, resulting in primary cycles and associated network imperfections [341]. This effect is less pronounced for the thiol-ene systems due to the orthogonal crosslinking occurring between complementary functionalities of gelatin and the applied thiolated crosslinker.

The water uptake capacity or swelling ratio can be an important aspect of a hydrogel in the framework of additive manufacturing. This is especially relevant when using high resolution technologies, as post-production swelling of the material can result in deviations from the applied CAD design [135,284] (see Chapter 2).

Based on the rheological and swelling ratio results, it can be concluded that, in general, the mechanical properties improve and the swelling ratio decreases when the number of thiols/crosslinker are increased. Furthermore, the mechanical properties of the hydrogels improve upon increasing the molecular weight of the applied crosslinker. However, this is due to the relative increase in polymer concentration (i.e. gelatin + crosslinker), thereby resulting in a denser hydrogel.

4.3.3. Influence of Physical Interactions on Mechanical Properties and Swelling Ratio of the Obtained Hydrogels

A second important aspect when applying gelatin for biofabrication application is physical gelation. Certain additive manufacturing techniques either benefit from or require this physical gelation behaviour to enable the generation of 3D structures prior to covalent crosslinking [48]. For example, deposition-based techniques often apply this physical gelation behaviour to lock the deposited structure prior to chemical crosslinking [127,161,342]. Additionally, in case of 2PP-processing, the presence of a physical gel can be a benefit as it provides mechanical support to the formed structure, which enables the construction of more complicated architectures [48,127,339]. Furthermore, when a material is crosslinked in a physical gel state, triple helices are formed. As a result, semi-crystalline junction zones are formed,

that can induce a proximity effect of the crosslinkable functionalities thereby resulting in a higher crosslink efficiency. Additionally, these semi-crystalline junction zones can partially be 'locked' by the introduction of chemical bonds [248,284] (Figure I.9).

As a consequence of both aspects, in general, a denser hydrogel network with superior mechanical properties is formed after crosslinking from a physical gel. This aspect is beneficial when using a solution containing only gelatin. However, when other polymers are introduced into the formulation, these supramolecular interactions can result in phase separation and solubility issues thereby resulting in inhomogeneous networks [235,296]. Thiol/ene systems typically require a thiolated (polymeric) crosslinker, that can result in phase separation during physical gelation. Therefore, the effect of physical gelation prior to crosslinking was assessed for the different formulations. To this end, hydrogel films were prepared using 2 mol% Irgacure 2959 as PI either via direct UV-induced crosslinking or following a 1 hour physical gelation period at 4°C (Figure IV.45 A & B).

In general, a similar trend is observed for all formulations as an increase in stiffness in combination with a decrease in swelling ratio can be observed for the physically gelled hydrogels (Figure IV.45 A & B). When physical gelation is first induced, the effect is most pronounced for the chain growth gel-MOD that outperforms all other formulations both in terms of stiffness and swelling ratio with a 5.5-fold increase in stiffness and a 1.4-fold decrease in swelling ratio compared to the gels which were crosslinked from solution. This result is anticipated as no phase separation can occur in this system. Additionally, the proximity effect of the methacrylamides due to triple helix formation also decreases the probability for the formation of primary cycles resulting in network imperfections. Because of the structural similarity between gel-NB and gel-SH, it is obvious that this combination results in the second stiffest hydrogel with a 4.3-fold increase in storage modulus and a 1.2-fold decrease in water uptake capacity. Alsofor the low molecular weight crosslinkers (i.e. DTT and TEG2SH) a significant effect is observed because their small molecular size (i.e. 154 g/mol and 226 g/mol vs > 3000 g/mol) and low concentration will not interfere substantially with the triple helix formation. As anticipated, the high molecular weight crosslinkers (i.e. the PEG-based crosslinkers) exhibit only a small benefit from physical gelation whereas the 4-arm PEG crosslinkers even result in a slight decrease in mechanical properties due to phase separation between both components.

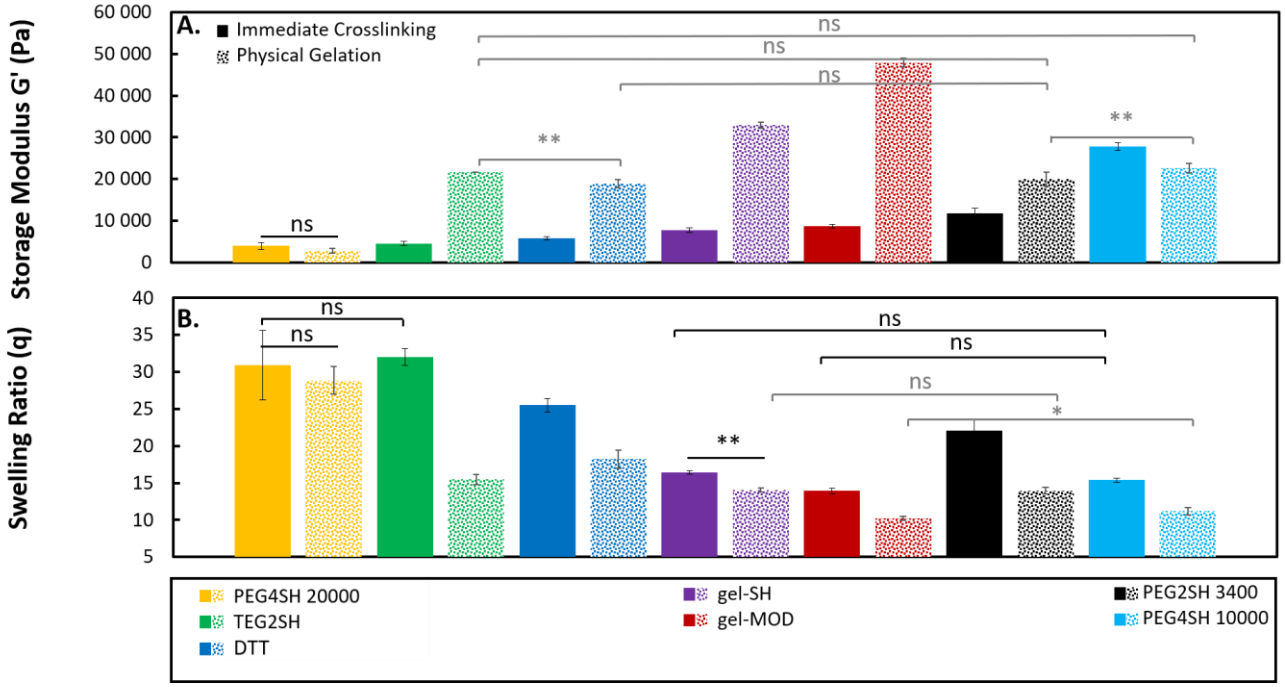

Figure IV.45: Influence of physical gelation prior to crosslinking using Irgacure 2959 as PI on storage modulus (A) and swelling ratio (B) with the full bars being crosslinked without physical crosslinking and the dotted bars after a 1 h incubation period at 4°C to induce physical crosslinking prior to UV irradiation. All statistical differences are significant with $p < 0.001$ unless stated differently with ** $p < 0.001$, * $p < 0.05$ and ns indicating no statistical significance.

Consequently, the use of gel-SH as crosslinker results in the most homogeneous network. This combination forms the closest mimic of the conventional gel-MOD hydrogel system in terms of swelling ratio and mechanical properties, with the additional benefit of the characteristic fast reaction kinetics of thiol-ene systems.

4.4. Influence of Applied Crosslinker on Laser-Based Processing Performance

To assess the processability differences of the different hydrogel formulations, a 2PP assay was performed in line with previous reports [230,284,336] (see Chapter 2 & 3). In this assay, cubes (r = 100 µm) were structured at different laser powers with a constant scanning speed of 100 mm/s on top of a methacrylated glass slide (Figure IV.46 A). As a result, an overview of the processing range of each derivative is obtained. Furthermore, measuring of the top surface of the cube, which is not limited in swelling by adhesion to the glass, provides an indication of the swelling degree which is closely related to the CAD-CAM reproducibility (Figure IV.46 B). In addition, it also provides insights in the crosslink density. In line with previous reports, it is anticipated that from a certain laser power onwards, no more decrease in swelling is observed, indicating a fully crosslinked network[336] (see Chapter 3).

The assay indicated the far superior processability of the thiol-ene hydrogels over the conventional chain growth hydrogels (see also Chapter 3) [336]. More specifically, the polymerization threshold for the different crosslinkers is similar and extremely low, around 4 to 5 mW average power, which is about 20-fold below the polymerization threshold for the conventional gel-MOD hydrogels (i.e. 80 to 90 mW average laser power). An exception in this respect is the high molecular weight PEG4SH 20000 and gel-SH (Figure IV.46). However, it should be noted that all hydrogels were crosslinked in the presence of 2 mol% P2CK as PI relative to the number of norbornene/methacrylamide functionalities, which corresponds to 0.68 mmolar of PI. However, for the gel-NB/gel-SH formulations, the total amount of gelatin was kept at 10 w/v% thereby maintaining a 1:1 thiol:ene ratio. Therefore, the PI concentration was lower because it was adjusted with respect to the amount of norbornene functionalites (i.e. 0.3 mmolar), resulting in a higher polymerization threshold and a higher energy dose before reaching a plateau value.

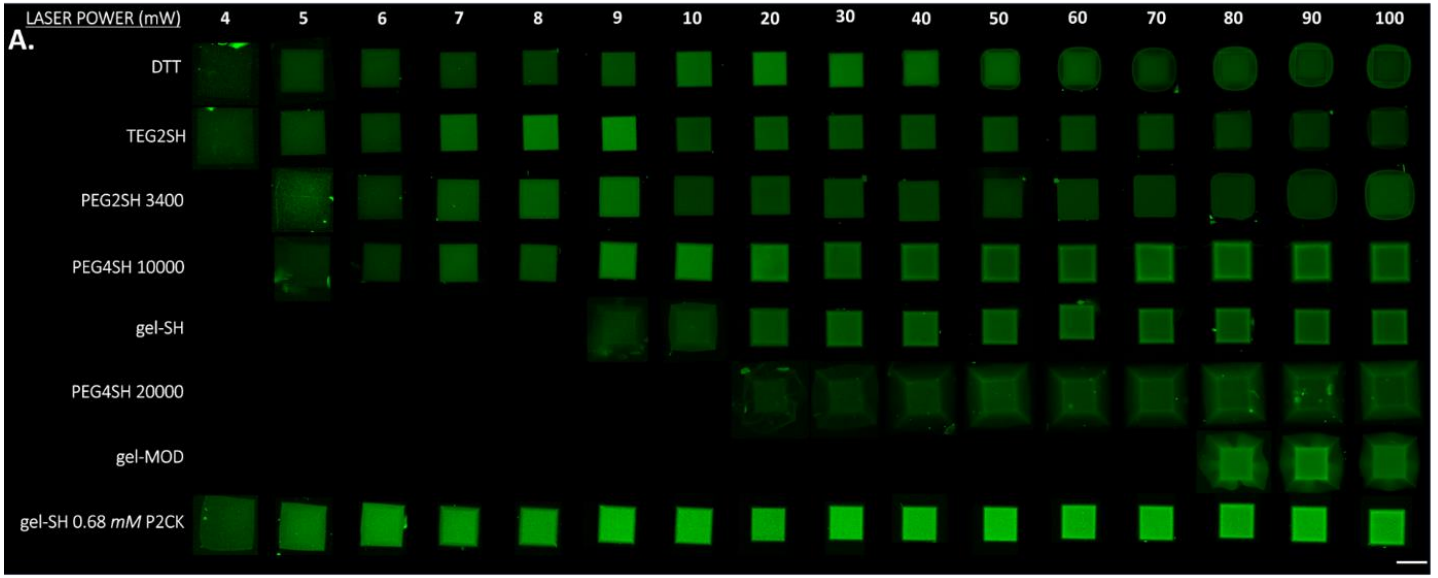

Figure IV.46: Overview of 2PP processing range at 100 mm/s scanning speed in terms of laser power by structuring cubes (r = 100 µm) in the different formulations (A). (Scale bar represents 100 µm. Volumetric swelling calculated from the comparison of the top surface area to the applied CAD design (B). ; Maximum volumetric swelling calculated from the surface area of the layer with the highest swelling degree relative to the applied CAD model for the different thiol-ene formulations (C). (Image continued on the next page)

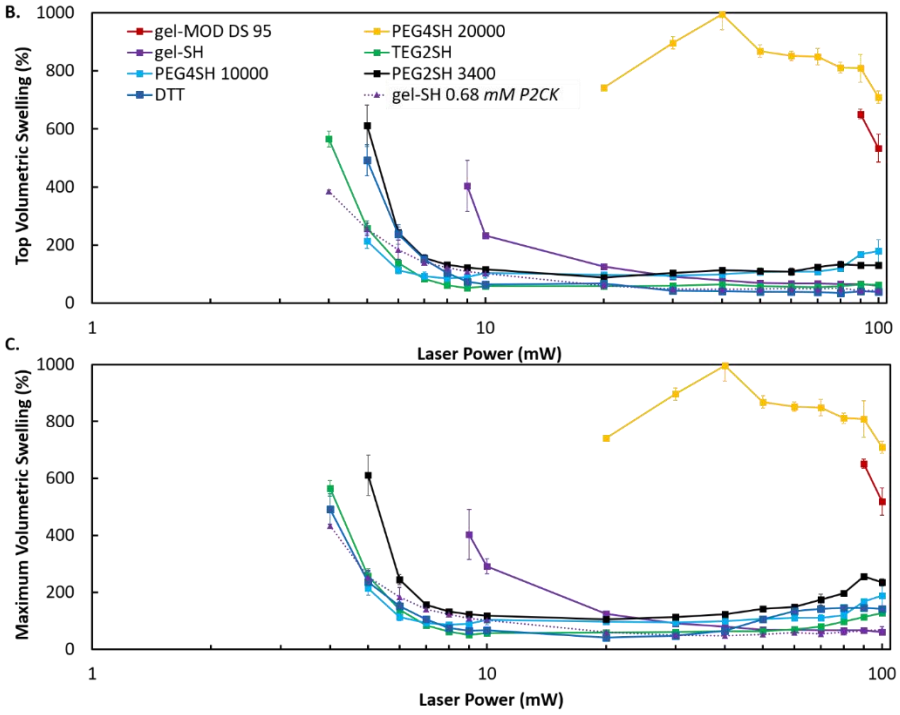

To provide a fair comparison, an additional experiment was performed where this hydrogel combination was crosslinked in the presence of 0.68 mmolar PI which resulted in a comparable polymerization threshold as for the other thiol:ene systems (i.e. 4 mW average laser power) (Figure IV.46).

For the high molecular weight, 4-arm PEG4SH 20000, the structuring threshold was observed at 20 mW. Although this is still significantly lower compared to the conventional gel-MOD, The swelling profile as a function of increasing laser powers appears quite random and is substantially higher compared to the other thiol:ene formulations. Furthermore, during structuring, it became apparent that phase separation between gel-NB and PEG4SH 20000 occurred as evidenced by the presence of spherical-shaped particles. This is further substantiated by the high amount of debris that can be observed on the LSM images after structuring (Figure IV.46 A and Figure IV.47).

This further confirms why the crosslink density was substantially lower compared to the other thiol:ene hydrogels in the single photon polymerization experiments (*vide supra*). Therefore, no further characterization experiments

were performed using this formulation, due to reproducibility issues. Furthermore, when considering the swelling behaviour of the top surface of the cubes in the different formulations, a plateau in swelling occurs around an average laser power of ± 10 mW for the thiol:ene systems.

This indicated the presence of a fully crosslinked network, in contrast with the gel-MOD hydrogel that exhibits a clear laser power dependency within the presented range as also previously reported [230,284] (see Chapter 2).

When the laser power is further increased, this plateau is maintained initially as expected, but at higher laser powers (i.e. above 30 to 40 mW), the swelling increases again. This can be attributed to some extent to the formation of a larger voxel with increasing laser powers [343,344]. However, these effects are considered to be of a lower order of magnitude as observed in the present experiments and would not result in deformations of the basic cubic structure [275].

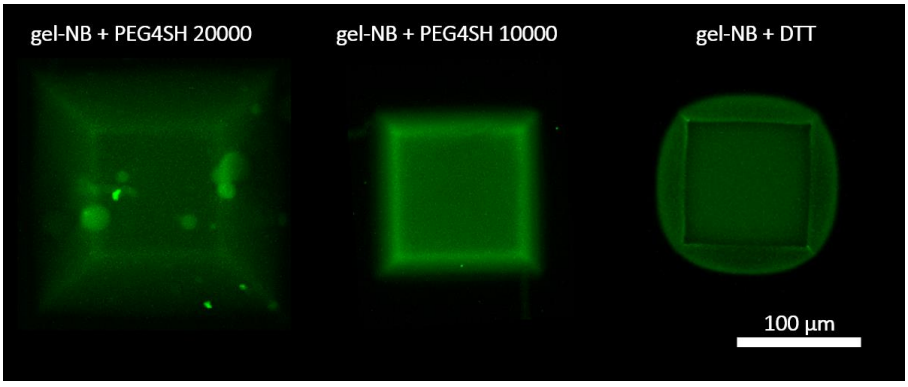

Figure IV.47: Zoom of cubes structured at 90 mW and 100 mm/s in different thiol-ene formulations indicating the presence of spheres in the gel-NB + PEG4SH 20 000 formulation due to phase separation occurring between gelatin and the crosslinker.

Furthermore, when observing the shape of the cubes (Figure IV.47 & 48), another phenomenon is clearly responsible for this effect at high laser powers. Indeed, instead of a gradual increase in swelling when moving away from the glass in the Z-direction as observed at lower laser powers and as previously reported (see Chapter 2 & 3), the swelling appears to reach a maximum first and then decreases again with increasing height. Therefore, besides measuring the top surface, also the maximum swelling for each cube

was assessed. This reflected the increase in volume with increasing laser powers even more (see Figure IV.46 C). A similar trend was also previously reported by Dobos et al. who observed this effect reflected in the mechanical properties of the obtained structures [341]. Since the swelling is larger halfway up the structure and decreases again, it is anticipated that this effect originates from a competitive photocleavage reaction. It is anticipated that this photocleavage occurs in the amide bonds of the gelatin backbone as it is known that amide bond photo-degradation can occur, especially in aqueous environments [345–347]. Additionally, it has been reported that the photo-lysis or photo-oxidation induced degradation of the amide bond in nylon occurs following a free-radical reaction [346]. These effects typically require very long irradiation times (i.e. weeks to months) in single photon experiments. However, in the present set up, very high laser light intensities are applied, resulting in a very high number of radicals that will be formed, especially at high average laser powers (Figure VII.70). This effect is especially anticipated considering some overlap of the different voxels in between the different layers (Figure IV.49). This voxel overlap was deliberately introduced to ensure proper adhesion between the different layers.

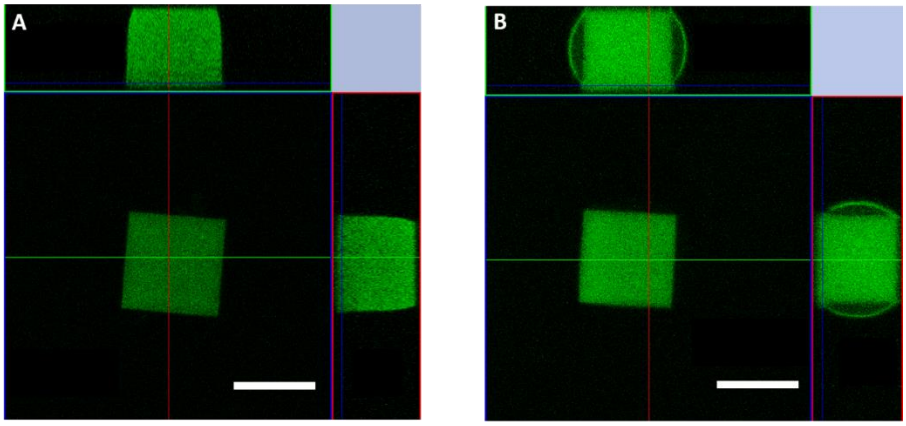

Figure IV.48: Orthogonal projection of the structured cubes indicating the anticipated swelling profile as observed at low laser power (A) and the deviations from this behaviour observed at high laser powers (B). (Scale bars represent 100 µm)

To quantify this overlap to some extent, the voxel dimensions can be calculated using the following formulas (see also Chapter 2) [275]:

$$\omega_{xy} = \frac{0.325\,\lambda}{\sqrt{2}\,NA^{0.91}}\ (if\ NA\ > 0.7) \tag{10}$$

$$\omega_z = \frac{0.532\,\lambda}{\sqrt{2}}\left(\frac{1}{n-\sqrt{n^2-NA^2}}\right) \tag{11}$$

With ω_{xy} being the radius of the voxel in the XY-plane and ω_z the radius of the voxel along the Z-axis; λ being the applied wavelength (i.e. 800 nm); NA being the numerical aperture of the applied objective (i.e. 0.85) and *n* being the refractive index, estimated to be around 1.35 based on previous measurements and the high dilution of the hydrogel precursors in the solution (see Chapter 2). As a consequence, the voxel has an XY-diameter equalling 2 times the (1/e²) radius or = $2\sqrt{2}$ * ω_{xy} (i.e. 602 nm) and a Z-length of $2\sqrt{2}$ * ω_z (i.e. 2826 nm)[275]. To assess how many times every voxel is exposed to the laser, these theoretical values can be compared to the applied hatching (slicing distance in the XY-plane) (i.e. 500 nm) and slicing distance (layer spacing in Z direction) (i.e. 1000 nm) and the fact that every layer is hatched in both X- and Y-direction to ensure proper contact between all lines. Consequently, every crosslinked voxel is exposed twice during the writing of a single layer. Furthermore, this voxel is exposed a third and a fourth time during the writing of the subsequent layer and partially exposed a fifth and sixth time during writing of the third layer since the slicing distance was set about 2.8 times lower in comparison to the intensity maximum of the illumination point spread function² (IPSF²) (Figure IV.49).

It should be noted that this overlap between the voxels of consecutive layers is performed deliberately to ensure proper attachment between the different layers as the voxel shape as defined by the IPSF² can be approximated by a three-dimensional Gaussian volume resulting in smaller thicknesses towards the Z-edges [275]. As a consequence, every structured voxel is 5*2 = 10 times (partially) exposed (5 consecutive layers, 2 times per layer due to X and Y hatching) to the laser in the bulk of the structure whereas for the last layer, this is only (partially) exposed 6 times - 2 times partially during the n-2 layer at lower intensity and 2 times during the previous (due to X and Y hatching) and two times in the centre of the focal spot during the writing of the layer, whereas there will be 1.8 additional layers above only exposed 1.8 times to the edge of the voxel. Therefore, the observed decrease in swelling properties

towards the top of the structure is consistent with partial cleavage of the bulk of the material (Figure IV.48).

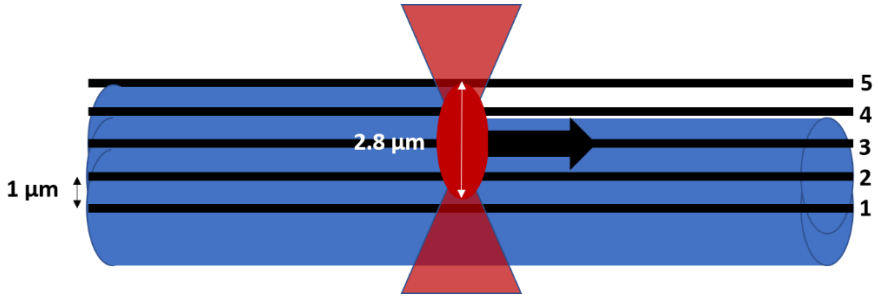

Figure IV.49: Schematic representation on how a voxel when scanned during the structuring of layer 3 will result in partial irradiation of the already structured layer 1 and 2 and layer 4 and 5 that still need to be polymerized.

To further substantiate this hypothesis, the effect of the laser on the hydrogel material was assessed by exposing UV-crosslinked hydrogel pellets to the laser according to a previously reported protocol [217]. To this end, first, a hydrogel pellet was obtained via crosslinking of a gel-NB/DTT solution on top of a methacrylated glass slide using UV-A irradiation in the presence of LAP as PI. Next, part of the pellet was cut with a scalpel and removed resulting in a clear edge (Figure IV.50). This edge was exposed to different laser intensities (i.e. 50 – 200 mW average power) at different scan speeds (i.e. 25 – 150 mm/s) using the same hatching properties as applied throughout the structuring experiments in an attempt to generate channels (350 µm * 30 µm * 100 µm) over the introduced edge of the hydrogel (Figure IV.50). For this experiment, pellets were made starting from the DTT-containing formulation as the effect was mostly pronounced for this condition (Figure IV.46 A).

During structuring, the samples were monitored to assess bubble formation as an indication of cleavage due to thermal effects. Next, the hydrogels were incubated in PBS at 37°C to remove any degraded material, followed by incubation in a solution containing a highly fluorescent FITC-dextran with a molecular weight of 2000 kDa, which cannot diffuse into the hydrogel due to its high molecular weight, but should be able to penetrate into any introduced channels in case of successful cleavage (Figure IV.50). Brightfield microscopy (Figure IV.51) already allowed to visualize some of the exposed regions as a consequence of a difference in refractive index due to partial degradation of the material, resulting in a less densely crosslinked network and a concomitant decrease in refractive index which is more apparent at

higher spatiotemporal irradiation doses (i.e. low scanning speed (< 100 mm/s) and high intensities (>100 mW)).

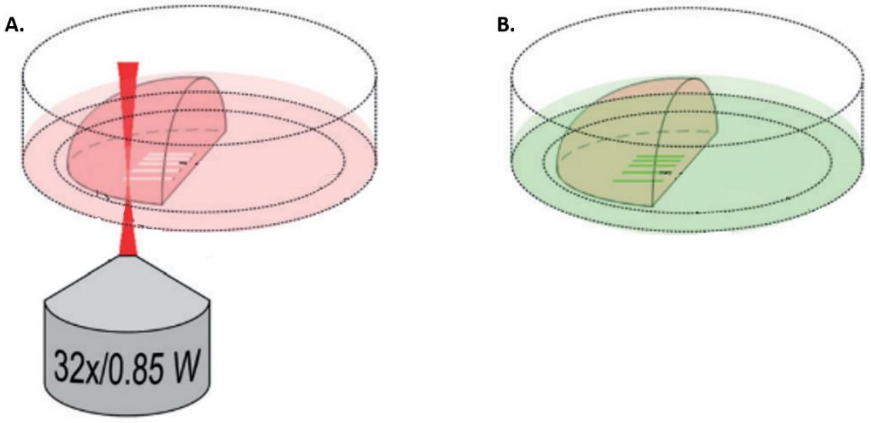

Figure 50: Principle of photocleaving experiment. Structuring channels in the pellet which is cut in half (A). Swelling in a solution containing FITC-dextran to visualise the formed channels (B). (Image adapted from [217])

Furthermore, when looking at the associated laser scanning microscopy images, the FITC-dextran could clearly penetrate the channels at 25 and 50 mm/s at high laser intensities (i.e. 150 and 200 mW average power) and at 75 mm/s at 200 mW. However, it should be noted that at 25 mm/s and 200 mW some bubble formation was observed during structuring which is a clear indication of (partial) cleavage by thermal effects. However, this was not the case at the higher writing speeds and when applying lower laser powers. The fact that not all channels could be penetrated by the fluorescent FITC-dextran, while being visible on brightfield microscopy images indicates that at lower doses, the cleavage is not complete as only part of the bonds will be broken resulting in increased swelling. Furthermore, the observed difference in refractive index cannot be attributed to additional polymerization, as it is known that during the UV polymerization of gel-NB/DTT hydrogels, full conversion was obtained (Figure III.35 A). Additionally, it should be noted that during this control experiment, only full cleavage occurred at lower speeds and higher intensities than during the actual structuring experiment. However, since at similar conditions and lower spatiotemporal energy doses, the channels are still visible, there will still be some photo-degradation ongoing during the structuring itself, especially at higher powers, resulting in the

observed unexpected swelling behaviour (Figure IV.46). In this respect, the deviations from the original cube seem to be mostly pronounced for the gels crosslinked with DTT (Figure IV.46, IV.47 & IV.48). Moreover, the quantitative analysis of the maximum swelling relative to the applied CAD (Figure IV.46 C), indicates that this effect is more pronounced in hydrogels crosslinked with the bifunctional crosslinkers (i.e. DTT, TEG2SH and PEG2SH 3400).

This is intuitive as in these hydrogels, a less densely crosslinked network is obtained, as each crosslinker only links 2 norbornene functionalities to each other. Therefore, only one amide bond in the backbone needs to be broken in between 2 norbornene functionalities to fully cleave this crosslink whereas in the gels with PEG4SH 10000, at least 3 bonds need to be broken to realize the same effect. When looking at the 4-arm PEG4SH 10000, this effect is less pronounced, although a higher volumetric swelling is obtained at 100 mW compared to low molecular weight crosslinkers (Table IV.5). Furthermore, the effect appears most pronounced when using PEG2SH 3400, because of the highly hydrophilic nature of PEG. After cleavage of some bonds, a less densely crosslinked network is obtained that will result in a larger additional water uptake in comparison to the low molecular weight crosslinkers. This phenomenon is a consequence of the larger distance between the different thiol:ene-crosslinks. When comparing this to the minimal volumetric swelling, a 2.1-fold increase in swelling due to photocleavage effects for PEG4SH 10000 vs a 3.8-fold increase for DTT and a 3.4-fold increase for the TEG2SH crosslinker is observed. This effect is lacking when using highly functionalized gel-SH as crosslinker. This is expected as this derivative exhibits around 0.27 mmol of thiols/g gelatin, corresponding to an average of around 14 thiols per gelatin chain. The effect of cleavage is not observed in this system, because full cleavage of one “junction zone” in the network is only obtained by cleaving a substantially higher number of bonds. For the conventional chain growth hydrogels (i.e. gel-MOD), the reasoning is similar. Upon crosslinking, kinetic non-biodegradable chains are formed which link multiple photo-crosslinkable functionalities into one junction zone.

As a result, multiple bonds need to be broken in order to result in an observable cleavage of the network [146,336,348]. Additionally, the photopolymerization of methacrylamides is characterized by slower crosslinking kinetics (Figure IV.43), therefore, both effects will occur simultaneously, with the polymerization reaction occurring more than the cleavage thereby resulting in a perceived decrease in swelling with increasing powers.

Table IV.5 Comparison of volumetric swelling at 100 mW average power and minimum swelling of different thiol-ene systems.

Crosslinker	Volumetric Swelling @ 100 mW (%)	Minimum Swelling	Molecular Weight Between Crosslinks (g/mol)
PEG4SH 10000	180 ± 40 %	85 ± 10 % (@ 8 mW)	2500
DTT	145.7 ± 3.1 %	38.3 ± 0.5 (@ 10 mW)	226
TEG2SH	128.2 ± 10.33 %	38.1 ± 4.3 (@ 20 mW)	154

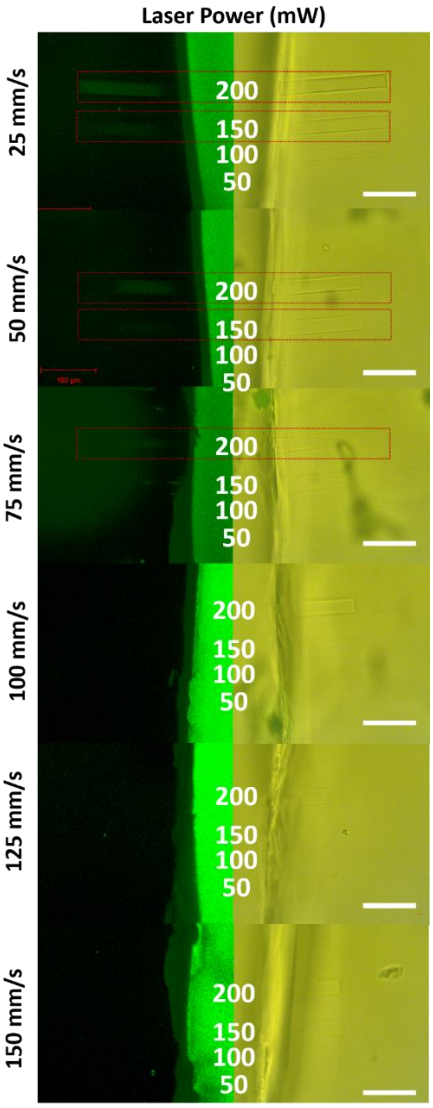

Figure IV.51: Laser scanning microscopy (left) and Brightfield (right) images of the 2PP-induced photocleavage of a gel-NB + DTT hydrogel as a function of laser scanning speed and average laser power in the presence of FITC-dextran 2000 kDa. The doses for which full hydrogel cleavage occurred as evidenced by penetration of the dye into the hydrogel are presented through a red square. The brightfield images show the weakening of the hydrogel as a consequence of partial cleavage resulting in a difference in refractive index due to a looser network. (Scale bars represent 100 µm)

In contrast, for the thiol-ene systems, full crosslinking already occurs at low laser powers (i.e. ± 20 – 30 mW) where further increasing the laser power will only result in more cleavage as it is no longer compensated for by concurrent polymerization reactions.

Finally, it should be noted that the lowest swelling degree and associated CAD-CAM reproducibility is obtained when using the highly functional gel-SH, rendering it the most suitable candidate for 2PP processing.

4.5. In Vitro Cell Viability

Another important feature of a hydrogel formulation for tissue engineering and biofabrication applications is its biological performance. In particular, the performance of the material in the presence of cells is of paramount importance if it would be used as a bioink (i.e. in the presence of cells during processing) or as a bioink component[349]. Therefore, cell encapsulation experiments as well as toxicity of the different components of the hydrogel formulation were tested. It should be noted that due to the poor performance of gel-NB/PEG4SH 20000, that resulted in heterogeneous, weak hydrogels in both the single- and two-photon processing experiments, this formulation was not assessed towards biological performance. The other formulations were subjected to a cell encapsulation assay by preparing hydrogel formulations consisting of the hydrogel precursors (i.e. gel-MOD or gel-NB and the corresponding thiolated crosslinker in the presence of 2 mol% LAP corresponding to around 0.55 *mM* because this is way below the cytotoxic limit (i.e. 1.12 *mM*)[292]) at a total concentration of 7.5 w/v% and containing 500 000/ml GFP-labelled ASCs. The samples were crosslinked during 10 mins UV-A irradiation (i.e. 365 nm and 25 mW/cm²). The metabolic activity and cellular morphology of the encapsulated cells was assessed at specific time points using a Presto blue assay and laser scanning confocal microscopy.

When looking at the cell morphology over time (Figure IV.52 A) clear differences can be observed between the different samples. More specifically, cells start to remodel the matrix sooner in the formulations applying the low molecular weight crosslinkers (i.e. DTT and TEG2SH) which is evidenced by an increase in average cell length (Figure IV.53 A). The fact that this is observed first with the low molecular weight crosslinkers is anticipated. First of all, these hydrogels are the softest, which is known to enhance matrix remodelling [152,341] (Figure IV.44 A). Secondly, remodelling of the matrix occurs via enzymatic cleavage of the gelatin backbone by collagenase

between Gly and Ile in Gly-Pro-Gln-Gly-Ile-Ala-Gly-Gln sequences [48,115] (see also Chapter 1).

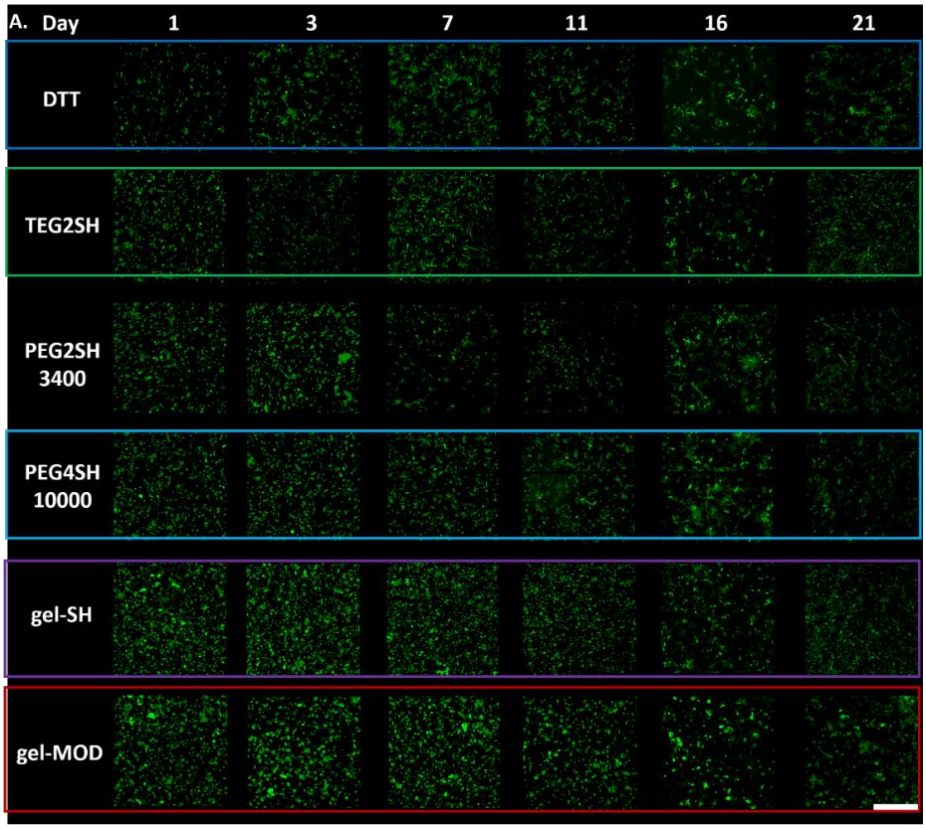

Figure IV.52: Z-stack confocal laser scanning microscope images of GFP labelled ASC's encapsulated in the different hydrogel formulations after 10 min UV exposure crosslinking at different time points (A). (scale bar represents 500 µm).

Because the hydrogels obtained using TEG2SH and DTT only link 2 norbornene functionalities to each other in each junction knot, cleavage of part of the backbone will have a more drastic effect on the network density in comparison to for example gel-MOD or gel-NB/gel-SH hydrogels where every junction knot consists of multiple methacrylamide or thiol/norbornene links. A similar trend was also observed in the photocleavage reaction. Because all hydrogels were immediately crosslinked after pipetting; the stiffest hydrogels are the ones obtained using gel-NB/PEG4SH 10000 (Figure IV.44 A).

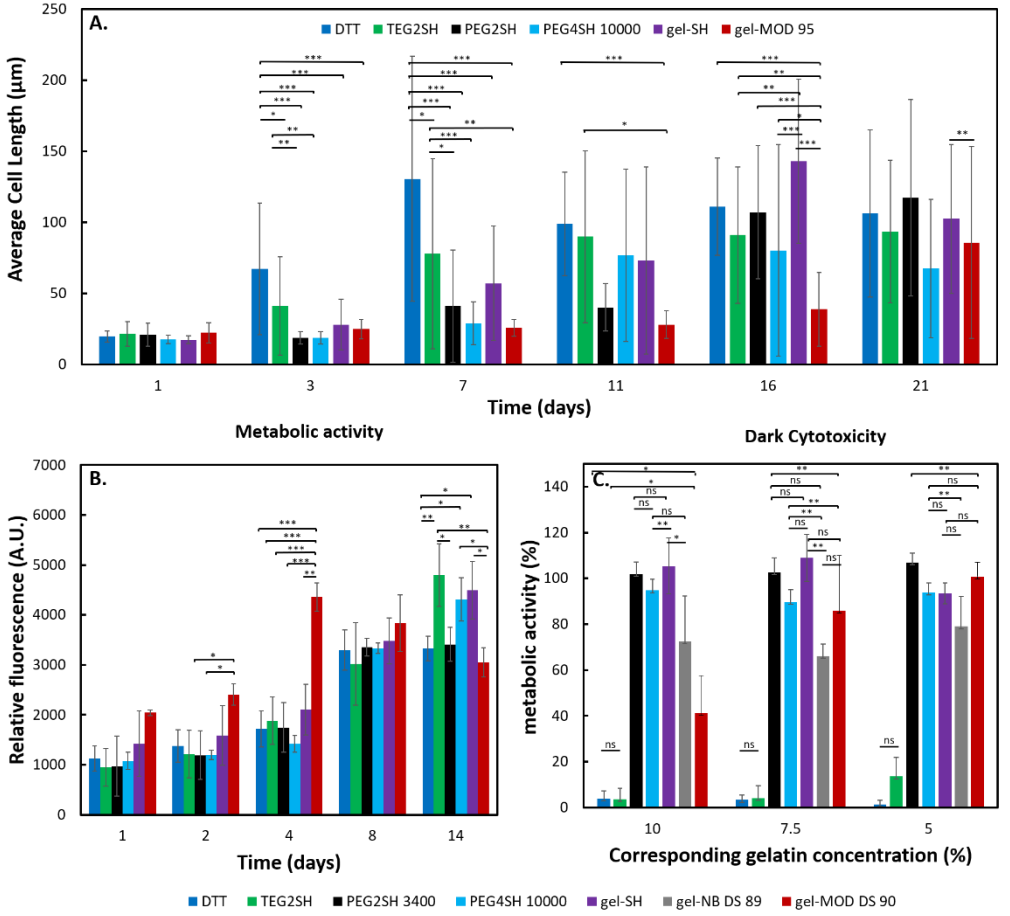
A.
DTT
TEG2SH
PEG2SH
PEG4SH 10000
gel-SH
gel-MOD 95
Average Cell Length (µm)
Time (days)
Metabolic activity
B.
Relative fluorescence (A.U.)
Time (days)
Dark Cytotoxicity
C.
metabolic activity (%)
Corresponding gelatin concentration (%)
DTT
TEG2SH
PEG2SH 3400
PEG4SH 10000
gel-SH
gel-NB DS 89
gel-MOD DS 90

Figure IV.53: Measured average cell lengths in the different hydrogel formulations at different time points (B). Metabolic activity of the encapsulated cells in the different hydrogel formulations at different time points (C). Dark cytotoxicity of the different components of the hydrogel formulations for 3 different corresponding gelatin concentrations (D). All statistical significant differences are denoted with *p<0.05, **p<0.01, ***p<0.005, except for panel D in which all differences are significant with p<0.005 unless denoted otherwise with ns representing no statistical difference (Image continued on the next page)

However, remodelling of the matrix occurs last in the gel-MOD hydrogels due to the presence of the kinetic chains linking more functionalities into one junction knot. Therefore, more bonds need to be cleaved before the cells can remodel the matrix in comparison to the thiol:ene systems. It is anticipated that remodelling occurs later (i.e. ≥ 7 days; Figure 42 A & B) in hydrogel systems with a higher number of thiol functionalities per crosslinker.

Consequently, remodelling should occur last in the gel-NB/gel-SH hydrogels with around 14 thiols/crosslinker. However, after 16 days of culture, the cell length is significantly higher in these hydrogels in comparison to the PEG4SH 10000 hydrogels with 4 thiols/crosslinker due to the fact that the gel-SH crosslinker is also prone to enzymatic degradation, which counterbalances this effect.

Another aspect to assess biocompatibility is monitoring of the metabolic activity of the cells, which is related to the cellular activity (Figure IV.53 B) [350]. In this respect, after one day of encapsulation, no significant differences are observed between the different thiol-ene systems and the gel-MOD reference material. Although after 2 and 4 days of culture, the gel-MOD reference exhibits a significantly higher metabolic activity in comparison to the PEG containing formulations, while there are no significant differences between the different thiol-ene systems as such. Furthermore, after 8 days of culture, there are no significant differences between the thiol-ene systems and the gel-MOD benchmark any longer, while after 14 days, the TEG2SH, PEG4SH 10 000 and gel-SH-containing systems significantly outperform the gel-MOD benchmark.

Therefore, it can be concluded that all assessed thiol-ene systems exhibit at least a comparable biocompatibility to gel-MOD, irrespective of the applied crosslinker. Additionally, they exhibit more favourable crosslinking kinetics, that can significantly decrease the writing times (*vide supra*). In addition, varying the crosslinker provides additional control over the mechanical properties, while maintaining the same amount of cell-interactive functionalities(i.e. RGD) [48,168]. Finally, the mechanical properties can further be fine-tuned by varying the thiol/ene ratio as previously reported [48,168,336] (see Chapter 3).

Another relevant aspect for bioink components, is the toxicity before crosslinking, or the “dark toxicity”, as depending on the printing time, the cells will be in the presence of these components for a considerable time. Therefore, the toxicity was screened for the different components at the relevant concentrations to yield hydrogels with a gelatin content of 10, 7.5 or

5 w/v%. To this end, a confluent monolayer of GFP-labelled ASCs was exposed to these components for 2 hours, followed by removal of the components followed by 24 hours of incubation prior to measuring the metabolic activity (Figure IV.53 C). Two hours was selected as a relevant time frame, as this is a reasonable estimation of a long printing process where cells would be in contact with the uncrosslinked components. Most importantly, this assay indicated the cytotoxicity of the small molecular weight thiolated crosslinkers (i.e. DTT and TEG2SH) at all assessed concentrations (Figure IV.53 C). This is probably due to the possibility for these molecules to penetrate the cell membrane, as also previously observed for low molecular weight PI [235]. Once inside the cell membrane, the thiols present on these crosslinkers can interact with thiols present within the cytoplasm such as kinases, transcription factors and phosphatases, thereby reducing disulphide bonds or forming disulphide bonds [194,351,352]. Consequently, this dark toxicity was not observed for the high molecular weight crosslinkers (i.e. PEG2SH 3400, PEG4SH 10 000 and gel-SH). In terms of gelatin materials, comparable biocompatibility is observed between gel-NB and gel-MOD at 7.5 w/v%, whereas at high concentrations, gel-NB appears to be less cytotoxic in comparison to gel-MOD. In general, gel-SH is more cytocompatible compared to both gel-NB and gel-MOD at 7.5 and 10 w/v%. Therefore, gel-NB thiol-ene systems prove to be suitable alternatives for the gel-MOD gold standard in terms of biocompatibility when selecting the correct crosslinker.

4.6. Conclusion

Thiol-norbornene gelatin hydrogels prove to be very relevant alternatives for the widely used gel-MOD as bioink or biomaterial ink (component) for biofabrication purposes. However, the use of thiol-ene photo-click chemistry allows to further tune the hydrogel properties in terms of reactivity, processability, mechanical properties and biological response by varying the thiolated crosslinker. Crosslinkers with a higher number of thiols (i.e. gel-SH or PEG4SH 10000) result in stiffer gels, thereby better mimicking the mechanical properties of the widely used gel-MOD in combination with more favourable crosslinking kinetics. The selection of the most appropriate crosslinker also depends on the processing method of the gelatin hydrogel. Indeed, when direct crosslinking from solution is desired, superior mechanical properties and the lowest swelling ratio are obtained when using PEG4SH 10000. If crosslinking is desired from a physical gel, the low molecular weight of gelatin based crosslinkers are preferred because phase separation can occur with the high molecular weight PEG crosslinkers resulting in a

heterogeneous network. In this respect, superior mechanical properties are obtained for the conventional gel-MOD, followed closely by the gel-NB/gel-SH system that also benefits from the physical gelation prior to crosslinking.

In terms of biological performance, no significant differences in metabolic activity were observed between the different gel-NB formulations and the gel-MOD benchmark, indicating a comparable, desirable cytocompatibility. However, the type of crosslinker does influence the remodelling behaviour of the encapsulated cells, as the low molecular weight crosslinkers (i.e. TEG2SH and DTT) induce faster matrix remodelling in comparison to the formulations with the high molecular weight crosslinkers and gel-MOD. In this respect, not only the mechanical properties of the hydrogel are of importance but also the type of crosslinks present in the hydrogel. Indeed, the stiffest formulation containing PEG4SH 10000, still exhibits matrix remodelling prior to gel-MOD because of the absence of kinetic chains following the chain-growth crosslinking approach. Furthermore, the dark toxicity of the components was also assessed to assess suitability for longer printing times, which indicated considerable toxicity for the low molecular weight crosslinkers (i.e. TEG2SH and DTT). It is anticipated that they can penetrate the cell membrane and react with thiols inside the cytoplasm, thereby inducing cytotoxicity. For the high molecular weight crosslinkers, no significant cytotoxicity was observed. Furthermore, gel-NB and gel-MOD exhibited a comparable dark cytotoxicity.

However, the real benefit of the thiol-ene systems lies in their use for light-based additive manufacturing applications, where the photo-reactivity has a great influence on the attainable writing speeds and associated writing times. This is especially relevant for high-resolution laser scanning-based systems such as SLA or 2PP. Indeed, it was shown that substantially (i.e. 20-fold) lower laser powers could be applied to crosslink the thiol-ene formulations, regardless of the applied crosslinker. The applied crosslinker does have a large influence on the volumetric swelling ratio and associated differences in CAD-CAM reproducibility. The high molecular weight, bifunctional PEG crosslinker (PEG2SH 3400) exhibited the highest water uptake capacity over the entire processing range due to the low amount of thiol functionalities, the large distance between two crosslinks and the highly hydrophilic nature of the crosslinker. The lowest swelling, was obtained for the crosslinker with the highest number of thiols (i.e. gel-SH). However, at high average laser powers, a specific non-anticipated increase in swelling was observed in all formulations due to photo-cleavage of the gelatin backbone. This effect was most pronounced for the low molecular weight bifunctional thiolated

crosslinkers (i.e. DTT and TEG2SH) while being absent for the highly functional gel-SH crosslinker as well as for gel-MOD. In those systems fewer bonds need to be cleaved upon applying the low molecular weight crosslinkers to result in real channels in the hydrogel.

Therefore, the most promising thiol-ene alternative for gel-MOD is the gel-NB/gel-SH formulation, because this benefits from the formation of hydrogels with mechanical properties mimicking those of gel-MOD, while also benefitting from the physical gelation behaviour prior to crosslinking in combination with a low cytotoxicity, fully biodegradable and biointeractive components, no issues with phase separation and best CAD-CAM mimicry, being the least susceptible to photocleavage.

Chapter 5:
Development of Artificial Descemet's Membranes Based on Poly(lactic acid) and Gelatin Hydrogels as Corneal Endothelial Scaffold

The *in vitro* cell biology in the present sample was performed by Bert van Den Bogerd. Part of the membranes were produced by Dhr. Jasper Delaey.

Parts of this chapter have been submitted to Advanced Healthcare Materials as:

> **J. Van Hoorick**, J. Delaey, J. Van Erps, H. Thienpont, P. Dubruel, N. Zakaria, C. Koppen, S. Van Vlierberghe, B. Van den Bogerd *Advanced Healthcare Materials,* **(submitted 2019)**

5.1. Introduction

The present chapter focusses on the application of the gelatin hydrogels developed in the previous chapters towards corneal endothelial regeneration.

As previously discussed in the introduction, the cornea is the clear membrane that provides the eye a window to the exterior world. Several diseases or trauma can lead to an opaque cornea resulting in impaired vision and eventually, in blindness.

A significant portion of these patients suffer from an oedematous cornea due to a dysfunctional corneal endothelium, a monolayer of hexagonally shaped cells that covers the posterior corneal surface [353]. This cell layer is principally responsible for maintaining the cornea in a physiological state of deturgescence, which is imperative for its transparency. Corneal endothelial cells are incapable to undergo *in vivo* regeneration, meaning that the absolute number of cells will only decrease throughout life, which can be further exacerbated by disease or trauma. When corneal endothelial cell density falls under a threshold of 500 cells/mm^2, corneal oedema ensues, leading to opacification and irreversible visual impairment [30] (Figure I.3).

Currently, the standard of care is to surgically strip the dysfunctional cell layer and its underlying Descemet's basement membrane from the corneal stroma and replace this with a viable corneal endothelium of a cadaveric donor cornea, termed endothelial keratoplasty [355]. More specifically, in Descemet's stripping automated endothelial keratoplasty (DSAEK), the graft consists of endothelial cells, the Descemet's membrane and some residual stroma that is inserted using a specialized cannula [354] (Figure V.54). In this respect, the graft is first rolled up during introduction in the specialized cannula. Next, the cannula is introduced into the anterior chamber, whereafter the graft is removed using a specialized surgical tool (Figure V.54 A & B). Due to the tension present on the graft in the cannula, automatic unfolding will occur once leaving this cannula inside the anterior chamber (Figure V.54 A & B). This unfolding is aided via the injection of phosphate buffered saline (PBS) into the anterior chamber [354]. Next, the graft is positioned on the back of the stroma using an air bubble or continuous air pressure [354] (Figure V.54 C & D). Finally, excessive fluid is removed via introduced incisions [354] (Figure V.54 E & F).

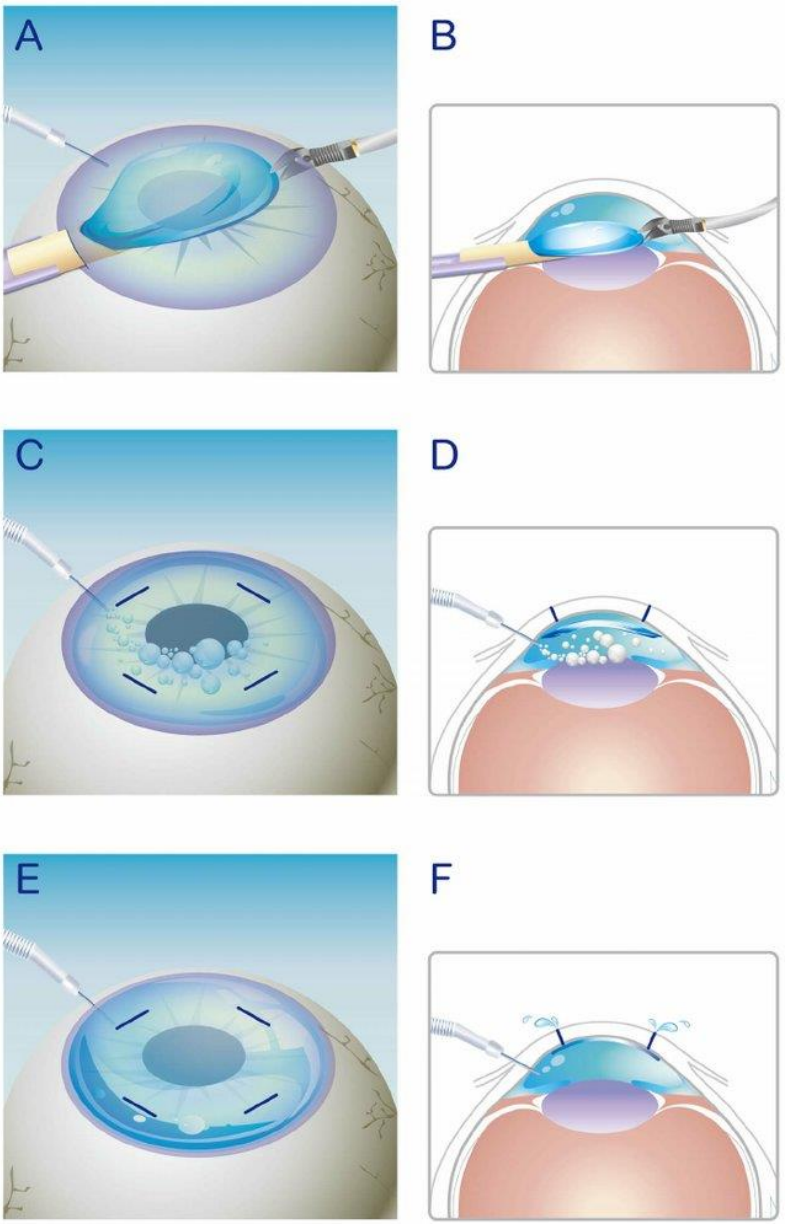

Figure V.54: Descemet's stripping automated endothelial keratoplasty (DSAEK): Introduction of the graft via removal of the specialized cannula (A & B). Placement of the graft on the back of the stroma via introduction of air (C & D). Removal of excessive interface fluid via introduced incisions (E & F). (Image reproduced from [354])

On the other hand, in Descemet's membrane endothelial keratoplasty (DMEK), there is no residual stroma, resulting in a thinner graft that spontaneously forms a roll that is subsequently unrolled by means of an air bubble in combination with manual tapping and manipulations on the anterior cornea by the surgeon [30,356] (Figure V.55). In the procedure, the membrane is also introduced using a cannula in combination with a surgical tool. However, the main difference with DSAEK is the need for more thorough surgical manipulation to unroll and position the membrane to the back of the stroma. Regardless of good visual outcomes and minimal surgery-related complications, there is a severe global donor shortage that limits the number of corneal (endothelial) transplantations. A recent survey estimates that in general for corneal transplantation, only 1 in 70 people requiring a donor cornea can be treated [15]. This unfortunate situation has inspired researchers to develop a cell therapy, based on the *ex vivo* expansion of corneal endothelial cells from one donor cornea to provide multiple patients with an answer to their sight-threatening condition.

Recently, Kinoshita et al. have treated the very first patients with an injection of a corneal endothelial cell suspension and reported good visual recovery up to 2 years later [44]. Nevertheless, the most investigated strategy is to create composite grafts of cells seeded onto a scaffold enabling transplantation similar to the currently applied corneal endothelial grafts. Such cell carriers, however, must exhibit very specific properties, such as transparency, glucose permeability, cytocompatibility and above all, they must maintain the correct endothelial cell phenotype [45]. To date, attempts have been made to find an ideal corneal endothelial scaffold, they range from biological and biosynthetic to fully synthetic membranes. However, no candidate scaffold has met all requirements yet, nor has one effectively entered the clinic [18].

An attractive scaffolding material in this respect is gelatin, because it is obtained via hydrolysis of collagen, the main constituent of the natural extracellular matrix (ECM), rendering it a promising material for tissue engineering [48]. Furthermore, it is inexpensive, non-immunogenic, considered safe by the Food and Drug Administration and exhibits the processing ability in line with a variety of applications [48,104,117]. Additionally, due to the breakdown of the tertiary collagen protein structure into gelatin, it contains RGD (Arginine-Glycine-Aspartic acid) motifs that promote cell attachment, rendering it cytocompatible and cell-interactive [110]. In the past, gelatin has already been used for corneal endothelial tissue engineering as a functionalized scaffold to grow cells on or as a bioadhesive gelatin disc for

transplantation [357,358]. However, these membranes were too thick (i.e. 50 - 750 µm) for clinically relevant application [357,358].

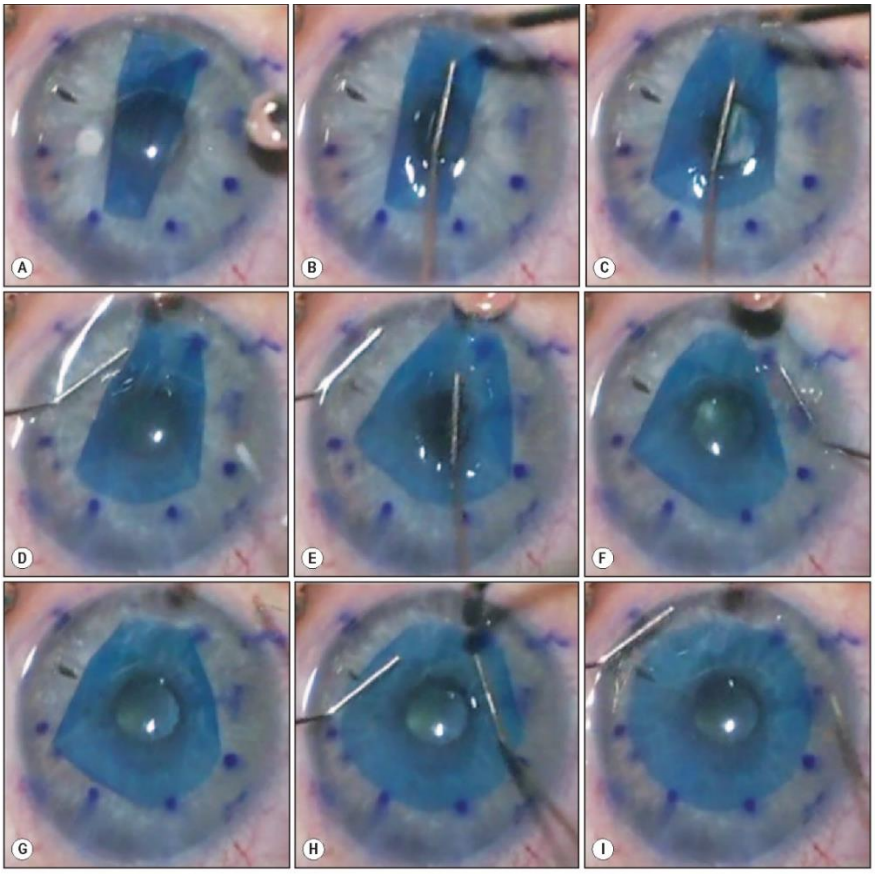

Figure V.55: Descemet's membrane endothelial keratoplasty (DMEK) : Correctly orienting of the graft with the overlapping edges facing forward (A). Unfolding of the graft by tapping on the anterior corneal surface with a cannula (B,C). Centering of the graft prior to complete unscrolling via tapping on the limbus and/or peripheral cornea (D-G). The peripheral edges of the graft are unfolded using specific taps on the cornea (H). The DMEK graft is fully unscrolled and at the correct position (I). (Image reproduced from [356])

In the present chapter, a combination of the modified gelatins discussed in the previous chapters and a biodegradable polyester (i.e. poly(D,L-lactic acid) (PDLLA)) was envisaged, to develop a biocompatible scaffold for corneal endothelial transplantation. On the one hand, modified and crosslinked

gelatins provide an ideal, stabilized ECM mimic to introduce cytocompatibility and cell interactivity. On the other hand, an underlying PDLLA polyester substrate should provide the transplant with mechanical strength, thereby enabling corneal endothelial transplantation.

5.2. Hydrogel Selection and Characterization

For the membrane scaffold development, 4 different gelatin hydrogels were selected based on gel-MOD, gel-MOD-AEMA and gel-NB [121,284,336] (Chapter 2 – 4). In this respect, gel-MOD and gel-MOD-AEMA are crosslinked following a free radical chain growth polymerization mechanism, whereas gel-NB is crosslinked using a thiol-ene step growth polymerization mechanism using DTT as thiolated crosslinker. Additionally, derivatives with a different number of crosslinkable groups were compared. The first and most common derivative, gel-MOD, was used with two different degrees of amine substitution, namely 63 and 95% (corresponding to 0.243 and 0.367 mmol/g gelatin respectively). These derivatives were obtained via the reaction of the primary amines present in the (hydroxy)lysine and ornithine amino acids with 1 or 2.5 equivalents of methacrylic anhydride respectively (Figure I.8 A)[121].

Apart from gel-MOD, gel-MOD-AEMA was also assessed, which is another derivative containing more crosslinkable functionalities [284] (see Chapter 2). This derivative is obtained starting from gel-MOD with a high degree of substitution (i.e. DS 95%) via subsequent reaction of the carboxylic acids present in the side chains of the glutamic acid and aspartic acid amino acids with 2-aminoethyl methacrylate (AEMA) using carbodiimide coupling chemistry (EDC/NHS) (see chapter 2 and figure 8 B). As a result, a DS for the carboxylic acids of 55% was obtained, corresponding to 0.604 mmol methacrylates/g gel-MOD-AEMA. When combining the latter value with the 0.367 mmol methacrylamides/g resulting from the amine substitution, a total of 0.97 mmol crosslinkable groups/g gel-MOD-AEMA was obtained [284].

A third crosslinkable gelatin derivative (gel-NB) applies thiol-ene photo-click chemistry to generate a crosslinked network. For this derivative, the primary amines of gelatin were functionalized with 5-norbornene-2-succinimidyl ester, yielding gel-NB with a DS of 63%, corresponding to 0.243 mmol/g gel-NB (see chapter 3) [336].

To compare the different reactivities of the applied derivatives, photo-rheological measurements were performed on 10 w/v% solutions in the presence of 2 mol% Irgacure 2959 as photoinitiator (with respect to the

amount of incorporated crosslinkable functionalities) and 0.5 equiv. of DTT (i.e a 1:1 thiol:ene ratio) with respect to the norbornene derivative. Irgacure 2959 was selected as photoinitiator, due to its known biocompatible behavior [292]. The assay provides insight in the reactivity of the materials as well as the mechanical properties of the gelatin coatings after crosslinking. In accordance to previous research, the material with the highest density of crosslinkable functionalities (gel-MOD-AEMA) resulted in the highest stiffness as reflected by the storage modulus (G') after 10 minutes crosslinking [284]. This derivative reached a storage modulus of around 15 kPa whereas gel-MOD DS95 reached a storage modulus of around 6 kPa. The gel-MOD DS63 and gel-NB DS63 derivatives yielded storage moduli around 4.5 kPa (Figure V.56 B).

When Palchesko et al. investigated the influence of mechanical properties on the expansion behavior of bovine corneal endothelial cells, they observed the optimal mechanical properties being around a Young's modulus (E') of 50 kPa [359,360]. To put this into perspective, we made an estimation for the Young's modulus (E') following the following equation [270]:

$$E' = 2G'(1+\mu) \quad (12)$$

Here, μ is the Poisson number that equals 0.5 for ideal rubbery materials, which is a good approximation for hydrogels [270,361]. As a consequence, the gel-MOD-AEMA derivative reaches a Young's modulus of around 45 kPa, while the high DS gel-MOD reach Young's moduli around 18 kPa and the low DS gel-MOD and the gel-NB derivatives around 13.5 kPa. As a consequence, gel-MOD-AEMA should provide the closest match with the required mechanical properties of the membrane. However, the natural Descemet's membrane is characterized by a Young's modulus of around 5 MPa [6]. Therefore, the combination with the more robust PDLLA membrane becomes apparent.

We compared the gel points of the different materials as an indicator for reactivity, thereby providing information about the minimally required irradiation time. Here, the drastic increase in reactivity for norbornene derivatives over the more conventional systems is apparent as also reported in chapters 3 & 4 (Figure 2; right panel). The norbornene derivative has a gel point in the range of a few seconds (i.e. 2 – 3 s) versus > 50 seconds for the gel-MOD derivatives, with the gel-MOD-AEMA derivative being intermediate, at approximately 15 seconds (Figure V.56 B).

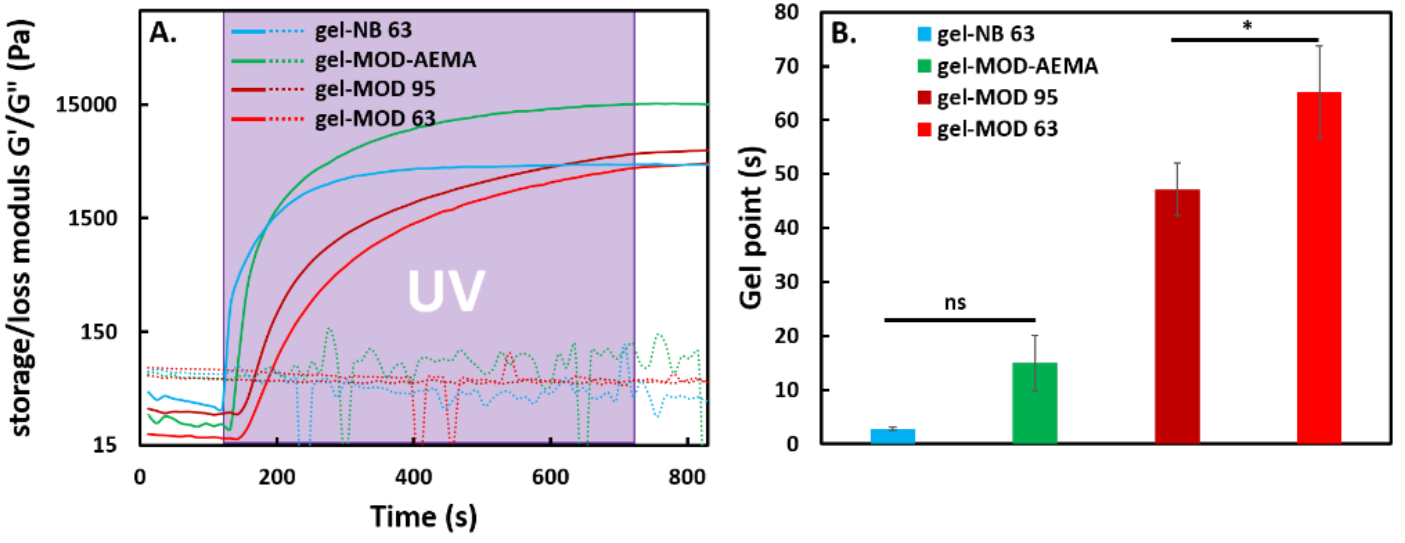

Figure V.56: Photo-rheological monitoring of crosslinking kinetics and resulting mechanical properties at 37°C with the evolution of the storage modulus (G') depicted as solid lines, whereas the loss modulus (G") is depicted using dashed lines. (A); Average gel points (in seconds) after switching on the UV light for the different crosslinking systems as a measure of crosslinking reactivity (n = 3) (B). ***All differences were significant with p < 0.001 except for the ones indicated in the picture with * (p < 0.05) or ns (not significant).***

5.3. Membrane Production

To obtain ultrathin membranes (i.e. the natural Descemet's membrane exhibits a thickness around 10 – 12 µm [362]), a multi-step spincoating approach was used. First, a layer of unmodified gelatin was applied on a supporting glass substrate. This layer enables straightforward membrane harvesting as this gelatin layer will selectively dissolve after incubation in water at 40°C (Figure V.57 C). Next, a polyester substrate was applied through spincoating, starting from a solution of PDLLA in THF. To this end, an amorphous poly(D,L-lactide) with a molecular weight of 150 kg/mol and a polydispersity of 1.13 was chosen for several reasons. First, PDLLA is an FDA approved material for use in the human body [67]. Secondly, PDLLA was chosen over the more conventional PLLA because PDLLA is an amorphous material thereby resulting in a higher transparency [70]. Finally, PDLLA is a biodegradable material resulting in non-toxic lactic acid-based degradation products (see also Chapter 1). This is a specific benefit towards corneal endothelial repair as *in vivo* 85% of the glucose nutrients that enter the cornea are metabolized into lactic acid, which diffuses back through the corneal endothelium. As a consequence, the tissue is characterized by relatively high lactic acid concentrations (i.e. 13 mM in the cornea and 7 mM in the anterior chamber) [49]. Therefore, it is anticipated that PDLLA is an ideal scaffolding material, as the degradation products will not induce any inflammation and the lactate is even considered as a contributing anion flux to maintain corneal transparency [49]. To allow covalent adhesion between the polyester and the subsequent crosslinkable gelatin layer, the surface was activated using a plasma treatment [57,69]. Finally, the crosslinkable gelatin solution was applied starting from a solution containing 2 mol% Irgacure 2959 and an equimolar amount of thiols (DTT) with respect to the NB functionalities for the gel-NB derivative [336]. Gelatin was chosen as an ECM mimic due to the structural similarities with collagen, the main component of the natural Descemet's membrane [21,48]. Furthermore, the material is known to be biodegradable, resulting in the formation of peptides *in vivo*, similarly to collagen breakdown in the human body [48,284,339]. Crosslinking and covalent attachment of this gelatin layer occurred by UV irradiation after prewetting of the surface with type I demineralized water [69].

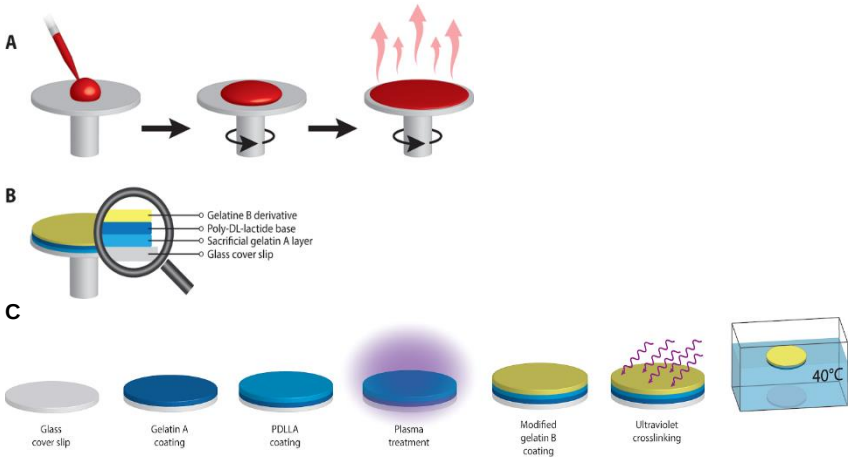

Figure V.57: The principle of spincoating (A). The final composition of the obtained membranes (B)Scheme of the multistep spincoating approach to produce the membranes (C).

Finally, the membranes were detached by immersion in water at 40°C which is above the gel temperature of gelatin (i.e. ± 30°C) (Figure V.57 C) [284]. With respect to membrane fabrication, it should be noted that the gel-MOD-AEMA derivative exhibits a benefit over the other reported derivatives, as the high degree of modification hampers triple helix formation resulting in solubility at room temperature [48,138,284] (see Chapter 3). As a consequence, material manipulation during spincoating becomes more straightforward (i.e. a more homogeneous deposition) because there are no issues with premature gel formation.

5.4. Membrane Characterization

X-ray photoelectron spectroscopy (XPS) elemental surface characterization was performed after each of the aforementioned steps in the multi-step spincoating process to validate the successful application of the respective layers. The results indicate that the elemental composition of the surface differed after each step. There was an anticipated high silicium level (i.e. ± 20 %) from the glass substrate and an anticipated nitrogen signal in the (modified) gelatin layers (i.e. ± 4 % to ± 16 %) (Figure V.58 A) as a consequence of the peptide backbone and the nitrogen atoms present in the side chains of the (hydroxy)lysine, ornithine, histidine, proline and arginine amino acids present in gelatin. Additionally, the N/C ratio diminished with increasing degree of substitution for the gelatin derivatives since more

carbons are attached per amine (i.e. from ± 0.18 to ± 0.05). Especially for gel-MOD-AEMA, this ratio drastically decreased since the introduced AEMA functionalities have a very high C/N ratio (i.e. 6/1). Furthermore, when looking at the O/C ratio of the PDLLA membrane, this corresponds to 0.67, thereby proving that indeed the surface was covered with PDLLA since every repeating unit in the polymer chain contains three carbon atoms and two oxygen atoms.

Further proof of a successful coating process could be found by measuring the static contact angle upon depositing water on the different substrates (Figure V.58 B). After initial coating of the glass with PDLLA, the contact angle increased (i.e. from 69 to 81°) due to the relatively hydrophobic nature of PDLLA. After plasma treatment, reactive oxygen-containing functional groups (i.e. peroxides and hydrogen peroxides) are introduced at the surface, that lead to an increased hydrophilicity as evidenced by a decreased contact angle (i.e. 55°) [69,363]. Subsequent coating with the gelatin derivatives reduces this hydrophilicity. Furthermore, when comparing the non-plasma treated PDLLA with the gelatin coatings, a significant difference can be observed, thereby again confirming successful membrane functionalization. Although some differences between the different gelatin coatings appear to be present, these are non-significant with exceptions between gel-MOD DS 63 and gel-MOD-AEMA with gel-MOD-AEMA being significantly more hydrophilic ($P < 0.05$).

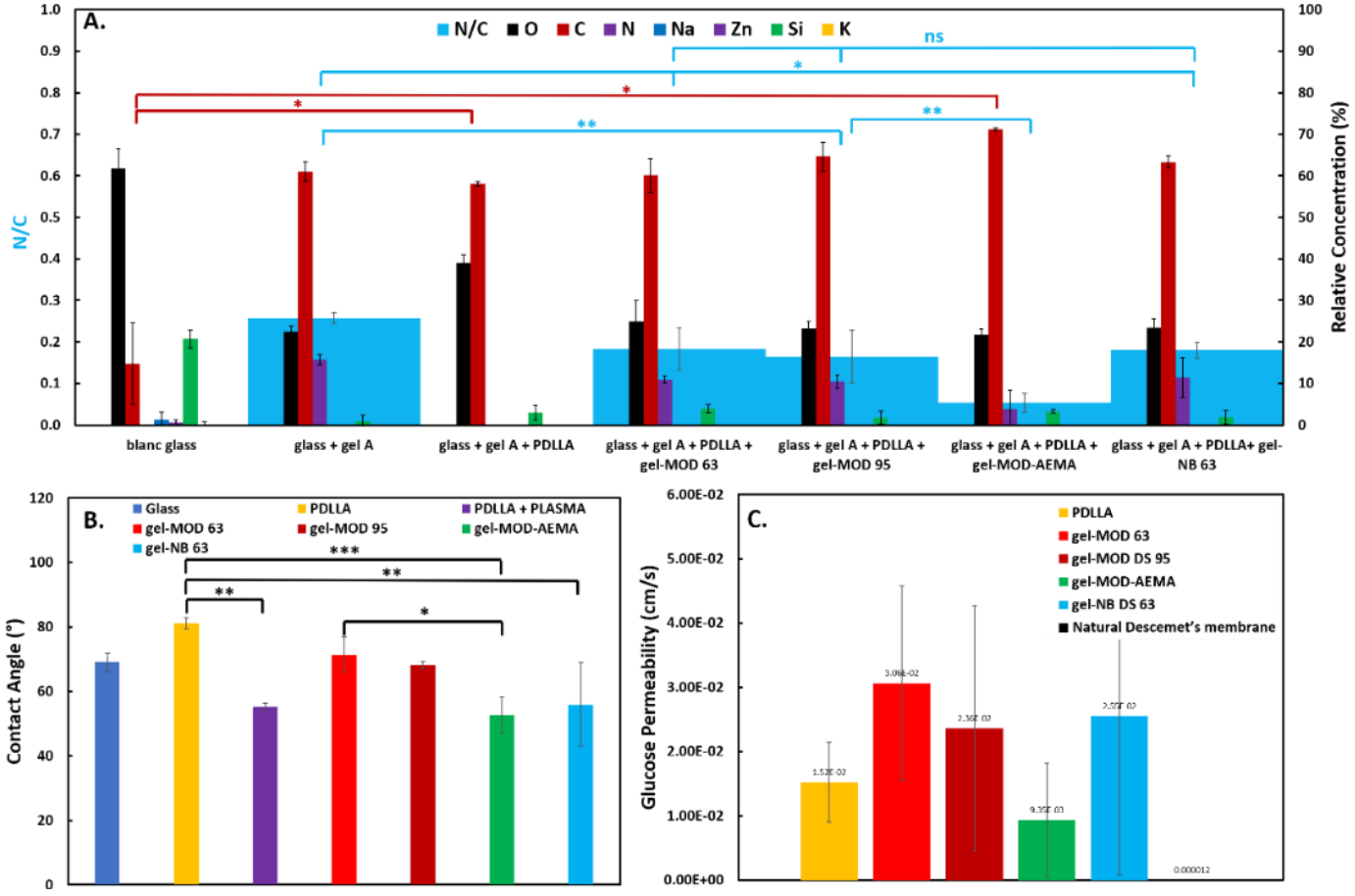
A.
N/C
O
C
N
Na
Zn
Si
K
ns
*
**
N/C
Relative Concentration (%)
blanc glass
glass + gel A
glass + gel A + PDLLA
glass + gel A + PDLLA + gel-MOD 63
glass + gel A + PDLLA + gel-MOD 95
glass + gel A + PDLLA + gel-MOD-AEMA
glass + gel A + PDLLA+ gel-NB 63
B.
Glass
PDLLA
PDLLA + PLASMA
gel-MOD 63
gel-MOD 95
gel-MOD-AEMA
gel-NB 63
***
**
*
Contact Angle (°)
C.
PDLLA
gel-MOD 63
gel-MOD DS 95
gel-MOD-AEMA
gel-NB DS 63
Natural Descemet's membrane
Glucose Permeability (cm/s)

Figure V.58 — X-ray photoelectron spectroscopy elemental analysis of the top layer of the membrane during stepwise membrane production (A). Static contact angle measurements indicating hydrophilicity/hydrophobicity of the different membranes (B). Glucose permeability of the different membranes (i.e. blank PDLLA and PDLLA with the different coatings) relative to the natural Descemet's membrane (C) [46]. (All statistical differences are denoted with * for $p < 0.05$, ** for $p < 0.01$ and * for $p < 0.001$ with the exception of panel A where all differences are $p < 0.001$ unless denoted otherwise (with "ns" representing no statistical significance).**

5.5 Assessing the Suitability of the Membrane as Descemet's Membrane Substitutes

One of the predominant requirements of an artificial Descemet's membrane is that it should be sufficiently transparent in the visible range (i.e. ≥ 90% for the natural Descemet's membrane [45]), not to impair the vision of the patient after transplantation [18]. When assessing the transparency of the produced membranes qualitatively, it seems that throughout the different production steps, the membranes exhibited comparable transparency compared to the glass slide on which they were coated, because the underlying pattern can clearly be distinguished (Figure V.59 A - G). Additionally, after isolation from the supporting glass slide by dissolution of the sacrificial gelatin layer, the membranes exhibited sufficient mechanical integrity to enable surgical manipulation. It should be noted that in contrast to natural donor endothelium, the currently reported membranes did not exhibit the same self-rolling behavior of a DMEK graft. However, it is anticipated, that the scaffold could be introduced into the eye by using a suitable surgical tool to introduce it into a cannula similar to that used during a DSAEK procedure [354,358].

As a proof of concept experiment towards surgical manipulation, the membranes were mounted into cell crowns (Figure V.59 K & L). Additionally, after membrane isolation, still sufficient transparency was observed (i.e. PDLLA + gel-MOD-AEMA in Figure V.59 I & J). Furthermore, the membranes proved prone to trypan blue staining, a stain which is also used in DMEK to better visualize the graft for surgical manipulation [356] (Figure V.59 M & N). It should be noted that transparency was somewhat compromised in the dry state (Figure V.59 I) due to wrinkling of the membrane. However, after rehydration, which is more representative for the membranes after implantation (Figure V.59 J), the underlying pattern becomes very clear again, indicating sufficient transparency. Quantitative spectrophotometric measurements indicated that all membranes exhibited over 90 % transparency in the visual spectrum in the dry state with gel-MOD-AEMA being the least transparent (i.e. 90 – 94 %) while still exhibiting a comparable transparency to the natural Descemet's membrane [45] (Figure V.60 A).

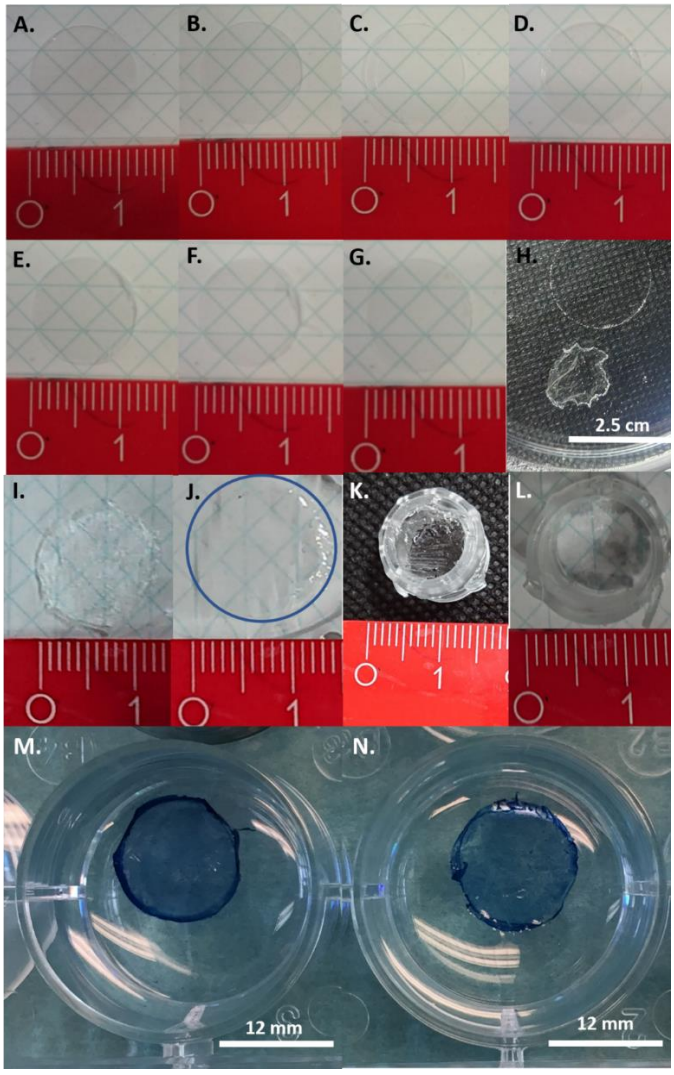

Figure V.59: Photographs of the produced membranes: after spincoating onto glass slides demonstrating the transparency qualitatively. (A) Blank glass; (B) glass + gelatin A; (C) glass + gelatin A + PDLLA; (D) glass + gelatin A + PDLLA + gel-MOD DS 63; (E) glass + gelatin A + PDLLA + gel-MOD DS 95; (F) glass + gelatin A + PDLLA + gel-MOD-AEMA; (G) glass + gelatin A + PDLLA + gel-NB DS 63. (scale in cm). After isolation from the glass slide: (H) PDLLA + gel-MOD-AEMA; (I) in the dry state; (J) after hydration; (K,L) mounted in a Cellcrown insert. Isolated membranes after staining with trypan Blue (a dye used during surgical manipulation) (M) with gel-MOD-AEMA; (N) without gelatin coating.

In addition, the transparency of the membranes was also assessed on hydrated samples to provide a closer mimic to natural tissue, being more representative for *in vivo* conditions. After hydration, the transparency of the gelatin-coated materials increased to > 97% for all membranes with no significant differences in transparency whereas the uncoated PDLLA membrane exhibited transparencies around 100% throughout the spectrum however also not significantly higher in comparison to the gelatin-coated membranes (Figure V.60 A). Since the natural Descemet's membrane is characterized by 90% transparency in the visual spectrum, these membranes prove to be suitable as a natural Descemet's membrane substitute with respect to optical characteristics [45].

To assess the thickness of the membranes, white light interferometry optical profilometry was performed on the membranes when still immobilized on the glass substrates (Figure V.61). To this end, the membranes were scratched to expose the surface of the glass slide. Next, the differences in height between membrane surface and the glass surface provide an indication of the membrane thickness (Figure V.61).

These experiments indicated that the thickness of the membranes can be tuned by application of multiple coatings on top of each other, rather than changing the concentration of the PDLLA in the spin-coating solution (Figure V.62). Furthermore, besides the thicker dimensions, the application of multiple coatings on top of each other did not elicit decreases in transparency (Figure V.62). When decreasing the concentration to 2 wt%, no homogeneous coating was obtained, resulting in scattering of the light when passing through the membrane (Figure V.62). Furthermore, application of different layers of the 4 wt% PDLLA solution did not result in a significant difference in transparency (Figure V.62).

The white light interferometry method allowed to distinguish between the sacrificial gelatin layer which is not covalently attached to the other layers and the combination of the PDLLA + gelatin coating. The fact that no distinction between the layers of the final graft (i.e. PDLLA + gelatin coating) could be made, further proves the successful attachment between these layers. After measuring the thickness of all membranes, they all exhibited thicknesses below 1 µm which is below the thickness of the natural Descemet's membrane (i.e. 10 – 12 µm) thereby qualifying as a proper surrogate Descemet's membrane in terms of dimensions. It should be noted that no significant differences between the different crosslinked gelatin coatings were observed.

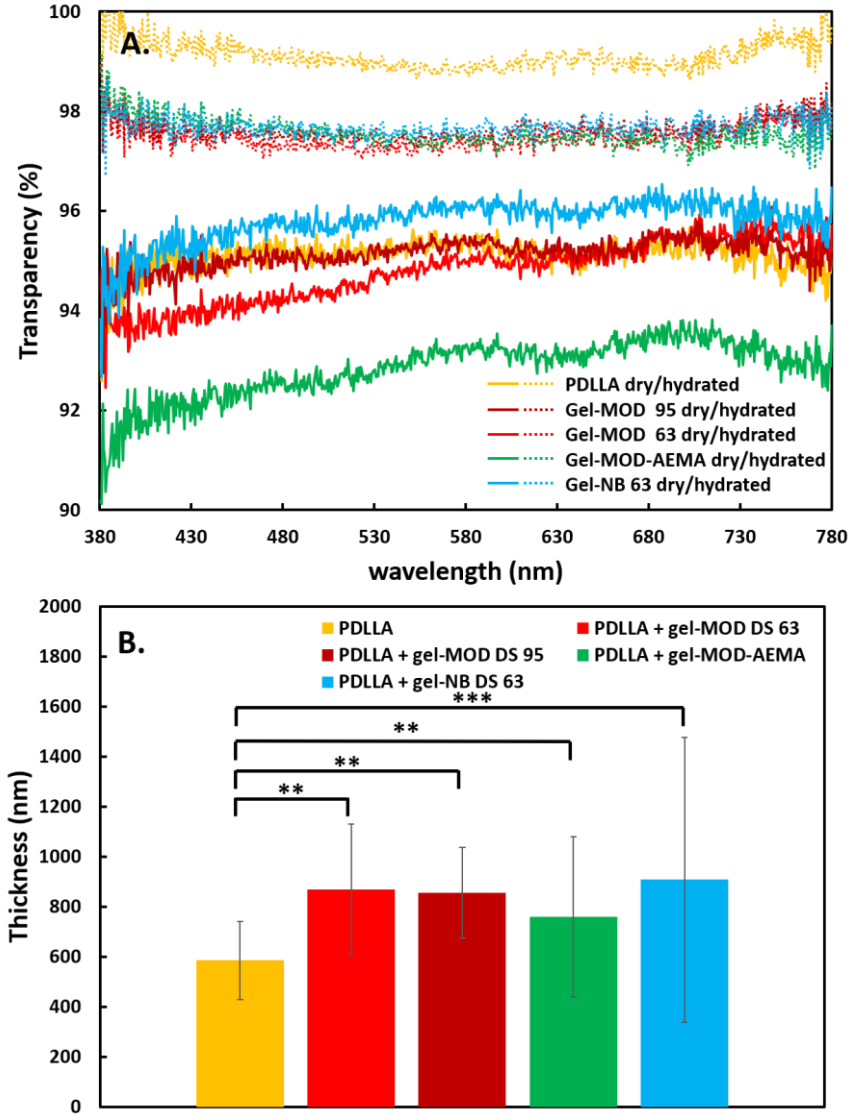

Figure V.60: Transparency of the different membranes throughout the visual spectrum both in the dry (solid lines) and in the hydrated state (dashed lines) (n = 4) (D). Membrane thickness measurements, as determined using optical profilometry (E). (All statistical differences are denoted with * for p < 0.05, ** for p < 0.01 and * for p < 0.001 with the exception of panel A where all differences are p < 0.001 unless denoted otherwise (with "ns" representing no statistical significance).**

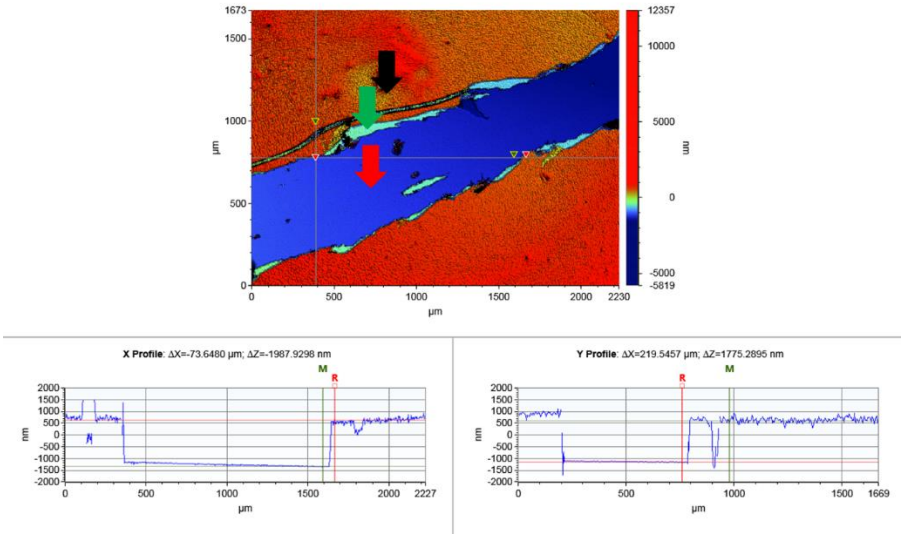

Figure V.61: Optical profilometry measurements to determine membrane thickness after making a scratch through the membrane. As a result, the different layers on top of the glass slide can clearly be distinguished: blank glass (red arrow), sacrificial gelatin A coating (green arrow) and PDLLA + covalently linked gelatin layer (black arrow).

However, the samples with gelatin coating were significantly thicker in comparison to the pure PDLLA membranes (Figure V.60 A). The dimensions of the developed membranes form the largest difference with previously reported work that also applied gelatin-based hydrogels for corneal endothelium regeneration. More specifically, previously reported studies using gelatin were either crosslinked with toxic reagents [364] or were thicker (i.e. 50 – 750 µm) [357,358,365]. However, thick constructs would eventually lead to loss of visual acuity in patients and compromise surgical introduction into the anterior chamber [45,362,366].

The most important function of corneal endothelial cells is to maintain the stroma in a state of deturgescence using a pump-and-leak mechanism, whilst providing the cornea with nutrients (mostly glucose) from the anterior chamber by passive leakage [30]. As a consequence, the synthetic membranes need to exhibit sufficient diffusion capacities, which was assessed using a glucose diffusion assay in a side-by-side diffusion cell set-up (Figure V.58 C). The results showed that the PDLLA membranes enable efficient trans-membrane diffusion of glucose (i.e. permeability coefficient of $P_{app} = 1.52*10^{-2} \pm 6.19*10^{-3}$ cm/s), which can be considered the limiting layer due to the hydrophobicity of the PDLLA.

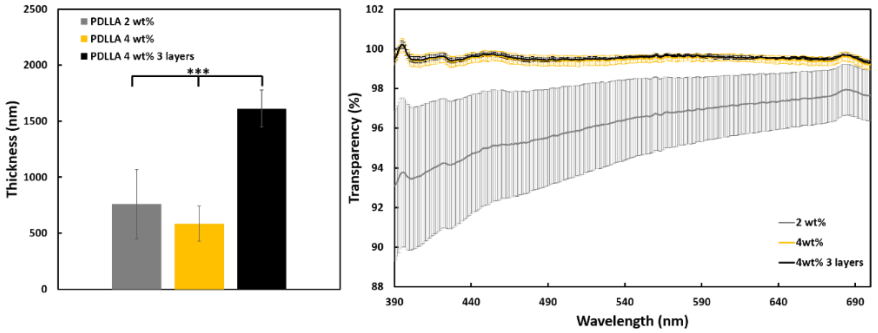

Figure V.62: Influence of PDLLA concentration and layer thickness on transparency.

Furthermore, introducing a crosslinked gelatin layer did not lead to any significant differences in permeability between the membranes, thereby confirming that the PDLLA layer is indeed the limiting factor (Table 5 & Figure V.58 C). When comparing these values to literature, the diffusion still outperforms that of natural Descemet's membranes (i.e. 1.2 * 10^{-5} cm/s) [46]. Indeed, the obtained permeability coefficients are several orders of magnitude higher than the ones recorded for the natural Descemet's membrane. We anticipate that higher diffusion values are more desirable than lower diffusion values as this does not preclude the pumping function of the cells, while allowing sufficient transport of nutrients towards the stroma. Furthermore, when combining the permeability coefficients with the measured membrane thicknesses, the diffusion coefficients (D) can be calculated based on equation 2 [365]:

$$D = P_{app} * T \tag{13}$$

With T being the membrane thickness (cm);

The obtained diffusion coefficients are presented in Table V.6. When comparing these values to previously reported values from literature (i.e. D = 2.55 * 10^{-7} cm²/s for gelatin and atelocollagen membranes), it can be concluded that a similar order of magnitude was obtained [357].

Table V.6: Comparison of the permeability coefficient (P_{app}), membrane thickness and calculated diffusion coefficient (D) from these values compared to the natural Descemet's membrane.

	gel-MOD 95	gel-Mod 63	gel-MOD-AEMA	gel-NB 63	PDLLA	Descemet's Membrane
P_{app} (cm/s)	**2.36E-02**	**3.06E-02**	**9.35E-03**	**2.55E-02**	**1.52E-02**	**1.20E-05** [46]
sd	1.90E-02	1.51E-02	8.85E-03	2.47E-02	6.19E-03	
Thickness (nm)	**8.58E+02**	**8.68E+02**	**7.60E+02**	**9.08E+02**	**5.85E+02**	**1.00E+04** [362]
sd	1.82E+02	2.62E+02	3.19E+02	5.69E+02	1.56E+02	
D (cm^2/s)	**2.03E-06**	**1.91E-06**	**7.10E-07**	**2.99E-06**	**8.87E-07**	**1.20E-08**
sd	1.75E-06	1.12E-06	6.72E-07	2.18E-06	3.62E-07	

5.6. In Vitro Biological Assays

5.6.1. Corneal Endothelial Cell culture

B4G12 immortalized corneal endothelial cells were seeded at a density of 15,000 cells/cm^2. Cell attachment to the membranes was observed four hours after seeding and the cells grew to confluency after one week of culture on a 12 mm diameter membrane. In every condition, the typical hexagonal morphology of corneal endothelial cells (CEnCs) was preserved. During these experiments, no form of additional coating agent was applied to enable the endothelial cells to adhere to any of the membranes. Corneal endothelial cells are known for their difficulty to expand *in vitro* regarding attachment and expansion, which emphasizes the propensity of the modified gelatin derivatives to mimic the extracellular matrix. Alternative approaches to enhance the attachment of cells to tissue culture plastic include the supplementation of ROCK inhibitor in the growth medium and through means of forced attachment with hyaluronic acid [367,368].

5.6.1.1. Phenotyping

To date, there is no consensus on the correct markers to demonstrate the phenotypic profile of properly cultured corneal endothelial cells. However, the combination of ZO-1 and Na^+/K^+ ATPase ion pumps are the most investigated combination of markers reported in literature, to represent the *in vivo* barrier and pump function of the cell layer, respectively.

In that regard, it is shown that ZO-1 is expressed along the lateral cell membranes of corneal endothelial cells cultured for one week on any of the gelatin-polyester combination membranes.

Additionally, the staining pattern clearly delineates the hexagonal shape of the cells which is an arbitrary parameter for “healthy” corneal endothelial cells [369] (Figure V.63). Furthermore, Na^+/K^+ ATPase are also expressed at the basolateral membranes of the corneal endothelial cells, proving that they still express a high density of ion pumps, which is typical for CEnCs. They do not attach well on FNC-coated glass cover slips. However, they were included to compare the control condition at the same magnification and resolution, which would not be possible with standard tissue culture plastic as it is too thick for fluorescence microscopy.

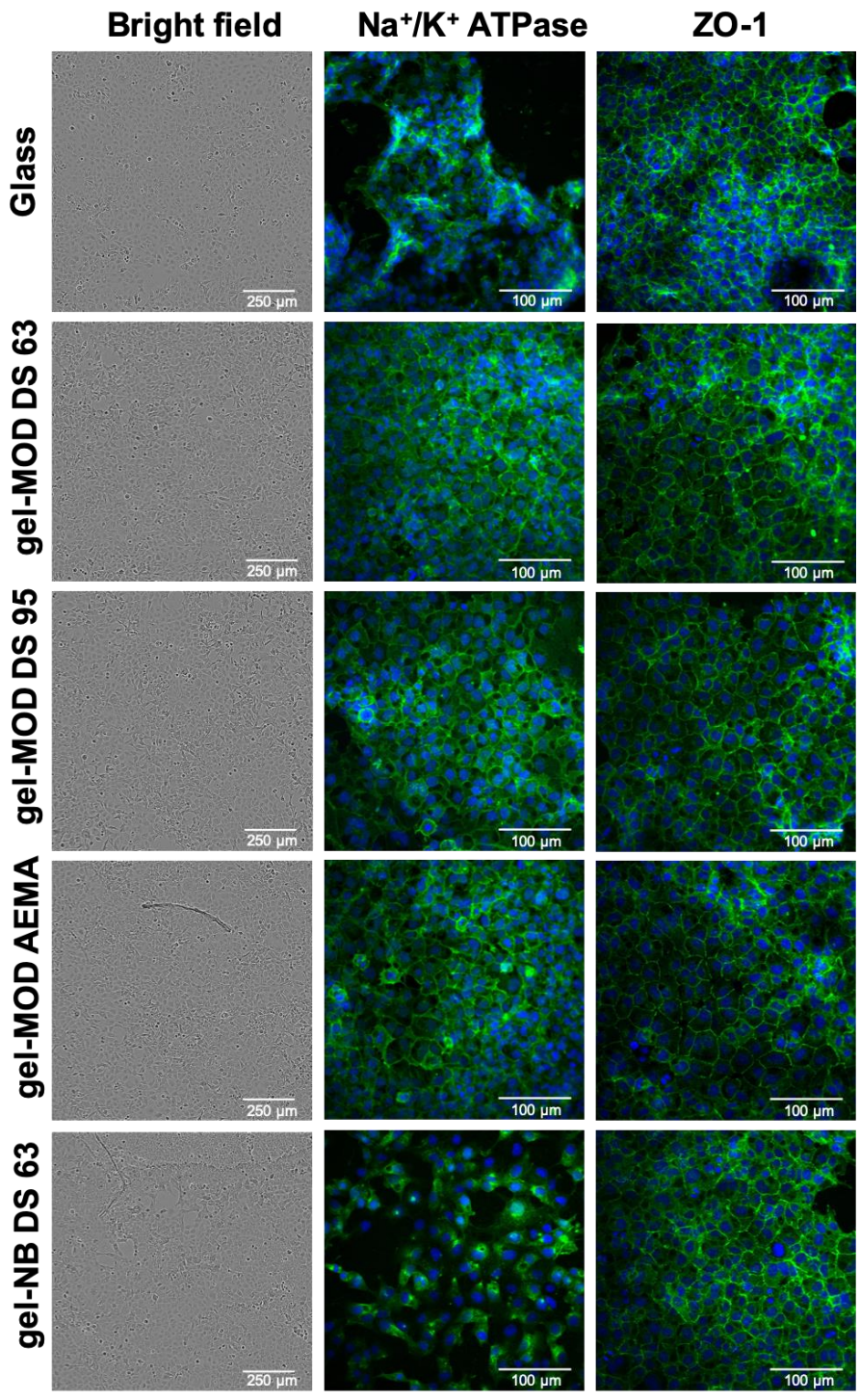
Bright field
Na+/K+ ATPase
ZO-1
Glass
gel-MOD DS 63
gel-MOD DS 95
gel-MOD AEMA
gel-NB DS 63
250 µm
100 µm

Figure V.63: Morphology and phenotype of cells grown on gelatin derivatives. Left column lists phase contrast images taken at 10x magnification. Middle and right column are fluorescence images of cells grown on gelatin derivatives and were stained for Na^+/K^+ ATPase and ZO-1 respectively.

The samples with higher crosslink density display a more specific membranous staining pattern than their less crosslinked counterparts. As mentioned before, the Young's modulus of gel-MOD-AEMA approaches that of the Descemet's membrane to the greatest extent, which could explain why the phenotype of cells grown on that membrane appears superior to that of less crosslinked membranes [359].

5.6.1.2. Adhesion Assay

To quantify the propensity of cells to initiate adhesion to the candidate scaffold materials, the surface area of focal adhesions (FA) per cell was quantified and divided by the surface area of the cell, 24 hours after seeding. There was no significant difference in this ratio between the positive control, i.e. cell culture plastic coated with the FNC coating mix, i.e. the most favorable *in vitro* growth condition, and the gelatin derivatives in terms of FA/cell surface area ratio. However, when looking to these parameters separately, the cells cultured on plastic displayed both a larger area of focal adhesions and a larger cell area (Figure V.64 B and C).

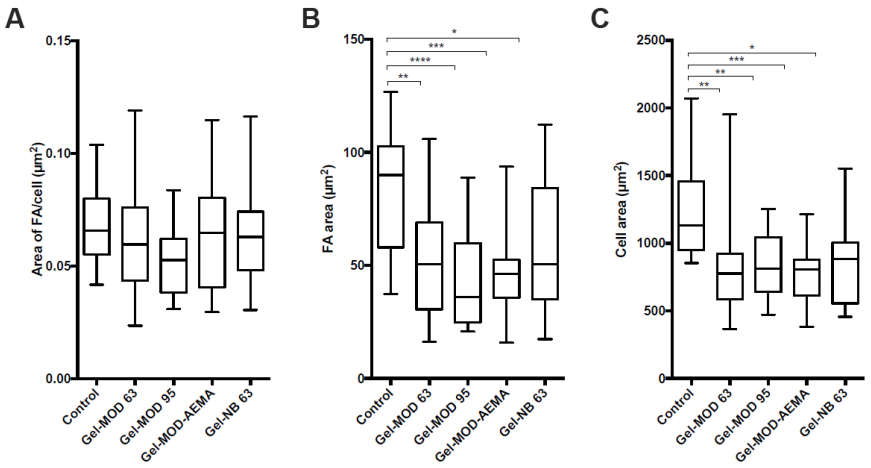

Figure V.64: Graphical representation of the ratio of the focal adhesion area of a cell divided by the cell surface area(A), the focal adhesion area per cell (B) and the cell surface area (C).

Previous studies have shown that cell size and the rate of spreading is higher with increased substrate stiffness [370]. This phenomenon can explain the larger size of cells grown on TCP, which has an elastic modulus around 100,000 kPa [371]. However, a similar FA area to cell size ratio on both plastic and gelatins indicates that within the first 24 hours, the cells are equally able to develop focal adhesions upon being seeded on tissue culture plastic and on the gelatin derivatives.

5.6.1.3. *Proliferation Assay*

From exponential growth curves, population doubling times (PDT) were calculated to compare the growth rate on the different scaffolds (Figure V.65). No significant difference was seen between the cells grown on gelatin scaffolds (range: 44-58 hours) or the positive control (35.84 ± 0.97 hours), (i.e. tissue culture plastic that was coated with FNC coating mix). However, the corneal endothelial cells that grew on coated glass cover slips had a significantly higher PDT compared to coated tissue culture plastic, as the high stiffness of glass creates an inhospitable environment for cell homeostasis. To conclude, every type of gelatin scaffold is able to sustain cell growth to the same degree as the coated culture plastic benchmark, thereby proving their cytocompatible features *in vitro*.

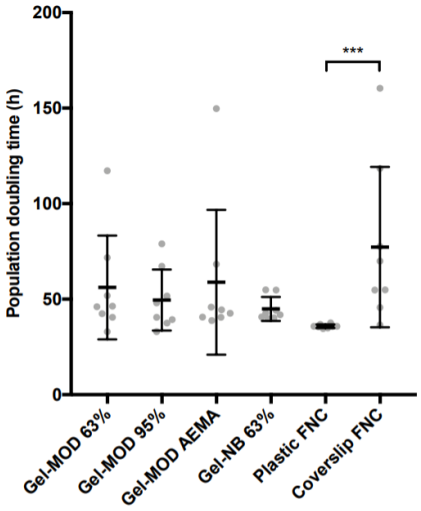

Figure V.65: Population doubling times of CEnC grown on modified gelatin. There was no significant difference between the positive control (plastic FNC) and the crosslinked gelatins. CEnC did grow slower on a glass coverslip coated with FNC.

5.7. Influence of 2PP Patterns on Cellular Behaviour

Besides the very beneficial 2D *in vitro* culture assay, the effect of 3D patterns on cellular behavior was assessed, as it is known that 3D patterns can influence cellular behavior [281–283,358].

For example, Karuri et al. observed cell alignment of human corneal epithelial cells on substrates with grooves ranging from 400 – 4000 nm [281]. Herein, membranes were prepared first using gel-NB/DTT at a 0.5 thiol:ene ratio to result in unreacted norbornene functionalities onto which 3D patterns can be attached (see Chapter 3). Next, gel-NB/gel-SH patterns were grafted at a thiol:ene ratio of 1, as this thiol-ene combination results in the lowest swelling ratio and least effects of photocleaving (see Chapter 4). As a control, gel-NB/gel-SH patterns were structured at a thiol/ene ratio of 1 on methacrylated glass slides, to enable sufficient adhesion to the glass. Patterns were structured at lower average laser powers (i.e. 35 mW) as the previous chapter showed that the higher intensities (i.e. 100 mW average power) result in undesired competitive gelatin cleaving, in particular for thiol-ene systems, whereas at 35 mW, the lowest swelling ratios were observed. These patterns were structured at a laser scanning speed of 100 mm/s.

After cell culture on the membranes (Figure V.66), it is clear that the cells tend to attach on the gel-NB coating in-between the patterns, whereas this trend is opposite for the patterns deposited onto methacrylated glass (Figure V.67). However, one thing that is clear for both types of samples is the fact that cells adapt to the morphology of the underlying pattern. This is in agreement with previous studies from literature studying the influence of patterns on cellular behavior [283]. Especially for the patterned membranes with gelatin coating, the influence of the patterns is clear, as a clear alignment of the cells is observed when seeded on the lines (Figure V.66 E – H). This effect is not apparent on the patterned glass slides (Figure V.67 C & D) where the cells randomly attached over different lines, whereas for the coated slides, they attached everywhere in-between the lines. For the other morphologies, there is still a clear effect as the cells tend to grow in-between the patterned structures on the gelatin-coated membranes.

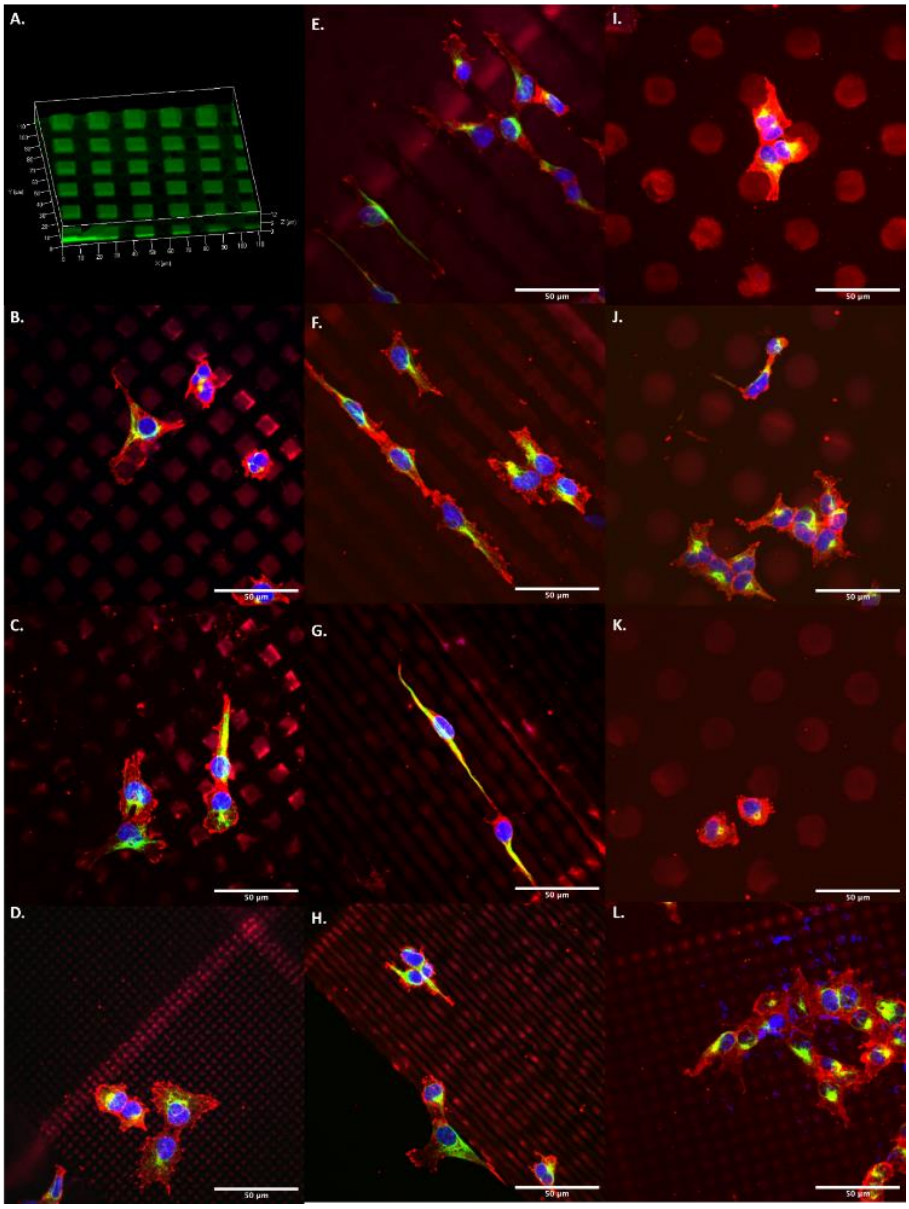

Figure V.66: Images obtained of seeded CEnCs (30000/sample) after 3 days of culture on 2PP patterns on PDLLA – gel-NB/DTT (0.5 thiol:ene ratio) membranes structured using gel-NB/gel-SH in a 1:1 thiol:ene ratio: A) LSM image of structured cubes on the membrane. Corneal endothelial cells seeded onto: (B,C) structured cuboids of 10 µm * 10 µm * 5 µm; (D) cuboids of 2.5 µm * 2.5 µm * 5 µm; (E) lines of 10 µm *

600 µm * 5 µm; (F-G) beams of 5 µm * 600 µm * 5 µm; (H) beams of 2.5 µm * 600 µm * 5 µm (I - K) solid half spheres with a diameter of 10 µm (L) half spheres with a diameter of 5 µm.(all patterns structured using a laser emitting at 780 nm with a 32X objective at 100 mm/s and 35 mW average laser power at a hatching distance of 0.2 µm and slicing distance dZ of 0.5 µm in the presence of 2 mol% P2CK) (samples stained with vinculin-CY3 (red) for focal adhesions and vimentin-FITC (green) for cytoskeleton and DAPI (blue) for nuclei).

However, the patterns still clearly influence the cellular behavior as they tend to grow in between the deposited membranes, thereby acting as guides for cell-growth. (Figure V.66 B – D & I – L). Additionally, when looking at the structures coated on the methacrylated glass slides, instead of in-between the structures, the cells tend to adhere randomly on top of the gelatin patterns, thereby being less influenced by the specific morphology of the patterns (Figure V.67).

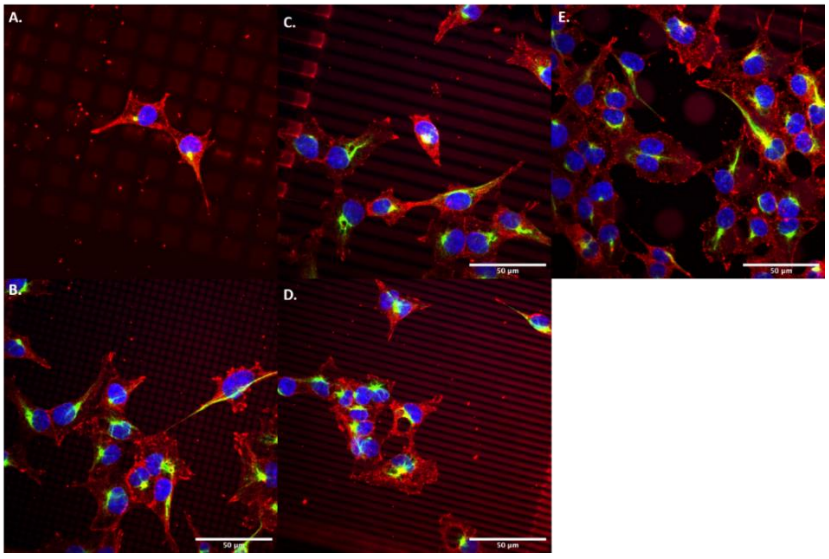

Figure V.67: Images obtained of CEnCs (30000/sample) after 3 days of culture on 2PP patterns structured using gel-NB/gel-SH in a 1:1 thiol:ene ratio on methacrylated glass slides: Corneal endothelial cells seeded onto: (A) structured cuboids of 10 µm * 10 µm * 5 µm; (B) cuboids of 2.5 µm * 2.5 µm * 5 µm; (C) lines of 5 µm * 600 µm * 5 µm; (D) beams of 2.5 µm * 600 µm * 5 µm; (E) half spheres with a diameter of 10 µm. (all patterns structured using a laser emitting at 780 nm with a 32X objective at 100 mm/s and 35 mW laser power at a hatching distance of 0.2 µm and slicing distance dZ of 0.5 µm in the presence of 2 mol% P2CK) (samples stained with vinculin-CY3 (red) for focal adhesions and vimentin-FITC (green) for cytoskeleton and DAPI (blue) for nuclei).

Unfortunately, for both types of samples (i.e. coated membranes and methacrylated glass slides), the cells lose their characteristic hexagonal morphology, as observed in the 2D samples (*vide supra*). Therefore, these preliminary experiments indicate that the introduction of 3D patterns on the samples is not a viable strategy towards the development of an artificial Descemet's membrane. However, in this respect, the use of 2PP and especially, the multiphoton-assisted grafting as discussed in Chapter 3 holds promise towards the stimulation of corneal cellular behavior [372][373].

5.8. Conclusion

In the present chapter, the potential of applying PDLLA-gelatin multilayer membranes for corneal endothelial tissue engineering was assessed. This strategy resulted in very thin membranes (i.e. < 1 µm thick) that benefit both from the mechanical strength from the PDLLA and the ECM-mimicking capacity of the gelatin derivatives. These materials were selected as every gelatin derivative will be hydrolyzed and broken down into peptides *in vivo*, similarly to collagen breakdown in the human body. The PDLLA supporting polymer will be degraded into lactic acid, which should not pose any problems in the corneal environment as 85% of glucose in the cornea is metabolized into lactate that is even considered as a contributing anion flux to maintain corneal transparency. Although the gelatin coatings have proven to be a very suitable ECM mimic in the present application, the experiments do not further reveal an outperforming candidate amongst the different modified gelatins both in terms of physico-chemical nor biological performance. However, the samples with the highest elastic moduli, namely gel-MOD-AEMA, can be considered to be a better mimic of the Descemet's membrane, due to a closer match to the native membrane in terms of mechanical properties. Therefore, in future studies, the choice for a suitable gelatin derivative can be made based on the most straightforward membrane fabrication. As a result, the most promising candidate gelatin derivative would be gel-MOD-AEMA due to the following reasons. First, gel-MOD-AEMA displays a higher elastic modulus which is a closer match to the *in vivo* value of the Descemet's membrane. Secondly, due to its higher degree of crosslinking, it is expected to swell less *in vivo* and degrade at a slower rate which is beneficial as corneal endothelial cells secrete only very limited extracellular matrix through life, rendering a slowly degrading ECM-mimicking material more interesting (see Chapter 2). Thirdly, gel-MOD-AEMA can be easily processed at room temperature in contrast with the other assessed gelatin derivatives. Furthermore, in contrast with the step-growth-based norbornene derivatives,

processing of a chain growth derivative (i.e. gel-MOD and gel-MOD-AEMA) can occur in a straightforward manner since there are no issues related to thiol stability at the required elevated temperatures to keep gelatin in solution or premature crosslinking due to the high reactivity. Through this innovative combination of PDLLA with gelatin, a maximum benefit of the mechanical strength of the polyester and the ECM-mimicking capacity of gelatin was realized thereby obtaining an ultra-thin scaffold for corneal endothelial transplantation. Furthermore, preliminary 2PP experiments proved the feasibility of post- membrane production patterning to influence cell behavior. Although a clear effect of the patterns on the cell growth/adhesion behavior was observed, the cells lost their characteristic hexagonal morphology and associated leaky barrier function.

Chapter 6:
General Conclusions and Future Perspectives

6.1. General Conclusions

The goal of the present work included the development of new hydrogel building blocks towards their application in (ocular) tissue engineering. In this respect, the research can be subdivided into two major parts. On the one hand, focus was placed on improving the laser-based processing performance of gelatin-based hydrogels while maintaining biocompatibility and cell interactivity. On the other hand, research was performed related to the development of functional membranes for ocular applications and more specifically, towards the development of membranes to regenerate the innermost part of the cornea, namely the corneal endothelium.

6.1.1. Improving the Laser-Based Processing Performance of Gelatin Hydrogels

The first aspect of the present work consisted in finding a suitable ECM mimic. To this end, gelatin was selected, as it is derived from collagen, the main constituent of the natural extracellular matrix in the cornea (i.e. collagen type IV in the natural Descemet's membrane), and in the human body in general [21,102]. As a consequence, gelatin exhibits structural similarities and similar properties to the natural ECM, including cell interactivity due to the presence of RGD sequences that can bind with the integrins present on the cell membrane [110]. However, it is characterized by a dissociation temperature (T_d) around 30°C resulting in solubility at elevated temperatures and the formation of a physical gel below the dissociation temperature. Consequently, it will dissolve at physiological temperature (i.e. 37°C). This undesirable behaviour can be circumvented via the introduction of covalent crosslinks into the material. In this respect, the most reported method consists of modification of the primary amines present in the (hydroxy)lysine and ornithine amino acids present in gelatin with methacrylic anhydride. Consequently, (photo-)crosslinkable methacryloyl functionalities are introduced resulting in the generation of gel-MOD [121][125]. This derivative can be considered as one of the gold standards in the field of biofabrication and tissue engineering, with a proven track record for 2PP processing [125][129][126]. Therefore, it was applied as a benchmark throughout the present work. However, for 2PP processing of gel-MOD, usually high concentrations (i.e. > 15 wt% [129]) and high laser powers (i.e. 330 mW at 7 mm/s [129]) are required to allow for acceptable structural integrity.

In a first attempt to improve the laser-based processing performance of gel-MOD, additional crosslinkable functionalities (i.e. methacrylates) were introduced via the reaction of the carboxylic acids present in the glutamic acid and aspartic acid amino acids in gelatin with 2-aminoethylmethacrylate (AEMA) using conventional carbodiimide coupling chemistry. To this end, first, all the primary amines in gelatin B were methacrylated to yield gel-MOD with a DS of ± 95%, thereby preventing zero-length crosslinking between the primary amines and the carboxylic acids present in gelatin. This gel-MOD starting material (i.e. DS 95 %) was also used as benchmark to assess the material properties and processing performance of the developed novel derivative (i.e. gel-MOD-AEMA). It was shown that the DS of the carboxylic acids could be tuned by varying the gel-MOD concentration during the reaction as 10, 5 and 2.5 w/v % mixtures resulted in a DS of around ± 35, ± 45 and ± 55 % respectively. Since the aim was to improve the mechanical properties along with the 2PP processing performance, all further characterization experiments were performed using gel-MOD-AEMA exhibiting the highest DS (i.e. 55%). When benchmarked to gel-MOD (DS 95 %), a comparable molecular weight for gel-MOD and gel-MOD-AEMA was obtained after the complete modification, indicating an acceptable degree of hydrolysis which occurred during modification while exhibiting a 2.7-fold increase in the number of crosslinkable functionalities (see Table VI.7). Furthermore, gel-MOD-AEMA exhibits faster crosslinking kinetics and higher storage moduli (see table VI.7). Additionally, it is characterized by a significantly lower swelling ratio (i.e. a 1.6 – 1.9-fold decrease) while still exhibiting a comparable biocompatibility upon cell seeding when compared to the gel-MOD benchmark. What's more, the additional modification results in solubility below the T_d as a consequence of triple helix formation disturbance due to the introduction of additional bulky side groups [138]. As a consequence, the material becomes suitable for additive manufacturing technologies requiring liquid resins (i.e. DLP, SLA, ink-jet) [138].

However, the real benefit of the gel-MOD-AEMA derivative becomes clear during 2PP processing. Not only do the improved reaction kinetics result in a larger 2PP processing window (i.e. > 40 mW vs > 60 mW at 15 w/v% and > 50 mW vs > 80 mW at 10 w/v% at 100 mm/s) but the presence of a denser network also resulted in nearly no post-production swelling to occur. Consequently, to the best of our knowledge, this is the first cell-interactive hydrogel system that exhibits a true CAD-CAM mimicry as structures with feature sizes down to 1 µm could successfully be reproduced. Additionally, due to the room temperature solubility, the material becomes accessible to so-called 'meso'-scale 2PP during which the objective is immersed inside the

polymer resin, allowing for stitching of different parts of a single CAD file into larger structures [299,323].

Although promising results were obtained using the gel-MOD-AEMA derivative, it is known that densely crosslinked hydrogel networks can compromise biocompatibility of the material when used as an ECM mimic for cell-encapsulation purposes [252]. Furthermore, these conventional chain-growth hydrogels are characterized by the formation of non-degradable (poly)methacryloyl chains that can pose problems upon degradation [146]. Therefore, another type of crosslinking chemistry was applied that is characterized by improved reaction kinetics and the formation of a more homogeneous network namely, thiol-ene photoclick chemistry [162,167]. To this end, gelatin was modified with norbornene functionalities, as it is known that they exhibit the fastest reaction kinetics of all ene functionalities. Additionally, they are not prone to competitive crosslinking via homo-polymerization or via thiol-Michael addition [167]. To this end, the primary amines present in gelatin were reacted with 5-norbornene-2-carboxylic acid using conventional carbodiimide coupling chemistry yielding gel-NB. It was shown that by varying the amount of 5-norbornene-2-carboxylic acid, the DS could be tuned up to 90 %. To the best of our knowledge, this is the highest DS ever reported in literature for gel-NB. Furthermore, by using the elaborated approach, not only a higher DS can be obtained in comparison to the conventionally reported approach using carbic anhydride, but also significantly shorter reaction times suffice (i.e. ≤ 45h vs 70h) [168].

Table VI.7: Comparison between material properties of gel-MOD vs gel-MOD-AEMA.

Material	DS_{NH2} (%)	DS_{COOH} (%)	# Double Bonds/g	Concentration (w/v%)	Gel Point (s)	Storage Modulus (kPa)	Swelling Ratio
gel-MOD	95		0.37	5		7.7 ± 1.7	18.5 ± 1.0
	95		0.37	10	47.2 ± 8.5	20.3 ± 3.5	10.1 ± 0.2
	95		0.37	15		31.8 ± 15	8.9 ± 0.1
gel-MOD-AEMA	95	55	0.99	5		7.1 ± 0.7	10.4 ± 2.2
	95	55	0.99	10	15.0 ± 5.2	49.8 ± 6.5	6.5 ± 0.2
	95	55	0.99	15		105.0 ± 33.8	4.7 ± 0.1

For characterization purposes, gel-NB with two different degrees of substitution was synthesized (i.e. 63 % & 89 %) which were benchmarked to gel-MOD with a comparable DS (i.e. 63 % & 95 %). The main difference between the gel-NB and gel-MOD hydrogels is the need for a thiolated crosslinker as the thiol/ene hydrogels are crosslinked using a step-growth polymerization approach between complementary functionalities (i.e. thiol and ene). To this end, for the first set of characterization experiments, gel-NB with a DS of 63% was crosslinked using DTT as thiolated crosslinker and was benchmarked to gel-MOD with a DS of 63 %. The most important benefit associated with the use of the thiol/ene system is the significantly faster crosslinking kinetics as evidenced by a decreased gel-point for 10 w/v% solutions (i.e. 2.8 s vs 65.2 s). However, lower storage moduli were obtained for the gel-NB hydrogels (see Table VI.8).This is a consequence of the orthogonal character of the thiol/ene system in combination with the use of a bifunctional crosslinker. As a consequence, only two norbornene functionalities are linked in each junction knot whereas in case of gel-MOD, multiple methacryloyl functionalities are polymerised in the same junction knot resulting in a stiffer material [146]. As a consequence, similar mechanical properties are obtained at low gel-MOD concentrations (i.e. 5 w/v%) for which the probability to link more than two methacryloyl functionalities in the same junction knot, will be limited. Furthermore, despite the difference in mechanical properties, comparable swelling ratios are observed for the gel-NB hydrogels. Another benefit of the gel-NB hydrogels is the fact that the number of reacted functionalities can be controlled by varying the thiol/ene ratio. When using a thiol/ene ratio of 1, all functionalities will react, whereas lower ratios result in unreacted norbornene functionalities that allows tuning of the mechanical properties while also allowing for post-crosslinking thiol-ene photografting [182]. Furthermore, a comparable biocompatibility is obtained between gel-NB/DTT and gel-MOD upon cell seeding.

The main benefit of the thiol-ene systems becomes apparent during 2PP processing, as very low laser powers already result in crosslinking, thereby holding potential to further increase the writing speeds. In the present work, the fastest reported writing speeds did not exceed 100 mm/s due to mechanical limitations of the 2PP set-up. However, other reports already indicate the feasibility of processing gel-NB/DTT systems at 1000 mm/s using comparable laser powers when using different optics (i.e. a 10 X objective with NA 0.4) [341].

Table VI.8: Comparison between material properties of gel-MOD vs gel-NB/DTT.

Material	DS_{NH2} (%)	Crosslinker	Thiol/Ene Ratio	# Double Bonds/g	Concentration (w/v%)	Gel Point (s)	Storage Modulus (kPa)	Swelling Ratio
gel-MOD	63			0.24	5		9.0 ± 0.3	21.6 ± 0.7
	63			0.24	10	65.2 ± 8.5	36.83 ± 1.6	10.5 ± 0.3
	63			0.24	15		75.6 ± 4.3	8.4 ± 0.3
gel-NB	63	DTT	1	0.24	5		8.6 ± 0.2	17.5 ± 2.4
	63	DTT	1	0.24	10	2.8 ± 0.3	24.0 ± 0.7	10.5 ± 0.3
	63	DTT	1	0.24	15		29.8 ± 1.1	7.5 ± 0.2

Table VI.9: Calculated maximal resolutions for different applied objectives.

Magnification (X)	NA	RI	Voxel Length (µm)	Voxel Width (µm)	Gausian Volume Approximation (µm³)
2.5	0.075	1.35	288.68	4.83	23392.91
10	0.4	1.35	9.93	0.91	28.29
32	0.85	1.35	2	0.43	1.26
63	1.4	1.51	0.64	0.27	0.16
100	1.4	1.51	0.64	0.27	0.16

Furthermore, the gel-NB/DTT system exhibited an unprecedented efficiency towards 2PP as for the first time ever, gelatin hydrogels were processed at concentrations below 10 w/v% in a reproducible way with a high degree of shape fidelity. Finally, by using thiol-ene ratios below 1, a fluorescent dye could successfully be grafted inside the hydrogel matrix using multi-photon photo-grafting. The use of multiphoton photo-grafting results in an extremely high spatiotemporal control that enables very defined grafting, which is depending on the applied focussing objective, in all three dimensions (see Table VI. 9). Since, the grafting occurs in equilibrium swollen hydrogels, it is anticipated, that the calculated voxel volumes are in close agreement with the real resolution, as no post processing swelling will occur in contrast to the 2PP of gelatin hydrogels.

Although previous reports already indicated the feasibility of multiphoton grafting, this is the first time that multi-photon thiol-ene grafting was reported [334]. As a consequence, it is anticipated that the combination of gel-NB and multiphoton lithography will allow to further tailor the hydrogel matrix via the grafting of biofunctional molecules (e.g. laminin) in a straightforward way as they often already contain thiol functionalities [374].

Furthermore, thiol:ene hydrogels exhibit an additional influence on the final hydrogel properties as different thiolated crosslinkers can be applied. To assess the influence of the applied crosslinker, hydrogels were prepared from gel-NB with a DS of 89 % using different thiolated crosslinkers (i.e. gel-SH with a DS of 72%, DTT, TEG2SH, PEG2SH 3400, PEG4SH 10000 and PEG4SH 20000) in a thiol/ene ratio of 1. These formulations were characterized in depth and benchmarked to gel-MOD with a DS of 95%. It was shown that high molecular weight crosslinkers (i.e. PEG4SH 20000) resulted in phase separation, rendering them not suitable for hydrogel formation. Looking at the reactivity, no significant differences were observed between the different crosslinkers. However, it was shown that by selecting the appropriate crosslinker, the mechanical properties of gel-MOD can be matched (i.e. when using gel-SH or PEG2SH 3400) or even outperformed (i.e. when using PEG4SH 10000). However, it should be noted that there is a huge difference in case the material is crosslinked after inducing physical gelation rather than directly from solution. When crosslinking is performed after physical gelation, the formulations where only gelatin based materials are applied (i.e. gel-MOD & gel-NB/gel-SH) exhibit the highest increase in storage modulus whereas the high molecular weight PEG4SH crosslinkers result in a decrease due to phase separation that occurs during physical gel formation. This can be of relevance when targeting deposition-based AM

techniques for which the physical gelation is often a requirement to enable straightforward processing. Additionally, all formulations exhibited a comparable biocompatibility after 7 days upon encapsulating ASC's, indicating their suitability as bioink (components) [349]. However, when the direct contact toxicity of the different components was assessed during two hours (i.e. a realistic estimation of the typical duration of a printing process), the low molecular weight crosslinkers (i.e. DTT and TEG2SH) exhibited considerable cytotoxicity. This effect is anticipated to be a consequence of cell membrane penetration by these crosslinkers followed by interaction with thiolated molecules in the cytoplasm. Furthermore, although the different formulations exhibited a comparable cytotoxicity after crosslinking, significant differences in cell morphology were observed during cell culture. The formulations characterized by the lowest storage moduli (i.e. low molecular weight crosslinkers) resulted in significantly faster matrix remodelling as evidenced by a faster increase in average cell length of the encapsulated cells over time [341]. As anticipated, the gel-MOD derivative resulted in the slowest matrix remodelling. Conversely, the cellular behaviour, the mechanical properties and the water uptake capacity can thus be tuned via variation of the thiolated crosslinker.

During 2PP processing, the different formulations were characterized by an extremely low polymerization threshold (i.e. 4 – 5 mW vs > 80 mW for gel-MOD at 100 mm/s). In this respect, clear differences in water uptake capacity were observed between the different formulations, with the lowest swelling degrees obtained for the gel-NB/gel-SH system, the latter being characterized by a high number of thiols (i.e. ± 14) per crosslinker. The highest swelling ratio was obtained for the highly hydrophilic, bifunctional PEG2SH. However, the most important aspect was the increase in volumetric swelling with increasing laser powers instead of the previously observed plateau as a consequence of a fully crosslinked network. A similar effect was previously reported by Dobos et al [341]. However, it is the first time that the origin of this phenomenon was elucidated. It was anticipated that this effect is the consequence of competitive photo-cleaving of the hydrogel matrix at high laser powers, which was substantiated by actual channel formation in crosslinked hydrogels following multiphoton irradiation. Although this effect is generally undesirable, the high reaction kinetics of the thiol-ene systems allow for crosslinking at significantly lower laser powers, with minima observed between 20 and 40 mW (at 100 mm/s writing speed). As a consequence, the materials are also suitable for processing using lower energy lasers, resulting in a decreased cost of the multiphoton setup, making them more relevant as bioink

components to be applied in more economically viable multiphoton lithography systems.

6.1.2. Development of Functional Artificial Descemet's Membranes for Corneal Endothelial Regeneration

In the second part of the current PhD, the developed gelatin hydrogel formulations were applied for the fabrication of functional membranes for corneal endothelial tissue engineering. These membranes need to comply with a series of requirements to consolidate proper in vivo function. First, they need to be sufficiently thin (i.e. the natural Descemet's membrane is around 10 – 12 µm in thickness [362]). They need to exhibit over 90% transparency throughout the visible spectrum [45]. Surgical manipulation should be feasible in accordance to the DSAEK or DMEK approach during which they need to be rolled up and introduced into a cannula, followed by unrolling in the anterior chamber [354,358]. Additionally, in order to act as a functional corneal endothelium, the cells and graft need to form a leaky barrier. To this end, the membranes need to allow sufficient diffusion of glucose (i.e. the natural Descemet's membrane exhibits a permeability coefficient of $1.2 * 10^{-5}$ cm/s [46]). Finally, the membranes should be cell-interactive towards corneal endothelial cells resulting in the correct phenotype and appropriate cell attachment [45].

In order to comply to all these requirements, crosslinked gelatin hydrogels were selected as they have a proven track record as transparent ECM mimics with cell-interactive properties. Furthermore, since gelatin is a hydrogel, it enables sufficient diffusion of small molecules through the network [375]. Additionally, during degradation, the backbone will be cleaved into peptides and amino acids, resulting in similar degradation products as for the natural collagen present in the eye. However, due to the desired small dimensions (i.e. ≤ 12 µm), gelatin as such will not exhibit sufficient structural integrity to enable proper surgical manipulation. Therefore, a second, stronger material was applied to ensure structural integrity. To this end, amorphous PDLLA was chosen due to its high transparency, biodegradability and FDA approval for clinical applications [67]. Furthermore, upon degradation, lactic acid molecules will be formed which are already naturally present in the cornea as 85% of glucose is naturally metabolized into lactate, thereby even contributing to the anion flux which maintains corneal transparency [49].

In order to comply to the thin dimensions, membranes were generated using a multi-step spincoating approach resulting in gelatin-coated PDLLA

membranes. To this end, four different gelatin formulations were applied, namely gel-MOD DS 63 %, gel-MOD DS 95 %, gel-MOD-AEMA and gel-NB/DTT with a DS of 63 %. All membranes proved to comply to the requirements in terms of thickness (i.e. all membranes exhibited thicknesses below 1 µm), glucose diffusion (i.e. the membranes exhibited permeability coefficients of $9.35 * 10^{-3}$ - $1.52 * 10^{-2}$ cm/s) and transparency (i.e. > 95 % throughout the visual spectrum). Finally, the corneal endothelial cells exhibited the correct phenotype on all membranes with no significant differences in proliferation observed between the different membranes and the positive control. Furthermore, the membranes proved to allow for manual manipulations without rupturing. As a consequence, viable membranes were obtained. Therefore, for future experiments, the gelatin derivative can be applied that allows for the most straightforward sample preparation. To this end, the most promising material is gel-MOD-AEMA due to its similar mechanical properties compared to the natural Descemet's membrane and room temperature solubility, resulting in more straightforward processing and more homogeneous samples. Furthermore, the influence of the introduction of 2PP patterns on the cellular behavior was assessed. It was shown that the cells did follow the morphology of the patterns, however thereby losing their characteristic hexagonal morphology which is required for the formation of a functional leaky barrier.

6.2. Future Perspectives

The developed gelatin hydrogel systems resulted in a significant improvement In terms of 2PP processing performance. In this respect, the introduction of additional crosslinkable functionalities to gel-MOD, resulting in gel-MOD-AEMA resulted in significant improvement in the attainable feature sizes of the final construct as a consequence of a decreased post production swelling. Indeed, these feature sizes are mainly determined by the applied optics of the system, but can be compromised to some extend by post production swelling, which is limited to completely absent in the gel-MOD-AEMA formulations. Furthermore, the use of thiol-ene photoclick chemistry via the introduction of norbornene functionalities to gelatin (i.e. gel-NB) resulted in a significant decrease in required energy for efficient 2PP processing. Additionally, this approach allowed to further expand the processing range in terms of applied concentration, since for the first time 2PP processing was possible below 10 w/v%. Although, the optimal selection of the applied thiolated crosslinker already allowed to obtain similar mechanical properties in comparison to gel-MOD, the structures are still characterised by considerable post production

swelling, resulting in losses of the maximum obtainable resolution. In this respect, it is anticipated that this phenomenon can be circumvented by also modifying the carboxylic acid functionalities in gel-NB with norbornene functionalities via the reaction with 5-norbornene-2-methylamine in a similar fashion as for the gel-MOD-AEMA.

Additionally, when focussing on cell-encapsulation during 2PP, it can be beneficial to immobilise a photoinitiator on a macromolecule, thereby circumventing cytotoxicity effects due to penetration of the cell-membrane by the PI [235]. To this end, previous research has shown the efficiency of this approach via the immobilisation of the PI on hyaluronic acid [235]. However, the immobilisation on hyaluronic acid resulted in phase-separation issues with gel-MOD [235]. It is anticipated that this can be circumvented by immobilisation of the photoinitiator on gelatin, to which currently already preliminary experiments are ongoing.

Finally, one of the issues of 2PP is that due to the high resolution in combination with the laser scanning principle, the structuring of larger objects typically requires a considerable amount of time. In this respect, improvement of the reaction kinetics of the photopolymer formulation can aid in decreasing the required writing time. Additionally, the writing time can also be further decreased via optimisation of the slicing parameters towards the applied hydrogel system and associated size of the voxel. Another approach can be the introduction of adjustable optics in order to influence the applied voxel sizes, resulting in larger voxels for parts of the design that do not require high resolution thereby drastically reducing the writing times [376]. Furthermore, the use of multi-focus 2PP has also been reported where simultaneous writing occurs in more than one focal spot [377][378]. Finally, use of a spatial light modulator where the shape of the voxel is adjusted to result in simultaneous polymerisation of a well-defined shape within the field of view within a single shot [379]. As a consequence, more high throughput fabrication of structures can be performed. The downside of this approach is that higher laser powers are required to compensate for this beam splitting, while multiple structures can only be printed within the field of view of the applied objective. Therefore, this approach is more suitable for high-throughput production of small scale structures [377]. In this respect, the improved reactivity of the gel-NB thiol-ene systems can circumvent the laser power drawback to some extent, as lower laser powers are required for the processing. Finally, currently research is ongoing into holographic 2PP, resulting in irradiation of the entire CAD model at once, which can further decrease the writing times, at the cost of much more powerful lasers resulting in very expensive systems [380].

In terms of the developed artificial Descemet's membranes, they already exhibit promising *in vitro* potential for use as scaffolds for corneal endothelium regeneration, but there are still some roadblocks ahead towards clinical application. Indeed, the surgical manipulation of the developed membranes should be assessed in depth on cadaveric eyes. It should be noted that preliminary experiments were performed that proved their loading capabilities into a DSAEK shooter cannula. Based on feedback from these experiments, the membrane fabrication process can be further fine-tuned, for example to generate thicker, more robust membranes. In this respect, also research can be performed to tune the diffusion capabilities via the introduction of cavities in the base membrane, either via laser ablation or via the introduction of soluble porogens in the polymer mixture prior to manufacturing. Additionally, with potential clinical applications in mind, a more scalable production method can be elaborated. A candidate that is currently under investigation is doctor blading, where large films can be generated at once, followed by cutting of each of the membranes in the desired diameter. After optimization of membrane production, the next step will be to perform animal experiments in rabbits to assess the *in vivo* performance of the proposed membranes. If successful, transfer towards clinical trials can be elaborated.

In parallel to the optimization of the developed membranes towards clinical trials, further research can be performed on the membranes itself. In this respect, the introduction of shape-memory properties to the polyester carrier membrane can be of specific interest to aid in unfolding after implantation. It is anticipated that this can potentially streamline the surgical procedure significantly. Currently, preliminary experiments are already ongoing.

Finally, the use of the developed membranes will be assessed towards other ocular applications. For example, already preliminary experiments are ongoing towards the regeneration of the retinal pigment epithelium for patients suffering from age-related macular degeneration. However, it is anticipated that these other applications will require further fine-tuning of the membranes in terms of diffusion and might require the presence of other ECM components. For example, research indicates the need for laminin as an ECM component for the culture of retinal pigment epithelial cells [381]. However, since laminin contains eight conserved cysteines [374], the thiol-ene (multi-photon) photografting approach can be a promising technique in this respect.

Chapter 7:
Applied Materials and Methods

7.1. Background on Applied Techniques

7.1.1. Two-photon polymerization

Two-photon polymerization (2PP), also referred to as multiphoton lithography is an extremely high resolution (i.e. ≤ 1 µm) additive manufacturing technology which benefits from the non-linear absorption of multiple photons thereby resulting in a very localised polymerisation. The technology finds its origin in 1930 when Maria Göppert-Mayer theoretically described that multiple photons of lesser energy can result in an excitation which is normally only observed by absorption of a single photon of higher energy [382].

In order to result in polymerization, two (or more) long wavelength (i.e. near-infrared) photons, each characterised by half the energy required to bridge the energy gap required to excite a photoinitiator molecule which is conventionally occurring via the absorption of a short wavelength (i.e. UV) photon, need to be absorbed nearly simultaneously (within 10^{-16} s) (Figure VII.68) [97,316,383–387]. However, the probability for a single photoinitiator to nearly simultaneously interact with two or more photons will only occur at very high photon densities [275]. These high photon densities are typically only obtained via the use of pulsed laser light with high laser powers (as high as 1 kW peak power) in combination with a very short pulse width (< 1 picosecond) to avoid thermal effects, and tightly focussing optics [379]. As a consequence of this tight focussing, the photon density is only high enough in a very small 3-dimensional volume pixel (i.e. voxel). Therefore, movement of the focal point through the solution results in the polymerization of the voxel path resulting in solidification of the material [96,97,383–386]. Consequently, 2PP additive manufacturing is not restricted to the conventional layer-by-layer deposition principle as observed for most other additive manufacturing technologies. In addition, it exhibits the benefit of having nearly no geometrical restrictions in the produced structure. Because of this working principle, 2PP exhibits a higher resolution (i.e. ≤ 1 µm), which can even extend to beyond the diffraction limit. The latter can be achieved by controlling the number and the energy of the applied laser pulses to only just overcome the polymerization energy threshold which results in sub-micrometer precision [96,316,383,384,386,388].

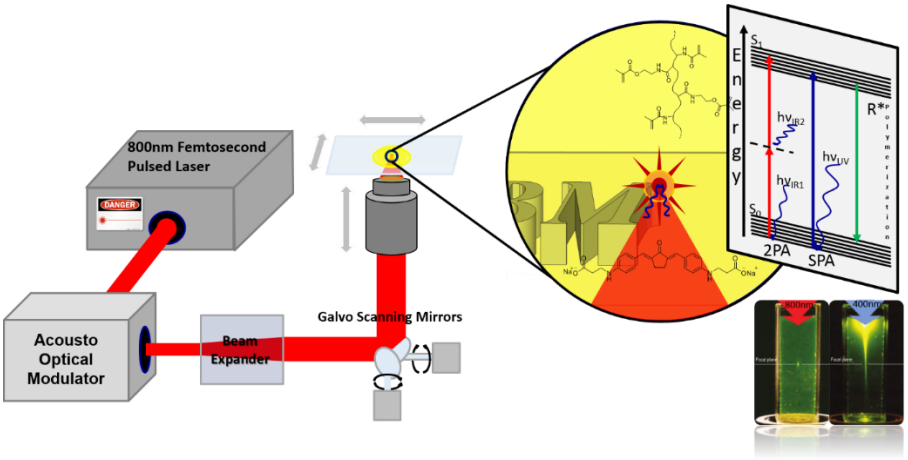

Figure VII.68: (left) Schematic representation of the most important components of a 2PP setup including a femtosecond pulsed laser, an acousto-optical modulator, a beam expander, a galvanometer scanner and a microscope stage. (right) Comparison of single-photon and two-photon polymerization as depicted in the Jablonski diagram, and the consequences for the obtained excitation volume (Figure adapted from [275,284]).

The attainable resolution is highly dependent on the applied optics, and more specifically, the applied focussing objective. In this respect, the maximally attainable resolution is dependent of the size of the voxel, which can be calculated from the illumination point spread function (ISPF) which describes the light intensity everywhere in 3D space near the focus [275]. Furthermore, an even closer definition of the real optical resolution is obtained when using IPSF² (Figure VII.69 a and b). The IPSF can be approximated by a three-dimensional Gaussian function which allows to calculate the 1/e radii of te obtained voxel in the XY (ω_{xy}) and Z (ω_z) direction (Figure VII.69 c). Furthermore, from these calculations, the full width at half maximum (FWHM) diameter can be calculated via multiplication of ω_{xy} and ω_z with $2\sqrt{ln2}$. The 1/e² radius (i.e. the voxel radius at the focal plane) can be calculated by multiplying with ω_{xy} and ω_z with $\sqrt{2}$ [275]. It is clear that the maximal resolution will be highly dependent on the numerical aperture (which characterizes the range of angles over which the objective can accept or emit light, and is defined by the refractive index of the medium in which the objective is focussed and the back aperture of the objective) of the applied objective. Furthermore, the voxel size also depends on the applied laser power, due to an accumulation in excited chromophores or photoinitiators (i.e. fluorophore

excitation saturation) resulting in larger voxels at higher laser powers (Figure VII.69 d)[275,343,344].

The multiphoton polymerization principle is in contrast with the conventional laser-based techniques which apply single-photon polymerization, resulting in photoinitiator excitation over the entire penetration depth of the beam in the polymerizable solution (Figure VII.68) [389]. In order to avoid competitive single-photon polymerisation processes in multiphoton lithography, it is important that no component of the photo-polymer formulation exhibits single-photon absorption at the wavelength of the applied laser. As a result, the use of NIR lasers has become very popular in the field, as besides the absence of absorption in most aromatic systems, the latter also have the additional benefit that at these wavelengths, natural tissue becomes transparent (without taking into account scattering effects), and NIR radiation typically does not result in any cellular damage, making processing possible in the presence of living cells [129,235,275].

Another aspect in which multiphoton lithography deviates from conventional stereolithography is that the initiation rate of the reaction does not exhibit a linear dependence towards the applied laser intensity. In multiphoton lithography, the rate of initiation (*Ri*) is related to the square of the laser intensity according to the following formula[344,379,390].

$$R_i = 2 * 1.17\delta_u\phi_u \frac{T}{\tau_P}\left(\frac{\lambda}{\pi hc\omega_{xy}^2}\right)^2 P_{avg}^2 VF[PI] \quad (14)$$

Where $\delta_u\phi_u$ is the two-photon cross-section of the initiator, T is the period of the laser pulses (or 1/repetition rate), τ_P is the pulse duration (i.e. about 70 fs in the setup at TUWien and 100 fs for the Nanoscribe), λ is the wavelength of the laser light (i.e. 800 nm at TUWien vs 780 nm at Nanoscribe), h is Planck's constant, c is the speed of light, ω_{xy} is the lateral focal radius of the laser, P_{avg} is the average laser power, VF is a volume factor (i.e. 0.63 for an axial cylinder[390]) and [*PI*] is the local concentration of the photoinitiator. The factor 2 is introduced based on the assumption that upon excitation of each photoinitiator molecule, two radicals are formed. As a consequence, a tenfold increase in average laser power will result in a 100-fold increase in initiation (Figure VII.70).

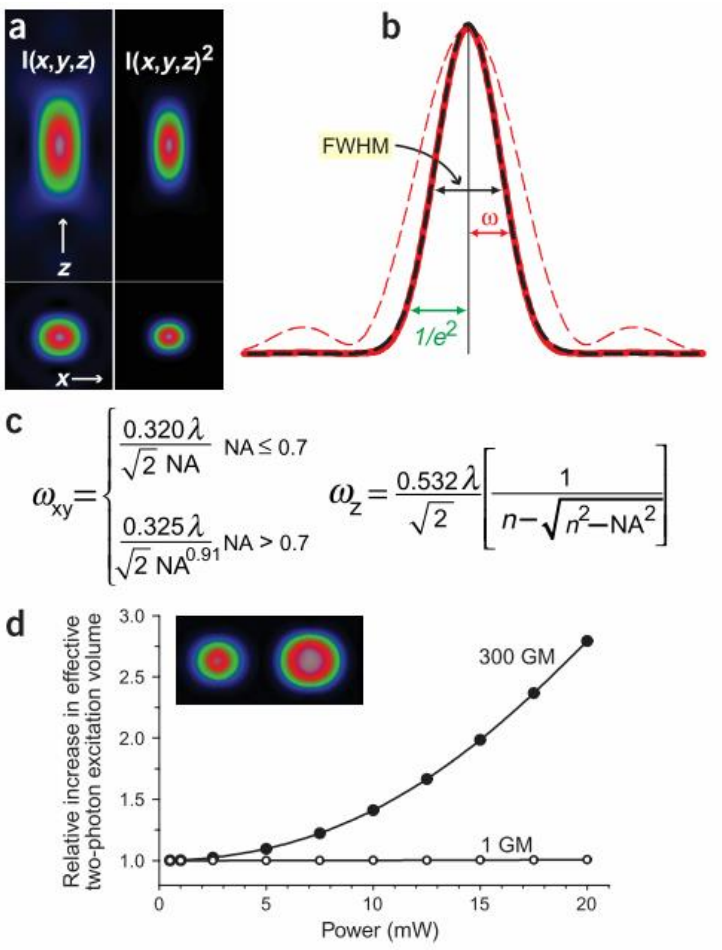

Figure VII.69: Representation of the two-photon excitation volume with (a) visual simulations of the IPSF and IPSF² and (b) the schematic axial profile of the IPSF (dashed red), the IPSF² (solid red) and Gaussian approximation (dashed black). (c) Equations to calculate the 1/e radii ω_{xy} and ω_z of the obtained voxels depending on the NA of the applied objective. (d) Influence of the applied laser power on voxel volume, which is highly dependent on the two-photon cross-section of the applied photoinitiator. (Figure reproduced from [275])

In order to apply 2PP as an additive manufacturing technique, a femtosecond pulsed laser setup is required which typically encompasses several components to enable spatiotemporal control (Figure VII.68). In this respect, the main component is a femtosecond pulsed laser source. Herein, a comparison between the laser system applied in the TUWien setup is made

with the laser system of the commercial Nanoscribe in terms of several key properties. The beam of the laser typically passes through a set of components along the optical path to enable 2PP. Starting from the laser, the first important component is the acousto-optical modulator which allows very fast control of the applied laser power. Next, the laser beam is expanded using a beam expander, which allows to irradiate the entire back aperture of the applied microscope objective to maximise the focussing power. These objectives are typically characterised by a large back aperture as well as a large numerical aperture, resulting in a high focussing power, and associated small voxel sizes (Figure VII.69 c).

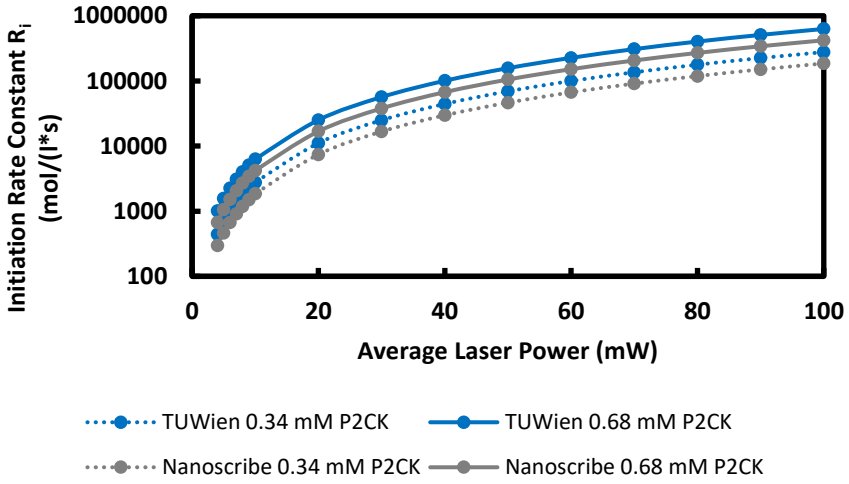

Figure VII.70: Calculated increase in initiation rate as a function of applied average laser power for the photoinitiator P2CK (176 GM @ 800 nm; 160 GM @ 780 nm) [230,232] using a 32X/0.85 objective at the photoinitiator concentrations and average laser powers as applied in chapter 4. The R_i was calculated both for the set-up at TUWien and the Nanoscribe present at B-PHOT based on table VII.10.

The objective typically focusses the laser beam into a sample which is mounted on a microscope stage, thereby allowing control in all 3 dimensions. Additionally, nowadays most 2PP systems are equipped with a galvanometer scanner, which allows to rapidly scan the laser beam within the XY plane prior to entering the objective, resulting in very fast scanning of the focal spot within the field of view of the microscope objective. As a consequence, the writing speeds can be significantly increased, up to several m/s. As a result, structures are typically written by dividing the applied CAD design in different

layers (i.e. slicing) where every layer is divided in lines over which the voxel will be scanned (i.e. hatching). In this respect, it is important that the slicing and hatching distance match with the size of the obtained voxel (as determined by the microscope objective). It is important, that there is enough overlap in of the different voxels in the XY planes (i.e. hatching) to avoid the presence of individual lines after structuring. Furthermore, the slicing distance should be lower than the obtained voxel height, to ensure proper attachment. In order to ensure proper contact between the different voxel paths, the hatching often occurs in both the X and Y direction, where scanning can be applied within the same layer, or alternating between the different layers.

In the present work, a tuneable femtosecond NIR laser (MaiTai eHP DeepSee, Spectra-Physics) with a pulse duration of 70 fs and a repetition rate of 80 MHz is used, in combination with a Plan-Apochromat, 32x NA 0.85 water immersion microscope objective. All experiments were performed at a wavelength of 800 nm. An overview of the specs of the applied laser source is presented in table VII.10 and compared to the laser applied in the commercial Nanoscribe GT system.

Table VII.10 Comparison between the laser sources of the commercially available Nanoscribe, and the experimental set-up at TUWIEN.

	2PP set-up (TU-WIEN)	**Nanoscribe**
Laser	Ti:sapphire laser	Ultrafast Erbium Fiber Laser
Wavelength	690 – 1040 nm	780 nm
Average power	2,400 mW	180 mW
Peak power	425 kW	25 kW
Pulse duration	70 fs	100 fs
Repetition rate	80 MHz	80 MHz
Feature size	Sub-micron – mm scale	Sub-micron – mm scale

7.1.2. (Photo-)Rheology

7.1.2.1. Viscous, Elastic and Visco-elastic Materials

Rheology studies the deformation of flow and matter under the influence of a certain applied stress [391]. It provides the ability to study materials with a mechanical behavior which cannot be described using conventional elasticity and Newtonian fluid mechanisms. Polymers are materials whose mechanical behavior can typically not be described using the conventional theories discussed below in brief.

The mechanical behavior of a material can typically be described using two ideal theories. On the one hand, an ideal elastic material will return back to its original shape after inducing a deformation and removing the external force applied to induce this deformation (i.e. spring model). The deformations in these materials can be described using Hooke's law [87,392].

$$\tau(t) = G^* * \gamma(t) \tag{15}$$

With $\tau(t)$ being the time-dependent shear stress, G^* the complex shear modulus and $\gamma(t)$ the time- dependent applied strain.

On the other hand, ideal viscous materials are materials which do not return to their original shape after inducing a deformation to the sample resulting in an irreversible deformation proportional to the applied tension and time and inverse to the viscosity (i.e. a dashpot model). As a consequence, these materials typically follow Newtonian fluid behaviour and can be described using the following equation [87,392]:

$$\tau(t) = \eta^* * \dot{\gamma}(t) \tag{16}$$

With $\tau(t)$ being the time-dependent shear stress, η^* the complex viscosity and $\dot{\gamma}(t)$ the time- dependent applied shear rate.

Finally, there are materials which are characterized by both viscous and elastic behaviour, which are generally referred to as visco-elastic materials. In this respect, the materials can be represented theoretically by a combination of a dashpot and a spring which are positioned in parallel to each other. If a deformation is induced, a certain force is required to induce this deformation by a consequence of a combination of Hooke's law and the Newtonian fluid behaviour. Once the force is released, the material will return

to its original shape with a certain delay as a consequence of the viscous behaviour. Polymers are typical materials which exhibit this type of behaviour. They will undergo a partial reformation with a delay when the applied stress is removed. To examine these materials, rheology is often applied to perform an oscillatory assay. In the present work, rheology was performed using a plate-plate geometry (Figure VII.71). In this geometry, the sample is placed onto a temperature-controlled glass plate under which a UV-light source can be mounted that can be triggered on demand. A second plate is placed on top at a predetermined distance (i.e. gap) to ensure close contact with the sample [391]. The tests are performed by applying a controlled shear strain characterized by an oscillatory sine function:

$$\gamma(t) = \gamma_0 \sin(\omega t) \tag{17}$$

With γ_0 being the applied amplitude of the shear strain and ω being the applied frequency of deformation. The corresponding resulting shear stress is then a phase-shifted sine function:

$$\tau(t) = \tau_0 \sin(\omega t + \delta) \tag{18}$$

With δ being the phase shift angle which corresponds to 0° for ideal elastic behavior and 90° for ideal viscous behavior and 0° < δ < 90° for visco-elastic behavior (see Figure VII.71).

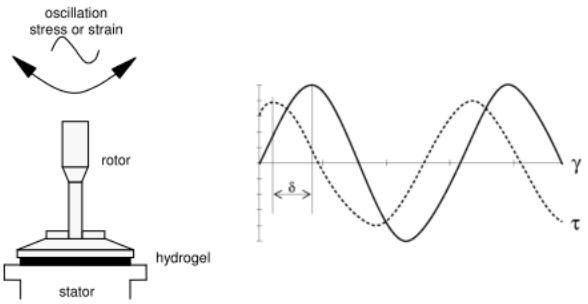

Figure VII.71 (left) Schematic representation of a rheometer with a plate-plate geometry with a moving top plate (rotor) and a static bottom plate (stator) and the gelatin hydrogel sample in between. (right) The shear strain function $\gamma(t)$ and the resulting shear stress function $\tau(t)$ as obtained during a rheological experiment. (Figure reproduced from [392])

Two important parameters for the characterization of visco-elastic materials include the storage modulus G' and the loss modulus G''. G' is a measure for the energy stored during deformation which will reverse deformation after

removal of the applied load and is thus associated with the elastic behavior of the sample. G" corresponds with the energy consumed by the sample during the deformation and is associated with the viscous behavior of the material [87,391,392].

$$G'(\omega) = \frac{\tau_0}{\gamma_0}\cos(\delta) \tag{19}$$

$$G"(\omega) = \frac{\tau_0}{\gamma_0}\sin(\delta) \tag{20}$$

These measurements have to be performed within the linear visco-elastic range (LVE range), which is the range in which deformations will remain reversible [391]. To determine the LVE range, typically a strain sweep (i.e. increasing the strain or amplitude of deformation at a constant frequency) are performed. The LVE is then determined on these graphs as the range where G' and G" remain constant.

For hydrogels, the storage modulus will mainly describe the stiffness of the hydrogel. Therefore, usually the storage modulus is applied to compare different hydrogel materials to each other and to biological tissues [306]. Furthermore, rheology also allows to perform dynamic measurements on hydrogel systems. Of specific relevance in the present work is assessing the rheological properties of hydrogel precursor solutions under the influence of UV-irradiation. In this respect, especially the cross-over point between the loss and storage modulus or gel-point is of specific importance. Before this point, the material exhibits predominantly viscous behaviour, meaning that it is still in solution, whereas after this point, the material exhibits mainly elastic behaviour, meaning a gel is present [393]. By measuring this point as a function of time, the reactivity of different hydrogel precursor formulations can be compared in a reproducible manner.

7.1.3. Confocal Laser Scanning Microscopy

Confocal laser scanning microscopy is a form of fluorescence microscopy which allows the generation of 3D images of fluorescently labelled structures. To this end, a laser at a specific wavelength is scanned through the sample to induce excitation of fluorescent components in the structure or tissue. Next, the resulting fluorescence emission is observed using a suitable detector at the correct wavelength. For example, when using a DAPI stain to visualize the cell-nuclei, the sample is irradiated at 461 nm, while fluorescence is detected at 461 nm (see Figure VII.72).

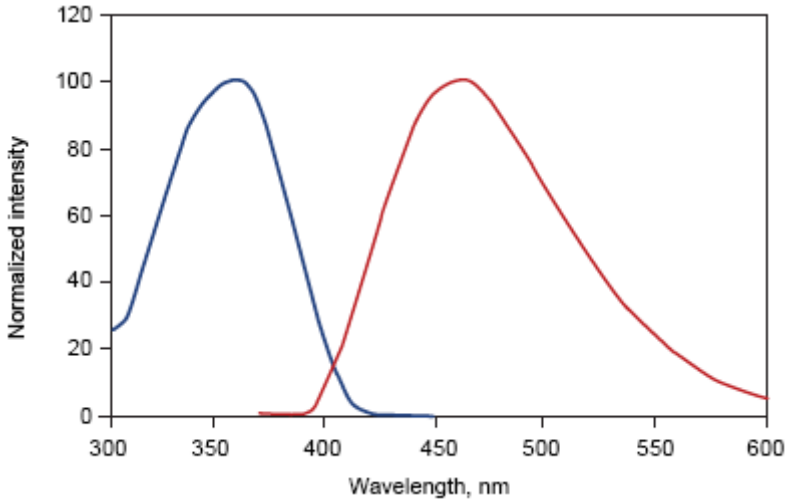

Figure VII.72 Absorption (blue) and emission red) spectrum of 4',6-diamidino-2-phynylindole (DAPI), a common nucleus staining dye. (Image reproduced from [394])

Furthermore, in contrast to conventional optical microscopy, confocal microscopy enables the generation of sharp images limited only to the exact plane of focus via the introduction of a pinhole before the detector. Because of this pinhole, all light originating from the background or out of focus artefacts will be blocked, thereby only allowing detection of the signals from the illuminated area [395] (Figure VII.73). By scanning the sample in a raster pattern, single plane images are created. By recording several of these images in consecutive focal planes along the Z direction, 3D images can be obtained (through a so called z-stack) [396]. Since often hydrogels and biological tissues are transparent for the induced fluorescence, also images within the structure or cells can be obtained by using specific stains. Furthermore, by using different laser wavelengths in combination with detectors at specific wavelengths, areas which contain different dyes can be imaged separately and compiled again afterwards, thereby allowing for example visualization of the nucleus and cytoskeleton of cells in a single image.

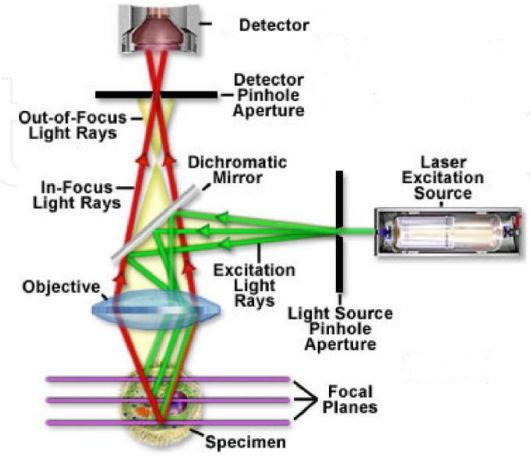

Figure VII.73 Schematic representation of the principle of confocal microscopy. (Image reproduced from [395])

7.1.4. Differential Scanning Calorimetry

Differential scanning calorimetry (DSC) is a characterization method which enables to determine phase transitions inside a material (i.e. glass transition temperature T_g and melting temperature T_m). Using this method, the required heat applied to a sample is quantified relative to the heat applied to a reference sample for a certain change in temperature at a predetermined rate. When a material undergoes a certain phase transition, it requires additional or less energy compared to the reference sample. By plotting these differences in applied heat (i.e. the enthalpy) versus the temperature, a thermogram is obtained in which the phase transitions are visualized as peaks or shifts in the baseline which represent the heat capacity (C_v).

7.1.5. Spincoating

Spincoating is a surface treatment method which allows to deposit thin films on a substrate. To this end, a droplet of the coating solution is dispensed on top of a substrate. Next, the surface is rotated at high speed (i.e. typically ≥ 1000 RPM), resulting in spreading of the solution as a consequence of centrifugal forces. As a consequence, the solution is uniformly spread on the surface, whereas excess solution evaporates of exits the surface at the edges

as a consequence of the centrifugal forces. After the coating process, often the film is stabilized by a UV- or thermal treatment.

7.2. Applied Materials

7.2.1. Applied Materials

All chemicals were used as received, unless stated otherwise. Gelatin type B (isolated from bovine hides by an alkaline process) and gelatin type A (isolated from porcine skin by an alkaline process)was supplied by Rousselot (Ghent, Belgium). 2-butanone (≥ 99 %); 2-mercaptoethanol (≥ 99%); 3-(trimethoxysilyl)propyl methacrylate (98%); 5-norbornene-2-carboxylic acid (mixture of endo and exo, predominantly endo (98%)); 1-ethyl-3-(3-dimethylaminopropyl)carbodiimide (EDC); Acetic acid 3-(trimethoxysilyl) propyl methacrylate (98%); D,L-dithiothreitol (DTT) (≥ 99%); D,L-homocysteine thiolactone hydrochloride (≥ 99%); deuterium oxide; EDTA tetrasodium tetrahydrate salt; Glucose (GO) Assay Kit, KH_2PO_4 (≥ 99%); LiBr (≥ 99%); Methacrylic anhydride (94%); Na_2HPO_4 (≥ 99%); Na_2CO_3 (≥ 99.5%); $NaHCO_3$ (≥ 99.7%); NaOH; n-butylamine (≥ 99%); o-phthaldialdehyde (≥ 99%); Poly(ethylene glycol) dithiol (3400 g/mol) (PEG2SH 3400); Tetra(ethylene glycol) dithiol (97%) and tetrahydrofurane (THF) were purchased at Sigma Aldrich (Diegem, Belgium). Dimethyl sulfoxide (DMSO) (99.85%) and N-hydroxysuccinimide (98%) (NHS) were purchased at Acros (Geel, Belgium). 2-Aminoethyl methacrylate hydrochloride (AEMA.HCl) was obtained from Polysciences (Conches, France). N-(3-dimethylaminopropyl)-N'-ethylcarbodiimide hydrochloride (EDC) (> 98 %) was obtained at TCI (Zwijndrecht, Belgium). Irgacure 2959® (1-[4-(2-hydroxyethoxy)-phenyl]-2-hydroxy-2-methyl-1-propane-1-one) was purchased at BASF (Antwerp, Belgium). FITC-dextran (2000 g/mol) was obtained from TdB Consultancy AB (Uppsala, Sweden). (2,4,6-trimethylbenzoyl)-phenyl-phosphinic acid ethyl ester (i.e. Speedcure TPO-L) was obtained from Lambson (West Yorkshire, UK).The 4-arm-PEG-SH-20 k (PEG4SH 20k) and 4-arm-PEG-SH-10k (PEG4SH 10k) were obtained from Laysan Bio Inc. (Alabama, USA). PURASORB® PDL 20 (PDLLA) was obtained at Corbion Purac and is FDA-approved and registered under DMF-21817. The dialysis membranes Spectra/Por® (MWCO 12.000-14.000 g/mol) were obtained from Polylab (Antwerp, Belgium).

7.3. Applied Methods

7.3.1. Chemical Modifications of Gelatin

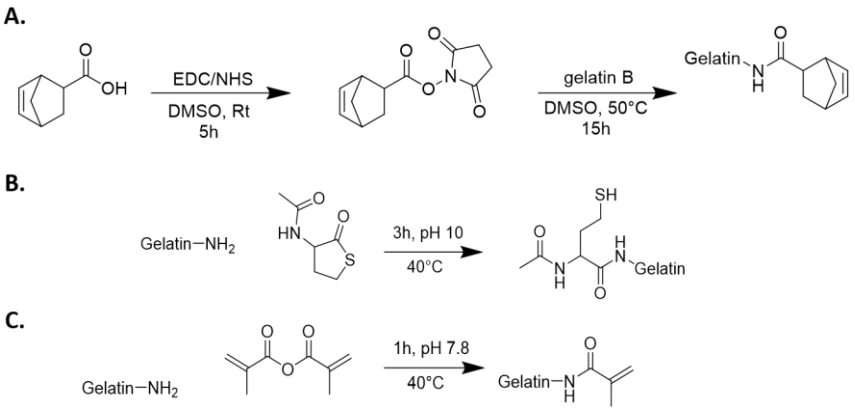

Figure VII.74 : Different gelatin modification strategies including: (A) the formation of gel-NB using 5-norbornene-2-carboxylic acid; (B) the formation of gel-SH using N-acetyl homocysteine thiolactone; (C) and the formation of gel-MA using methacrylic anhydride

7.3.1.1.Methacrylation of the Primary Amines in Gelatin B Yielding gel-MOD/gel-MA

The methacrylation of gelatin B, with the aim of obtaining gel-MOD (also commonly referred to as gel-MA), was performed as described earlier [121] (see Figure VII.74 C). Briefly, 100 g gelatin type B (38.5 mmol amines) was dissolved in 1 L of phosphate buffer (0.2 molar, pH 7.8) at 40 °C under continuous mechanical stirring. Next, either 1 (i.e. 5.736 mL, 38.5 mmol) or 2.5 equivalents (equiv.) (i.e. 14.34 mL, 96.25 mmol) methacrylic anhydride were added and allowed to react for one hour to obtain a high and a low degree of substitution (DS). After one hour, the reaction mixture was diluted with 1 L double distilled water (DDW) (ρ = 18.2 MΩ cm) followed by dialysis against distilled water (MWCO 12000−14000 g/mol) during 24 h at 40 °C, with the water being changed 5 times. The pH of the solution was adjusted to ~7.4 using a 5 *M* NaOH solution. Finally, the gel-MA was isolated by freezing and lyophilization (Christ freeze-dryer alpha I-5). The degree of substitution (DS) was determined using ^{1}H-NMR spectroscopy using D_2O as solvent at elevated temperature (40°C) as reported earlier resulting in derivatives with a DS of 63 or 95%, respectively [289].

7.3.1.2. Methacrylation of the Carboxylic Acids in gel-MOD Yielding gel-MOD-AEMA

Fully functionalized gel-MOD (DS 95%) (10 g, 10.980 mmol carboxylic acids) was dissolved in 300 mL of dry DMSO (obtained via vacuum distillation over CaH_2) at 50°C under inert Argon atmosphere. After complete dissolution, 1 equiv. of 1-ethyl-3-(3-(dimethylamino)propyl)carbodiimide hydrochloride (EDC) (2.1 g; 10.980 mmol) and 1.5 equiv. N-hydroxysuccinimide (NHS) (1.895 g; 16.48 mmol) were added together with 50 mL dry DMSO. After 30 min, 1.5 equiv. 2-aminoethyl methacrylate hydrochloride (AEMA.HCl) (2.729 g, 16.47 mmol) were added together with 0.01 equivalents (18 mg; 0.1098 mmol) of 4-tert-butyl catechol (i.e. inhibitor) and 50 mL of dry DMSO after which the solution was shielded from light and stirred overnight at 50°C. DMSO was removed by dialysis (MWCO 12000 - 14000 g/mol) at 40°C during 24 h in distilled water followed by freezing and lyophilisation.

The modification was quantified via ^{1}H-NMR spectroscopy (Bruker WH 500 MHz) using D_2O as solvent at elevated temperature (40°C). The integrations characteristic for methacrylamide (5.5 ppm (s,1H) and 5.51 ppm (s, 1H)) (gel-MOD) or methacrylate (6.20 ppm (s, 1H) and 5, 80 (s, 1H) (gel-MOD-AEMA) were compared with the integration corresponding with the inert hydrogens of Val, Leu and Ile at 1.01 ppm (18H) according to the following formula (based on the amino acid composition see Table II.1).

$$DS_{Carboxylic\ acids}(\%) = \left[\frac{\frac{I_{6.20ppm}}{0.1098 \frac{mol}{100g}}}{\left(\frac{I_{1.01ppm}}{0.3836\ mol/100g}\right)} \right] * 100\ \% \qquad (21)$$

7.3.1.3. Introduction of Norbornene Functionalities onto Gelatin Type B Yielding gel-NB

For the preparation of 10 g gel-NB, the carboxylic acid functionalities in 5-norbornene-2-carboxylic acid were converted into an activated succinimidyl ester via reaction with EDC and NHS during 25 hours, using a 1.25 – 1.5 times excess of 5-norbornene-2-carboxylic acid (relative to the amount of EDC added i.e. 600 mg, 4.35 mmol – 2000 mg, 14.5 mmol) to prevent the presence of unreacted EDC molecules which can on the one hand result in the formation of zero-length crosslinks between the primary amines and the carboxylic acids present in gelatin (see Figure VII.74 A) [48]. On the other hand, it is of predominant importance that all EDC is reacted prior to the

addition to gelatin, as the combination of a carbodiimide and an acid catalyst (5-norbornene-2-carboxylic acid) in DMSO could result in oxidation of the alcohols present in gelatin into their respective aldehyde or ketone following a Pfitzner-Mofatt-oxidation[326]. These aldehydes could also result in crosslinking of gelatin via reaction with the primary amines of gelatin resulting in Schiff's base formation [48]. To this end, 5-norbornene-2-carboxylic acid was dissolved in 50 ml of dry DMSO followed by dissolution of the EDC (555 mg, 2.9 mmol -1860 mg, 9.7 mmol) and NHS in a respective 1:1.5 ratio. After 25 hours of reaction, the temperature was raised to 50°C and gelatin type B (10 g) was added together with 250 ml of dry DMSO to the reaction mixture resulting in 0.75 - 2 equiv. of norbornene succinimidyl ester relative to the primary amines present in gelatin (0.385 mmol/g) followed by 3 times degassing and allowed to react for another 20h. Next, the mixture was precipitated in a ten-fold excess of acetone, filtered on filter paper (VWR, pore size 12-15 µm) using a Büchner filter to remove the formed ureum side products and DMSO, followed by dissolving in DDW and dialysis for 24 hours against distilled water (MWCO 12- 14 kDa). After dialysis, a turbid solution was obtained. Next, the pH of the mixture was adjusted to ~7.4 using a 5 *M* NaOH solution resulting in a clear solution. Finally, the pure product was isolated by freezing and lyophilisation. The DS was assessed using ^{1}H-NMR spectroscopy in D_2O at 40°C.

In order to determine the DS, the characteristic signals for the protons on the vinyl group present in the norbornene functionalities were used. However, since the applied norbornene derivative is a mixture of both endo- and exo-5-norbornene-2-carboxylic acid, four signals are observed instead of two, of which two peaks correspond to the endo-form (6.33 ppm (m, 0.06-0.75 H depending on the DS) and 6.00 ppm (m, 0.06-0.75 H depending on the DS)) and the two other signals (6.28 ppm (m, 0.05-0.45H depending on the DS) and 6.26 ppm (m, 0.05-0.45H depending on the DS)) to the exo-derivative [327]. Consequently, the four peaks need to be taken into account for the integration. Furthermore, since the peaks of the exo-derivative cannot be separated fully, these signals are grouped and the DS can be obtained by taking the average of these signals and comparing with the reference signal at 1.01 ppm (s, 9.96 H) resulting in the following equation (2):

$$DS(\%) = \left[\frac{\frac{I_{6.33\ ppm} + I_{6.28\ \&\ 6.26\ ppm} + I_{6.00\ ppm}}{2 * 0.0385\ mol/100g}}{\frac{I_{1.01\ ppm}}{0.3836\ mol/100g}}\right] * 100 =$$

$$= \left[\frac{I_{6.33\ ppm} + I_{6.28\ \&\ 6.26\ ppm} + I_{6.00\ ppm}}{2 * I_{1.01\ ppm}}\right] * 9.96 * 100 \qquad (22)$$

The derivatives exhibited a DS ranging from 63 % to 90%.

7.3.1.3. Thiolation of the Amine Functionalities in Gelatin Type B Yielding gel-SH

Thiolation of the primary amines in gelatin type B was performed according to a previously reported protocol [187] (see Figure VII.74 B). In brief, 20 gram of gelatin type B (7.7 mmol reactive amines) was dissolved in 200 ml carbonate buffer (pH 10) at 40°C. After complete dissolution, the solution was degassed and placed under inert atmosphere. Next, 0.045 g (1.5 mM) of ethylenediaminetetraacetate tetrasodium tetrahydrate salt (EDTA) was added in order to complex any metals which can catalyze the disulfide forming oxidation reaction. Next, 5 equiv. (relative to the primary amines of gelatin) of N-acetyl homocysteine thiolactone (38.5 mmol, 6.193 mg) were added to the reaction mixture. After addition, the reaction was allowed to proceed for 3 hours under inert (Ar) atmosphere at 40°C. The gel-SH was purified using dialysis (spectrapor MWCO 12,000 – 14,000 Da) for 24 hours under inert atmosphere and the water was changed 5 times. After dialysis, the gel-SH was immediately frozen in liquid nitrogen and isolated via freeze-drying (Christ freeze-dryer alpha I-5). The DS was determined using a ortho-phthalic dialdehyde amine determination assay as reported earlier yielding a DS of 72% [339].

7.3.2. Synthesis of Lithium (2,4,6-trimethylbenzoyl) phenylphosphinate (LAP)

The photoinitiator Li-TPO-L or LAP was synthesized according to a previously reported protocol [292].

To this end, 8.60 g (27.2 mmol) of (2,4,6-trimethylbenzoyl)-phenyl-phosphinic acid ethyl ester (i.e. speedcure TPO-L by Lambson) was dissolved in 150 ml butanone followed by the addition of 9.45 g (109 mmol) lithium bromide. The mixture was allowed to react for 24 hours at 65°C under reflux conditions. The formed precipitate was isolated via filtration, washed with petroleum ether and dried under vacuum at room temperature.

7.3.3. Primary Amine Determination Using an Ortho-Phthalic Dialdehyde Assay

An ortho-phthalic dialdehyde (OPA) assay was performed following a protocol previously reported in literature [187]. First, 20 mg ortho-phthalic dialdehyde (OPA) was dissolved in 10 ml ethanol. After complete dissolution, the mixture was diluted to 50 ml with DDW to yield stock solution 1. A second stock solution was prepared by dissolving 25 µl 2-mercaptoethanol in 50 ml borate buffer (pH 10).

First a calibration curve was obtained using n-butylamine solutions with known concentrations (0.002 M to 0.01 M). To this end, 50 µl of one of these calibration solutions, 950 µl DDW, 1500 µl mercapto-ethanol stock solution and 500 µl of the OPA stock solution was pipetted into a cuvette followed by vigorous stirring. Finally, the absorbance at 335 nm was determined relative to a blank consisting of the same mixture using 1000 µL of DDW with the omission of an n-butylamine solution.

Next, the same protocol was applied on a gelatin, gel-MOD, gel-NB or gel-SH solution (25 mg/ ml in DDW, 40°C). All measurements were performed in triplicate.

7.3.4 Preparation of Gelatin Films via Film Casting

All hydrogels were crosslinked starting from 5-15 w/v% solutions of gel-NB, gel-MOD-AEMA or gel-MOD using PBS as solvent at 40 °C. After complete dissolution, 2 mol% Irgacure 2959 was added (relative to the number of crosslinkable functionalities) using a stock solution containing 8 mg/ml of Irgacure 2959 while to gel-NB, 1,4-dithiotreitol (DTT) was also added (0.5 equivalents, relative to the number of norbornene functionalities) using a stock solution containing 80 mg/ml of DTT in PBS. Prior to injection in between the glassplates, the solutions were degassed for at least 30 seconds. Next, the heated solution was injected between two parallel glass plates coated with Teflon release foil and separated by a 1 mm thick silicone spacer. Prior to 30 minutes of UV-A irradiation from both sides (365nm, 8mW/cm²), the plates were stored at 4 °C during 1 h to induce physical. Following irradiation, the films were incubated in 20 ml DDW at 37 °C during 48h to induce equilibrium swelling.

7.3.5. Gel Fraction and Swelling Ratio Determination

From the obtained films, 3 samples with a diameter of 0.8 cm were punched to determine the gel fraction. The remaining films were incubated in 20 ml DDW at 37°C during 48 hours to obtain equilibrium swelling.The gel fraction was determined by freeze-drying films with a diameter of 0.8 cm immediately after crosslinking. Next, the dry mass of these films was determined ($m_{d,1}$) and the films were incubated in DDW at 37°C for 24 hours. After equilibrium swelling, the films were freeze-dried again and the dry mass was determined again ($m_{d,2}$). The gel fraction was determined by comparing the final dry mass to the original one:

$$gel\ fraction\ (\%) = \frac{m_{d,2}}{m_{d,1}} \tag{23}$$

All measurements were performed in triplicate and the standard deviation was calculated.

The equilibrium swelling ratio was determined using circular films with a diameter of 0.8 cm punched from equilibrium swollen sheets. Before determining the swollen mass (m_s) of the films, the excess water on the surface was gently removed using tissue paper. Afterwards, the samples were freeze-dried to determine the dry mass (m_d). The swelling ratio was then calculated using the following formula:

$$mass\ swelling\ ratio\ (q) = \frac{m_s}{m_d} \tag{24}$$

7.3.6. Statistical Analysis

Statistical significance was analyzed using GraphPad Instat using a one-way analysis of Variance (ANOVA) with Bonferroni post-test in case of a normal distribution and adequate sample size. Non-parametric Kruskal-Wallis was applied in case of a lower sample. Statistical significance was defined as *** $p < 0.001$, ** $p < 0.01$, * $p < 0.05$.

7.3.9 Applied Methods in Chapter 2

7.3.9.1.Molecular Weight Determination via Gel Permeation Chromatography (GPC)

GPC measurements were performed on a Waters 610 fluid unit and a Waters 600 control unit equipped with a Waters 410 RI detector. Samples were prepared by dissolving approximately 10 mg material in 1 ml DMSO. The mobile phase consisted of DMSO in the presence of 0.2 M LiCl. All samples were measured at 40°C. A five point calibration curve was prepared using pullulan standards (i.e. 9890 - 276500 g/mol). The obtained results were analyzed using Waters Empower 2 software.

7.3.9.2.Physical Gelation Study via Differential Scanning Calorimetry

Hydrogel building block solutions (10w/v%, 40 mg each) in double distilled water were placed into a hermetic Tzero pan (TA instruments, Zellik, Belgium). As a reference, an empty hermetic Tzero pan was applied. The samples were subjected to a preparatory program as described by Prado et al.[240]. First, a temperature ramp of 20.00 °C/min was applied to reach a temperature of 60.00 °C. The sample was stabilized for 20 minutes. Next, a ramp of 10.00 °C/min was applied to cool down to a temperature of 15.00 °C, followed by stabilizing the samples at 15 °C for 20 minutes prior to applying a temperature ramp of 20.00 °C/min until a temperature of -10.00 °C was reached followed by a final ramp of 5.00 °C/min until a temperature of 60.00 °C was obtained. All measurements were performed on a TA instruments Q 2000 with an RSC 500 cooler (Zellik, Belgium). The results were analyzed using Q series software. 10 w/v% solutions were applied for most characterization experiments as they enable straightforward sample manipulation, while both physical and chemical crosslinking can clearly be observed.

7.3.9.5. Rheological Monitoring of the Crosslinking Reaction and Determining the Mechanical Properties of Hydrogel Films.

A rheometer type Physica MCR-301 (Anton Paar, Sint-Martens-Latem, Belgium) with a parallel plate geometry (upper plate diameter of 25 mm) was applied. For monitoring the crosslinking reaction, 300 µl of each solution containing 2 mol% Irgacure 2959 (relative to the amount of crosslinkable functionalities) was placed between the plates using a gap setting of 0.35 mm. The edges were trimmed and sealed using silicone grease (mittelviskös, Bayer, Sigma-Aldrich, Diegem, Belgium) to prevent sample drying. An oscillation frequency of 1 Hz and a strain of 0.1% were applied as these values are within the linear visco-elastic range as determined by isothermal measurements (37°C) of the storage (G') and loss moduli (G") as a function of deformation at a constant frequency (1Hz) and varying strain (0.01% - 10%). Next, the solutions were either cooled to 5°C to induce physical gelation which was monitored during 10 min prior to irradiation or immediately irradiated at 37°C using UV-A light (10 min, EXFO Novacure 2000 UV light source at 365 nm using a power density of 500 mW/cm²) followed by 2 min of post-curing monitoring. To assess the effect of the irradiation dose on the final mechanical properties, the same protocol was performed using either 215, 360 or 500 mW/cm² power density and the final storage modulus was plotted. The obtained power density was obtained by entering a UV dose of either 1500, 2500 or 3500 mW/cm² on the light source, followed by measuring the actual value at the site of crosslinking using a smart UV intensity meter (Accu-Cal-50, DYMAX)
Rheology on thin films was performed by cutting equilibrium swollen gelatin films (1 mm thick, 48 hours in double distilled water at 37°C) with a diameter of 14 mm and placing them in between the spindle (d = 15mm) and the bottom plate of the rheometer at 37°C. Next, a normal force of 1 N was applied to ensure proper contact between the thin film and both plates. Then, the storage modulus was monitored at 37° using an amplitude of 0.1% over a frequency range from 0.01 Hz to 10 Hz.

7.3.9.6. Enzymatic Degradation Assay

The *in vitro* degradation of the hydrogels was studied by freeze-drying thin films (1 mm thick, 0.8 cm diameter) followed by determining their initial dry mass. Next, the samples were incubated in 0.5 ml Tris–HCl buffer (0.1 M, pH 7.4) in the presence of 0.005 % w/v NaN_3 and 5 mM $CaCl_2$ at 37 °C. After 1

h, 0.5 ml collagenase (200 U/ml) dissolved in Tris–HCl buffer, was added. At different time points, enzymatic degradation was inhibited through addition of 0.1 ml EDTA solution (0.25 M) and subsequent cooling of the sample on ice. Next, the hydrogels were washed three times during ten minutes with ice-cooled Tris–HCl buffer and three times with DDW and after freeze-drying, the gel fraction of the samples for each time point was determined.

7.3.9.7. Applied Cell Lines and In Vitro Biological Assay

Mouse fibroblast cells (L929) obtained from Sigma and mouse calvaria-derived preosteoblast cells (MC3T3-E1 Subclone 4) from ATCC-LGC Standards were used for cell viability testing. The L929 cells were cultured in Dulbecco's Modified Eagle's Medium (DMEM) with 4500 mg/L glucose, L-glutamine, and sodium bicarbonate, without sodium pyruvate (Sigma). The MC3T3-E1 cells were expanded in Alpha Minimum Essential Medium (aMEM) containing ribonucleases, deoxyribonucleases and 2mM L-glutamine, in the absence of ascorbic acid (Gibco). Both media were supplemented with 10% fetal bovine serum (Sigma) and 1% of 10000 U/mL Penicillin/Streptomycin (Lonza). The cells were cultivated in an incubator in a humid atmosphere at 37°C containing 5% carbon dioxide. The cell medium was refreshed every other day.

Presto Blue Metabolic Activity Assay

10 w/v% solutions of the gelatin derivatives were prepared in PBS using 2 mol% of Irgacure 2959.
For each sample, an aliquot of 15 µl was pipetted onto a Teflon plate and a glass coverslip activated with 3-(trimethoxysilyl)propyl methacrylate was pressed on top to evenly cover the glass surface. Afterwards, samples were stored at 4°C for 1 hour to induce physical crosslinking, followed by 10 minutes UV-A induced crosslinking (365 nm, 4 mW/cm^2). Next, samples were removed from the Teflon surface, transferred to a 12 well plate, and soaked in medium. To sterilize the coated samples, UV-C irradiation (254 nm, 30 min) was applied prior to storage in the incubator overnight (5% carbon dioxide, 37°C) in appropriate medium to remove any uncrosslinked material and induce equilibrium swelling on all samples. Next, all medium was aspirated from the samples and 50 µL medium containing either 20000 MC3T3-E1 or L929 cells was seeded per well. After 30 minutes of settling time, 1 ml of appropriate medium was added. During further culture, the appropriate cell

medium was replaced every other day. At specific time points (1, 2 , 3 and 7 days), the metabolic activity was assessed using a Presto Blue Cell Viability test (Life technologies). For these tests, Presto Blue, a Resazurin-based reagent, was diluted 1:10 with appropriate medium and 500 µl of solution was applied per well followed by incubation during 1 h. In the presence of viable cells, resazurin is reduced thereby becoming highly fluorescent. From each well 100 µL of solution was transferred to a 96 well plate for fluorescence measurements, while the remaining cell medium was aspirated and replaced by new appropriate medium followed by incubation. The fluorescence was measured with a plate reader (Synergy Bio-Tek, excitation 560 nm, emission 590 nm). After subtraction of the sample blank, (diluted PrestoBlue incubated for 1h in appropriated medium) the different substrates were compared to each other and to the “dead cell” control (cells in 50% DMSO and 50 % medium for 1 h). The fluorescence value obtained for the cells cultivated on tissue culture plastic (TCP) after 7 days of culture was considered as 100% viability. Next, all fluorescence values were normalized against this control and expressed relative to this 100% viability.

7.3.9.9. Two-Photon Polymerization of Gelatin Derivatives

Two-photon polymerization experiments were performed on a setup which was previously reported. [129,232] A water immersion objective (C-Achroplan 32X, NA = 0.85, water immersion, Zeiss) was used in combination with a femtosecond pulsed NIR (800 nm) laser with 70 fs pulse duration. The scan speed was set at 100 mm/s for all samples. The CAD design was sliced with a layer spacing of 1 µm and hatched with 0.5 µm line spacing. In every layer the focal spot was scanned both in the x and y direction for all samples.
Average laser powers varying from 10 to 100 mW in 5, 10 and 15 w/v% hydrogel precursor solutions in DMEM medium containing 2 mol% P2CK as a two-photon initiator (relative to the amount of double bonds present) were applied at a constant scan speed of 100 mm/s. To prevent sample drying, approximately 50 µl of each solution was placed in a micro-well (µ-Dish 35 mm, Ibidi) consisting of two glass plates separated by a silicone spacer with a diameter of 6 mm and a thickness of 1 mm. The bottom plate was silanized with 3-(trimethoxysilyl)propyl methacrylate to enable sufficient attachment.[129] After structuring, 2 ml of PBS was added to each sample, and samples were stored in the incubator at 37°C for at least 24 hours to wash away all uncrosslinked material and induce equilibrium swelling of the microstructures.

Swelling of Microstructures

For each hydrogel building block concentration, an array of ten cubes was structured (each 100 x 100 x 100 µm) at a scan speed of 100 mm/s using average laser powers in the range of 10 mW to 100 mW in steps of 10 mW. Laser scanning microscopy (LSM 700, Carl Zeiss) images using the same objective as for structuring were obtained for analysis. The surface of the bottom part of the structures where swelling is constrained due to attachment to the glass slide was analyzed using ImageJ software and compared to the surface of the top of the structures which is not constrained in swelling by the glass slide after 24 hours incubation in PBS buffer.

7.3.10. Applied Methods in Chapter 3

7.3.10.1.High Resolution- Magic Angle Spinning 1H-NMR spectroscopy

The analysis of the crosslinking efficiency of the developed hydrogels was performed according to a previously reported protocol [289].

All HR-MAS ^{1}H-NMR spectroscopy measurements were performed on a Bruker Avance II 700 spectrometer (700.13 MHz) using a HR-MAS probe equipped with a ^{1}H, ^{13}C and ^{119}Sn and gradient channel. Samples were spun at a spinning rate of 6 kHz. Freeze-dried samples of crosslinked hydrogels were cut into small pieces and introduced in a 4-mm MAS rotor (50 µL) in D_2O and allowed to swell. Sample homogeneity was achieved by manual stirring within the rotor.

The amount of cross-linkable groups was determined prior to and after crosslinking using HR-MAS ^{1}H-NMR spectroscopy. To determine the amount of reacted functionalities (RF), the DS was evaluated before and after crosslinking as mentioned previously [111,289]

$$RF\ (\%) = \left(\frac{DS_{before} - DS_{after}}{DS_{before}}\right) * 100 \qquad (25)$$

7.3.10.4. Rheological Analysis

The mechanical properties of the crosslinked hydrogels were determined as described in chapter 2.

To assess the crosslinking kinetics of the different hydrogel formulations, *in situ* photo-rheology experiments were performed on an Anton Paar Physica MCR-301 with a plate plate geometry (d = 25 mm) with a quartz glass bottom plate through which UV-A irradiation occurred (EXFO Novacure 2000 UV, 365 nm at a power density of 500 mW/cm² as determined using a smart UV intensity meter (Accu-Cal-50, DYMAX) at a gap setting of 300 µm at 37°C to exclude any physical gelation. To this end, 300 µl of each solution applied for the film casting was injected between the two plates. After trimming the edges of the sample, it was sealed using silicone grease to prevent sample drying (Bayer mittelviskös, Sigma Aldrich). The measurement occurred at an oscillatory frequency of 1 Hz and a strain of 0.1% as these values remain within the linear viscoelastic region of the hydrogels (data not shown). During the measurement, the storage (G') and loss modulus (G") were monitored over a total course of 14 minutes. After 2 minutes, the UV light was switched on to induce crosslinking for 10 minutes followed by post-curing monitoring during 2 minutes. To quantitively compare the crosslinking kinetics, the gel point of the different formulations was assessed as the cross-over point between the loss modulus and storage modulus, indicating a transition from a primarily liquid to a primarily elastic state. All measurements were performed in triplicate.

7.3.10.5. Two-Photon Polymerization and Laser Scanning Microcopy Analysis of Generated Structures.

Two-photon polymerization experiments were performed on the same set-up as mentioned in chapter 2. Average laser powers varying from 10 to 100 mW with a 10 mW increment were applied in 5, 10, and 15 w/v % hydrogel precursor solutions using PBS as solvent in the presence of 2 mol % Sodium 3,3'-((((1E,1'E)-(2-oxocyclopentane-1,3-diylidene) bis (methanylylidene)) bis(4,2-phenylene)) bis(methylazanediyl)) dipropanoate (P2CK) as two-photon photo-initiator (relative to the amount of double bonds present) [232].

An important difference with the previously reported protocol was that structuring in the present chapter occurred in PBS instead of Dulbecco's modified Eagle's medium (DMEM) since the cysteine amino acids present in DMEM might interfere in the thiol/ene crosslinking reaction. Furthermore, for the structuring of Gel-NB, this protocol was adapted in the sense that besides the addition of 2 mol% P2CK also 0.5 equivalents (relative to the norbornene functionalities) DTT were added to realize an equimolar ratio between the thiols and the norbornene functionalities.

Laser scanning microscopy (LSM 700, Carl Zeiss) and post-production swelling assessment were performed as reported in chapter 2. The surface area of the top of the structures, which is not constrained in swelling was compared to the applied CAD design, after 24 h incubation in PBS buffer. From these results, also the linear swelling of the cubes was calculated being the one- dimensional swelling of the structure relative to the CAD design following the following formula with L_{MAX} & L_{CAD} being the calculated length of the cube calculated from the surface of the structure and CAD design respectively and A_{MAX} being the measured top surface area and A_{CAD} the surface area according to the applied CAD design i.e. 100 µm * 100 µm.

$$linear\ swelling = \frac{L_{max}}{L_{CAD}} = \frac{\sqrt{A_{max}}}{\sqrt{A_{max}}} \quad (26)$$

7.3.10.6. Applied Cell Line and in vitro Biological Assays

L929 mouse fibroblasts were obtained from Sigma. Cell culturing occurred in Dulbecco's modified Eagle's medium (DMEM) with 4500 mg/L glucose, L-glutamine, sodium bicarbonate, sodium pyruvate (Sigma) and supplemented with 10% fetal bovine serum (Sigma) and 1% of 10000 U/ml penicillin/streptomycin (Lonza) in an incubator at 37°C in a humid atmosphere containing 5 % carbon dioxide. Fresh cell medium was introduced every other day.

Presto Blue Metabolic Activity Assay

The metabolic activity assay was performed similar as reported in chapter 2. Cell seeding occurred by pipetting 50 µL medium containing 20,000 L929 cells onto the coated slides. After 30 min of settling time, 1 ml medium was added which was replaced every other day. After 1, 2, 3 and 7 days, the metabolic activity was assessed using a resazurin-based Presto Blue Cell Viability test (Life technologies). The metabolic activity of the different samples was compared using tissue culture plastic (TCP) as a positive and a 50/50 DMSO/culture medium as a negative control. For normalization purposes, the fluorescence of the positive control after 7 days was considered to correspond with a viability of 100%.

Cell Seeding and Live/Dead Staining Assay on Cell-Seeded Micro-Scaffolds

A similar seeding protocol was applied as reported for the metabolic activity tests, as multiple micro-scaffolds were printed into a methacrylated micro-well

(35mm IBIDI µ-dish). To this end, after development of the structures, all PBS was aspirated from the samples, and 50 µL medium containing 20 000 L929 cells was seeded on top of the structure. After 30 min settling time, 3 ml medium was added which was replaced every other day. After 2 or 7 days, a live/dead staining (Molecular Probes, Life Technology) was performed. To this end, the culture medium was removed and the samples were rinsed three times with PBS followed by adding the staining solution containing 0.2 µ*M* calcein AM and 0.6 µ*M* propidium iodide. After 20 min incubation at 37 °C, the samples were again washed three times with PBS and imaged using the LSM with the excitation/emission filter set at 488/530 nm to visualize the living cells (green) and 530/580 nm to observe dead cells (red) [235,292].

7.3.10.7. Photo-Grafting Experiments

Single-Photon Photo-Grafting

Gel-MOD (DS 63%) and Gel-NB/DTT (DS 63%) films were crosslinked at 10 w/v% via film casting in the presence of 2 mol% Irgacure 2959 and at a 0.5 thiol/ene ratio for the gel-NB hydrogels via UV-A irradiation (365 nm 8 mW/cm²) for 30 minutes. Next, they were allowed to reach equilibrium swelling via incubation in DDW for 48 hours at 37°C. Next, samples with a diameter of 8 mm were punched from the sheets, frozen, and dehydrated via freeze-drying. After freeze-drying, each sample was placed in a well from a 96 well plate. Next, the samples were split up into four experimental conditions:

Condition 1: 750 µL of a solution containing 10 mmolar of 7-mercapto-4-methylcoumarin was added to wells containing gel-NB samples; in the dark. Next, the samples were shielded from light and placed in an incubator at 37°C. After 2 hours of incubation, the solvent was removed, and the samples were exposed to UV-A irradiation for 30 min (i.e. 365 nm, 8 mW/cm²). Finally, the samples were shielded from light and washed 3 times with DMSO to remove unbound 7-mercapto-4-methylcoumarin for 1 hour each at 37°C followed by 3 times washing with DDW and incubated at 37°C overnight to remove residual DMSO.

Condition 2: Control: This experiment is equal to condition 1, however they were incubated in 750 µL of DMSO in the absence of the dye in the first step.

Condition 3: gel-MA control: This experiment is equal to condition 1, however instead of gel-NB samples, crosslinked gel-MOD samples were applied.

Condition 4: dark control: This experiment is equal to condition 1, however the samples were kept in the dark and not irradiated using UV-A light.

Multi-photon Photo-Grafting

Gel-NB hydrogel pellets were generated in a similar way as the sample preparation for 2PP experiments. In Brief, 60 µL of a 10 w/v% solution of gel-NB/DTT at a thiol/ene ratio of 0.5 in the presence of 2 mol% Irgacure 2959 was pipetted into a silicone mold (d = 6 mm, h = 0.5 mm) placed in a methacrylated glass bottom dish (IBIDI) followed by sealing with a microscope cover slip to prevent sample drying. Next, the sample was irradiated using UV-A irradiation for 10 min (365 nm, 25 mW/cm²). After crosslinking, the sample was incubated in DMSO at 40°C for 24 hours to dissolve uncrosslinked material. Next, the DMSO was removed and replaced with a 10 mmolar solution of 7-mercapto-4-methylcoumarin and incubated in the dark for at least 1 hour at 40°C to allow complete penetration of the hydrogel with the coumarin dye. Next, the sample was mounted on the 2PP device using the same optics as for the 2PP processing experiments (i.e. 32X 0.85 NA objective) and atomiums were structured with a height of 210 µm at a slicing distance of 1 µm and a hatching distance of 0.5 µm at different scanning speeds (i.e. 25 to 150 mm/s with a 25 mm/s increment) and different laser powers (i.e. 50 to 200 mW with a 50 mW increment).

As a negative control, samples were subjected in parallel to the same protocol in the absence of the 7-mercapto-4-methylcoumarin dye.

Success of the grafting was visualised using Fluorescence microscopy with a 10X objective and a 1X tube lens. To this end, the samples were excited by irradiation at 340 nm and the fluorescence was detected at 350 nm using an Andor 897 (X-2726) detector at an exposure time of 32 ms. Images were generated using FEO Live acquisition software. The obtained images were processed using ImageJ software.

7.3.10.8. *Gel Permeation Chromatography*

GPC was performed in PBS buffer on a setup using a Millipore-Waters 510 pump and Waters 410 Differential Refractometer for detection in combination with Waters Ultrahydrogel columns 250-500 (300 mm * 7.8 mm) at 50°C to prevent physical gelation. Phosphate buffer (0.2 molar, pH 7.4) was applied as an eluent with a flow rate of 1 ml/min. Gelatin samples were prepared by dissolving 20 mg in 2 ml of buffer followed by filtering (0.22 µm) and injection

(20 µL) into the system. For molecular weight calibration pullulan standards with different molecular weights were applied (i.e. 9890; 21400 and 276500 g/mol) and a calibration curve was obtained (R^2 = 0.99).

7.3.11. Applied Methods in Chapter 4

7.3.11.1. Preparation of Gelatin Films via Film casting

To determine the swelling ratio and gel fraction of hydrogel films, they were first processed into thin films using a film casting approach. To this end 10 w/v% solutions of gel-NB or gel-MOD were prepared using PBS as a solvent at 40°C. In this respect, the total gelatin concentration was always set at 10 w/v% meaning that for the gel-NB-gel-SH hydrogels, the total amount of gelatin was 10 w/v% with a 1:1 thiol:ene ratio. After complete dissolution, either 2 mol% (relative to the number of norbornene or methacrylate functionalities present in the mixture) of Irgacure 2959 or LAP was added to the solution. Finally, the respective thiolated crosslinker was added to the solution in a 1:1 thiol:ene ratio. Next, the heated solution was injected in between two parallel glass plates coated with Teflon release foil and separated by a 1 mm thick silicon spacer. Next, the plates were either exposed to UV-A (at 365nm and a power density of 8 mW/cm²) from both sides during 30 min (i.e. corresponding to a total dose of 14400 J/cm²) either immediately after casting or after first storing them 4°C for 1 h to induce physical gelation prior to crosslinking. Following irradiation, 3 samples (d = 8 mm) were removed from the film to analyse gel fraction while the remaining part of the films were incubated in 20 ml DDW at 37°C for 48 hours to study equilibrium swelling.

7.3.11.2. Gel-fraction and Swelling-Ratio Determination

The gel fraction and swelling ratio determination were performed analogously as for chapter 2.

7.3.11.3. Rheological analysis

All rheological measurements were performed as reported in chapter 3.

7.3.11.4. In vitro Biological Experiments

Cell Culture

For the cell experiments, a hTERT immortalized human adipose-derived stem cell ASC/TERT1 (Evercyte GmbH, Austria) was used which was transfected with green fluorescent protein (GFP) to obtain permanently transfected green labelled cells according to a previously reported protocol[397]. Cells were cultured at 5% CO_2 at 37°C in EGM-2 medium (Lonza) supplemented with 10% fetal bovine serum (Gibco). Cells were detached with 0.5% Trypsin-EDTA upon 90% confluency.

Cell Encapsulation Experiments

For cell encapsulation experiments, passage 17 GFP labelled adipose tissue derived stem cells (ASC-GFPs) were encapsulated in 7.5 w/v% of the different thiol-ene formulations, in the presence of 2 mol% LAP (relative to the number of crosslinkable functionalities) and an equimolar thiol:ene ratio. To this end, first 600 µl of each gelatin formulation was prepared at 10 w/v% in PBS the presence of the photoinitiator (PI) and thiolated crosslinker. After complete dissolution, the samples were diluted with 200 µL of a stock solution containing 2 million cells/ml as counted using a Neubauer chamber resulting in a final cell density of 500 000 cells/ml. From the obtained solution, 3 pellets of 30 µl were pipetted in a methacrylated glass bottom dish (IBIDI) [336] followed by 10 minutes of UV-A irradiation (365 nm, 25 mW/cm² corresponding to 15 000 J/cm²). After crosslinking, the samples were incubated in appropriate cell culture medium and were maintained at 37°C in an incubator (high humidity, 5% CO_2). At different time points, the metabolic activity of the cells was measured using a Presto Blue assay and the cellular morphology was monitored using LSM. The medium was replaced every other day.

Presto Blue Metabolic Activity Assay

After 1, 2, 4 and 8 days, the metabolic activity was assessed using a resazurin-based Presto Blue Cell Viability test (Life technologies) according to the manufacturer's protocol. In brief, the Presto Blue reagent was diluted with cell culture medium (1:10). Next, 500 µL of the solution was pipetted to each sample followed by a 1 h incubation period. In viable cells, the blue colored resazurin is reduced to the pink colored resorufin which allows for

fluorescence detection of the product. From each IBIDI dish, 100 µL solution was pipetted into a 96-well plate for measurement. The remaining medium was replaced by fresh medium followed by incubation at 37°C for further culture. The fluorescence was measured with a plate reader (Synergy Bio-Tek, excitation 560 nm, emission 590 nm). After subtraction of the sample blank (diluted Presto Blue for 1h in medium without cells), the metabolic activity of the different samples was compared using tissue culture plastic (TCP) as a positive and a 50/50 DMSO/culture medium as a negative control.

Dark Toxicity Screening

To assess the cytotoxicity of the components of the different gel-NB formulations, a dark toxicity assay was performed. To this end, a 96 well plate was seeded with 100 µL of a stock solution containing 2 million cells/ml of passage 17 ASC-GFPs which were cultured for 24 hours in appropriate medium to obtain confluency. Next, these well plates were exposed to solutions (100 µL) containing the required concentrations of the crosslinkers used to formulate 10 , 7.5 and 5 w/v% gelatin solutions for a duration of 2 hours, which is typically around the maximum time the cells will be exposed to these uncrosslinked components during a 2PP structuring process. After 2 hours of contact, the solution containing the potentially cytotoxic component was replaced by appropriate medium and the cells were incubated for 24 hours at 37°C. After 24 hours of incubation, the metabolic activity of the different conditions was assessed and normalised to confluent cells cultured on tissue culture plastic (set as 100 %). As a negative control, the cells were exposed to a 50/50 DMSO cell medium solution for 2 hours. All experiments were performed in six-fold.

7.3.11.5. Two-Photon Polymerization Processing

2PP processing

Two-photon polymerization experiments were performed on a previously reported in-house developed set-up [336]. More specifically, a water immersion objective (C-Achroplan 32×, NA = 0.85, water immersion, Zeiss) was used in combination with a femtosecond pulsed NIR laser (800 nm) with 70 fs pulse duration. The scan speed was set at 100 mm/s for all samples. The CAD design was sliced with a layer spacing of 1 µm and hatched with 0.5 µm line spacing. In every layer, the focal spot was scanned in both the x- and y-directions for all samples. Average laser powers varying from 1 to 100 mW

with a 1 mW increment for 1 to 10 mW and a 10 mW increment from 10 mW onwards were applied in 10 w/v % (total gelatin concentration) hydrogel precursor solutions using PBS as solvent in the presence of 2 mol % Sodium 3,3'-((((1E,1'E)-(2-oxocyclopentane-1,3-diylidene) bis (methanylylidene))bis(4,2-phenylene))bis(methylazanediyl))dipropanoate (P2CK) as two-photon photo-initiator (relative to the amount of double bonds present) and the respective thiolated crosslinker in a 1:1 thiol:ene ratio[232]. To prevent sample drying, approximately 50 µL of each solution was pipetted into a micro-well (µ-Dish 35 mm, Ibidi) consisting of two glass plates separated by a silicone spacer with a diameter of 6 mm and a thickness of 1 mm. The bottom plate was silanized using 3-(trimethoxysilyl)propyl methacrylate to enable sufficient attachment of the generated structures during sample development[336]. For sample development, 2 mL PBS was added followed by storage in an incubator at 37 °C for at least 24 h to allow dissolution of uncrosslinked material while inducing equilibrium swelling of the microstructures.

Laser scanning microscopy (LSM 700, Carl Zeiss) and post-production swelling assessment of the obtained microstructures was performed as previously reported[336][284]. For each hydrogel precursor concentration, an array of twenty cubes was structured (each 100 µm × 100 µm × 100 µm). Laser scanning microscopy (LSM 700, Carl Zeiss) images using the same objective as for 2PP processing were applied for analysis of the produced structures. The surface area of the top of the structures, which is not constrained in swelling was compared to the applied CAD design, after 24 h incubation in PBS buffer. To this end, the surface of the top of the cubes was measured as well as the maximum swelling, of the structures as measured from Z stack composite images. From these measurements, the volumetric (i.e. 3D) swelling was calculated by taking the square root of the measured surface area resulting in linear swelling followed by taking the third power of this value to obtain swelling in all 3 dimensions as described in the following equation. With A_{max} (in µm²) being the measured maximum surface area and A_{CAD} (in µm²) being the surface area according to the CAD model (i.e. 100 µm x 100 µm) and V_{max} and V_{CAD} being the corresponding calculated volumes.

$$volumetric\ swelling = \frac{V_{max}}{V_{CAD}} = \frac{(\sqrt{A_{max}})^3}{(\sqrt{A_{CAD}})^3} \quad (27)$$

2PP Photo-Cleaving

To assess potential cleaving of the hydrogels under the influence of two-photon absorption, an assay was performed to assess the influence of laser dose on potential cleavage similar to a previously reported assay [217]. To this end, a gel-NB hydrogel was crosslinked inside a methacrylated IBIDI dish in the same spacer as applied in the 2PP experiments using 2 mol% LAP in the presence of DTT in an equimolar thiol:ene ratio by using UV-A (365 nm, 25 mW/cm^2) irradiation for 30 min. Next, the sample was equilibrium swollen in PBS and cut in half using a scalpel to have a clear edge. Next, “channels” (350 x 30 x 100 µm) were structured using the same setup as for the 2PP structuring of the material spanning over this “edge” by scanning both in X and Y direction with a hatch distance of 0.5 µm and Z distance of 1 µm. To this end, an array was structured with varying scanning speed of 25 – 150 mm/s with a 25 mm/s increment and varying laser powers of 50 to 200 mW with a 50 mW increment. Next, the sample was incubated at 37°C for 24 hours to remove any cleaved material. Finally, the samples were incubated in a solution containing FITC-dextran with a molecular weight of 2000 kg/mol at a concentration of 0.1mg/ml. Since the FITC-dextran has a high molecular weight, it will only be able to penetrate the channels and not diffuse into the hydrogel matrix, allowing for visualisation of the channels if they are truly cleaved. Next, the samples were imaged using both optical microscopy and LSM microscopy, as cleaving of the network will result in a less crosslinked network, characterised by a difference in refractive index, making it visible using optical microscopy, whereas the LSM can indicate if indeed channels are formed as a consequence of complete decrosslinking of the material or partial decrosslinking resulting in localised increased swelling.

7.3.12. Applied Methods in Chapter 5

7.3.12.1. Gel Permeation Chromatography

GPC was performed on the PDLLA polyesters to determine the number average molecular weight (Mn), weight average molecular weight (Mw) and polydispersity index (PDI). The measurements were performed on a Waters Alliance 2695 set-up (Zellik, Belgium) coupled to an Agilent (Diegem, Belgium) guard column (PLGel 5 µm) and a mixed-D LS polystyrene-divinylbenzene (300 * 7.5 *5 µm) column from Polymer Laboratories (Middelburg, The Netherlands). Detection was based on a Waters refractive

index detector 2414. The molecular weights were determined from the obtained retention times via an external calibration curve using polystyrene standards (1.2 - 177 kg mol^{-1}). As eluent, HPLC grade chloroform at a flow rate of 1 ml min^{-1} was applied.

Samples were prepared by dissolving 10 mg of polymer in 2 ml HPLC grade chloroform. The resulting solutions were passed through a 0.45 µm syringe filter, transferred to a mass vial and subsequently analysed. Furthermore, a correction factor of 0.58 was applied to the results to compensate for the difference in hydrodynamic volume between the polystyrene standards and the PDLLA [398].

7.3.12.2. Membrane Production

Membranes were produced by a multistep spincoating process in the following order: (i) Gelatin A, (ii) PDLLA and (iii) cross-linkable Gelatin B derivatives, with the specific parameters mentioned in table 1. After the PDLLA layer was deposited, the samples were subjected to a 0.8 mbar Argon plasma treatment for 30 seconds with a Diener electronic plasma treatment device to enable a better compatibility and covalent attachment of the gelatin derivatives to the PDLLA after crosslinking[57,69]. Finally, crosslinking of the gelatin B derivatives was performed by hydrating the coated gelatin layer with 60 or 250 µL of DDW (for respectively samples with a diameter of 12 and 25 mm) and irradiating the samples for 10 min from top and bottom with UV-A light at a wavelength of 365 nm with anof 8 mW/cm^2 using a high performance ultraviolet transilluminator (Ultra Violet Products).

Table VII.12 Overview of applied spincoating parameters for membrane production.

#	Type		Concentration	Spincoating Parameter (Acceleration in RPM/S²) Speed (RPM)	Photoinitiator	Crosslinker	Volume 12 mm ø	Volume 25 mm ø
1	Gelatin A		10 w/v% (in DDW)	750 RPM/s² (2000 RPM for 60 s)	/	/		
2	PDLLA		4 w/w% (in THF)	1000 RPM/s² (3000 RPM for 60 s)	/	/		
3	Gelatin B	gel-MOD	10 w/v% (in PBS)	750 RPM/s² (2000 RPM for 60 s)	Irgacure 2969 2 mol%	/	60 µL	250 µL
		Gel-MOD-AEMA	10 w/v% (in PBS)			/		
		Gel-NB	10 w/v% (in PBS)			DTT (1 to 1 thiol/ene ratio)		

7.3.12.3. Membrane Characterization

X-ray Photoelectron Spectroscopy

X-ray photoelectron spectroscopy (XPS) measurements were performed on four random locations of the measured samples in duplicate for elemental analysis of the spincoated layers. An ESCA S-probe VG monochromatic spectrometer with an Al Kα X-ray source (1486 eV) was used to measure a spot size of 250 µm by 1000 µm, which was analyzed using the Casa XPS software package.

Static Contact Angle Determination

Static contact angles of the produced membranes were determined using an OCA 20 device using the software provided by the supplier (i.e. SCA 20, version 2.1.5 build 16). A 1 µL droplet of DDW was used to determine the contact angles. The contact angle for each sample was determined as the average during the first 30 seconds. All measurements were performed in triplicate.

Determining the Membrane Transparency

Transparency of the membranes coated on glass plates was measured using a custom-made set-up consisting of a broadband halogen light source (Avantes Avalight-Hal) which was guided towards the sample holder using an optical fiber. The transmitted light was transferred to a broadband spectrum analyzer (Avantes Avaspec – 2048). In this way, transmission at all wavelengths was measured simultaneously after performing a baseline correction. Furthermore, during the measurement, the sample holder was covered with a black case to remove the influence of stray light. Transmission of all coated glass slides was compared relative to a glass slide with a gelatin A coating. For the hydrated samples, a droplet of deionized water (300 µL) was placed on each sample, and they were allowed to reach equilibrium swelling during 90 min prior to the measurement.

Determining the Membrane Thickness

The thickness of the membranes was determined with the use of a BRUKER Contour GT-I white light interferometric 3D surface metrology optical

microscope. Samples were scratched with metal forceps to expose the multiple layers. The thickness was then measured from the glass to the top of the coating using depth profilometry.

Determining the Membrane Diffusion Capabilities

Glucose diffusion was evaluated by placing a membrane in a side-by-side diffusion set up. To this end, a 10 w/v% glucose solution in double distilled water was prepared with 0.5 w/v% sodium azide added to prevent growth of micro-organisms. The setup consists of 2 diffusion cells, where each diffusion cell is supplied with a stirring bar and kept at a constant temperature of 37°C. The produced membranes were clamped between the diffusion cells. One of the two diffusion cells is filled with 2.5 ml of the previously prepared glucose solution, termed the donor cell. The other diffusion cell is filled with 2.5 ml of double distilled water, which is the acceptor cell. The acceptor cell is periodically emptied inside a mass tube and then refilled with 2.5 ml double distilled water. The collected fractions of the acceptor cell are then diluted 100 times and analysed using a glucose oxidase assay. The apparent permeability constant (P_{app}) was calculated according to the following equation.[365]

$$P_{app} = \frac{\frac{dC}{dt}}{(A * C_0)} \quad (28)$$

Where $\frac{dC}{dt}$ is the change in concentration over time as determined by the linear regression of the measurements at different time points. (mol/s)

A is the exposed surface of the membrane (cm^2) (i.e. 0.79 cm^2)

C_0 is the initial glucose concentration (mol/cm^3) (i.e. 0.55 * 10^{-3} mol/cm^3)

7.3.12.4. Biological Assays

Glass coverslips coated with the gelatin B derivatives were used in order to test the interaction between gelatin and endothelial cells without the sacrificial gelatin A layer or the PDLLA. The glass coverslips were first methacrylated to ensure covalent attachment between the gelatin derivatives and the glass coverslips.

To this end, they were cleaned with DDW, acetone and subjected to a 3-minute argon plasma treatment. Following this, they were incubated in a

mixture containing 50 ml DDW, 48 ml ethanol, 0.3 ml acetic acid and 2 ml 3-(trimethoxysilyl) propyl methacrylate for 30 min followed by thorough rinsing with DDW.

In brief, the spincoated samples on glass coverslips (diameter 12 mm) were secured into a 24 well tissue culture plate using the cellcrown insert (Scaffdex, Tampere, Finland).

To sterilize the samples, they were incubated in a range from 30 % - 70% ethanol solution with a 10% increment every 30 min. They were stored overnight in a 70% solution, and irradiated with UV-C for 30 min. Next, they were rinsed with sterile PBS (3X) and exposed to UV-C irradiation for another 30 min prior to use.

Cell Culture

B4G12 immortalized corneal endothelial cells (DSMZ, Braunschweig, Germany) were cultured according to the manufacturer's instructions with minor modifications. In brief, the cells were grown on tissue culture treated plastic ware, coated with an FNC coating mix (Athena Enzyme systems, Baltimore, USA). The growth medium consisted of human endothelial serum free medium (Life Technologies) supplemented with 10 ng/mL basic fibroblast growth factor (Life Technologies) without antibiotics. B4G12 cells were detached using 0.05% Trypsin-EDTA (Life Technologies) and subcultured or seeded according to the downstream assay.

Immunocytochemistry

Corneal endothelial cells were cultured on glass coverslips coated with gel-MOD-AEMA, gel-MOD DS63, gel-MOD DS95, gel-NB DS63. After 7 days in culture, the samples were fixated in ice cold paraformaldehyde 4% for 30 minutes, rinsed three times in PBS 1X (Life Technologies) and stained within one week. The samples were permeabilized with PBS1X containing 1% Triton X-100 for 30 minutes and incubated overnight with a primary antibody raised against ZO-1 (1:200; Thermo Fisher Scientific, Massachusetts, USA) or Na^+/K^+ ATPase (1:40; Santa Cruz Biotechnology, Texas, USA) for phenotyping. The secondary antibody (goat anti-mouse FITC 1:500; Jackson Immunoresearch, West Grove, USA) was incubated for 2 hours at room temperature in the dark, followed by a nuclear stain with 100 µg/mL 4′,6-diamidino-2-phenylindole (DAPI) (Sigma, St. Louis, USA) and mounted using Citifluor to reduce fading (Citifluor, Hatfield, USA). Images were captured

using an UltraView VOX laser spinning disk confocal microscope (Perkin Elmer, Massachusetts, USA) at 20 times magnification and processed using ImageJ.

For the adhesion assay, samples seeded with 25,000 cells for 24 hours were subjected to a similar protocol with primary anti-vinculin antibodies (1:200, Abcam, Cambridge, United Kingdom) and secondary goat anti-mouse PE conjugated antibodies. Images were processed according to a previous published protocol.[45] Both primary and secondary antibodies were diluted in 0.01 M PBS containing 0.5% Thimerosal, 0.1% NaN_3, 10% normal horse serum and 0.3% bovine serum albumin.

Proliferation Assay

A proliferation assay was performed in the Incucyte (Sartorius, Göttingen, Germany), a high-throughput live-cell imaging system. B4G12 cells were seeded with a density of 30,000 cells per well and incubated for 4 hours (37°C, 5% CO2) until adherent. Next, the nuclei were counterstained with NucLight Rapid Red Reagent 1:2000 (Sartorius, Göttingen, Germany) and imaged every 2 hours (see video 1 in supporting information). Using the built-in software, custom masking algorithms were generated to quantify cellular growth expressed as #nuclei/mm^2 as a function of time. Growth curves were fitted using Graphpad Prism 8.0 using an exponential growth fitting curve model and population doubling times (PDT) were extracted. PDT were then statistically compared to each other using a non-parametric Kruskal-Wallis test where $p<0.05$ was deemed significant.

Chapter 8:
Nederlandstalige Samenvatting

8.1. Inleiding

Het doel van het huidige doctoraat bestond uit de ontwikkeling van nieuwe hydrogelbouwstenen voor toepassingen in de (oculaire) regeneratieve geneeskunde. In dit opzicht kan het onderzoek worden onderverdeeld in twee grote luiken. In het eerste luik lag de nadruk op het verbeteren van de laser-gebaseerde verwerkbaarheid van gelatine-gebaseerde hydrogelen met het behoud van hun biologische compatibiliteit en cel-interactiviteit. In het tweede luik werden de ontwikkelde hydrogel-formulaties aangewend voor onderzoek naar de ontwikkeling van functionele membranen voor oculaire toepassingen en meer specifiek, voor de ontwikkeling van artificiële Descemet's membranen om de binnenste laag van het hoornvlies te regenereren, namelijk het endotheel.

8.2. Verbeteren van de verwerkbaarheid van gelatine gebaseerde hydrogelen in laser-gebaseerde 3D print processen

In het eerste luik van dit werk werd onderzoek gedaan naar geschikte extracellulaire matrix (ECM) analogen. Hiervoor werd gelatine gekozen als basismateriaal omdat het afgeleid is van collageen, het hoofdbestanddeel van de natuurlijke extracellulaire matrix in het hoornvlies (i.e. collageen type IV in het natuurlijke Descemet's membraan) en in het menselijk lichaam in het algemeen [21][102]. Hierdoor vertoont gelatine sterke structurele gelijkenissen met de natuurlijke ECM. Zo is gelatine onder andere cel-interactief door de aanwezigheid van RGD-sequenties die kunnen binden met de aanwezige integrines op het celmembraan [110]. Het wordt echter gekenmerkt door een dissociatietemperatuur (Td) rond 30 ° C waardoor het in oplossing kan gaan bij verhoogde temperatuur terwijl er een fysische gel zal ontstaan onder deze dissociatietemperatuur. Bijgevolg is het onstabiel bij fysiologische condities (i.e. 37 ° C), waarbij het zal oplossen. Dit ongewenste gedrag kan omzeild worden door het materiaal covalent te vernetten. De meest gangbare strategie om gelatine te vernetten bestaat uit de modificatie van de primaire amines die aanwezig zijn in de zijketens van de (hydroxy)lysine en ornithine aminozuren in gelatine met methacrylzuuranhydride. Hierdoor worden (foto-)vernetbare methacryloyl-functionaliteiten geïntroduceerd waardoor gemodificeerd gelatine of kortweg gel-MOD verkregen wordt [121,125]. Dit derivaat kan beschouwd worden als een

van de gouden standaarden in de wereld van 3D-print gebaseerde regeneratieve geneeskunde en weefselregeneratie. Daarnaast laat dit materiaal ook verwerking via twee-foton polymerisatie (2PP) toe [125,126,129]. Daarom werd gel-MOD doorheen dit doctoraatswerk als referentiemateriaal toegepast voor nieuw ontwikkelde gelatine derivaten. Ondanks de succesvol gerapporteerde 2PP-verwerking van gel-MOD, zijn gewoonlijk hoge concentraties (d.w.z.> 15 gew.% [129]) en hoge gemiddelde laservermogens (d.w.z. 330 mW bij 7 mm / s [129]) vereist om acceptabele structurele integriteit te verzekeren. Bijgevolg is er duidelijk nog ruimte voor verbetering.

In een eerste poging om de laser-gebaseerde verwerkbaarheid van gel-MOD te verbeteren, werden extra vernetbare groepen (i.e. methacrylaten) geïntroduceerd via de reactie van de carbonzuren in de zijketens van de glutaminezuur en asparaginezuur aminozuren aanwezig in gelatine met 2-aminoethylmethacrylaat (AEMA) via conventionele carbodiimide koppelingschemie. Hiertoe werden eerst alle primaire amines in gelatine B gemethacryleerd tot gel-MOD met een substitutiegraad (DS) van ± 95%, waardoor ongewenste vernetting tussen de primaire amines en de carbonzuren aanwezig in gelatine vermeden wordt. Het gel-MOD startmateriaal (DS 95%) werd ook gebruikt als referentiemateriaal om de materiaaleigenschappen en verwerkingscapaciteiten van het nieuwe derivaat (gel-MOD-AEMA) dat we ontwikkeld hebben te beoordelen. Tijdens de chemische modificatie werd aangetoond dat de substitutiegraad (DS) van de carbonzuren beïnvloed kan worden door de gel-MOD concentratie in het reactiemengsel te variëren. Zo resulteerden mengsels met gel-MOD concentraties van respectievelijk 10, 5 en 2.5 w/v% in een DS van ongeveer ± 35, ± 45 en ± 55% . Gezien het doel van deze extra modificatie erin bestond om de mechanische eigenschappen en de verwerkbaarheid via 2PP te verbeteren, werden alle verdere experimenten uitgevoerd met gel-MOD-AEMA met de hoogste DS (55%). Na de modificatie werden vergelijkbare moleculaire massa's bekomen voor zowel gel-MOD als gel-MOD-AEMA, wat aangeeft dat de extra modificatie niet leidt tot ongewenste hydrolyse. Desondanks nam het aantal vernetbare groepen op gelatine toe met een factor 2,7 (zie Tabel VIII.12). Bovendien vertoont gel-MOD-AEMA een snellere reactie kinetiek en worden stijvere hydrogelen bekomen (zie Tabel VIII.12). Verder werden aanzienlijk lagere post-vernetting zwellingsgraden bekomen voor gel-MOD-AEMA (i.e. een 1,6 - 1,9-voudige afname ten opzichte van gel-MOD) terwijl het een vergelijkbare biocompatibiliteit vertoont. Hiernaast bleek gel-MOD-AEMA oplosbaar bij kamertemperatuur (beneden de T_d) als gevolg van de introductie van extra zijgroepen die het tripel helix vormingsproces, dat verantwoordelijk is voor de fysische gel-

vorming, verstoren [138]. Bijgevolg ontstaat de mogelijkheid om gel-MOD-AEMA te verwerken via 3D-print technieken waarbij vloeibare (pre)polymeermatrixe essentieel zijn (i.e. Digital light projection (DLP), stereolithografie (SLA), inkt jet) [138].

Het grootste voordeel van het gel-MOD-AEMA-derivaat manifesteert zich echter tijdens 2PP-verwerking. Niet alleen resulteert de verbeterde reactiekinetiek in een groter 2PP-verwerkingsbereik (i.e. > 40 mW versus > 60 mW bij 15 w/v% en > 50 mW versus > 80 mW bij 10 w/v% bij een scansnelheid van 100 mm/s) maar treedt er ook zo goed als geen post-productie zwelling op bij het gel-MOD-AEMA derivaat door de aanwezigheid van een denser netwerk. Voor zover wij weten is dit bijgevolg het eerste cel-interactieve hydrogel-systeem dat een echte replicatie van het aangewende design toelaat. Dit werd gereflecteerd door de mogelijkheid om structuren met extreem kleine details (van 1 µm) succesvol te reproduceren. Hiernaast zorgt de oplosbaarheid bij kamertemperatuur ervoor dat het materiaal gebruikt kan worden voor zogenaamde 'meso'-schaal 2PP waarbij het objectief wordt ondergedompeld in de polymeermatrix, waardoor grotere structuren geprint kunnen worden door het CAD-model op te splitsen in verschillende deelstructuren [299,323].

Hoewel reeds veelbelovende resultaten werden verkregen voor het gel-MOD-AEMA-derivaat, kan het dens netwerk een negatieve invloed hebben op de biocompatibiliteit van het materiaal bij cel-encapsulatie [252]. Bovendien ontstaan er bij vernetting van deze conventionele ketting-groei *hydrogelen* niet-degradeerbare (oligo)methacryloyl-ketens tussen de gelatineketens die problemen kunnen veroorzaken bij biodegradatie [146]. Om deze problemen te omzeilen, werd ook een ander type vernettingschemie (thiol-een foto-click chemie) toegepast dat gekenmerkt wordt door een verbeterde reactiekinetiek en de vorming van homogenere netwerken [162,167]. Hiertoe werden norborneen groepen geïntroduceerd op gelatine omdat deze de snelste reactiekinetiek van alle ‘-een’ functionaliteiten vertonen en hiernaast ook ongevoelig zijn voor concurrerende vernettingsreacties (i.e. homopolymerisatie en thiol-Michael addities) [167].

Tabel VIII.12: Vergelijking van de materiaaleigenschappen van gel-MOD en gel-MOD-AEMA hydrogelen.

Materiaal	DS_{NH2} (%)	DS_{COOH} (%)	# Dubbele Bindingen/g	Concentratie (w/v%)	Gel Punt (s)	Opslag Modulus (kPa)	Zwellings Ratio
gel-MOD	95		0.37	5		7.7 ± 1.7	18.5 ± 1.0
	95		0.37	10	47.2 ± 8.5	20.3 ± 3.5	10.1 ± 0.2
	95		0.37	15		31.8 ± 15	8.9 ± 0.1
gel-MOD-AEMA	95	55	0.99	5		7.1 ± 0.7	10.4 ± 2.2
	95	55	0.99	10	15.0 ± 5.2	49.8 ± 6.5	6.5 ± 0.2
	95	55	0.99	15		105.0 ± 33.8	4.7 ± 0.1

Voor verdere karakterisatie experimenten werd gel-NB met twee verschillende substitutiegraden ontwikkeld (nl. 63% & 89%) waarbij gel-MOD met een vergelijkbare DS (d.w.z. 63% & 95%) gebruikt werd als referentiemateriaal. Het belangrijkste verschil tussen de gel-NB en gel-MOD hydrogelen is de nood aan gethioleerde crosslinkers gezien de vernetting gebeurt via een stap-groei polymerisatie tussen complementaire functionaliteiten (nl. thiolen en "een"-functionaliteiten). In een eerste set karakterisatie experimenten werd gel-NB met een DS van 63% vernet door gebruik te maken van dithiothreitol (DTT) als gethioleerde crosslinker, welke dan vergeleken werd met gel-MOD met een DS van 63%. Het belangrijkste voordeel van het thiol/een-systeem is de aanzienlijk snellere reactiekinetiek welke gereflecteerd wordt door vergelijking van het gel-punt van 10 w/v % oplossingen (nl. 2,8 s versus 65,2 s). Ondanks de gunstigere reactiesnelheden werden echter lagere opslagmoduli verkregen voor de gel-NB hydrogelen (zie Tabel VIII.13). Dit is een gevolg van het orthogonale karakter van het thiol/een-systeem in combinatie met het gebruik van een bifunctionele vernetter. Hierdoor zullen telkens slechts twee norborneen groepen verbonden worden in elk netwerk-knooppunt, terwijl bij gel-MOD, meerdere methacryloyl-functionaliteiten deel zullen uitmaken van een netwerk-knooppunt door de vorming van oligo(methacryloyl) ketens waardoor stijvere gelen bekomen worden [146]. Bij lage gelatine-concentraties (5 w/v%) zijn de verschillen in stijfheid tussen gel-MOD en gel-NB/DTT echter niet significant omdat bij deze lage concentraties, de probabiliteit om meer dan twee methacryloyl-functionaliteiten in hetzelfde knooppunt te polymeriseren beperkt is. Hiernaast worden, ondanks het verschil in mechanische eigenschappen, vergelijkbare zwellingsgraden waargenomen voor de gel-NB en gel-MOD hydrogelen. Naast de voordeligere reactiekinetiek, vertonen de gel-NB hydrogelen nog een extra voordeel gezien ze controle over het aantal gereageerde functionaliteiten toelaten door de thiol/een-verhouding te variëren. Wanneer een thiol/een-verhouding van 1 gebruikt wordt, zullen alle functionaliteiten reageren, terwijl er bij lagere verhoudingen niet-gereageerde norborneen groepen aanwezig zullen blijven in het netwerk. Hierdoor kunnen de mechanische eigenschappen van de finale hydrogel gevarieerd worden, terwijl de aanwezigheid van niet-gereageerde "een"-functionaliteiten ook toelaat om deze te gebruiken voor thiol-een-fotografting [182]. Hierbij wordt een vernette hydrogel ondergedompeld in een oplossing welke een actieve gethioleerde component bevat. Door dit vervolgens enkel zeer lokaal te bestralen (hetzij met UV licht of een multiphoton NIR licht) zal deze component enkel op deze plaats ingebouwd worden, waardoor de hydrogel

zeer lokaal gemodificeerd kan worden. Naast deze voordelen vertonen de gel-NB/DTT en gel-MOD hydrogelen bovendien een vergelijkbare biocompatibiliteit na uitzaaien van cellen.
Het belangrijkste voordeel van de thiol/een systemen wordt echter duidelijk tijdens de verwerking via 2PP. Hieruit bleek namelijk dat zeer lage laser vermogens reeds aanleiding gaven tot een reproduceerbare vernetting (d.w.z. vanaf 4 – 5 mW gemiddeld vermogen). Hierdoor kunnen in theorie hogere schrijfsnelheden aangewend worden waardoor de gemiddelde printtijd drastisch verlaagd zou kunnen worden. In het huidige werk werden maximale schrijfsnelheden van 100 mm/s gebruikt vanwege mechanische limitaties in de gebruikte 2PP-opstelling. Echter ondertussen zijn er reeds experimenten gerapporteerd waarbij gel-NB/DTT-hydrogelen aan 1000 mm/s verwerkt werden door gebruik van een aangepaste opstelling (namelijk een 10X-objectief met een numerieke apertuur (NA) van 0,4 ipv 32X met NA van 0,85) [341]. Hiernaast vertoonde het gel-NB/DTT-systeem een ongekende efficiëntie op gebied van 2PP verwerking, daar voor de eerste keer ooit gelatine-gebaseerde hydrogelen op een reproduceerbare manier verwerkt konden worden onder de 10 w/v% concentratie. Tot slot liet de combinatie van 2PP en thiol/een verhoudingen kleiner dan 1 toe om een fluorescerende kleurstof in de hydrogelmatrix te verankeren met een hoge spatio-temporele controle in de drie dimensies. De mogelijke resoluties in dit opzicht zijn sterk afhankelijk van het gebruikte objectief (zie Tabel VIII. 14). Omdat de modificatie op reeds gezwollen hydrogel netwerken gebeurt, zullen de berekende voxel volumes zeer sterk overeenkomen met de uiteindelijke resolutie, gezien geen extra zwelling meer zal optreden na verwerking, in tegenstelling tot wat het geval zou zijn bij conventionele 2PP van gelatine hydrogelen.
Hoewel multi-foton grafting in het verleden reeds gerapporteerd werd, is het voor zover wij weten de eerste keer dat multi-foton thiol-een grafting succesvol toegepast werd [334]. Bijgevolg verwachten wij dat de combinatie van gel-NB en multifoton-lithografie het mogelijk maken om nog een betere kopie te genereren van de natuurlijke ECM via het graften van bio-functionele moleculen die ook aanwezig zijn in de natuurlijke ECM (bijv. laminine) omdat deze vaak reeds thiol-functionaliteiten bevatten [374].

Tabel VIII.13. Vergelijking tussen de materiaaleigenschappen van gel-MOD vs gel-NB/DTT hydrogelen.

Materiaal	DS_{NH2} (%)	Crosslinker	Thiol/Een Ratio	# Dubbele Bindingen/g	Concentratie (w/v%)	Gel Punt (s)	Opslag Modulus (kPa)	Zwellings Ratio
gel-MOD	63			0.24	5		9.0 ± 0.3	21.6 ± 0.7
	63			0.24	10	65.2 ± 8.5	36.83 ± 1.6	10.5 ± 0.3
	63			0.24	15		75.6 ± 4.3	8.4 ± 0.3
gel-NB	63	DTT	1	0.24	5		8.6 ± 0.2	17.5 ± 2.4
	63	DTT	1	0.24	10	2.8 ± 0.3	24.0 ± 0.7	10.5 ± 0.3
	63	DTT	1	0.24	15		29.8 ± 1.1	7.5 ± 0.2

Tabel VIII.14: Berekende maximale resoluties voor verschillende gebruikte objectieven.

Vergroting (X)	NA	brekingsindex	Voxel Lengte (µm)	Voxel Breedte (µm)	Gaussiaanse Benadering van het Voxel Volume (µm³)
2,5	0.075	1,35	288,68	4,83	23392,91
10	0,4	1,35	9.93	0,91	28,29
32	0,85	1,35	2	0,43	1,26
63	1,4	1,51	0,64	0,27	0,16
100	1,4	1,51	0,64	0,27	0,16

Hiernaast laten thiol-een systemen ook toe om de finale hydrogeleigenschappen nog beter te gaan controleren door het variëren van de gebruikte gethioleerde crosslinker. Om dit te onderzoeken, werden hydrogelen bereid uit gel-NB met een DS van 89% door gebruik te maken van verschillende gethioleerde crosslinkers (nl. gel-SH met een DS van 72%, DTT, TEG2SH, PEG2SH 3400, PEG4SH 10000 en PEG4SH 20000) in een thiol/een-verhouding van 1. Deze formulaties werden uitvoerig gekarakteriseerd waarbij opnieuw gel-MOD met een vergelijkbare DS (nl. 95%) als referentiemateriaal gehanteerd werd. Uit deze experimenten bleek dat crosslinkers met een hoge moleculaire massa (nl. PEG4SH 20000) aanleiding gaven tot ongewenste faseseparatie. Hiernaast werden geen significante verschillen waargenomen tussen de verschillende vernetters op gebied van reactiekinetiek. Er werd echter wel aangetoond dat door de juiste crosslinker te selecteren, de mechanische eigenschappen van gel-MOD benaderd (bij gebruik van gel-SH of PEG2SH 3400) of zelfs overstegen kunnen worden (bij gebruik van PEG4SH 10000). Verder werd ook aangetoond dat er een enorm verschil is indien de vernetting uitgevoerd wordt nadat het materiaal reeds in de fysische geltoestand is in vergelijking met wanneer er vernet wordt vanuit oplossing. Wanneer het materiaal vernet werd in gel-toestand, werden gewoonlijk stijvere gelen bekomen. Dit effect was het meest uitgesproken indien enkel gelatine-gebaseerde componenten gebruikt werden (nl. bij gel-MOD & gel-NB/gel-SH), en dit terwijl bij de PEG4SH-crosslinkers met een hoge moleculaire massa juist een afname in stijfheid bekomen werd als gevolg van faseseparatie gedurende het fysische geleringsproces. Dit fenomeen kan van groot belang zijn indien men de hydrogelen wil verwerken via depositie-gebaseerde 3D-print technieken waarbij fysische gelering dikwijls essentieel is voor de verwerkbaarheid Bovendien vertoonden alle geteste thiol-een formulaties een vergelijkbare biocompatibiliteit na 7 dagen voor geëncapsuleerde adipose weefsel afgeleide stamcellen (ASCs), wat aantoont dat de formulaties uitermate geschikt zijn als bio-inkt of bio-inkt component [349]. Hiernaast werd ook de toxiciteit van de verschillende componenten van de hydrogelsystemen nagegaan gedurende twee uur (dit is een realistische schatting van de typische duur van een printproces). Uit deze experimenten bleek dat de crosslinkers met laag moleculair gewicht (DTT en TEG2SH) aanleiding gaven tot een aanzienlijke cytotoxiciteit. We verwachten dat dit effect een gevolg is van celmembraanpenetratie door deze vernetters waarna deze kunnen interageren met gethioleerde moleculen binnen het cytoplasma. Ondanks het feit dat de verschillende formulaties een vergelijkbare biocompatibiliteit

vertoonden na vernetting, konden er toch significante verschillen waargenomen worden op het gebied van celmorfologie gedurende de cultuurperiode. In de zachtste formulaties (bekomen na vernetting met de crosslinkers met een lage moleculaire massa) werd een snellere toename van gemiddelde cel-lengte waargenomen als gevolg van een snellere modellering van de matrix [341]. Zoals verwacht resulteerde het gel-MOD-derivaat in de traagste matrix modellering vanwege de hoogste stijfheid. Bijgevolg laat variatie van de gebruikte crosslinker toe om het cellulaire gedrag, de mechanische eigenschappen en de zwellingscapaciteit van de hydrogel te sturen.
Wanneer de verschillende formulaties aangewend werden voor 2PP-verwerking werd duidelijk dat de verschillende thiol-een formulaties over een extreem lage polymerisatiedrempel beschikken (nl. 4 - 5 mW versus > 80 mW voor gel-MOD bij 100 mm/s). Ook hier werden duidelijke verschillen in zwellingsratio waargenomen tussen de verschillende formulaties waarbij de laagste zwellingsgraden verkregen werden voor het gel-NB/gel-SH-systeem. Dit is logisch gezien gel-SH over het grootst aantal thiolen (± 14) per crosslinker molecule beschikt. De hoogste zwellingsgraad werd verkregen voor de zeer hydrofiele bifunctionele PEG2SH crosslinker. Echter, naast deze verwachte effecten bleek ook dat de verschillende thiol-een formulaties gekenmerkt werden door een toename in zwellingsgraad bij toenemend gemiddeld laservermogen in plaats van het eerder waargenomen plateau als gevolg van de aanwezigheid van een volledig vernet netwerk. Een soortgelijk effect voor gel-NB/DTT systemen werd reeds gerapporteerd door Dobos *et al.* [341]. Voor zover wij weten is het echter de eerste keer dat de oorsprong van dit fenomeen werd besproken. Wij verwachten dat dit effect het gevolg is van een competitieve foto-splitsingsreactie van de hydrogelmatrix bij hoge laser vermogens. Om deze hypothese kracht bij te zetten werd een experiment uitgevoerd op een vernette hydrogel waarbij kanaalvorming optrad na bestraling met de laser. Hoewel dit effect in het algemeen ongewenst is, laat de gunstige reactiekinetiek van de thiol/een-systemen toe om het materiaal te vernetten bij aanzienlijk lagere laservermogens, met minima tussen 20 en 40 mW (bij een schrijfsnelheid van 100 mm/s). Bijgevolg zijn deze thiol-een formulaties ook geschikt voor verwerking met behulp van minder performante gepulseerde lasers. Hierdoor kunnen goedkopere 2PP systemen aangewend worden voor de verwerking van de hydrogelsystemen. Dit maakt de ontwikkelde systemen relevanter als bioinkt-componenten in meer economisch relevante multi-foton lithografiesystemen.

8.3. Ontwikkeling van functionele artificiële Descemet's membranen voor corneale endotheel regeneratie.

In het tweede deel van dit doctoraat werden de ontwikkelde gelatine-hydrogelformulaties toegepast voor de ontwikkeling van functionele artificiële Descemet's membranen voor regeneratieve toepassingen van het corneale endotheel. Om hun functie te kunnen uitvoeren dienen deze membranen te voldoen aan een reeks strikte vereisten. Ten eerste moeten ze voldoende dun zijn (het natuurlijke Descemet's membraan heeft een dikte van ongeveer 10 - 12 µm [362]). Verder is een transparantie van meer dan 90% over het gehele zichtbare spectrum wenselijk [45]. Hiernaast is het essentieel dat de membranen robuust genoeg zijn om chirurgische manipulatie toe te laten. Idealiter moeten ze gemanipuleerd kunnen worden op een analoge wijze als de momenteel toegepaste Descemet's stripping automated endothelial keratoplasty (DSAEK)- of Descemet's membrane endothelial keratoplasty (DMEK)-methode, waarbij ze worden opgerold in een canule om vervolgens ontrold te worden in de voorste kamer van het oog [358][354]. Om als een werkend endotheel te functioneren moet de combinatie van de cellen met het implantaat een lekkende barrière vormen om zo de hydratatie van het stroma te controleren. Hiertoe moeten de membranen voldoende glucose permeabiliteit mogelijk maken (het natuurlijke Descemet's membraan vertoont een glucose permeabiliteitscoëfficiënt van 1,2 * 10-5 cm / s [46]). Tenslotte moeten de membranen voldoende cel-interactief zijn en aanleiding geven tot het juiste fenotype [45].
Om aan al deze eisen te voldoen, werden covalent vernette gelatine-gebaseerde hydrogelen geselecteerd gezien de structurele gelijkenis met de natuurlijke ECM. Gezien gelatine een hydrogel is, is diffusie van kleine moleculen door het netwerk mogelijk zonder problemen [375]. Bovendien geeft gelatine aanleiding tot de vorming van peptiden en aminozuren bij degradatie, welke zeer analoog zijn aan de afbraakproducten van natuurlijk collageen in het oog. Gezien de geringe dikte van het implantaat (nl. <12 µm) zal enkel gelatine over onvoldoende structurele integriteit beschikken om chirurgische manipulatie mogelijk te maken. Daarom werd gekozen om dit te combineren met een tweede sterker materiaal. Hiertoe is gekozen voor het amorfe poly(D,L-lactic acid) PDLLA vanwege de hoge transparantie, biologische afbreekbaarheid en U.S. Food & Drug Administration (FDA)-goedkeuring voor klinische toepassingen[67]. Bovendien zullen bij afbraak van dit polyester, melkzuurmoleculen worden gevormd welke ook al van nature aanwezig zijn in het hoornvlies, waar 85% van de aanwezige glucose op natuurlijke wijze

wordt omgezet in lactaat. De aanwezigheid van dit lactaat levert zelf een positieve bijdrage aan de anionflux die een rol speelt bij het onderhouden van de transparantie van het cornea [49].
Om de benodigde dunne afmetingen te bekomen, werd gebruik gemaakt van een meerstaps spincoating proces waarbij achtereenvolgens het polyester en het vernetbaar gelatine aangebracht werden. Hiertoe werden vier verschillende gelatine formulaties aangewend, namelijk gel-MOD DS 63%, gel-MOD DS 95%, gel-MOD-AEMA en gel-NB/DTT met een DS van 63%. Alle membranen bleken te voldoen aan de vereisten op het gebied van dikte (t.t.z. alle membranen hadden een dikte beneden 1 µm), glucosediffusie (t.t.z. de membranen vertoonden glucose-permeabiliteitscoëfficiënten van 9,35 * 10^{-3} tot 1,52 * 10^{-2} cm/s) en transparantie (> 95% over het gehele zichtbare spectrum). Tenslotte vertoonden de endotheelcellen het juiste fenotype op alle membranen zonder dat er significante verschillen in proliferatie werden waargenomen tussen de verschillende gelatine formulaties en de positieve controle. Bovendien konden de membranen met behulp van scalpels en pincetten gemanipuleerd worden zonder te scheuren. Gezien er geen significante verschillen op gebied van biologische respons waarneembaar waren tussen de verschillende gelatine formulaties, kan voor verdere experimenten gebruik gemaakt worden van het derivaat dat aanleiding geeft tot de meest eenvoudige productie methode. Hiervoor is gel-MOD-AEMA de meest veelbelovende formulatie-component gezien het vergelijkbare mechanische eigenschappen vertoont als het natuurlijke Descemet's membraan terwijl de oplosbaarheid bij kamertemperatuur resulteert in een meer eenvoudige verwerking van het materiaal. Hiernaast werd ook de invloed van aanwezigheid van 2PP patronen op de cellulaire respons nagegaan. Er werd aangetoond dat de cellen de morfologie van de patronen volgden, maar daardoor hun karakteristieke hexagonale morfologie verliezen die nodig is voor de vorming van een functionele lekbarrière. Hierdoor werden deze membranen minder geschikt geacht voor cornea endotheel regeneratie.

Bibliography

[1] WHO, “Priority eye diseases,” **2015**.

[2] J. P. Whitcher, M. Srinivasan, M. P. Upadhyay, **2001**, *79*, 214.

[3] D. T. Tan, J. K. Dart, E. J. Holland, S. Kinoshita, *Lancet* **2012**, *379*, 1749.

[4] “WHO | Causes of blindness and visual impairment,” **2017**.

[5] R. Edgar, Y. Mazor, A. Rinon, J. Blumenthal, Y. Golan, E. Buzhor, I. Livnat, S. Ben-Ari, I. Lieder, A. Shitrit, et al., *PLoS One* **2013**, *8*, DOI 10.1371/journal.pone.0066629.

[6] F. A. Guarnieri, in *Corneal Biomech. Refract. Surg.*, Springer New York, New York, NY, **2015**, pp. 7–31.

[7] C. E. Ghezzi, J. Rnjak-Kovacina, D. L. Kaplan, *Tissue Eng. Part B Rev.* **2015**, *21*, 278.

[8] Eye Bank Association of America, *2015 Eye Banking Statistical Report*, **2016**.

[9] H. Elhalis, B. Azizi, U. V. Jurkunas, *Ocul Surf* **2010**, *8*, 173.

[10] A. Shah, J. Brugnano, S. Sun, A. Vase, E. Orwin, *Pediatr. Res.* **2008**, *63*, 535.

[11] I. The Lewin Group, *Cost-Benefit Analysis of Corneal Transplant Prepared for the Eye Bank Association of America*, **2013**.

[12] D. C. Musch, L. M. Niziol, J. D. Stein, R. M. Kamyar, A. Sugar, *Investig. Opthalmology Vis. Sci.* **2011**, *52*, 6959.

[13] P. Gain, R. Jullienne, Z. He, M. Aldossary, S. Acquart, F. Cognasse, G. Thuret, *JAMA Ophthalmol.* **2016**, *134*, 167.

[14] M. T. Feng, M. O. Price, J. M. Miller, F. W. Price, *J. Cataract Refract. Surg.* **2014**, *40*, 1116.

[15] P. Gain, R. Jullienne, Z. He, *JAMA Ophthalmol.* **2015**, 1.

[16] S. Madi, P. Leon, Y. Nahum, S. D’Angelo, G. Giannaccare, J. Beltz, M. Busin, *Cornea* **2019**, *38*, 1192.

[17] A. Einan-Lifshitz, Z. Mednick, A. Belkin, N. Sorkin, S. Alshaker, T. Boutin, C. C. Chan, D. S. Rootman, *Cornea* **2019**, *38*, 1077.

[18] J. Navaratnam, T. P. Utheim, V. K. Rajasekhar, *J. fun* **2015**, *6*, 917.

[19] S. Gandhi, S. Jain, *Keratoprostheses Artif. Corneas Fundam. Surg. Appl.* **2015**, *37*, 19.

[20] J. Teichmann, M. Valtink, M. Nitschke, S. Gramm, R. H. W. Funk, K. Engelmann, C. Werner, *J. Funct. Biomater* **2013**, *4*, 178.

[21] S. Matthyssen, B. Van Den Bogerd, S. Ni, DhubhGhaill, C. Koppen, N. Zakaria, in *Neurol. Regen.*, Springer, **2017**, pp. 213–255.

[22] B. Vojniković, N. Gabrić, I. Dekaris, B. Jurić, *Coll. Antropol.* **2013**, *37*, 93.

[23] C. Xue, Y. Xiang, M. Shen, D. Wu, Y. Wang, *J. Ophthalmol.* **2018**, *2018*, DOI 10.1155/2018/5392041.

[24] J. V. Jester, *Semin. Cell Dev. Biol.* **2008**, *19*, 82.

[25] M. Aldrovani, A. M. A. Guaraldo, B. C. Vidal, *Vision Res.* **2007**, *47*, 3229.

[26] S. Patel, J. Marshall, F. W. Fitzke, *J. Refract. Surg.* **1995**, *11*, 100.

[27] J. Zhang, D. V. Patel, *Exp. Eye Res.* **2015**, *130*, 97.

[28] W. M. Bourne, *Eye* **2003**, *17*, 912.

[29] A. O. Eghrari, S. A. Riazuddin, J. D. Gottsch, in *Prog. Mol. Biol. Transl. Sci.*, Elsevier Inc., **2015**, pp. 79–97.

[30] B. Van den Bogerd, S. N. Dhubhghaill, C. Koppen, M. J. Tassignon, N. Zakaria, *Surv. Ophthalmol.* **2018**, *63*, 149.

[31] B. Van den Bogerd, S. N. Dhubhghaill, C. Koppen, M. Tassignon, N. Zakaria, *Surv. Ophthalmol.* **2018**, *63*, 149.

[32] A. Agarwal, S. Jacob, A. Agarwal, S. Agarwal, A. Kumar M, *J. Cataract Refract. Surg.* **2006**, *32*, 895.

[33] M. Fuest, M. Ang, H. M. Htoon, D. Tan, J. S. Mehta, *Am. J. Ophthalmol.* **2017**, *182*, 62.

[34] M. A. Nanavaty, X. Wang, A. J. Shortt, *Cochrane Database Syst. Rev.* **2014**, DOI 10.1002/14651858.CD008420.pub3.

[35] A. P. Adamis, V. Filatov, B. J. Tripathi, R. A. mes. C. Tripathi, *Surv. Ophthalmol.* **1993**, *38*, 149.

[36] S. Daljit, “Fuchs Endothelial Dystrophy Treatment &; Management,” **n.d.**

[37] F. W. Price, M. O. Price, *Cornea* **2013**, *32 Suppl 1*, S28.

[38] A. Jun, G. Vedana, G. Villarreal Jr., *Clin. Ophthalmol.* **2016**, *8*, 321.

[39] M. Claesson, *Br. J. Ophthalmol.* **2002**, *86*, 174.

[40] S. Vira, U. Abugo, C. Y. Shih, I. J. Udell, B. Sperling, S. B. Hannush, S. Basti, C. S. Bouchard, **2014**, *33*, 1.

[41] P. Maier, T. Reinhard, C. Cursiefen, *Dtsch. Arztebl. Int.* **2013**, *110*, 365.

[42] J. L. Güell, M. a. El Husseiny, F. Manero, O. Gris, D. Elies, *Ophtalmol. Ther.* **2014**, *3*, 1.

[43] E. Flockerzi, P. Maier, D. Böhringer, H. Reinshagen, F. Kruse, C. Cursiefen, T. Reinhard, G. Geerling, N. Torun, B. Seitz, *Am. J. Ophthalmol.* **2018**, DOI 10.1016/j.ajo.2018.01.018.

[44] S. Kinoshita, N. Koizumi, M. Ueno, N. Okumura, K. Imai, H. Tanaka, Y. Yamamoto, T. Nakamura, T. Inatomi, J. Bush, et al., *N. Engl. J. Med.* **2018**, 995.

[45] B. Van den Bogerd, S. N. Dhubhghaill, N. Zakaria, *J. Tissue Eng. Regen. Med.* **2018**, 1.

[46] J. H. Kim, K. Green, M. Martinez, D. Paton, *Exp. Eye Res.* **1971**, *12*, 231.

[47] M. M. Jumblatt, D. M. Maurice, J. P. McCulley, *Invest. Ophthalmol. Vis. Sci.* **1978**, *17*, 1135.

[48] J. Van Hoorick, L. Tytgat, A. Dobos, H. Ottevaere, J. Van Erps, H. Thienpont, A. Ovsianikov, P. Dubruel, S. Van Vlierberghe, *Acta Biomater.* **2019**, DOI 10.1016/j.actbio.2019.07.035.

[49] J. A. Bonanno, *Exp. Eye Res.* **2012**, *95*, 2.

[50] D. K. Schneiderman, M. A. Hillmyer, *Macromolecules* **2017**, *50*, 3733.

[51] A. Gandini, *Macromolecules* **2008**, *41*, 9491.

[52] Y. Zhu, C. Romain, C. K. Williams, *Nature* **2016**, *540*, 354.

[53] G. Z. Papageorgiou, *Polymers (Basel).* **2018**, *10*, DOI 10.3390/polym10090952.

[54] V. Siracusa, P. Rocculi, S. Romani, M. D. Rosa, *Trends Food Sci. Technol.* **2008**, *19*, 634.

[55] H. Seyednejad, A. H. Ghassemi, C. F. Van Nostrum, T. Vermonden, W. E. Hennink, *J. Control. Release* **2011**, *152*, 168.

[56] G. Graulus, T. Billiet, S. Van Vlierberghe, H. Thienpont, H. Ottevaere, P. Dubruel, in *Handb. Sustain. Polym. Process. Appl.*, **2016**, pp. 753–802.

[57] E. De Jaeghere, E. De Vlieghere, J. Van Hoorick, S. Van Vlierberghe, G. Wagemans, L. Pieters, E. Melsens, M. Praet, J. Van Dorpe, M. N. Boone, et al., *Biomaterials* **2018**, *158*, 95.

[58] M. Markovic, J. Van Hoorick, K. Hölzl, M. Tromayer, P. Gruber, S. Nürnberger, P. Dubruel, S. Van Vlierberghe, R. Liska, A. Ovsianikov, *J. Nanotechnol. Eng. Med.* **2015**, *6*, 0210011.

[59] M. van den Oever, K. Molenveld, M. van der Zee, H. Bos, *Bio-Based and Biodegradable Plastics – Facts and Figures – Focus on Food Packaging in the Netherlands*, **2017**.

[60] K. Madhavan Nampoothiri, N. R. Nair, R. P. John, *Bioresour. Technol.* **2010**, *101*, 8493.

[61] W. Amass, A. Amass, B. Tighe, *Polym. Int.* **1998**, *47*, 89.

[62] M. Vagenende, G. Graulus, J. Delaey, J. Van Hoorick, F. Berghmans, H. Thienpont, S. Van Vlierberghe, P. Dubruel, *Eur. Polym. J.* **2019**, *118*, 685.

[63] A. P. Gupta, V. Kumar, *Eur. Polym. J.* **2007**, *43*, 4053.

[64] G. Perego, G. Cella, C. Bastioli, *J. Appl. Polym. …* **1996**, *59*, 37.

[65] N. Passerini, D. Q. . Craig, *J. Control. Release* **2001**, *73*, 111.

[66] H. K. Makadia, S. J. Siegel, *J. Polym. Sci. Part B Polym. Phys.* **2011**, *3*, 832.

[67] A. Gierej, M. Vagenende, A. Filipkowski, B. Siwicki, R. Buczynski, H. Thienpont, S. Van Vlierberghe, T. Geernaert, P. Dubruel, F. Berghmans, *J. Light. Technol.* **2019**, *PP*, 1.

[68] H. Xu, J. Dong, G. Chai, Z. Yu, W. Lang, *Int. J. Med. Robot. Comput. Assist. Surg.* **2010**, *6*, 66.

[69] T. Desmet, T. Billiet, E. Berneel, R. Cornelissen, D. Schaubroeck, E. Schacht, P. Dubruel, *Macromol. Biosci.* **2010**, *10*, 1484.

[70] G. Graulus, N. Van Herck, K. Van Hecke, G. Van Driessche, B. Devreese, H. Thienpont, H. Ottevaere, S. Van Vlierberghe, P. Dubruel, *React. Funct. Polym.* **2018**, *128*, 16.

[71] B. V. Karmegam, P. Soltantabar, E. J. L. Calubaquib, R. N. Kularatne, M. C. Stefan, M. Matters, *Mater. Matters* **2017**, *12*, 1.

[72] P. X. Ma, *Adv. Drug Deliv. Rev.* **2008**, *60*, 184.

[73] D. W. Hutmacher, *Biomaterials* **2000**, *21*, 2529.

[74] M. L. Goodwin, J. E. Harris, M. Ed, A. Hernández, L. B. Gladden, D. Ph, *J. Diabetes Sci. Technol.* **2007**, *1*, 558.

[75] D. Garlotta, *J. Polym. Environ.* **2001**, *9*, 63.

[76] J. Torgersen, X.-H. Qin, Z. Li, A. Ovsianikov, R. Liska, J. Stampfl, *Adv. Funct. Mater.* **2013**, *23*, 4542.

[77] J. R. Dorgan, B. Braun, J. R. Wegner, D. M. Knauss, *Degrad. Polym. Mater. Princ. Pract.* **2006**, 102.

[78] G. Graulus, **2018**.

[79] S. Inkinen, M. Hakkarainen, A. C. Albertsson, A. Södergård, *Biomacromolecules* **2011**, *12*, 523.

[80] Y. Zhao, Z. Wang, J. Wang, H. Mai, B. Yan, F. Yang, *J. Appl. Polym. Sci.* **2004**, *91*, 2143.

[81] H. R. Kricheldorf, I. Kreiser-Saunders, C. Boettcher, *Polymer (Guildf).* **1995**, *36*, 1253.

[82] O. Coulembier, P. Degée, J. L. Hedrick, P. Dubois, *Prog. Polym. Sci.* **2006**, *31*, 723.

[83] H. R. Kricheldorf, C. Boettcher, K. U. Tönnes, *Polymer (Guildf).* **1992**, *33*, 2817.

[84] B. J. O'Keefe, M. A. Hillmyer, W. B. Tolman, *J. Chem. Soc. Dalt. Trans.* **2001**, 2215.

[85] M. K. Kiesewetter, E. J. Shin, J. L. Hedrick, R. M. Waymouth, **2010**, 2093.

[86] S. Van Vlierberghe, P. Dubruel, E. H. Schacht, *Biomacromolecules* **2011**, *12*, 1387.

[87] P. Dubruel, F. Du Prez, *Polymer Materials*, University Of Ghent, Ghent, **2012**.

[88] N. a Peppas, P. Bures, W. Leobandung, H. Ichikawa, *Eur. J. Pharm. Biopharm.* **2000**, *50*, 27.

[89] P. Dubruel, R. Unger, S. Van Vlierberghe, V. Cnudde, P. J. S. Jacobs, E. Schacht, C. J. Kirkpatrick, *Biomacromolecules* **2007**, *8*, 338.

[90] S. Van Vlierberghe, S. K. Samal, P. Dubruel, *Macromol. Symp.* **2011**, *309–310*, 173.

[91] A. Houben, Design and Development of Porous Pluronic ® Based Scaffolds for Tissue Engineering, Ghent University, **2013**.

[92] R. Ricciardi, G. Mangiapia, F. Lo Celso, L. Paduano, R. Triolo, F. Auriemma, C. De Rosa, D. Chimica, C. Uni, V. Uni, *Chem. Mater.* **2005**, *17*, 1183.

[93] W. E. Hennink, C. F. van Nostrum, *Adv. Drug Deliv. Rev.* **2012**, *64*, 223.

[94] Y. Zheng, M. Micic, S. V. Mello, M. Mabrouki, F. M. Andreopoulos, V. Konka, S. M. Pham, R. M. Leblanc, *Macromolecules* **2002**, *35*, 5228.

[95] K. Arcaute, B. K. Mann, R. B. Wicker, *Ann. Biomed. Eng.* **2006**, *34*, 1429.

[96] A. Ovsianikov, A. Deiwick, S. Van Vlierberghe, P. Dubruel, M. Lena, G. Dräger, B. Chichkov, *Biomacromolecules* **2011**, *12*, 851.

[97] A. Ovsianikov, A. Deiwick, S. Van Vlierberghe, M. Pflaum, M. Wilhelmi, P. Dubruel, B. Chichkov, *Materials (Basel).* **2011**, *4*, 288.

[98] S. C. Rodrigues, C. L. Salgado, A. Sahu, M. P. Garcia, M. H. Fernandes, F. J. Monteiro, *J. Biomed. Mater. Res. A* **2013**, *101*, 1080.

[99] E. Vanderleyden, L. Van Hoorebeke, E. Schacht, P. Dubruel, *Macromol. Symp.* **2011**, *309–310*, 190.

[100] J. Groll, T. Boland, T. Blunk, J. A. Burdick, D.-W. Cho, P. D. Dalton, B. Derby, G. Forgacs, Q. Li, V. A. Mironov, et al., *Biofabrication* **2016**, *8*, 013001.

[101] Z. Li, T. Qu, C. Ding, C. Ma, H. Sun, S. Li, X. Liu, *Acta Biomater.* **2015**, *13*, 88.

[102] J. F. Pan, H. F. Yuan, C. A. Guo, J. Liu, X. H. Geng, T. Fei, S. Li, W. S. Fan, X. M. Mo, Z. Q. Yan, *RSC Adv.* **2015**, *5*, 40820.

[103] I. Steyaert, H. Rahier, S. Van Vlierberghe, J. Olijve, K. De Clerck, *Food Hydrocoll.* **2016**, *57*, 200.

[104] R. Schrieber, H. Gareis, *Gelatine Handbook: Theory and Industrial Practice*, **2007**.

[105] J. L. Gornall, E. M. Terentjev, *Soft Matter* **2008**, *4*, 544.

[106] J. Van Hoorick, H. Declercq, A. De Muynck, A. Houben, L. Van Hoorebeke, R. Cornelissen, J. Van Erps, H. Thienpont, P. Dubruel, S. Van Vlierberghe, *J. Mater. Sci. Mater. Med.* **2015**, *26*, 247.

[107] a I. Van Den Bulcke, B. Bogdanov, N. De Rooze, E. H. Schacht, M. Cornelissen, H. Berghmans, *Biomacromolecules* **2000**, *1*, 31.

[108] J. Van Hoorick, P. Gruber, M. Markovic, M. Tromayer, J. Van Erps, H. Thienpont, R. Liska, A. Ovsianikov, P. Dubruel, S. Van Vlierberghe, *Biomacromolecules* **2017**, DOI 10.1021/acs.biomac.7b00905.

[109] S. Sakai, K. Hirose, K. Taguchi, Y. Ogushi, K. Kawakami, *Biomaterials* **2009**, *30*, 3371.

[110] I. Van Nieuwenhove, A. Salamon, K. Peters, G. Graulus, J. C. Martins, D. Frankel, K. Kersemans, F. De Vos, S. Van Vlierberghe, P. Dubruel, *Carbohydr. Polym.* **2016**, *152*, 129.

[111] G.-J. Graulus, A. Mignon, S. Van Vlierberghe, H. Declercq, K. Fehér, M. Cornelissen, J. C. Martins, P. Dubruel, *Eur. Polym. J.* **2015**, DOI 10.1016/j.eurpolymj.2015.06.033.

[112] T. Greene, C. Lin, *ACS Biomater. Sci. Eng.* **2015**, *1*, 1314.

[113] S. T. Koshy, R. M. Desai, P. Joly, J. Li, R. K. Bagrodia, S. A. Lewin, N. S. Joshi, D. J. Mooney, *Adv. Healthc. Mater.* **2016**, *5*, 541.

[114] J. Van Hoorick, P. Gruber, M. Markovic, M. Tromayer, J. Van Erps, H. Thienpont, R. Liska, A. Ovsianikov, P. Dubruel, S. Van Vlierberghe, *Biomacromolecules* **2017**, DOI 10.1021/acs.biomac.7b00905.

[115] T. Greene, T. Lin, O. M. Andrisani, C. Lin, *J. Appl. Polym. Sci.* **2017**, *44585*, 1.

[116] A. Ito, A. Mase, Y. Takizawa, M. Shinkai, H. Honda, K.-I. Hata, M. Ueda, T. Kobayashi ' ", *J. Biosci. Bioeng.* **2003**, *95*, 196.

[117] "Gelatin, Report No. 58," can be found under http://wayback.archive-it.org/7993/20171031062708/https://www.fda.gov/Food/IngredientsPackagingLabeling/GRAS/SCOGS/ucm261307.htm, **1979**.

[118] J. B. Rose, S. Pacelli, A. J. El Haj, H. S. Dua, A. Hopkinson, L. J. White, F. R. a J. Rose, *Materials (Basel).* **2014**, *7*, 3106.

[119] S. Van Vlierberghe, *J. Mater. Sci.* **2016**, *51*, 1.

[120] a. Bigi, G. Cojazzi, S. Panzavolta, K. Rubini, N. Roveri, *Biomaterials* **2001**, *22*, 763.

[121] A. I. Van Den Bulcke, B. Bogdanov, N. De Rooze, E. H. Schacht, M. Cornelissen, H. Berghmans, *Biomacromolecules* **2000**, *1*, 31.

[122] E. H. Schacht, A. I. Van Den Bulcke, B. Delaey, J.-P. Draye, *Medicaments Based on Polymers Composed of Methacrylamide-Modified Gelatin*, **2002**, US 6458386 B1.

[123] E. Schacht, A. I. Van Den Bulcke, B. Delaey, J.-P. Draye, *Medicaments Based on Polymers Composed of Methacrylamide-Modified Gelatin*, **2002**.

[124] H. Shih, T. Greene, M. Korc, C. Lin, *Biomacromolecules* **2016**, *17*, 3872.

[125] B. J. Klotz, D. Gawlitta, A. J. W. P. Rosenberg, J. Malda, F. P. W. Melchels, *Trends Biotechnol.* **2016**, *34*, 394.

[126] L. Brigo, A. Urciuolo, S. Giulitti, G. Della, M. Tromayer, R. Liska, N. Elvassore, G. Brusatin, *Acta Biomater.* **2017**, *55*, 373.

[127] T. Billiet, E. Gevaert, T. De Schryver, M. Cornelissen, P. Dubruel, *Biomaterials* **2014**, *35*, 49.

[128] M. Markovic, J. Van Hoorick, K. Hölzl, M. Tromayer, P. Gruber, S. Nürnberger, P. Dubruel, S. Van Vlierberghe, R. Liska, A. Ovsianikov, *J. Nanotechnol. Eng. Med.* **2015**, *6*, 021004.

[129] A. Ovsianikov, S. Mühleder, J. Torgersen, Z. Li, X.-H. Qin, S. Van Vlierberghe, P. Dubruel, W. Holnthoner, H. Redl, R. Liska, et al., *Langmuir* **2014**, *30*, 3787.

[130] A. Ovsianikov, A. Deiwick, S. Van Vlierberghe, M. Pflaum, M. Wilhelmi, P. Dubruel, B. Chichkov, *Materials (Basel).* **2011**, *4*, 288.

[131] J. Van Rie, H. Declercq, J. Van Hoorick, M. Dierick, L. Van Hoorebeke, R. Cornelissen, H. Thienpont, P. Dubruel, S. Van Vlierberghe, *J. Mater. Sci. Mater. Med.* **2015**, *26*, 5465.

[132] D. Loessner, C. Meinert, E. Kaemmerer, L. C. Martine, K. Yue, P. A. Levett, T. J. Klein, F. P. W. Melchels, A. Khademhosseini, D. W. Hutmacher, *Nat. Protoc.* **2016**, *11*, 727.

[133] K. S. Lim, R. Levato, P. F. Costa, M. D. Castilho, C. R. Alcala-Orozco, K. M. A. Van Dorenmalen, F. P. W. Melchels, D. Gawlitta, G. J. Hooper, J. Malda, et al., *Biofabrication* **2018**, *10*, DOI 10.1088/1758-5090/aac00c.

[134] K. Yue, G. Trujillo-de Santiago, M. M. Alvarez, A. Tamayol, N. Annabi, A. Khademhosseini, *Biomaterials* **2015**, *73*, 254.

[135] K. Hölzl, S. Lin, L. Tytgat, S. Van Vlierberghe, L. Gu, A. Ovsianikov, *Biofabrication* **2016**, *8*, 032002.

[136] "Allevi3D," can be found under https://allevi3d.com/shop/, **n.d.**

[137] X. Zhou, H. Cui, M. Nowicki, S. Miao, S. J. Lee, F. Masood, B. T. Harris, L. G. Zhang,

ACS Appl. Mater. Interfaces **2018**, *10*, 8993.

[138] E. Hoch, T. Hirth, G. E. M. Tovar, K. Borchers, *J. Mater. Chem. B* **2013**, *1*, 5675.

[139] T. Billiet, B. Van Gasse, E. Gevaert, M. Cornelissen, J. C. Martins, P. Dubruel, *Macromol. Biosci.* **2013**, *13*, 1531.

[140] F. A. Pennacchio, C. Fedele, S. De Martino, S. Cavalli, R. Vecchione, P. A. Netti, *ACS Appl. Mater. Interfaces* **2018**, *10*, 91.

[141] F.-C. Ding, S. Hsu, W.-Y. Chiang, *J. Appl. Polym. Sci.* **2008**, *109*, 589.

[142] I. Van Nieuwenhove, S. Birgit, G.-J. Graulus, S. Van Vlierberghe, P. Dubruel, *Macromol. Rapid Commun.* **2014**, *35*, 1351.

[143] R. Liska, M. Schuster, R. Inführ, C. Turecek, C. Fritscher, B. Seidl, V. Schmidt, L. Kuna, a. Haase, F. Varga, et al., *J. Coatings Technol. Res.* **2007**, *4*, 505.

[144] M. Schuster, C. Turecek, F. Varga, H. Lichtenegger, J. Stampfl, R. Liska, *Appl. Surf. Sci.* **2007**, *254*, 1131.

[145] Y. Cao, B. H. Lee, H. B. Peled, S. S. Venkatraman, *J. Biomed. Mater. Res. - Part A* **2016**, *104*, 2401.

[146] S. Bertlein, G. Brown, K. S. Lim, T. Jungst, T. Boeck, T. Blunk, J. Tessmar, G. J. Hooper, T. B. F. Woodfield, J. Groll, *Adv. Mater.* **2017**, *1703404*, 1.

[147] J. Van Hoorick, P. Gruber, M. Markovic, M. Rollot, G. Graulus, M. Vagenende, M. Tromayer, J. Van Erps, H. Thienpont, J. C. Martins, et al., *Macromol. Rapid Commun.* **2018**, *1800181*, 1.

[148] O. Bas, E. M. De-Juan-Pardo, M. P. Chhaya, F. M. Wunner, J. E. Jeon, T. J. Klein, D. W. Hutmacher, *Eur. Polym. J.* **2015**, *72*, 451.

[149] J. Visser, F. P. W. Melchels, J. E. Jeon, E. M. van Bussel, L. S. Kimpton, H. M. Byrne, W. J. a Dhert, P. D. Dalton, D. W. Hutmacher, J. Malda, *Nat. Commun.* **2015**, *6*, 6933.

[150] C. Claaßen, M. H. Claaßen, V. Tru, L. Sewald, G. E. M. Tovar, K. Borchers, A. Southan, *Biomacromolecules* **2018**, *19*, 42.

[151] A. Houben, N. Pien, X. Lu, F. Bisi, J. Van Hoorick, M. N. Boone, P. Roose, H. Van den Bergen, D. Bontinck, T. Bowden, et al., *Macromol. Biosci.* **2016**, 1.

[152] S. Žigon-Branc, M. Markovic, J. Van Hoorick, S. Van Vlierberghe, P. Dubruel, E. Zerobin, S. Baudis, A. Ovsianikov, *Tissue Eng. Part A* **2019**, *43*, ten. tea.2018.0237.

[153] Y.-C. Chen, R.-Z. Lin, H. Qi, Y. Yang, H. Bae, J. M. Melero-Martin, A. Khademhosseini, *Adv. Funct. Mater.* **2012**, *22*, 2027.

[154] X. Zhao, Q. Lang, L. Yildirimer, Z. Y. Lin, W. Cui, N. Annabi, K. W. Ng, M. R. Dokmeci, A. M. Ghaemmaghami, A. Khademhosseini, *Adv. Healthc. Mater.* **2016**, *5*, 108.

[155] J. W. Nichol, S. T. Koshy, H. Bae, C. M. Hwang, S. Yamanlar, A. Khademhosseini, *Biomaterials* **2010**, *31*, 5536.

[156] A. Mignon, D. Pezzoli, E. Prouvé, L. Lévesque, A. Arslan, N. Pien, D. Schaubroeck, J. Van Hoorick, D. Mantovani, S. Van Vlierberghe, et al., *React. Funct. Polym.* **2019**, *136*, 95.

[157] D. Mandt, P. Gruber, M. Markovic, M. Tromayer, M. Rothbauer, S. Rudi, A. Kratz, S. F.

Ali, J. Van Hoorick, W. Holnthoner, et al., *Int. J. Bioprining* **2018**, *4*, 1.

[158] M.-H. Chang, Y.-P. Hsiao, C.-Y. Hsu, P.-S. Lai, *Nanomaterials* **2018**, *8*, 791.

[159] R. Stevens, L. Stevens, N. C. Price, in *Biochem. Educ. 11*, **1983**, p. 70.

[160] A. L. Freeman, G. R. Buttermann, B. P. Beaubien, W. E. Rochefort, *J. Biomech.* **2013**, *46*, 1714.

[161] R. F. Pereira, P. J. Bartolo, *J. Appl. Polym. Sci.* **2015**, *1*, DOI 10.1002/app.42889.

[162] C. E. Hoyle, C. N. Bowman, *Angew. Chemie* **2010**, *49*, 1540.

[163] K. S. Lim, B. S. Schon, N. V. Mekhileri, G. C. J. Brown, C. M. Chia, S. Prabakar, G. J. Hooper, T. B. F. Woodfield, *ACS Biomater. Sci. Eng.* **2016**, *2*, 1752.

[164] F. Yu, X. Cao, L. Zeng, Q. Zhang, X. Chen, *Carbohydr. Polym.* **2013**, *97*, 188.

[165] H. C. Kolb, M. G. Finn, K. B. Sharpless, *Angew. Chemie - Int. Ed.* **2001**, *40*, 2004.

[166] T. O. Machado, C. Sayer, P. H. H. Araujo, *Eur. Polym. J.* **2017**, *86*, 200.

[167] C. E. Hoyle, T. Y. Lee, T. Roper, *J. Polym. Sci. Part A Polym. Chem.* **2004**, *42*, 5301.

[168] Z. Mũnoz, H. Shih, C.-C. Lin, *Biomater. Sci.* **2014**, *2*, 1063.

[169] C. E. Hoyle, T. A. I. Y. Lee, T. Roper, *J. Polym. Sci. Part A Polym. Chem.* **2004**, *42*, 5301.

[170] L. Tytgat, L. Van Damme, J. Van Hoorick, H. Declercq, H. Thienpont, H. Ottevaere, P. Blondeel, P. Dubruel, S. Van Vlierberghe, *Acta Biomater.* **2019**, 1.

[171] L. Russo, A. Sgambato, R. Visone, P. Occhetta, M. Moretti, M. Rasponi, F. Nicotra, L. Cipolla, *Monatshefte fur Chemie* **2016**, *147*, 587.

[172] L. Li, C. Lu, L. Wang, M. Chen, J. White, X. Hao, K. M. McLean, H. Chen, T. C. Hughes, *ACS Appl. Mater. Interfaces* **2018**, *10*, 13283.

[173] M. M. Perera, N. Ayres, *Polym. Chem.* **2017**, *8*, 6741.

[174] K. Xu, Y. Fu, W. Chung, X. Zheng, Y. Cui, I. C. Hsu, W. J. Kao, *Acta Biomater.* **2012**, *8*, 2504.

[175] Y. Dong, A. Sigen, M. Rodrigues, X. Li, S. H. Kwon, N. Kosaric, S. Khong, Y. Gao, W. Wang, G. C. Gurtner, *Adv. Funct. Mater.* **2017**, *27*, 1.

[176] C.-C. Lin, C. S. Ki, H. Shih, *J. Appl. Polym. Sci.* **2015**, *132*, 1.

[177] C. Resetco, B. Hendriks, N. Badi, F. Du Prez, *Mater. Horizons* **2017**, *4*, 1041.

[178] C.-C. Lin, C. S. Ki, H. Shih, *J. Appl. Polym. Sci.* **2015**, *132*, 1.

[179] J. D. Mccall, K. S. Anseth, *Biomacromolecules* **2012**, *13*, 2410.

[180] A. Dobos, W. Steiger, D. Theiner, P. Gruber, M. Lunzer, J. Van Hoorick, S. Van Vlierberghe, A. Ovsianikov, *Analyst* **2019**, DOI 10.1039/C9AN00068B.

[181] D. L. Alge, M. A. Azagarsamy, D. F. Donohue, K. S. Anseth, *Biomacromolecules* **2013**, *14*, 949.

[182] W. M. Gramlich, I. L. Kim, J. A. Burdick, *Biomaterials* **2013**, *34*, 9803.

[183] R. F. Pereira, P. J. Bártolo, *Engineering* **2015**, *1*, 090.

[184] C. F. Hansell, P. Espeel, M. M. Stamenovi??, I. A. Barker, A. P. Dove, F. E. Du Prez, R. K. Oreilly, *J. Am. Chem. Soc.* **2011**, *133*, 13828.

[185] F. Goethals, D. Frank, F. Du Prez, *Prog. Polym. Sci.* **2017**, *64*, 76.

[186] M. Gajendiran, J.-S. Rhee, K. Kim, *Tissue Eng. Part B Rev.* **2017**, *24*, ten. TEB.2016.0442.

[187] S. Van Vlierberghe, E. Schacht, P. Dubruel, *Eur. Polym. J.* **2011**, *47*, 1039.

[188] S. Duggan, O. O'Donovan, E. Owens, W. Cummins, H. Hughes, *Eur. J. Pharm. Biopharm.* **2015**, *91*, 75.

[189] J. Rohrer, A. Partenhauser, O. Zupančič, G. Leonavičiūtė, S. Podričnik, A. Bernkop-Schnürch, *Eur. Polym. J.* **2017**, *87*, 48.

[190] Y. Fu, K. Xu, X. Zheng, A. J. Giacomin, A. W. Mix, W. J. Kao, *Biomaterials* **2012**, *33*, 48.

[191] J. Rohrer, O. Zupancic, W. Suchaoin, K. Netsoomboon, F. Laffleur, S. Oh, A. Bernkop-Schnürch, *Eur. Polym. J.* **2015**, *73*, 268.

[192] X. Z. Shu, Y. Liu, F. Palumbo, G. D. Prestwich, *Biomaterials* **2003**, *24*, 3825.

[193] J. M. Heffernan, D. J. Overstreet, L. D. Le, B. L. Vernon, R. W. Sirianni, *Ann. Biomed. Eng.* **2015**, *43*, 1965.

[194] S. T. Koshy, R. M. Desai, P. Joly, J. Li, R. K. Bagrodia, S. A. Lewin, N. S. Joshi, D. J. Mooney, *Adv. Healthc. Mater.* **2016**, *5*, 541.

[195] E. Hoch, C. Schuh, T. Hirth, G. E. M. Tovar, K. Borchers, *J. Mater. Sci. Mater. Med.* **2012**, *23*, 2607.

[196] X. H. Qin, J. Torgersen, R. Saf, S. Mühleder, N. Pucher, S. C. Ligon, W. Holnthoner, H. Redl, A. Ovsianikov, J. Stampfl, et al., *J. Polym. Sci. Part A Polym. Chem.* **2013**, *51*, 4799.

[197] D. P. Nair, M. Podgórski, S. Chatani, T. Gong, W. Xi, C. R. Fenoli, C. N. Bowman, *Chem. Mater.* **2013**, *26*, 724.

[198] Y. Jiang, J. Chen, C. Deng, E. J. Suuronen, Z. Zhong, *Biomaterials* **2014**, *35*, 4969.

[199] B. V Sridhar, E. A. Dailing, J. L. Brock, J. W. Stansbury, M. A. Randolph, K. S. Anseth, *Regen. Eng. Transl. Med.* **2015**, *1*, 11.

[200] C. García-Astrain, A. Gandini, C. Peña, I. Algar, A. Eceiza, M. Corcuera, N. Gabilondo, *RSC Adv.* **2014**, *4*, 35578.

[201] C. García-Astrain, O. Guaresti, K. González, A. Eceiza, M. A. Corcuera, N. Gabilondo, *Mater. Lett.* **2016**, *182*, 134.

[202] A. N. Zelikin, J. F. Quinn, F. Caruso, *Biomacromolecules* **2006**, *7*, 27.

[203] B. Gyarmati, Á. Némethy, A. Szilágyi, *Eur. Polym. J.* **2013**, *49*, 1268.

[204] S. Kommareddy, M. Amiji, *Bioconjug. Chem.* **2005**, *16*, 1423.

[205] A. Bernkop-Schnürch, *Adv. Drug Deliv. Rev.* **2005**, *57*, 1569.

[206] T. Seki, H. Kanbayashi, T. Nagao, S. Chono, M. Tomita, M. Hayashi, Y. Tabata, K. Morimoto, *Biol. Pharm. Bull.* **2005**, *28*, 510.

[207] A. J. Kowaltowski, A. E. Vercesi, *Free Radic. Biol. Med.* **1998**, *26*, 463.

[208] B. Sarker, D. G. Papageorgiou, R. Silva, T. Zehnder, F. Gul-E-Noor, M. Bertmer, J. Kaschta, K. Chrissafis, R. Detsch, A. R. Boccaccini, *J. Mater. Chem. B* **2014**, *2*, 1470.

[209] Y. Liu, M. B. Chan-Park, *Biomaterials* **2009**, *30*, 196.

[210] Y. Liu, M. B. Chan-Park, *Biomaterials* **2009**, *30*, 196.

[211] S. H. Medina, J. P. Schneider, in *Chemoselective Bioorthogonal Ligation React.* (Eds: W. R. Algar, P. E. Dawson, I. L. Medintz), **2017**, pp. 497–542.

[212] K. M. Gattás-Asfura, E. Weisman, F. M. Andreopoulos, M. Micic, B. Muller, S. Sirpal, S. M. Pham, R. M. Leblanc, *Biomacromolecules* **2005**, *6*, 1503.

[213] C. García-Astrain, C. Peña-Rodriguez, A. Retegi, A. Eceiza, M. A. Corcuera, N. Gabilondo, *Mater. Lett.* **2015**, *160*, 142.

[214] L. A. Wells, M. A. Brook, H. Sheardown, *Macromol. Biosci.* **2011**, *11*, 988.

[215] S. Sirpal, K. M. Gattás-Asfura, R. M. Leblanc, *Colloids Surfaces B Biointerfaces* **2007**, *58*, 116.

[216] K. M. C. Tsang, N. Annabi, F. Ercole, K. Zhou, D. J. Karst, F. Li, J. M. Haynes, R. A. Evans, H. Thissen, A. Khademhosseini, et al., *Adv. Funct. Mater.* **2015**, *25*, 977.

[217] M. Lunzer, L. Shi, O. G. Andriotis, P. Gruber, M. Markovic, P. J. Thurner, D. Ossipov, R. Liska, A. Ovsianikov, *Angew. Chemie - Int. Ed.* **2018**, *57*, 15122.

[218] N. N. Ferreira, L. M. B. Ferreira, V. M. O. Cardoso, F. I. Boni, A. L. R. Souza, M. P. D. Gremião, *Eur. Polym. J.* **2018**, *99*, 117.

[219] T. Il Son, M. Sakuragi, S. Takahashi, S. Obuse, J. Kang, M. Fujishiro, H. Matsushita, J. Gong, S. Shimizu, Y. Tajima, et al., *Acta Biomater.* **2010**, *6*, 4005.

[220] T. Mazaki, Y. Shiozaki, K. Yamane, A. Yoshida, M. Nakamura, Y. Yoshida, D. Zhou, T. Kitajima, M. Tanaka, Y. Ito, et al., *Sci. Rep.* **2014**, *4*, 1.

[221] S. AnilKumar, S. C. Allen, N. Tasnim, T. Akter, S. Park, A. Kumar, M. Chattopadhyay, Y. Ito, L. J. Suggs, B. Joddar, *J. Biomed. Mater. Res. - Part B Appl. Biomater.* **2019**, *107*, 314.

[222] S. Anil Kumar, N. Tasnim, E. Dominguez, S. C. Allen, L. J. Suggs, Y. Ito, B. Joddar, *Gels* **2018**, *4*, 1.

[223] A. M. Braun, H. Dahn, E. Gassmannt, L. Jakobsl, J. Katevall, C. G. Martinez, E. Oliverosl, *Photochem. Photobiol.* **1999**, *70*, 868.

[224] Y. Tajima, H. Arai, Y. Tezuka, T. Ishii, K. Takeuchi, *Fuller. Sci. Technol.* **1997**, *5*, 1531.

[225] M. Yao, J. Zhang, F. Gao, Y. Chen, S. Ma, K. Zhang, H. Liu, F. Guan, *ACS Omega* **2019**, *4*, 8334.

[226] H. Degn, *Nature* **1968**, *217*.

[227] S. Sakai, H. Ohi, T. Hotta, H. Kamei, M. Taya, *Biopolymers* **2018**, *109*, 1.

[228] R. G. W. Norrish, C. H. Bamfore, *Nature* **1937**, *140*, 195.

[229] K. S. Lim, B. J. Klotz, G. C. J. Lindberg, F. P. W. Melchels, G. J. Hooper, J. Malda, D. Gawlitta, T. B. F. Woodfield, *Macromol. Biosci.* **2019**, 1.

[230] M. Tromayer, A. Dobos, P. Gruber, A. Ajami, R. Dedic, A. Ovsianikov, R. Liska, *Polym. Chem.* **2018**, *9*, 3108.

[231] D. A. Fancy, C. Denison, K. Kom, Y. Xie, T. Holdeman, F. Amini, T. Kodadek, *Chem. Biol.* **2000**, *7*, 697.

[232] Z. Li, J. Torgersen, A. Ajami, S. Mühleder, X. Qin, W. Husinsky, W. Holnthoner, A. Ovsianikov, J. Stampfl, R. Liska, *RSC Adv.* **2013**, *3*, 15939.

[233] L. Brigo, A. Urciuolo, S. Giulitti, G. Della Giustina, M. Tromayer, R. Liska, N. Elvassore, G. Brusatin, *Acta Biomater.* **2017**, *55*, 373.

[234] X. Wang, X. H. Qin, C. Hu, A. Terzopoulou, X. Z. Chen, T. Y. Huang, K. Maniura-Weber, S. Pané, B. J. Nelson, *Adv. Funct. Mater.* **2018**, *28*, 1.

[235] M. Tromayer, P. Gruber, M. Markovic, A. Rosspeintner, E. Vauthey, H. Redl, A. Ovsianikov, R. Liska, *Polym. Chem.* **2017**, *8*, 451.

[236] J. E. Mark, *Polymer Data Handbook*, **1999**.

[237] M. Schuster, C. Turecek, G. Weigel, R. Saf, J. Stampfl, F. Varga, R. Liska, *J. Polym. Sci. Part A Polym. Chem.* **2009**, *47*, 7078.

[238] J. E. Mark, *Polymer Data Handbook*, **1999**.

[239] R. Zamani Alavijeh, P. Shokrollahi, J. Barzin, *J. Mater. Chem. B* **2017**, *5*, 2302.

[240] J. R. Prado, S. Vyazovkin, *Macromol. Chem. Phys.* **2014**, *215*, 867.

[241] P. De Meuter, H. Rahier, B. Van Mele, *Int. J. Pharm.* **1999**, *192*, 77.

[242] E. Hoch, T. Hirth, G. E. M. Tovar, K. Borchers, *J. Mater. Chem. B* **2013**, *1*, 5675.

[243] L. Rebers, T. Granse, G. Tovar, A. Southan, K. Borchers, *Gels* **2019**, *5*, 4.

[244] L. Rebers, T. Granse, G. Tovar, A. Southan, K. Borchers, *Gels* **2019**, *5*, 4.

[245] B. Sen Chiou, R. J. Avena-Bustillos, P. J. Bechtel, H. Jafri, R. Narayan, S. H. Imam, G. M. Glenn, W. J. Orts, *Eur. Polym. J.* **2008**, *44*, 3748.

[246] A. A. Karim, R. Bhat, *Trends Food Sci. Technol.* **2008**, *19*, 644.

[247] E. Hoch, K. Borchers, G. E. M. Tovar, *Modifizierte Gelatine, Verfahren Zu Ihrer Herstellung Und Verwending*, **2012**, DE 10 2012 219 691 A1 2014.04.30.

[248] S. Ma, M. Natoli, X. Liu, M. P. Neubauer, F. M. Watt, A. Fery, W. T. S. Huck, *J. Mater. Chem. B* **2013**, *1*, 5128.

[249] B. Sara Žigon-Branc, M. Markovic, J. Van Hoorick, S. Van Vlierberghe, P. Dubruel, E. Zerobin, S. Baudis, A. Ovsianikov, S. Žigon-Branc, *Tissue Eng. Part A* **2018**, *43*, 1.

[250] C. D. O'Connell, B. Zhang, C. Onofrillo, S. Duchi, R. Blanchard, A. Quigley, J. Bourke, S. Gambhir, R. Kapsa, C. Di Bella, et al., *Soft Matter* **2018**, *14*, 2142.

[251] W. Schuurman, P. A. Levett, M. W. Pot, P. R. van Weeren, W. J. A. Dhert, D. W. Hutmacher, F. P. W. Melchels, T. J. Klein, J. Malda, *Macromol. Biosci.* **2013**, *13*, 551.

[252] J. Malda, J. Visser, F. P. Melchels, T. Jüngst, W. E. Hennink, W. J. A. Dhert, J. Groll,

D. W. Hutmacher, *Adv. Mater.* **2013**, *25*, 5011.

[253] L. Tytgat, M. Vagenende, H. Declercq, J. C. Martins, H. Thienpont, H. Ottevaere, *Carbohydr. Polym.* **2018**, *189*, 1.

[254] M. F. Butler, M. Heppenstall-Butler, *Biomacromolecules* **2003**, *4*, 928.

[255] L. Tytgat, M. Vagenende, H. Declercq, J. C. Martins, H. Thienpont, H. Ottevaere, *Carbohydr. Polym.* **2018**, *189*, 1.

[256] W. Zhu, H. Cui, B. Boualam, F. Masood, E. Flynn, R. D. Rao, Z. Y. Zhang, L. G. Zhang, *Nanotechnology* **2018**, *29*, DOI 10.1088/1361-6528/aaafa1.

[257] W. Jia, P. S. Gungor-Ozkerim, Y. S. Zhang, K. Yue, K. Zhu, W. Liu, Q. Pi, B. Byambaa, M. R. Dokmeci, S. R. Shin, et al., *Biomaterials* **2016**, *106*, 58.

[258] X. Hu, L. Ma, C. Wang, C. Gao, *Macromol. Biosci.* **2009**, *9*, 1194.

[259] S. Van Vlierberghe, S. K. Samal, P. Dubruel, *Macromol. Symp.* **2011**, *309–310*, 173.

[260] C. S. Nickerson, J. Park, J. A. Kornfield, H. Karageozian, *J. Biomech.* **2008**, *41*, 1840.

[261] K. Comley, N. A. Fleck, *J. Biomech.* **2010**, *43*, 1823.

[262] K. Comley, N. A. Fleck, *Int. J. Solids Struct.* **2010**, *47*, 2982.

[263] K.-H. Chang, H.-T. Liao, J.-P. Chen, *Acta Biomater.* **2013**, *9*, 9012.

[264] R. J. Dewall, T. Varghese, M. A. Kliewer, J. M. Harter, M. Hartenbach, *Ultrason Imaging* **2011**, *32*, 214.

[265] S. Cheng, E. C. Clarke, L. E. Bilston, *Med. Eng. Phys.* **2008**, *30*, 1318.

[266] M. Zhang, P. Nigwekar, B. Castaneda, K. Hoyt, J. V. Joseph, A. Di Sant' Agnese, E. M. Messing, J. G. Strang, D. J. Rubens, K. J. Parker, *ultrasound Med. Biol.* **2008**, *34*, 1033.

[267] A. L. Freeman, G. R. Buttermann, B. P. Beaubien, W. E. Rochefort, *J. Biomech.* **2013**, *46*, 1714.

[268] H. Frank, A. J. Grodzinsky, **1987**, *20*, 629.

[269] H. Wang, P. L. Prendiville, P. J. McDonnell, W. V. Chang, *J. Biomech.* **1996**, *29*, 1633.

[270] T. K. L. Meyvis, B. G. Stubbe, M. J. Van Steenbergen, W. E. Hennink, S. C. De Smedt, J. Demeester, *Int. J. Pharm.* **2002**, *244*, 163.

[271] O. Bas, E. M. De-Juan-Pardo, M. P. Chhaya, F. M. Wunner, J. E. Jeon, T. J. Klein, D. W. Hutmacher, *Eur. Polym. J.* **2015**, *72*, 451.

[272] J. Van Hoorick, H. Ottevaere, H. Thienpont, P. Dubruel, S. Van Vlierberghe, *Polymer and Photonic Materials Towards Biomedical Breakthroughs*, Springer International Publishing, Cham, **2018**.

[273] X.-H. Qin, A. Ovsianikov, J. Stampfl, R. Liska, *BioNanoMaterials* **2014**, *15*, 49.

[274] A. Ovsianikov, V. Mironov, J. Stampf, R. Liska, *Expert Rev. Med. Devices* **2012**, *9*, 613.

[275] W. R. Zipfel, R. M. Williams, W. W. Webb, *Nat. Biotechnol.* **2003**, *21*, 1369.

[276] S. Engelhardt, E. Hoch, K. Borchers, W. Meyer, H. Krüger, G. E. M. Tovar, A. Gillner, *Biofabrication* **2011**, *3*, 025003.

[277] J. Van Hoorick, P. Gruber, M. Markovic, M. Tromayer, J. Van Erps, H. Thienpont, R. Liska, A. Ovsianikov, P. Dubruel, S. Van Vlierberghe, *Biomacromolecules* **2017**, *18*, 3260.

[278] S. Engelhardt, E. Hoch, K. Borchers, W. Meyer, H. Krüger, G. E. M. Tovar, A. Gillner, *Biofabrication* **2011**, *3*, 025003.

[279] C. C. Danielsen, **2004**, *79*, 343.

[280] B. Ozcelik, K. D. Brown, A. Blencowe, K. Ladewig, G. W. Stevens, J. Y. Scheerlinck, K. Abberton, M. Daniell, G. G. Qiao, *Adv. Healthc. Mater.* **2014**, *3*, 1496.

[281] N. W. Karuri, S. Liliensiek, A. I. Teixeira, G. Abrams, S. Campbell, P. F. Nealey, C. J. Murphy, *J. Cell Sci.* **2004**, *117*, 3153.

[282] J. Mitra, S. Jain, A. Sharma, B. Basu, *Carbon N. Y.* **2013**, *65*, 140.

[283] B. C. Isenberg, D. E. Backman, M. E. Kinahan, R. Jesudason, B. Suki, P. J. Stone, E. C. Davis, J. Y. Wong, *J. Biomech.* **2012**, *45*, 756.

[284] J. Van Hoorick, P. Gruber, M. Markovic, M. Tromayer, J. Van Erps, H. Thienpont, R. Liska, A. Ovsianikov, P. Dubruel, S. Van Vlierberghe, *Biomacromolecules* **2017**, *18*, 3260.

[285] S. Van Vlierberghe, P. Dubruel, E. Schacht, *J. Bioact. Compat. Polym.* **2010**, *25*, 498.

[286] S. Van Vlierberghe, V. Cnudde, P. Dubruel, B. Masschaele, A. Cosijns, I. De Paepe, P. J. S. Jacobs, L. Van Hoorebeke, J. P. Remon, E. Schacht, *Biomacromolecules* **2007**, *8*, 331.

[287] S. Van Vlierberghe, P. Dubruel, E. Lippens, M. Cornelissen, E. Schacht, *J. Biomater. Sci. Polym. Ed.* **2009**, *20*, 1417.

[288] S. Van Vlierberghe, P. Dubruel, E. Lippens, B. Masschaele, L. Van Hoorebeke, M. Cornelissen, R. Unger, C. J. Kirkpatrick, E. Schacht, *J. Mater. Sci. Mater. Med.* **2008**, *19*, 1459.

[289] S. Van Vlierberghe, B. Fritzinger, J. C. Martins, P. Dubruel, *Appl. Spectrosc.* **2010**, *64*, 1176.

[290] S. Van Vlierberghe, M. Sirova, P. Rossmann, H. Thielecke, V. Boterberg, B. Rihova, E. Schacht, P. Dubruel, *Biomacromolecules* **2010**, *11*, 2731.

[291] M. A. Daniele, A. A. Adams, J. Naciri, S. H. North, F. S. Ligler, *Biomaterials* **2014**, *35*, 1845.

[292] M. Markovic, J. Van Hoorick, K. Hölzl, M. Tromayer, P. Gruber, S. Nürnberger, P. Dubruel, S. Van Vlierberghe, R. Liska, A. Ovsianikov, *J. Nanotechnol. Eng. Med.* **2015**, *6*, 021001.

[293] J. Van Rie, H. Declercq, J. Van Hoorick, M. Dierick, L. Van Hoorebeke, R. Cornelissen, H. Thienpont, P. Dubruel, S. Van Vlierberghe, *J. Mater. Sci. Mater. Med.* **2015**, *26*, 123.

[294] A. I. Ciuciu, P. J. Cywiński, *RSC Adv.* **2014**, *4*, 45504.

[295] J. Van Hoorick, H. Declercq, A. De Muynck, A. Houben, L. Van Hoorebeke, R. Cornelissen, J. Van Erps, H. Thienpont, P. Dubruel, S. Van Vlierberghe, *J. Mater. Sci. Mater. Med.* **2015**, *26*, 247.

[296] I. Van Nieuwenhove, A. Salamon, K. Peters, G. Graulus, J. C. Martins, D. Frankel, K.

Kersemans, F. De Vos, S. Van Vlierberghe, P. Dubruel, *Carbohydr. Polym.* **2016**, *152*, 129.

[297] I. Van Nieuwenhove, Development of Hydrogel Precursors for Stem Cell-Based Tissue Engineering, Ghent university, **2013**.

[298] I. Dranca, S. Vyazovkin, *Polymer (Guildf).* **2009**, *50*, 4859.

[299] K. Obata, A. El-Tamer, L. Koch, U. Hinze, B. N. Chichkov, *Light Sci. Appl.* **2013**, *2*, e116.

[300] S. Giraudier, D. Hellio, M. Djabourov, V. Larreta-Garde, *Biomacromolecules* **2004**, *5*, 1662.

[301] A. Houben, P. Roose, H. Van den Bergen, H. Declercq, J. Van Hoorick, P. Gruber, A. Ovsianikov, D. Bontinck, S. Van Vlierberghe, P. Dubruel, *Mater. Today Chem.* **2017**, *4*, 84.

[302] A. J. Kuijpers, G. H. M. Engbers, J. Feijen, S. C. De Smedt, T. K. L. Meyvis, J. Demeester, J. Krijgsveld, S. A. J. Zaat, J. Dankert, *Macromolecules* **1999**, *32*, 3325.

[303] J. Yao, C. W. Ko, P. Y. Baranov, C. V. Regatieri, S. Redenti, B. a. Tucker, J. Mighty, S. L. Tao, M. J. Young, *Tissue Eng. Part A* **2015**, *21*, 1247.

[304] R. Holmes, X. B. Yang, A. Dunne, L. Florea, D. Wood, G. Tronci, *Polymers (Basel).* **2017**, *9*, 226.

[305] C. Z. Liu, Z. D. Xia, Z. W. Han, P. a Hulley, J. T. Triffitt, J. T. Czernuszka, *J. Biomed. Mater. Res. B. Appl. Biomater.* **2008**, *85*, 519.

[306] J. Van Hoorick, A. Ovsianikov, P. Dubruel, S. Van Vlierberghe, *Mater. Matters* **2018**, *13*, 75.

[307] P. Martens, K. . Anseth, *Polymer (Guildf).* **2000**, *41*, 7715.

[308] K. Y. Lee, K. H. Bouhadir, D. J. Mooney, *Biomaterials* **2004**, *25*, 2461.

[309] F. Ganji, S. Vasheghani-Farahani, E. Vasheghani-Farahani, *Iran. Polym. J.* **2010**, *19*, 375.

[310] M. Sutter, J. Siepmann, W. E. Hennink, W. Jiskoot, *J. Control. Release* **2007**, *119*, 301.

[311] A. Veis, *The Macromolecular Chemistry of Gelatin*, Academic Press, New York, **1964**.

[312] S. Van Vlierberghe, P. Dubruel, E. Lippens, M. Cornelissen, E. Schacht, *J. Biomater. Sci. Polym. Ed.* **2008**, *0*, 1.

[313] I. Mironi-Harpaz, D. Y. Wang, S. Venkatraman, D. Seliktar, *Acta Biomater.* **2012**, *8*, 1838.

[314] R. B. Corey, L. Pauling, *Proc. R. Soc. B* **1953**, *141*, DOI 10.1098/rspb.1953.0011.

[315] R. A. Jackson, S. Murali, A. J. Van Wijnen, G. S. Stein, V. Nurcombe, S. M. Cool, *J. Cell. Physiol.* **2007**, *210*, 38.

[316] T. Billiet, M. Vandenhaute, J. Schelfhout, S. Van Vlierberghe, P. Dubruel, *Biomaterials* **2012**, *33*, 6020.

[317] J. Torgersen, A. Ovsianikov, V. Mironov, N. Pucher, X. Qin, Z. Li, K. Cicha, T. Machacek, R. Liska, V. Jantsch, et al., *J. Biomed. Opt.* **2012**, *17*, 105008.

[318] S. Inoué, R. Oldenbourg, in *Handb. Opt. Devices, Meas. Prop.* (Eds: M. Bass, E. W. Van Stryland, D. R. Williams, W. L. Wolfe), McGraw-Hill, **1995**, pp. 17.1-17.52.

[319] M. J. Nasse, J. C. Woehl, *J. Opt. Soc. Am. A* **2010**, *27*, 295.

[320] J. D. Auran, C. J. Koester, N. J. Kleiman, R. Rapaport, J. S. Bomann, B. M. Wirotsko, G. J. Florakis, J. P. Koniarek, *Ophthalmology* **1995**, *102*, 33.

[321] J. C. Culver, J. C. Hoffmann, R. a Poché, J. H. Slater, J. L. West, M. E. Dickinson, *Adv. Mater.* **2012**, *24*, 2344.

[322] M. J. Booth, T. Wilson, *J. Biomed. Opt.* **2001**, *6*, 266.

[323] T. Bückmann, N. Stenger, M. Kadic, J. Kaschke, A. Frölich, T. Kennerknecht, C. Eberl, M. Thiel, M. Wegener, *Adv. Mater.* **2012**, *24*, 2710.

[324] F. Li, V. X. Truong, H. Thissen, J. E. Frith, J. S. Forsythe, *ACS Appl. Mater. Interfaces* **2017**, *9*, 8589.

[325] N. B. Cramer, J. P. Scott, C. N. Bowman, *Macromolecules* **2002**, *35*, 5361.

[326] K. E. Pfitzner, J. G. Moffatt, *J. Am. Chem. Soc.* **1963**, *85*, 3027.

[327] M. Kanao, A. Otake, K. Tsuchiya, K. Ogino, *Int. J. Org. Chem.* **2012**, *02*, 26.

[328] "www.chemspider.com," can be found under www.chemspider.com, **n.d.**

[329] K. Sangamesh, C. Laurencin, M. Deng, *Natural and Synthetic Biomedical Polymers*, Elsevier, **2014**.

[330] Y. Li, J. Yang, B. C. Benicewicz, *J. Polym. Sci. Part A Polym. Chem.* **2007**, *45*, 4300.

[331] J. Liu, A. O. Burts, Y. Li, A. V Zhukhovitskiy, M. F. Ottaviani, N. J. Turro, J. a Johnson, *J. Am. Chem. Soc.* **2012**, *134*, 16337.

[332] Z. Li, J. Torgersen, A. Ajami, S. Mühleder, X. Qin, W. Husinsky, W. Holnthoner, A. Ovsianikov, J. Stampfl, R. Liska, *RSC Adv.* **2013**, *3*, 15939.

[333] A. E. Lanterna, M. González-Béjar, M. Frenette, J. C. Scaiano, *Photochem. Photobiol. Sci.* **2017**, *16*, 1284.

[334] A. Ovsianikov, Z. Li, A. Ajami, J. Torgersen, W. Husinsky, J. Stampfl, R. Liska, *Appl. Phys. A* **2012**, *108*, 29.

[335] K. Vanmol, S. Tuccio, V. Panapakkam, H. Thienpont, J. Watté, J. Van Erps, *Opt. Laser Technol.* **2019**, *112*, 292.

[336] J. Van Hoorick, P. Gruber, M. Markovic, M. Rollot, G. Graulus, M. Vagenende, M. Tromayer, J. Van Erps, H. Thienpont, J. C. Martins, et al., *Macromol. Rapid Commun.* **2018**, *39*, 1800181.

[337] W. M. Gramlich, I. L. Kim, J. A. Burdick, *Biomaterials* **2013**, *34*, 9803.

[338] A. Dobos, W. Steiger, D. Theiner, P. Gruber, M. Lunzer, J. Van Hoorick, S. Van Vlierberghe, A. Ovsianikov, *Analyst* **2019**, *144*, 3056.

[339] L. Tytgat, L. Van Damme, J. Van Hoorick, H. Declercq, H. Thienpont, H. Ottevaere, P. Blondeel, P. Dubruel, S. Van Vlierberghe, *Acta Biomater.* **2019**, *94*, 340.

[340] B. D. Fairbanks, M. P. Schwartz, C. N. Bowman, K. S. Anseth, *Biomaterials* **2009**, *30*, 6702.

[341] A. Dobos, J. Van Hoorick, W. Steiger, P. Gruber, M. Markovic, O. G. Andriotis, A. Rohatschek, P. Dubruel, P. J. Thurner, S. Van Vlierberghe, et al., *Adv. Healthc. Mater.* **2019**, *1900752*, 1900752.

[342] F. P. W. Melchels, W. J. A. Dhert, D. W. Hutmacher, J. Malda, *J. Mater. Chem. B* **2014**, *2*, 2282.

[343] Y. J. Heo, S. Iwanaga, S. Takeuchi, *Proc. IEEE Int. Conf. Micro Electro Mech. Syst.* **2012**, 997.

[344] R. Kumar, S. Anantha Ramakrishna, *Curr. Sci.* **2017**, *112*, 1668.

[345] B. MAREK, E. LERCH, *J. Soc. Dye. Colour.* **1965**, *81*, 481.

[346] R. Shamey, K. Sinha, *Rev. Prog. Color. Relat. Top.* **2003**, *33*, 93.

[347] C. H. Do, E. M. Pearce, B. J. Bulkin, H. K. Reimschuessel, *J. Polym. Sci. Part A Polym. Chem.* **1987**, *25*, 2301.

[348] F. P. W. Melchels, J. Feijen, D. W. Grijpma, *Biomaterials* **2010**, *31*, 6121.

[349] J. Groll, J. A. Burdick, D. Cho, B. Derby, M. Gelinsky, S. C. Heilshorn, T. Jüngst, J. Malda, *Biofabrication* **2018**, *11*, DOI 10.1088/1758-5090/aaec52.

[350] X. Wang, X.-H. Qin, C. Hu, A. Terzopoulou, X.-Z. Chen, T.-Y. Huang, K. Maniura-Weber, S. Pané, B. J. Nelson, *Adv. Funct. Mater.* **2018**, *1804107*, 1804107.

[351] B. Mannervik, K. Axelsson, A. C. Sundewall, A. Holmgren, *Biochem. J.* **1983**, *213*, 519.

[352] H. R. López-Mirabal, J. R. Winther, *Biochim. Biophys. Acta - Mol. Cell Res.* **2008**, *1783*, 629.

[353] Eye Bank Association of America, *2016 Eye Banking Statistical Report*, **2017**.

[354] C.-M. Liang, Y.-H. Chen, D.-W. Lu, J.-T. Chen, M.-C. Tai, *PLoS One* **2013**, *8*, e72089.

[355] M. O. Price, P. Gupta, J. Lass, F. W. Price, **2017**, DOI 10.1146/annurev-vision-102016-061400.

[356] K. J. Shah, M. D. Straiko, M. A. Greiner, in *Cornea* (Eds: M. J. Mannis, E. J. Holland), Elsevier, **2017**, pp. 1468–1479.

[357] R. Watanabe, R. Hayashi, Y. Kimura, Y. Tanaka, T. Kageyama, S. Hara, Y. Tabata, K. Nishida, *Tissue Eng. Part A* **2011**, *17*, 2213.

[358] M. Rizwan, G. S. L. Peh, H. Ang, N. Chan, K. Adnan, J. S. Mehta, W. Siew, E. K. F. Yim, *Biomaterials* **2017**, *120*, 139.

[359] R. N. Palchesko, K. L. Lathrop, J. L. Funderburgh, A. W. Feinberg, *Sci. Rep.* **2015**, *5*, 32.

[360] J. A. Last, S. J. Liliensiek, P. F. Nealey, C. J. Murphy, *J. Struct. Biol.* **2009**, *167*, 19.

[361] C. W. Macosko, *Rheology: Principles, Measurements, and Application*, Wiley-VCH Verlag GmbH & Co. KGaA, **1994**.

[362] J. Teichmann, M. Valtink, M. Nitschke, S. Gramm, R. Funk, K. Engelmann, C. Werner, *J. Funct. Biomater.* **2013**, *4*, 178.

[363] Q. Shi, Q. Fan, W. Ye, J. Hou, S. C. Wong, X. Xu, J. Yin, *ACS Appl. Mater. Interfaces* **2014**, *6*, 9808.

[364] M. M. Jumblatt, D. M. Maurice, B. D. Schwartz, *Transplantation* **1980**, *29*, 498.

[365] G. Niu, J. Choi, Z. Wang, A. Skardal, M. Giegengack, S. Soker, *Biomaterials* **2014**, *35*, 4005.

[366] K. H. Kurji, A. Y. Cheung, M. Eslani, E. J. Rolfes, D. Y. Chachare, N. J. Auteri, M. L. Nordlund, E. J. Holland, *Cornea* **2018**, *37*, 1226.

[367] M. Parekh, S. Ahmad, A. Ruzza, S. Ferrari, *Sci. Rep.* **2017**, *7*, DOI 10.1038/s41598-017-00209-5.

[368] N. Okumura, R. Inoue, Y. Okazaki, S. Nakano, H. Nakagawa, S. Kinoshita, N. Koizumi, *Invest. Ophthalmol. Vis. Sci.* **2015**, *56*, 6067.

[369] G. S. L. Peh, K.-P. Toh, H.-P. Ang, X.-Y. Seah, B. L. George, J. S. Mehta, *BMC Res. Notes* **2013**, *6*, 176.

[370] T. Yeung, P. C. Georges, L. A. Flanagan, B. Marg, M. Ortiz, M. Funaki, N. Zahir, W. Ming, V. Weaver, P. A. Janmey, *Cell Motil. Cytoskeleton* **2005**, *60*, 24.

[371] A. Skardal, D. Mack, A. Atala, S. Sokern, *J. Mech. Behav. Biomed. Mater.* **2012**, *17*, 307.

[372] G. Kumar, C.-C. Ho, C. C. Co, *Adv. Mater.* **2007**, *19*, 1084.

[373] B. Van den Bogerd, G. Garbenciute, C. Koppen, S. Ni DhubhGhaill, R. Valiokas, N. Zakaria, in *Belgian Symp. Tissue Eng. Newt Gener. Tissue Eng.*, Ghent, **2018**, p. 42.

[374] J. Engel, *FEBS Lett.* **1989**, *251*, 1.

[375] A. . Kuijpers, P. . van Wachem, M. J. . van Luyn, G. H. . Engbers, J. Krijgsveld, S. A. . Zaat, J. Dankert, J. Feijen, *J. Control. Release* **2000**, *67*, 323.

[376] A. Ovsianikov, J. Stampfl, R. Liska, P. Gruber, *Method for Lithography-Based Generative Production of Three-Dimensional Components*, **2019**, US 2019/02555773 A1.

[377] S. D. Gittard, A. Nguyen, K. Obata, A. Koroleva, R. J. Narayan, B. N. Chichkov, *Biomed. Opt. Express* **2011**, *2*, 267.

[378] K. Obata, J. Koch, U. Hinze, B. N. Chichkov, *Opt. Express* **2010**, *18*, 17193.

[379] J. Stampfl, R. Liska, A. Ovsianikov, *Multiphoton Lithography*, **2016**.

[380] M. P. Matheu, *Methods and Systems for Printing Biological Material*, **2018**, WO 2018/165613 A1.

[381] A. Subrizi, H. Hiidenmaa, T. Ilmarinen, S. Nymark, P. Dubruel, H. Uusitalo, M. Yliperttula, A. Urtti, H. Skottman, *Biomaterials* **2012**, *33*, 8047.

[382] M. Göppert-Mayer, *Ann. Phys.* **1931**, *9*, 273.

[383] A. Ovsianikov, A. Ostendorf, B. N. Chichkov, *Appl. Surf. Sci.* **2007**, *253*, 6599.

[384] S. a Skoog, P. L. Goering, R. J. Narayan, *J. Mater. Sci. Mater. Med.* **2013**, *25*, 845.

[385] A. Ovsianikov, B. N. Chichkov, O. Adunka, H. Pillsbury, A. Doraiswamy, R. J. Narayan, *Appl. Surf. Sci.* **2007**, *253*, 6603.

[386] M. Emons, K. Obata, T. Binhammer, A. Ovsianikov, B. N. Chichkov, U. Morgner, *Opt. Mater. Express* **2012**, *2*, 942.

[387] W. Denk, J. H. Strickler, W. W. Webb, *Science (80-.).* **1990**, *248*, 73.

[388] J. Seppälä, H. Korhonen, R. Hakala, M. Malin, *Macromol. Biosci.* **2011**, *11*, 1647.

[389] M. T. Raimondi, S. M. Eaton, M. M. Nava, M. Laganà, G. Cerullo, R. Osellame, *J. Appl. Biomater. Biomech.* **2012**, 0.

[390] N. I. Kiskin, R. Chillingworth, J. A. McCray, D. Piston, D. Ogden, *Eur. Biophys. J.* **2002**, *30*, 588.

[391] T. G. Mezger, *The Rheology Handbook: For Users of Rotational and Oscillatory Rheometers*, Hannover, **2006**.

[392] S. Van Vlierberghe, Cell-Interactive Biopolymer-Based Hydrogels Designed for Tissue Engineering(PhD), **2007**.

[393] H. H. Winter, *Rheol. J.* **1999**, *11*, 275.

[394] BIO-Rad, "PureBlu™ DAPI Nuclear Staining Dye #1351303," can be found under https://www.bio-rad.com/en-be/sku/1351303-pureblu-dapi-nuclear-staining-dye?ID=1351303, **n.d.**

[395] A. Basil, W. Wassef, in *Confocal Laser Microsc. - Princ. Appl. Med. Biol. Food Sci.*, InTech, **2013**, p. 13.

[396] S. W. Paddock, *Confocal Microscopy: Methods and Protocols*, Humana Press Inc., **1999**.

[397] L. Knezevic, M. Schaupper, S. Mühleder, K. Schimek, T. Hasenberg, U. Marx, E. Priglinger, H. Redl, W. Holnthoner, *Front. Bioeng. Biotechnol.* **2017**, *5*, 25.

[398] M. Save, A. Soum, *Macromol. Chem. Phys.* **2002**, *203*, 2591.

Appendix: Curriculum Vitae

Personal Details

Name: Van Hoorick Jasper
Date of Birth: 08/12/1989
Place of Birth: Asse
Nationality: Belgian
Marital Status: Married
Email: Vanhoorickjasper@gmail.com
Linkedin : https://www.linkedin.com/in/jasper-van-_hoorick-b42b49a7/
Researchgate : https://www.researchgate.net/profile/Jasper_Van_Hoorick

Short Description

Jasper Van Hoorick graduated his master in Chemistry in 2014 with distinction with a major in Molecular and Macromolecular design and a minor in Industry and Management. In his master thesis he focussed on the development of tunable hydrogel-polyester combination scaffolds for tissue engineering purposes. The master thesis was awarded with the Agoria award to technological master dissertations, part of the Vlaamse Scriptieprijs in 2014. Part of the award was an executive masterclass in Innovation and Enterpreneurship organized by Vlerick business school which he successfully completed. In 2015 he obtained an FWO SB mandate for a joint PhD project between the Polymer Chemistry & Biomaterials Research group (PBM) at Ghent University Brussels Photonics (B-PHOT) at the Vrije Universiteit Brussel. In his PhD research he focussed on the development of novel biodegradable polymer materials including aliphatic polyesters as well as hydrogels and their processing into membranes for ocular tissue regeneration. During this research a large focus lies into (high resolution) additive manufacturing using the laser based multiphoton lithography technique. He co-authored 17 Web of Science Core Collection cited papers, 1 book chapter and co-edited one book. Additionally, he attended multiple international conferences to present the results he obtained during his PhD research, which led to receiving a WBC trainee merit award at the 2016 World Biomaterials Conference in Montreal and the Biointerphases student award for best poster presentation at the European Society for Biomaterials annual meeting in 2016. During his PhD he also participated in a summerschool on Biofabriaction organized by Utrecht University. Additionally, he obtained funding for 5 international research stays in Vienna, Austria (Prof. Dr. Aleksandr Ovsianikov) to perform detailed 2PP experiments on hydrogel formulations developed during his PhD. Finally, the work performed during

his PhD also resulted in the filing of a patent on bifunctional modified biopolymers (PCT/EP2019/063995). In 2018 he aided in consolidating funding from the Research Foundation Flanders thereby aiming to further develop the corneal membranes towards (pre)clinical applications.

Honors & Awards

Grants

- **FWO SB PhD grant**: "Biopolymers Immobilised on Polyester Membranes: A New Vision Towards Ocular Repair." (2015, Brussels, Belgium)
- **FWO Research Project**: "Introducing Smart Polymers in The Field of Corneal Endothelial Tissue Engineering: Solving a Blinding Disease." (€ 542320) (Prof. Dr. Peter Dubruel (Ugent) & Prof. Dr. Carina Koppen) (2018, Brussels, Belgium)

Awards

- **Agoria award** as part of the Vlaamse Scriptieprijs for Technological Master Dissertations (**2014**, Kortrijk Belgium)
- **Utrecht Summer School on 3D Printing and Biofabrication:** IOP publishing award: Best oral presentation teamwork (**2015**, Utrecht, the Netherlands)
- **World Biomaterials Conference trainee merit award** (**2016**, Montreal, Canada)
- **Biointerphases Student Award** for best poster presented at the annual 28th annual Conference of the European Society for Biomaterials (**2017**, Athens, Greece)

Honorary Mentions

- Third place for oral presentations in the Macromolecular and Materials Chemistry session at the Chemistry Conference for Young Scientists "CHEMCYS" (**2018,** Blankenberghe, Belgium)

Student Supervision

- **Nils Callens** (Professional Bachelor Project, AP Hogeschool, Antwerpen, Belgium): "*Een indirecte benadering voor de ontwikkeling van hydrogel scaffolds op basis van gelatine en silica." (**2016**)*
- **Mélanie Rollot** (3 month Internship from ESCOM, Compiegne, France): *"Research on Hydrogel Coatings for Tissue Engineering Applications." (**2017**)*
- **Jasper Delaey** (Master Thesis, Ghent University, Ghent, Belgium): (**2018-2019**)

List of Publications

Publications in Peer-Reviewed Journals Related to the PhD

1. **J. Van Hoorick***, L. Tytgat*, A. Dobos, H. Ottevaere, J. Van Erps, H. Thienpont, A. Ovsianikov, P. Dubruel, S. Van Vlierberghe, *"(Photo-) crosslinkable gelatin derivatives for biofabrication applications"* *Acta Biomater*. **2019**, DOI 10.1016/j.actbio.2019.07.035.
(*both authors contributed equally)

2. A. Dobos, **J. Van Hoorick**, W. Steiger, P. Gruber, M. Markovic, O. G. Andriotis, A. Rohatschek, P. Dubruel, P. J. Thurner, S. Van Vlierberghe, et al., *"Thiol–Gelatin–Norbornene Bioink for Laser-Based High-Definition Bioprinting"* *Adv. Healthc. Mater*. **2019**, 1900752, 1900752.

3. M. Vagenende, G. Graulus, J. Delaey, **J. Van Hoorick**, F. Berghmans, H. Thienpont, S. Van Vlierberghe, P. Dubruel, *"Amorphous random copolymers of lacOCA and manOCA for the design of biodegradable polyesters with tuneable properties"* *Eur. Polym. J.* **2019**, 118, 685.

4. **J. Van Hoorick**, P. Gruber, M. Markovic, M. Rollot, G. Graulus, M. Vagenende, M. Tromayer, J. Van Erps, H. Thienpont, J. C. Martins, et al., *"Highly Reactive Thiol-Norbornene Photo-Click Hydrogels: Toward Improved Processability"* *Macromol. Rapid Commun.* **2018**, 39, 1800181.

5. **J. Van Hoorick**, P. Gruber, M. Markovic, M. Tromayer, J. Van Erps, H. Thienpont, R. Liska, A. Ovsianikov, P. Dubruel, S. Van Vlierberghe, *"Cross-Linkable Gelatins with Superior Mechanical Properties Through Carboxylic Acid Modification: Increasing the Two-Photon Polymerization Potential"* *Biomacromolecules* **2017**, 18, 3260.

Other Publications related to the PhD Research

1. **J. Van Hoorick**, A. Ovsianikov, P. Dubruel, S. Van Vlierberghe, ***"****Photo-Crosslinkable Gelatin Hydrogels, Versatile Materials for (High Resolution) Additive Manufacturing"* *Mater. Matters* **2018**, 13, 75.

Other Publications in Peer-Reviewed Journals

1. Dobos, W. Steiger, D. Theiner, P. Gruber, M. Lunzer, **J. Van Hoorick**, S. Van Vlierberghe, A. Ovsianikov, *"Screening of two-photon activated photodynamic therapy sensitizers using a 3D osteosarcoma model".* *Analyst* **2019**, 144, 3056.

2. A. Mignon, D. Pezzoli, E. Prouvé, L. Lévesque, A. Arslan, N. Pien, D. Schaubroeck, **J. Van Hoorick**, D. Mantovani, S. Van Vlierberghe, et al., *"Combined effect of Laponite and polymer molecular weight on the cell-interactive properties of synthetic PEO-based hydrogels"* *React. Funct. Polym.* **2019**, 136, 95.

3. W. Steiger, P. Gruber, D. Theiner, A. Dobos, M. Lunzer, **J. Van Hoorick**, S. Van Vlierberghe, R. Liska, A. Ovsianikov, *"Fully automated z-scan setup based on a tunable fs-oscillator" Opt. Mater. Express* **2019**, 9, 3567.

4. S. Žigon-Branc, M. Markovic, **J. Van Hoorick**, S. Van Vlierberghe, P. Dubruel, E. Zerobin, S. Baudis, A. Ovsianikov, *"Impact of Hydrogel Stiffness on Differentiation of Human Adipose-Derived Stem Cell Microspheroids" Tissue Eng. Part A* **2019**, 43, ten. tea.2018.0237.

5. L. Tytgat, L. Van Damme, **J. Van Hoorick**, H. Declercq, H. Thienpont, H. Ottevaere, P. Blondeel, P. Dubruel, S. Van Vlierberghe, *"Additive manufacturing of photo-crosslinked gelatin scaffolds for adipose tissue engineering" Acta Biomater*. **2019**, 94, 340.

6. D. Mandt, P. Gruber, M. Markovic, M. Tromayer, M. Rothbauer, S. R. A. Krayz, F. Ali, **J. Van Hoorick**, W. Holnthoner, S. Mühleder, et al., *"Fabrication of biomimetic placental barrier structures within a microfluidic device utilizing two-photon polymerization" Int. J. Bioprinting* **2018**, 4, 1.

7. E. De Jaeghere, E. De Vlieghere, **J. Van Hoorick**, S. Van Vlierberghe, G. Wagemans, L. Pieters, E. Melsens, M. Praet, J. Van Dorpe, M. N. Boone, et al., *"Heterocellular 3D scaffolds as biomimetic to recapitulate the tumor microenvironment of peritoneal metastases in vitro and in vivo" Biomaterials* **2018**, 158, 95.

8. A. Houben, P. Roose, H. Van den Bergen, H. Declercq, **J. Van Hoorick**, P. Gruber, A. Ovsianikov, D. Bontinck, S. Van Vlierberghe, P. Dubruel, *"Flexible oligomer spacers as the key to solid-state photopolymerization of hydrogel precursors" Mater. Today Chem.* 2017, 4, 84.

9. A. Houben*, **J. Van Hoorick***, J. Van Erps, H. Thienpont, S. Van Vlierberghe, P. Dubruel, *"Indirect Rapid Prototyping: Opening Up Unprecedented Opportunities in Scaffold Design and Applications" Ann. Biomed. Eng.* **2017**, 45, 58.
(*both authors contributed equally)

10. A. Houben, N. Pien, X. Lu, F. Bisi, **J. Van Hoorick**, M. N. Boone, P. Roose, H. Van den Bergen, D. Bontinck, T. Bowden, et al., *"Indirect Solid Freeform Fabrication of an Initiator-Free Photocrosslinkable Hydrogel Precursor for the Creation of Porous Scaffolds" Macromol. Biosci*. **2016**, 16, 1883.

11. **J. Van Hoorick**, H. Declercq, A. De Muynck, A. Houben, L. Van Hoorebeke, R. Cornelissen, J. Van Erps, H. Thienpont, P. Dubruel, S. Van Vlierberghe, *"Indirect additive manufacturing as an elegant tool for the production of self-supporting low density gelatin scaffolds" J. Mater. Sci. Mater. Med.* **2015**, 26, 247.

12. J. Van Rie, H. Declercq, **J. Van Hoorick**, M. Dierick, L. Van Hoorebeke, R. Cornelissen, H. Thienpont, P. Dubruel, S. Van Vlierberghe, *"Cryogel-PCL combination scaffolds for bone tissue repair" J. Mater. Sci. Mater. Med*. **2015**, 26, 123.

13. M. Markovic, **J. Van Hoorick**, K. Hölzl, M. Tromayer, P. Gruber, S. Nürnberger, P. Dubruel, S. Van Vlierberghe, R. Liska, A. Ovsianikov, *"Hybrid Tissue Engineering Scaffolds by Combination of Three-Dimensional Printing and Cell Photoencapsulation" J. Nanotechnol. Eng. Med*. **2015**, 6, 021001.

Book Chapters

1. **J. Van Hoorick**, H. Thienpont, P. Dubruel, S. Van Vlierberghe, *"Cell Regeneration: Current Knowledge and Evolutions"* in *Surg. Spine Spinal Cord*, Springer International Publishing, **2016**, pp. 15–63.

Books as Editor

1. **J. Van Hoorick**, H. Ottevaere, H. Thienpont, P. Dubruel, S. Van Vlierberghe, *Polymer and Photonic Materials Towards Biomedical Breakthroughs*, Springer International Publishing, **2018**.

Conference Proceedings

1. M. Steuperaert, C. Debbaut, P. Dubruel, S. Van Vlierberghe, **J. Van Hoorick**, W. Ceelen, P. Segers, *"Quantifying and Modeling the Fluid Transport Through Polylactic Acid Scaffolds"* 4th International Conference on Computational and Mathematical Biomedical Engineering – CMBE2015, **2015**

Patents

1. **J. Van Hoorick** *et al. "Bifunctional Modified Biopolymer Based Polymers and Hydrogels Obtainable from Such Bifunctional Modified Biopolymer Based Hydrogels"* (PCT/EP2019/063995)

Submitted to Peer Reviewed Journals

1. **J. Van Hoorick**, J. Delaey, J. Van Erps, H. Thienpont, P. Dubruel, N. Zakaria, C. Koppen, S. Van Vlierberghe, B. Van den Bogerd.- "*Designer Descemet Membranes Constituted of PDLLA and Functionalized Gelatins as Corneal Endothelial Scaffold", Advanced Healthcare Materials,* **(submitted 2019)**

2. **J. Van Hoorick**, A. Dobos, L. Tytgat, M. Markovic, P. Gruber, J. Van Erps, H. Thienpont, A.Ovsianikov, P. Dubruel and S. Van Vlierberghe. -*Varying Thiolated Crosslinkers in Thiol-norbornene Photo-Click Gelatin-based Hydrogels to Tune Physico-Chemical Properties and Laser Based Processing Capabilities*, *Biofabrication* **(submitted 2019)**

3. A. Dobos, F. Gantner, M. Markovic, **J. Van Hoorick**, S. Van Vlierberghe, A. Ovsianikov. **– "***On-Chip High-Definition Bioprinting of Microvascular Structures"***,** *Biofabrication* **(submitted 2019)**

Oral Presentations at International Conferences

1. **Van Hoorick J**, Van den Bogerd B, Delaey J, Van Erps J, Thienpont H, Koppen C, Zakaria N, Dubruel P, Van Vlierberghe S - *"Gelatin-Polyester Membranes for Regenerating the Corneal Endothelium."*
   (**2019**, Tissue Engineering and Regenerative Medicine – EU Annual Meeting, Rhodos, Greece)
2. **Van Hoorick J**, Markovic M, Gruber P, Tytgat L, Van Erps, J, Thienpont H, Ovsianikov A, Dubruel P, Van Vlierberghe S. - *"Thiolated crosslinker effect on physico-chemical properties and laser-based processing of gelatin thiol-ene hydrogels"*
   (**2018**, Biofabrication, Würzburg, Germany)
3. **Van Hoorick J**, Van den Bogerd B, Van Erps J, Thienpont H, Koppen C, Zakaria N, Dubruel P, Van Vlierberghe S. - *"Towards Corneal Endothelium Repair Using Synthetic Polymer Membranes"*
   (**2018**, European Society for Biomateriasl Annual Meeting, Maastricht, The Netherlands)
4. **Van Hoorick J**, Markovic M, Gruber P, Tytgat L, Van Erps J, Thienpont H, Ovsianikov A, Dubruel P, Van Vlierberghe S. - *"Thiol-ene Click Hydrogels: Influence of Crosslinker on Network Properties."*
   (**2018**, European Symposium on Photopolymer Science, Mulhouse, France)
5. **Van Hoorick J**, Van den Bogerd B, Van Erps J, Thienpont H, Koppen C, Zakaria N, Dubruel P, Van Vlierberghe S. - *"Polyester Membranes with Crosslinkable Gelatins: A Perfect Marriage for Corneal Endothelial Repair?"*
   (**2018**, Chemistry Conference for Young Scientists, Blankenberge, Belgium)
6. **Van Hoorick J**, Gruber P, Markovic M, Zegwaart JP, Van Erps J, Thienpont H, Ovsianikov A, Dubruel P, Van Vlierberghe S.- *"Expanding the crosslinkable gelatin toolbox broadens the biofabrication highway."*
   (**2017**, China-European Society for Biomaterials, Porto, Portugal)
7. **Van Hoorick J**, Gruber P, Markovic M, Van Erps J, Tienpont H, Ovianikov A, Dubruel P, Van Vlierberghe S - *"Gelatin Derivatization Enables High Resolution Additive Manufacturing"*
   (**2017**, Belgian Symposium on Tissue Engineering, Leuven, Belgium)
8. **Van Hoorick J**, Markovic M, Gruber P, Tytgat L, Van Erps, J, Thienpont H, Ovsianikov A, Dubruel P, Van Vlierberghe S. - *"Increasing the Two-Photon Polymerization Performance of Crosslinkable Gelatins: Towards Ocular Applications"*
   (**2016**, Young Scientist Forum Germany, Annual Meeting: Translational Research Towards Clinic, Frankfurt, Germany)
9. **Van Hoorick J**, Gruber P, Hölzl K, Van Erps J, Thienpont H, OVsianikov A, Dubruel P, Van Vlierberghe S. -*"Crosslinkable Gelatin Hydrogels for Two-Photon Polymerization: Towards a New Ocular Treatment"*
   (**2016**, Chemistry Conference for Young Scientists, Blankenberge, Belgium)
10. **Van Hoorick J**, Markovic M, Declercq H, Cornelissen M, Fowler T, Hoffmann O, Ovsianikov A, Van Erps J, Thienpont H, Dubruel P, Van Vlierberghe S. - *"Cryogel-Polyester Combination Scaffolds for Hard Tissue Engineering"*
    (**2015**, International Materials Research Society Annual Meeting, Cancùn, Mexico)
    (Invited)

Poster Presentations at International Conferences

1. **Van Hoorick J**, Markovic M, Gruber P, Tytgat L, Van Erps J, Thienpont H, Ovsianikov A, Dubruel P, Van Vlierberghe S. - *"Gelatin Thiol-ene Crosslinkable Hydrogels for Tissue Engineering"*
   (**2018**, Belgian Symposium on Tissue Engineering)
2. **Van Hoorick J**, Van den Bogerd B, Van Erps J, Thienpont H, Zakaria N, Dubruel P, Van Vlierberghe S. - *"Biodegradable Membranes for Corneal Endothelial Repair."*
   (***2017***, Advanced Materials for Biomedical Applications, Ghent, Belgium)
3. **Van Hoorick J**, Gruber P, Markovic M, Zegwaart JP, Van Erps J, Thienpont H, Ovianikov A, Dubruel P, Van Vlierberghe S. - *"Gelatin Functionalization Strategies Enhance Biofabrication Versatility on the Micro- and Macro Scale"*
   (**2017**, European Society for Biomaterials Annual Meeting, Athens, Greece)
4. **Van Hoorick J**, Gruber P, Markovic M, Zegwaart JP, Tromayer M, Van Erps J, Thienpont H, Ovsianikov A, Dubruel P, Van Vlierberghe S. - *"A range of gelatin derivatization strategies lead to biofabrication versatility."*
   (**2017**, Tissue Engineering and Regenerative Medicine – EU Annual Meeting, Davos, Switzerland)
5. **Van Hoorick J**, Markovic M, Gruber P, Ovsianikov A, Van Erps J, Thienpont H, Dubruel P, Van Vlierberghe S. - *"Photo-Crosslinkable Gelatin Blends for Tissue Engineering Purposes: The Perfect Marriage Between Biocompatibility, Mechanical Control and Laser-Based Processing"*
   (**2016**, Belgian Polymer Group Annual Meeting, Hasselt, Belgium)
6. **Van Hoorick J**, Gruber P, Hölzl K, Markovic M, Van Erps J, Ovsianikov A, Thienpont H, Dubruel P, Van Vlierberghe S. - *"Surpassing Currently Encountered Drawbacks in Two-Photon Polymerization of Gelatin Hydrogels by Carboxylic Acid Modification"*
   (**2016**, World Biomaterials Conference, Montreal, Canada)
7. **Van Hoorick J**, Declercq H, De Muynck A, Houben A, Van Hoorebeke L, Cornelissen R, Van Erps J, Thienpont H, Dubruel P, Van Vlierberghe S. - *"Surpassing Concentration Limitations in Gelatin Scaffold Production via Indirect Additive Manufacturing"*
   (**2015**, Biofabrication, Utrecht, The Netherlands)
8. **Van Hoorick J**, Van Erps J, Thienpont H, Dubruel P, Van Vlierberghe S. - "Two-Photon polymerization: the masterkey to microfabrication?"
   (**2015**, Belgian Polymer Group Annual Meeting, Houffalize, Belgium)
9. **Van Hoorick J**, Ovsianikov A, Markovic L, Fowler T, Hoffman O, Dubruel P, Van Vlierberghe S.- *"Hydrogel-Polyester Combination Scaffolds for Tissue Engineering Purposes"*
   (**2014**, Advanced Materials for Biomedical Applications, Ghent, Belgium)
10. **Van Hoorick J**, Declercq H, Cornelissen M, Dubruel P, Van Vlierberghe S. - *"Surpassing the Mechanical Boundaries of Crosslinkable Gelatin."*
    (**2014**, Advanced Materials for Biomedical Applications, Ghent, Belgium)

International Research Stays

10/03/2019 – 22/03/2019	**Institute of Applied Synthetic Chemistry, Division of Macromolecular Chemistry, TUWIen,(Vienna, Austria)** „Synthesis of a macromolecular two-photon photoinitiator.“
05/11/2018 – 16/11/2018	**3D Printing an Biofabrication Group, Institute of Materials Science and Technology, TUWIen, (Vienna, Austria)** „2PP processing of crosslinkable gelatins onto membranes for cornea endothelial regeneration”
12/03/2018 – 26/05/2018	**3D Printing an Biofabrication Group, Institute of Materials Science and Technology, TUWIen, (Vienna, Austria)** “2PP processing of gelatin derivatives using different crosslinkers. Grafting experiments in hydrogel material and synthesis of a macromolecular photo-initiator.”
10/04/2016 – 14/05/2016	**3D Printing an Biofabrication Group, Institute of Materials Science and Technology, TUWIen, (Vienna, Austria)** “2PP experiments on gel-MOD-AEMA, gel-MOD, and gel-NB”
20/04/2015 – 01/05/2015	**3D Printing an Biofabrication Group, Institute of Materials Science and Technology, TUWIen, (Vienna, Austria)** “2PP/biocompatibility experiments on novel gelatin derivative.”

Scientific Training and Courses

28/11/2016 – 30/11/2016	**“Winterschool on Functional Coatings” –** Doctoral School for Sciences & Technology, Universiteit Hasselt (Diepenbeek, Belgium)
18/01/2016 – 19/01/2016	**„Flow Chemistry Workshop“** - Doctoral School for Sciences & Technology, Universiteit Hasselt (Diepenbeek, Belgium)
2015 - 2016	**“Executive Masterclass in Innovation and Entrepreneurship“** – Vlerick Business School (Ghent, Leuven, Brussels, Belgium)
13/07/2015 – 17/07/2015	**„Summer School on 3D Printing and Biofabrication“** – Utrecht Medical University (UMC) (Utrecht, The Netherlands)
02/06/2015	**Studienamiddag: „Extrusion Based Manufacturing“** - Centexbel & Sirris (Leuven, Belgium)
20/05/2015	**Workshop: „Biobased Polymers and Materials“** – Partnership in International Research & Education (Houffalize, Belgium)
05/02/2015	**Workshop: “3D Prtining: Concrete Toepassingen vandaag & mogelijkheden op textiel en kunststoffen.”** - Centexbel & Materialise (Leuven, Belgium)